OXIDATION and SORPTION MECHANISMS of HYDROLYZABLE METAL IONS on OXIDE SURFACE

by

Scott E. Fendorf

A dissertation submitted to the Faculty of the University of Delaware in partial fulfillment of the requirements for the degree of Doctor of Philosophy in Soil Science

December 1992

OXIDATION and SORPTION MECHANISMS of HYDROLYZABLE METAL IONS on OXIDE SURFACES

by

Scott E. Fendorf

Approved: Donald L. Sparks

Donald L. Sparks, Ph.D.
Chairman of the Department of Plant and Soil Sciences

Approved: John C Nye

John C. Nye, Ph.D.
Dean of the College of Agricultural Sciences

Approved: Carol E. Hoffecker

Carol E. Hoffecker, Ph.D.
Acting Associate Provost for the Graduate Studies

I certify that I have read this dissertation and that in my opinion it meets the academic and professional standard required by the University as a dissertation for the degree of Doctor of Philosophy.

Signed: _____

Donald L. Sparks, Ph.D.
Professor in charge of dissertation

I certify that I have read this dissertation and that in my opinion it meets the academic and professional standard required by the University as a dissertation for the degree of Doctor of Philosophy.

Signed: _____

Theodore H. Carski, Ph.D.
Member of dissertation committee

I certify that I have read this dissertation and that in my opinion it meets the academic and professional standard required by the University as a dissertation for the degree of Doctor of Philosophy.

Signed: _____

Douglas J. Doren, Ph.D.
Member of dissertation committee

I certify that I have read this dissertation and that in my opinion it meets the academic and professional standard required by the University as a dissertation for the degree of Doctor of Philosophy.

Signed: _____

Michael J. Kelley, Ph.D.
Member of dissertation committee

I certify that I have read this dissertation and that in my opinion it meets the academic and professional standard required by the University as a dissertation for the degree of Doctor of Philosophy.

Signed: _____

J. Thomas Sims, Ph.D.
Member of dissertation committee

ACKNOWLEDGMENTS

Pursuit of my doctoral degree has been both a trying and exhilarating experience. The encouragement, support, and collaboration of numerous individuals has made this research possible. I would like to thank each of my committee members: Dr. T.H. Carski for his encouragement and for providing me the valuable definition of pita, Dr. D.J. Doren for our numerous and enlightening discussions, Dr. M.J. Kelley for his surface science expertise, and Dr. T.J. Sims for keeping my research of practical significance. I would especially like to thank my major professor, Dr. Donald L. Sparks, for his support, encouragement, and guidance. I believe that I could not have received a finer doctoral training anywhere. I would also like to gratefully acknowledge the financial support provided by a research fellowship from the University of Delaware

Interaction, both professionally and personally, with many people has greatly enriched my graduate experiences. I have had the pleasure to work at numerous National Laboratories and would like to thank and acknowledge those with whom I have worked. Drs. J.A. Franz, D.M. Camaioni, and T. Autrey, and C.C. Ainsworth at Battelle Pacific Northwest Laboratory were instrumental in my EPR-SF studies. I cannot begin to thank Dr. Gerry Lamble, Brookhaven National Lab, enough for her patience, help, and guidance in XAFS experiments. A major portion of my research was conducted at the Lawrence Berkeley Lab, and I am grateful for the use of these facilities. I am particularly grateful to my brother Mark for collaboration on many aspects of this research. Without his aid this research would not have been possible; and, besides, Berkeley was a great place to visit. In addition to the National Laboratories, the Soil Chemistry research group has provided a wonderful environment for my scholastic endeavors. Apart from

the scientific benefits, we have had great personal interactions and had a great humor department. Matt Eick, Paul Grossl, Jerry Hendricks, Michael Stapleton, Yigal Salinger, Chip Toner (CVT), and ZZ Zhang have been a fabulous group to work with, and around. More than anything else during my stay in Delaware, my memories of our relationships will be cherished.

My family and friends have provided support and encouragement throughout my life. My parents have always had the wisdom and thoughtfulness to support my efforts while giving me the freedom to choose in which direct they will go. They have been instrumental in my scholastic endeavors. Finally, I would like to thank Elizabeth for enduring the distance which has separated us during my doctoral research. Although we were physically distant, our bond became increasingly strengthened. Her continued patience, understanding, encouragement, and support have continually enlightened me.

TABLE OF CONTENTS

LIST OF FIGURES

LIST OF TABLES

ABSTRACT

Metal ion reactions at the solid/solution interface are one of the primary processes which determine their fate in soils and waters. Ascertaining interfacial metal ion reaction rates and mechanisms is essential for determining reaction pathways and conditions which influence these processes. In this study, the sorption and redox reactions of Cr(III) at the oxide/solution interface were investigated by employing an array of sophisticated atomic-resolution experimental techniques and a novel electron paramagnetic resonance spectroscopically monitored stopped-flow (EPR-SF) techniquekinetic technique for studying rapid colloidal reactions *in situ*.

The oxidation of nonhazardous Cr(III) to the hazardous Cr(VI) by Mn-oxide, the only known naturally occurring oxidant of Cr(III), was investigated. The EPR-SF technique was used to determine the redox reaction rate between Cr(III) and δ-MnO_2 (birnessite). An overall second-order reaction was ascertained that exhibited a first-order dependence on $[Cr(III)]_o$ and $\{MnO_2\}_o$. A four step reaction mechanism was postulated: (i) Cr(III) adsorption, (ii) a two electron transfer, (iii) a single electron transfer and ligand exchange, (iv) and desorption of the reaction products. The adsorption step was rate limiting. At pH > 4, surface precipitation of Cr-hydroxide effectively inhibited oxidation. Aluminum also poisoned the reaction in a similar manner. Surface precipitation was catalyzed in the electrified interface and occurred at an ion activity product 10^3 times lower than would be expected for precipitation in solution.

The surface structure of Cr(III) sorbed on silica was ascertained using extended X-ray absorption fine structure (EXAFS) and diffuse reflectance infrared Fourier transform (DRIFT) spectroscopies, along with high-resolution transmission electron

microscopy. A monodentate Cr(III) surface complex formed at surface site occupancies < 20%, while Cr-hydroxide nucleation, with the γ-CrOOH type local structure, occurred at coverages > 20%. At the Cr-Si interface, a shorter corner sharing Cr octahedra distance occurred due to the structural constraints imposed by the silica. The energetics of the strained structure promoted the nucleation growth to progress away from the silica surface rather than across it, i.e., discrete crystalline γ-CrOOH surface clusters formed.

CHAPTER 1

INTRODUCTION

The mechanisms of heavy metal retention and oxidation by colloidal particles is of great interest to colloidal, environmental, and soil scientists. The fate of multivalent cationic metals (hydrolyzable metal ions) in the environment has increasingly become a focal point of study due to the potential toxicity and longevity of these elements. Metal ions are an environmental concern to agriculture, industry, and the public. Reactions at solid/solution interfaces, which are ubiquitous in surface and subsurface environments, are the primary determinant in the fate of heavy metals. Furthermore, metals may influence the properties of solid constituents in the environment through adsorption, redox, or surface precipitation reactions. After reacting with hydrolyzable metal ions, colloids may exhibit markedly different properties which will influence their subsequent behavior.

Although oxide materials may constitute only a small fraction of the solid composition in surface environments, their reactivity, high surface area, and coating ability make them very influential in sorption reactions. Moreover, oxides can be used in relatively pure phases allowing for the use of model systems to investigate metal reactions with solid components of soils and waters. Determining the interactions of heavy metals with several oxide materials will provide important information about the transport and fate of metal contaminants in natural systems, and will help to elucidate unresolved sorption mechanisms.

Oxidation/reduction reactions are also very important in determining the hazard and mobility of some heavy metals. Chromium is one such metal which is stable in two

oxidation states under surface environmental conditions, Cr(III) and Cr(VI). Chromium(VI) is more toxic and generally more mobile in soils and waters than Cr(III). Chromium(VI) readily penetrates plant and animal cell membranes and is toxic as an oxidizing agent; consequently, the drinking water standard maximum for Cr is 0.05 ppm (U.S. EPA, 1984). Concentrations as low as 5 ppm Cr(VI) in soils can be toxic to plants (Turner and Rust, 1971). Furthermore, anionic forms of Cr(VI) predominate under surface environments, resulting in a greater mobility of this species than Cr(III) due to the abundance of negatively charged surfaces in soils and the low hydroxide solubility of the Cr(III). In contrast to Cr(VI), Cr(III) is not known to be toxic to plants and is essential in animal nutrition (Bartlett and James, 1988).

Chromium is used in a variety of industrial processes which include alloying, tanneries, plating, and as water corrosion inhibitors. Environmental contamination of Cr arises from sludges, fly ash, industrial waste, and leakage of waters treated with Cr (which is present as an anti-corrosion agent). Commonly, municipal sludges contain Cr levels in excess of 1000 ppm (Grove and Ellis, 1980), and U.S. tanneries alone generate 80,000 to 100,000 tons of Cr-sludge per year (Makdisi, 1992) which may contain 21,000 to 55,000 ppm Cr on a dry weight basis (Federal Register, 1980a). Although these levels of Cr are extremely high, the sludges are not designated as hazardous waste because they are composed primarily of Cr(III) (Federal Register, 1980b). However, Cr(VI) levels of greater than 150 ppm were reported in soils at a Berkeley tannery only one year after the site was closed (Makdisi, 1992).

Although Cr(III) was once considered relatively harmless in the environment, recent evidence for Cr(III) oxidation by Mn-oxides potentially makes its hazard tantamount to that of Cr(VI). Because of the dramatic differences in toxicity and mobility between Cr species, it is imperative to determine reactions which influence potential oxidation state transformations. Determining the mechanism of Cr(III) oxidation to Cr(VI) is necessary to

accurately assess its potential hazard, and to determine safe disposal methods for this environmentally hazardous element. In addition, the reaction mechanisms of Cr may give important insights as to reaction pathways for other redox reactive heavy metals.

Manganese oxides are one of the most reactive inorganic constituents in surface environments, acting as both a strong sorbent and oxidizing agent, and are the only known natural occurring oxidant of Cr(III) (Eary and Rai, 1987). Chromium(III) oxidation by δ-MnO_2 is rapid, but the extent of reaction is limited at higher pH values (Fendorf and Zasoski, 1992). Molecular level information on this reaction is limited. This study will investigate the mechanism of Cr(III) oxidation by δ-MnO_2.

In general, the mechanisms of hydrolyzable metal ion sorption and oxidation are not resolved and much of the current knowledge is based only on macroscopic data. This investigation will employ several sophisticated surface probing techniques to obtain direct atomic level information on reaction mechanisms. Accurate knowledge of reaction rates and mechanisms is necessary to predict and control the fate of metal ions in the environment, which allows for risk assessment of the metal contaminants. While many sorption/desorption and redox reactions are relatively rapid (occurring in less than 1 s), rate information is necessary to determine competitive reaction processes which may occur in the complex matrices of soils and waters. Reaction mechanisms are needed to better understand the influences of other constituents present in these systems, reaction pathways, and possibly alter reaction pathways.

Manganese-, Si-, and Ti-oxides have differing physical and chemical properties which cover a broad spectrum of sorbent properties present in natural systems. They exhibit wide variations in their dielectric constants, zero points of charge (ZPC), surface morphology, redox reactivity, surface area, and surface charge. These oxides will be used to investigate the sorption and oxidation mechanisms of Al(III), La(III), and Cr(III). These hydrolyzable metal ions were chosen due to their environmental significance, and because

they provide a variety of sorbate properties while having similar valences. This allowed greater mechanistic information to be obtained on sorption mechanisms. Both Al(III) and Cr(III) have similar ionic radii and hydrolysis constants, but La(III) has a much larger ionic radius and smaller hydrolysis constant. The first hydrolysis constant ($Me^{3+} + H_2O$ <--> $MeOH^{2+} + H^+$) for La is at least 10^5 times smaller than that of Cr(III), Fe(III), or Al(III) (log $K_{1_{Fe}}$ = -3.05, log $K_{1_{Al}}$ = -4.97, log $K_{1_{Cr}}$ = -4.01, log $K_{1_{La}}$ = -9.06; Baes and Mesmer, 1976).

1.2 Sorption Mechanisms

Numerous studies have been conducted on metal ion sorption to colloidal surfaces, many of which have employed pure phase clay minerals or metal (hydr)oxides. Various thermodynamic approaches have arisen from these studies to describe metal sorption processes on oxide surfaces (James and Healy, 1972a,b; Schindler and Stumm, 1987; Burube and De Bruyn, 1968a,b; Davis et al., 1978; Hayes and Leckie, 1986; Dzombak and Morel, 1990). However, these macroscopic approaches do not give direct evidence for surface reaction mechanisms and differ in their physical conception of the solid/solution interface. Furthermore, many of these approaches model sorption reactions over a range of pH and metal concentrations entirely as a single mechanism. It is possible that numerous mechanisms of metal sorption occur over a range in system parameters. Advancements in surface spectroscopic and microscopic techniques allow direct mechanistic evidence to be obtained for metal ion reactions at the solid/solution interface.

The retention of multivalent cationic metals by oxide surfaces typically undergoes a dramatic increase over a solution pH increase of a few units. The mechanisms of hydrolyzable metal ion sorption on oxide surfaces have been questioned. Hypothesized mechanisms include: adsorption of the free ion or hydrolysis products, sorption of

polymerized species, surface cluster formation, and the formation of a surface precipitate. Surface precipitation has been proposed as an explanation for the sharp increase in metal sorption over a narrow increase in solution pH (James and Healy, 1972a,b; Tewari and Lee, 1975; Murray and Dillard, 1979; Benjamin, 1983; Crowther et al., 1983). Surface precipitation or surface polymerization appears to be the only plausible explanation for the retention of anions on amorphous $Fe_2O_3 \cdot H_2O$ after reaction with cationic metals (Benjamin, 1983).

James and Healy (1972a,b) proposed that the electric field induced by a charged colloid reduces the dielectric constant of the interfacial region, thereby reducing the solvation energy needed for precipitation reactions. The solubility constant of metal-hydroxide species is thus reduced in the electric double layer, allowing for precipitation prior to that in bulk solution. This hypothesis explains the sigmoidal curve generally shown with metal retention as a function of solution pH. Surface complexation has also been proposed as an explanation for the sharp increase in sorption, and for the electrophoretic mobility behavior of colloids in a system with hydrolyzable metal ion solutions (Schindler, 1981). Farley et al. (1985) introduced a more comprehensive thermodynamic model which combines surface complexation with surface precipitation reactions. However, these models are all based on a single surface functional group. Recent crystallographic assessment of oxide surfaces indicates that the 2 pKa single functional-group reaction mechanism of the previous adsorption models would be inaccurate (Torrent et al., 1990; Hiemstra et al., 1989a,b). A proton adsorption model based on both chemical and crystallographic considerations has recently been developed (Hiemstra 1989a,b) which will be discussed in the following section.

1.2.1 Multisite Surface Complexation Model

Various models have been proposed for proton adsorption on oxide surfaces in aqueous environments (Schindler and Stumm, 1987; Davis et al., 1978; Yates et al., 1974; Burube and De Bruyn, 1968a,b). Predominantly, these models have employed a 2 pKa single site surface functional group as described by the following generalized protonation equations.

$$Me\text{-}O^- + H^+ \text{ <----> } Me\text{-}OH^o \quad (1.1)$$

$$Me\text{-}OH^o + H^+ \text{ <----> } Me\text{-}OH_2^+ \quad (1.2)$$

However, various anomalies arise with these models, e.g., estimated surface site densities which are physically unrealistic, and the consideration of a homogeneous surface, and therefore a new approach was taken by Hiemstra et al. (1989a,b). This series of papers presents a general multisite complexation model (MUSIC), which is based on crystallographic and chemical/physical considerations. The MUSIC model was tested on a variety of well characterized oxides and found to describe proton titration data quite well. In this section, a very brief summary of the prominent features in the development, utility, and accuracy of the MUSIC model is presented. Clearly, this model indicates that many of the previous models were curve fitting exercises and do not provide sorption mechanisms. In this study, obtaining direct information on sorption and oxidation mechanisms will be emphasized to facilitate the development of accurate surface complexation models. This should ensure one of accurately predicting metal ion behavior in colloidal systems.

The presence of various surface groups on oxides has been known for some time (Kinselev and Lygin, 1975). However, until the development of the MUSIC model, proton adsorption models only considered one type of site (homogeneous surface sites). The MUSIC model considers at least three types of surface groups: singly, doubly, and triply metal coordinated. While the MUSIC model makes advancements in representing the

heterogeneous nature of surface functional groups, it does not consider complex particle morphology (i.e., surface plane distributions and edge or kink sites) of colloidal suspensions.

In the MUSIC model, protonation reactions for each of the surface site types were developed based on their chemical and structural environment. Proton affinity constants are dependent on many factors: valence of the central cation (Me), its electron configuration, Me-H distances, Me coordination number (CN), ligand CN, and the type of ligand. In an ionic solid, the bond valence (v), a concept introduced by Pauling (1960), is described as the charge (Z) of the cation divided by its CN. At the surface, bonds and CN are not satisfied, and consequently, when in an aqueous environment -O and-OH groups of oxide surfaces will coordinate protons. The number of protons (0, 1, or 2) depends on the solution and surface characteristics. The protonation can be represented for a general case as:

$$Me_n\text{-}O^{(n \cdot v - 2)} + H_s^+ \text{ <--> } Me_n\text{-}OH^{(n \cdot v - 1)} \qquad (1.3)$$

$$Me_n\text{-}OH^{(n \cdot v - 1)} + H_s^+ \text{ <--> } Me_n\text{-}OH_2^{(n \cdot v)} \qquad (1.4)$$

where n is the number of cations and v is the bond valence reaching the oxygen or hydroxyl. The intrinsic free energies of the groups in reactions (1.3) and (1.4) are made up of local electrostatic forces and other contributions shown in Eq. (1.5).

$$\Delta G^{\circ}_{intr} = \Delta G^{*} + \Delta G^{\circ}_{coul} \qquad (1.5)$$

In principle, the local electrostatic energy contribution to the adsorption of protons cannot be calculated as isolated from the rest of the surface. However, conveniently, Pauling's (1960) concept of bond valence, v, (or the strength of the electrostatic bond) accounts for potential fields exerted by surrounding ligands of the central cation. Thus,

using the relationship between the intrinsic free energy change and intrinsic affinity constant (K_{intr}) one obtains:

$$\log K_{intr} = A - B\,(n \bullet \nu / L) \tag{1.6}$$

where,

$$A = \frac{-Z_H Z_{o(H)} N e^2}{2.3\,RT\,4\pi\varepsilon_1 r} - \frac{\Delta G^*}{2.3\,RT} \tag{1.7}$$

and,

$$B = \frac{-Z_H N e^2}{2.3\,RT\,4\pi\varepsilon_1 L} \tag{1.8}$$

in which n is the number of metal ions coordinated with a surface group, Z_H=1, and $Z_{O(H)}$ is the valence of the surface oxygen or hydroxyl (-2 and -1, respectively), N is Avogadro's number, and ε_1 and ε_2 are effective microscopic dielectric constants. The distance of charge separation , L, is the distance from the center of the metal nucleus to that of H^+. Proton affinity constants are thus a function of the bond valence (ν), distance of charge separation (L), and the number of cations coordinated to a surface species (n), Eq. (1.6). However, the constants, A and B, of Eq. (1.6) must be determined in order to solve for the proton affinity constants.

Determining these constants, Eq. (1.6), is arduous due to the difficulty in obtaining physically accurate values for many of the parameters in the equation, e.g., the effective dielectric constants in the interfacial region. Yet, Hiemstra et al. (1989a) cleverly used solution monomers of cation species common to oxides (Al, Fe, Si, ...) as analogs to surface groups and plotted known log K values as a function of v / L. This is done for two types of similar electronic species: those with configurations of noble gases, and those with filled d-orbitals (d_{10}). The resulting plot showed very good linearity for such a simple

approach. The constants A and B were obtained graphically, avoiding calculations based on unknown or estimated physical parameters.

The resulting parameters, A and B, can then be used to calculate the proton affinity constants of an oxide with already well known constants (gibbsite, $Al(OH)_3$). However, Hiemstra et al. (1989a) noted a discrepancy between the calculated and known proton affinity constants for gibbsite and attributed this discrepancy to slight differences in the arrangements of -OH(H) species and solute molecules in a flat surface structure as opposed to those with a spatial arrangement for the monomer. The parameters A and B were thus altered by inducing a surface correction factor for use in calculating proton affinity constants of surfaces (Hiemstra et al, 1989a). In addition, charge effects of 'oxo' species were also accounted for, which resulted in a slight drop for such species. Finally, the surface charge can be related to surface potential by using an electrostatic model, e.g., the basic Stern model, completing the MUSIC model depiction of proton adsorption to oxide surfaces.

Hiemstra et al. (1989b) tested the MUSIC model on various well characterized oxides in which the proportions of surface planes were known, allowing calculations of weighted site densities for different surface group types. The resulting predictions were in very good agreement with proton titration data. The model was able to predict proton reactions over a broad range of pH values ($3 < pH < 11$) and with different types of surfaces (Al-, Fe-, Si-, and Ti-oxides). The results of the MUSIC model indicate that many important factors which determine proton affinities were not previously considered in surface complexation models. Firstly, a single surface functional group will only undergo one protonation step rather than two protonation steps because the difference in the pK's ($\Delta pK \approx 14$) is larger than the range of pH values encountered in the environment ($\Delta pK \approx 7$). Secondly, previously believed two pK models are actually due to more than one surface group type (singly, doubly, or triply coordinated groups). And finally, some

surface groups do not undergo protonation reactions under the normal pH range encountered in the surface environment. The findings of the MUSIC model account for the lower reactive surface site density observed with proton titration data than would be calculated by crystallographic considerations of a closest packed surface layer.

In short, the MUSIC model appears to offer a new, more accurate depiction of the oxide solid/solution interface and should be incorporated into a generalized surface complexation model. The results of this study, which will employ various advanced surface probing techniques to obtain direct information on the nature of metal ion reactions at the oxide/solution interface, should thus allow for confirmation or refutation of various aspects of the current surface complexation models. Such information will be useful in developing more accurate physical models of surficial sorption processes.

1.2.2 Direct Evidence for Sorption Reaction Mechanisms

Spectroscopic studies indicate various mechanisms for hydrolyzable metal ion sorption. Extended x-ray absorption fine structure (EXAFS) spectroscopy has recently been employed to study Co(II) and Pb(II) sorption on oxide surfaces (Brown et al., 1989). They indicated that sorbed Co(II), at approximately 10% surface coverage, formed small multi-nuclear species on γ-Al_2O_3, TiO_2 (rutile), and kaolinite. Lead(II) was observed as a mixture of monomeric and small multi-nuclear species at 10% monolayer coverage on γ-Al_2O_3. A detailed depiction of Cr(III) coprecipitates with Fe(III) and sorbed complexes on α-FeOOH (goethite) were also obtained with EXAFS (Charlet and Manceau, 1992). Homogeneous solution precipitation of Cr-hydroxide resulted in γ-CrOOH, and coprecipitates of $Cr,Fe(OH)_3 \cdot nH_2O$ also yielded the γ-MeOOH type structure. When Cr(III) sorbed on α-FeOOH at low surface coverage the α-CrOOH structure was discerned. With increasing Cr(III) levels, the nucleation growth occurred across the

surface (Charlet and Manceau, 1992). Beyond monolayer coverage the Cr-hydroxide precipitate underwent a phase transition to the γ-CrOOH local structure.

Bleam and McBride (1986), using EPR spectroscopy, found that Cu(II) and Mn(II) sorbed on TiO_2 at isolated sites under very low surface coverage, followed by the formation of surface nucleated clusters with increasing surface coverage. Mass action balance based on the pH, solution metal concentration, and sorbent surface area (surface site density) was postulated to control the growth of surface clusters relative to adsorption at isolated sites (Bleam and McBride, 1986). Copper(II) adsorbed on singly coordinated O(H) groups of Al-oxides, with $Cu(OH)_2$ surface nucleation occurring at only fractional surface coverage and well before solution precipitation (McBride et al., 1984; McBride, 1982). The Al-oxides lowered the apparent solubility of $Cu(OH)_2$ (McBride et al., 1984). Direct evidence has also been obtained for the formation of a Co(II) surface precipitate on oxide surfaces (Tewari and Lee, 1975; Murray and Dillard, 1979; Crowther et al., 1983). Crowther et al. (1983) observed XPS spectra characteristic of $Co(OH)_2$ on the surface of a synthetic birnessite when critical pH and Co(II) concentrations were exceeded.

The multi-nuclear metal species observed at lower surface coverage by other spectroscopic techniques (Charlet and Manceau, 1992; Manceau and Charlet, 1992; Brown et al., 1989; Bleam and McBride, 1986) may be a precursor to the formation of a surface precipitate. The mass action balance proposed by Bleam and McBride(1986) to explain the progression from isolated site binding to the formation of multi-nuclear sorbed clusters with increased solution metal concentration may explain the formation of a surface precipitate at even greater solution metal ion concentrations. Recently, we have employed an array of surface spectroscopic/microscopic techniques to investigate metal ion sorption and redox reactions at the oxide/water interface. Preliminary results provide direct experimental evidence that surface precipitation can occur prior to bulk solution precipitation and is influenced by the type of surface, pH, and the metal ion concentration

(these topics will be addressed in subsequent chapters). Consequently, such phenomena need to be considered in catalytic and environmental processes. Mechanistic models proposed to describe hydrolyzable metal ion sorption reactions need to incorporate surface nucleation reactions rather than assuming the total sorption process to be a single isolated site binding mechanism.

1.3 Kinetics of Metal Reactions at the Oxide/Water Interface

Equilibrium studies alone do not provide definitive information on reaction mechanisms and provide no insight as to reaction rates. Studies on the rates of heavy metal reactions on oxide materials would prove invaluable in providing mechanistic data, reaction time scales, and competitive sorption influences (competing time dependencies).

To accurately assess the fate of metals in surficial systems and to model their mobility, it is critical to determine the mechanisms of chemical reactions and the time frame in which they occur. Few studies have appeared on rates of hydrolyzable metal ion sorption on soil materials. Accurate rates are necessary to determine reaction mechanisms, and to assess the kinetic competition in sorption processes. Moreover, kinetic rate parameters can be coupled with equilibrium-based modeling to determine the accuracy, and thus, validity of the thermodynamic model employed. Hence, one of the major objectives of this research will be to develop a kinetic technique capable of determining heavy metal ion sorption/desorption rates and mechanisms on oxide surfaces.

Unfortunately many kinetic reactions on soils and soil components are extremely rapid, thus precluding the use of batch or flow techniques (Sparks, 1989). Heavy metal sorption reactions appear to be rapid, which may have prevented researchers from measuring the kinetics of these environmentally important reactions. Fortunately, there are

chemical relaxation techniques that measure reaction rates on millisecond and microsecond time scales.

1.3.1 Chemical Relaxation Techniques

Chemical relaxation techniques operate on the principle that the equilibrium of a reaction mixture is perturbed by a rapid alteration of some external factor, e.g., pressure or temperature. The pressure-jump (p-jump) method is based on the fact that chemical equilibria have a pressure dependence (Bernasconi, 1976). A pressure perturbation shifts the equilibrium; the return to equilibrium is related to the rates of all elementary reaction steps. Thus, the determination of the relaxation time may be used as a basis for formulating reaction mechanisms. The time required to reach the new equilibrium from the sudden pressure release is related to the relaxation time (τ). The perturbation is small such that the equilibrium is shifted by only a small amount. Because of the small perturbation, all rate expressions are linearized regardless of molecularity or reaction order and transport phenomena are minimized, which greatly simplifies the elucidation of complex reaction mechanisms (Bernasconi, 1976; Sparks, 1989).

Zhang and Sparks (1989, 1990a,b) have successfully used p-jump relaxation to ascertain molybdate, sulfate, selenite, and selenate adsorption/desorption reaction mechanisms at the goethite/water interface. Pressure-jump relaxation was also used by Hayes and Leckie (1986) and Hachiya et al. (1979) to study the kinetics of Pb^{2+} adsorption/desorption on goethite and γ-Al_2O_3 surfaces. Such studies are unique in that relaxation techniques measure chemical kinetics (devoid of transport phenomena). This allows one to more accurately ascertain sorption/desorption reaction rates. When these measurements are coupled with equilibrium model approaches, mechanistic information on sorbent retention on solids can be obtained.

1.3.2 EPR-SF Kinetics

Although p-jump relaxation provides a valuable tool for investigating sorption/desorption reactions on oxides, it is limited to the investigation of fully reversible reactions. In addition, many relaxation techniques monitor the reaction process indirectly. Thus, in complex systems, or for non-reversible reactions, relaxation kinetics may not be suitable. Another limitation of chemical relaxation techniques is that often determination of rate constants is dependent on equilibrium-based parameters. Because of these deficiencies, a novel approach for measuring rapid reactions in colloidal systems was employed. This technique is capable of directly measuring reaction rates in colloidal systems, regardless of reversibility, on a millisecond time scale *in situ*: an electron paramagnetic resonance (EPR) spectroscopically monitored stopped-flow (EPR-SF) kinetic technique.

This technique was used to determine the kinetics of Mn(II) sorption/desorption on δ-MnO_2 and Cr(III) oxidation by δ-MnO_2. A stopped-flow mixing cell located in an EPR spectrometer was equipped with a rapidly injecting dual-port syringe drive pump. The pump rapidly injects and mixes the reactants in the reaction cell, and the reaction is monitored by EPR detection of Mn(II). An advantage of the EPR-SF procedure is that the need for filtration is eliminated since with EPR, only Mn(II) is measured even in the presence of colloidal Mn or any other physical form of Mn (McBride, 1989a). Therefore, one can detect fast reactions and obtain high accuracy due to direct monitoring of the Mn(II) produced during the reactions.

The EPR-SF method is a novel approach for measuring rapid redox and sorption/desorption reaction rates at the oxide/solution interface. It also has many advantages for investigating reaction rates in colloidal suspensions. However, this technique is not without limitations. Unfortunately, the reaction being measured must involve an EPR active constituent. While this restriction does limit the applicability of

EPR-SF kinetics to some environmental systems, there are many systems for which this technique is ideally suited. One of its greatest utilities is the ability to monitor the oxidation of substances, e.g., organic molecules, Cr(III), As(III), by Mn-oxides. Because Mn(II) is liberated from the reductive dissolution of Mn-oxides, the production of oxidation products can thus be measured.

1.4 Chromium(III) Oxidation by Manganese Oxides

Oxidation/reduction reactions involving Cr are of considerable environmental importance because changes in the behavior and hazard of this element are induced. Chromium(VI) reduction decreases the potential hazard of Cr, but oxidation reactions of Cr(III) make it as potentially hazardous as Cr(VI). Chromium(VI) is reduced in natural systems by organic material, Fe(II), and sulfides. However, early studies indicated that oxidation of Cr(III) did not occur in soil systems (Bartlett and Kimble, 1976). Subsequently, Bartlett and James (1979) found that Cr(III) was readily oxidized by soils if fresh soil samples were used, rather than dried, aged samples. Manganese oxides were the oxidizing agent important in the soil systems (Bartlett and James, 1979). Research utilizing different forms of MnO_2 substantiated its role in oxidizing Cr(III) (Amacher and Baker, 1982; Eary and Rai, 1987). Manganese oxides can also oxidize many organic compounds. Much of the recent work on redox reactions has involved low molecular weight organic compounds and manganese oxides (McBride, 1987, 1989a,b; Stone, 1991).

Chromium(III) was oxidized over a range of pH values and Cr(III) concentrations by δ-MnO_2 (a common soil Mn-oxide, birnessite), but the reaction was limited as pH and Cr(III) concentrations increased (Fendorf and Zasoski, 1992). However, oxidation occurred at environmentally hazardous levels throughout the range of parameters studied

(i.e., greater than 1.7 ppm Cr(VI) formed even when the reaction was limited). Thermodynamically, Cr(III) oxidation should be more favorable as pH and initial Cr(III) concentrations increase. However, the extent of oxidation was contradictory, it was limited as pH and Cr(III) concentration increased. At pH < 3.5, the reaction went to completion but was limited at higher pH values when the initial Cr(III) concentration exceeded 77 μM. The reaction products were not the cause of the oxidation inhibition.

In agreement with Amacher and Baker (1982), Fendorf and Zasoski (1992) found the initial δ-MnO_2 levels were a controlling parameter affecting the degree of oxidation at higher pH values. Electrokinetic studies indicated a marked change in the electrophoretic mobility (EM) of δ-MnO_2 after reaction with Cr(III). The change in EM was due to Cr(III) rather than to other constituents in the system. As pH and Cr(III) concentration increased, the amount of Cr sorbed on the δ-MnO_2 increased, the EM became more positive, and the extent of oxidation was limited. At certain pH values and concentrations, Cr(III) appears to induce a surface alteration of the MnO_2 which limits the extent of oxidation (Fendorf and Zasoski, 1992).

Manceau and Charlet (1992) employed EXAFS spectroscopy to investigate the Cr(III) oxidation reaction mechanism. A bidentate inner-sphere Cr(III) surface complex on δ-MnO_2 was discerned, which led to the develop of a γ-CrOOH surface precipitate. In the structure of δ-MnO_2, 1 out of 6 Mn(VI) sites is vacant. Manceau and Charlet (1992) postulated that diffusion of Cr(III) into these vacancy sites was necessary for oxidation. However, their hypothesis is not consistent with oxidation rate, or the oxidation of Cr(III) by Mn-oxides which do not contain site vacancies, e.g., γ-MnOOH and β-MnO_2. Further investigation of the inhibitory mechanism of Cr(III) oxidation by δ-MnO_2 is discussed in the following chapter.

Although Cr(III) oxidation by δ-MnO_2 was more extensive at lower pH values, the initial reaction rate was much faster at pH 5 than at pH 3 (Fendorf and Zasoski, 1992).

Unfortunately, the initial reaction rate at pH 5 exceeded the detection times of the stirred-flow apparatus used and only general rate information was obtained. A definitive determination of the reaction mechanism could not be obtained. A kinetic technique capable of measuring rapid reaction kinetics must be used to obtain accurate rate parameters for Cr(III) oxidation. The rate of Cr(III) oxidation by γ-MnOOH had a first-order dependency on Cr(III) concentration and MnOOH suspension density (Johnson and Xyla, 1991). At pH > 4.5, a Cr(III) sorption term describes the reaction rate decline and thus indicated the presence of a surface limiting rate factor.

Prior to the Cr(III)-MnO_2 redox reaction, Cr(III) is sorbed to the surface, with subsequent oxidation. The Cr(III) sorption mechanism appears to be a primary factor in determining the extent of oxidation. However, studies of Cr(III) sorption on δ-MnO_2 are complicated by subsequent Cr(III) oxidation and the rapid desorption of the anionic Cr(VI) species produced. Moreover, the postulates of Manceau and Charlet (1992) for the sorption mechanism necessary for oxidation, i.e., diffusion of Cr(III) into site vacancies, seem inconstant with observed reaction rates, pH effects, and oxidizing ability of oxides without site vacancies. Analog systems of Cr(III)-MnO_2, which do not undergo oxidation/reduction reactions, could provide valuable information on the Cr(III) sorption mechanism. Aluminum(III) is predicted to behave in a similar manner to Cr(III) (Bartlett and James, 1979); therefore, data from this species may be similar to those for Cr(III) prior to oxidation. Moreover, information gained from the unique boundaries imposed on the sorption of Cr(III) to MnO_2 (i.e., the ensuing electron transfer) should be applicable to other hydrolyzable metal ion sorption processes. Competing metal ion influences, e.g., Al(III), on Cr(III) oxidation may also be an important consideration in complex matrices such as soils or waters. Accordingly, in this study we investigate the sorption mechanisms of Al, La, and Mn(II) and their influences on Cr(III) oxidation by δ-MnO_2.

A definitive Cr(III) oxidation mechanism should be ascertained by determining: (i) rate parameters for the oxidation reaction, (ii) Cr(III) sorption mechanisms, and (iii) the solid phase transformation induced by Cr(III) to δ-MnO_2.

1.5 Surface Spectroscopies/Microscopies

A multitude of macroscopic investigations on metal sorption reactions at the solid/solution interface have been conducted. While meaningful and important data were obtained from these studies, direct evidence for reaction mechanisms was not obtained. Nevertheless, reaction mechanisms were proposed to explain the observed solution trends. One cannot be certain that such reaction mechanisms are accurate, and, in fact, recent studies employing atomic level experimental techniques have indicated that early postulates were incorrect. The development of experimental techniques capable of ascertaining reaction mechanisms directly needs to be implemented to determine metal ion reactions at the solid/solution interface. This should facilitate the development of mechanistic models necessary to predict metal behavior in colloidal systems. Therefore, a primary objective of this study was to use a variety of atomic resolution surface probing techniques to investigate metal ion reactions at the oxide/water interface.

A multitude of techniques are available for investigating surface reactions, which yield a host of information. At present, no single technique is a panacea for investigating colloidal surface reactions. However, through the employment of different techniques one can obtain an accurate and detailed depiction of surface reactions. The molecular data can be combined with macroscopic data to provide a complete depiction of reaction mechanisms in colloidal suspensions. In this study, a range of experimental techniques were employed to thoroughly and accurately deduce redox and sorption reaction mechanisms.

Electron microscopies are useful in investigating solid state structures. Resolution better than 0.2 nm is easily achievable with transmission electron microscopes (TEM), while recent advancements in scanning electron microscopes (SEM) provides better than 3 nm resolution. Atomic resolution is thus possible with TEM, which may be coupled with electron spectroscopies to obtain elemental analysis. A detailed analysis of surface structural alterations induced by metal ion reactions with surfaces can thus be acquired. Unfortunately, a vacuum environment is necessary and sample damage may occur from electron bombardment. In addition, TEM analysis only forms a 2 dimensional image of the surface structure, although some information in the third dimension (depth) can be obtained from focal distortions. Hence, TEM gleans information on the atomic structure of surfaces and provides one a means for obtaining the spatial locality of surface modifications after metal ion sorption processes.

While high-resolution TEM has been very useful in discerning surface structural alteration of colloids after reaction with metals, this technique only gives evidence for the development of a new solid phase. It does not give information on the ion binding process--structural information is obtained rather than the local environment of a particular element. Fortunately, surface spectroscopies allow for direct atomic level information to be obtained on metal binding process, even at lower surface coverage, giving the local chemical environment of a particular species. Therefore, by combining a spectroscopic technique, e.g., X-ray absorption fine structure spectroscopy with TEM one is able to determine the surface structural modifications and the local structural/chemical environment of the sorbing species (i.e., the metal ion which sorbed on the surface).

X-ray absorption fine structure spectroscopy (XAFS) has recently been used to investigate the sorption of various heavy metals on oxide surfaces (Charlet and Manceau, 1992; Manceau and Charlet, 1992; Chrisholm-Brause et al., 1989; Hayes et al., 1987). A distinct advantage of synchrotron XAFS is that many systems can be investigated *in situ*.

However, XAFS is not without limitations. Because the X-ray absorption edge of many environmentally important elements lie at relatively low energies, high vacuum conditions are necessary. Furthermore, multiple chemical environments may be difficult to resolve, and the need for a synchrotron source may be restrictive. In this study, we will employ HRTEM (with associated electron spectroscopies), diffuse reflectance infrared Fourier transform (DRIFT), and XAFS spectroscopy to investigate metal ion reactions at the oxide/solution interface. The HRTEM provides information on the surface structure and spatial locality of the modifications. The spectroscopic analyses, DRIFT and XAFS, were conducted to determine the local environment of the sorbed species. The DRIFT results provided molecular information, structural information of which was qualified using XAFS. This allowed an extensive range of reaction parameters (surface coverage, pH, metal concentration, and surface type) to be evaluated as to their effects on the sorption complex.

1.6 Objectives of Research

Accordingly, the objectives of this research were to:

1) obtain equilibrium data on the sorption of Al(III), La(III), Mn(II) and Cr(III) on δ-MnO_2, and Cr(III) on SiO_2.

2) determine the binding structure of sorbed metal ions on oxide surfaces over a range of system parameters.

3) discern surface structural alterations of the metal oxide after reaction with hydrolyzable metal ions over a range of reaction conditions.

4) develop the application of a novel kinetic technique for the study of colloidal reactions with the capacity to measure rapid sorption/desorption and redox reactions.

1.7 References

Amacher, M.C., and D.E. Baker. 1982. Redox reactions involving chromium, plutonium, and manganese in soils. DE-AS08-77DPO4515. Inst. for Res. on Land and Water Res., Penn State Univ, PA.

Baes, C.F., and B.E. Mesmer. 1976. The hydrolysis of cations. Wiley and Sons, New York.

Bartlett, R.J., and J.M. Kimble. 1976. Behavior of chromium in soils: I. Trivalent forms. *J. Environ. Qual.* 5:379-383.

Bartlett, R.J., and B.R. James. 1988. Mobility and bioavalability of chromium in soils. pp. 267-303. *In* J.O. Nraigu and E. Nieborer (eds.) Chromium in the natural and human environments. Wiley and Sons, New York.

Bartlett, R.J., and B. James. 1979. Behavior of chromium in soils: III. Oxidation. *J. Environ. Qual.* 8:31-35.

Benjamin, M.M. 1983. Adsorption and surface precipitation of metals on amorphous iron oxyhydroxide. *Environ. Sci. Technol.* 17:686-692.

Bernasconi, C.F. 1976. Relaxation kinetics. Academic Press, New York.

Bleam, W.F., and M.B. McBride. 1986. The chemistry of adsorbed Cu(II) and Mn(II) in aqueous titanium dioxide suspensions. *J. Colloid Interface Sci.* 110: 335-346.

Brown, G.E. Jr., G.A. Parks, and C.J. Chisholm-Brause. 1989. In-situ x-ray absorption spectroscopic studies of ions at oxide-water interfaces. *Chimia.* 43: 248-256.

Burube, Y.G., and P.L. De Bruyn. 1968a. Adsorption at the rutile-solution interface. I: Thermodynamic and experimental study. *J. Colloid Interface Sci.* 27: 305-316.

Burube, Y.G., and P.L. De Bruyn. 1968b. Adsorption at the rutile-solution interface. II: Model of the electrochemical double layer. *J. Colloid Interface Sci.* 28: 92-105.

Charlet, L. and A.A. Mancaeu. 1992. X-ray absorption spectroscopic study of the sorption of Cr(III) at the oxide-water interface: I. Molecular mechanism of Cr(III) oxidation on Mn oxides. *J. Colloid Interface Sci.* 148: 425-442.

Chisholm-Brause, C.J., G.E. Brown, Jr., G.A. Parks, and J.O. Leckie. 1989. XANES and EXAFS study of aqueous Pb(II) absorbed on oxide surfaces. *Physica B* (Amsterdam) 158:674-675.

Cowley, J.M. 1981. Diffraction physics. North Holland, Amsterdam.

Crowther, D.L., J.G. Dillard, and J.W. Murray. 1983. The mechanism of Co(II) oxidation on synthetic birnessite. *Geochim. Cosmochim. Acta.* 47:1399-1403.

Davis, J.A., R.O. James, and J.O. Leckie. 1978. Surface ionization and complexation at the oxide/water interface. I.Computation of electrical double layer properties in simple electrolytes. *J. Colloid Interface Sci.* 63:480-499.

Dzombak, D.A., and F.M.M. Morel. 1990. Surface complexation modeling-hydrous ferric oxide. Wiley and Sons, NY.

Eary, L.E., and D. Rai. 1987. Kinetics of chromium(III) oxidation to chromium (VI) by reaction with manganese dioxide. *Environ. Sci. Technol.* 21:547-552.

Farley, K.J., Dzombak, D.A., and F.M.M. Morel. 1985. A surface precipitation model for the sorption of cations on metal oxides. *J. Colloid Interface Sci.* 106:226-242.

Federal Register. 1980a. pp. 33084-33139. Vol. 45, No. 98. Goverment Printing Office, Washington, D.C.

Federal Register. 1980b. pp. 74884-74894. Vol. 45, No. 220. Goverment Printing Office, Washington, D.C.

Fendorf, S.E., and R.J. Zasoski. 1992. Chromium(III) oxidation by δ-MnO_2. I: Characterization. *Environ. Sci. Technol.* 26: 79-85.

Grove, J.H., and B.G. Ellis. 1980. Extractable chromium as releated to soil pH and applied chromium. *Soil Sci. Soc. Am. J.* 44:238-242.

Hachiya, K, M. Ashida, M. Saski, H. Kan, T. Inoue, and T. Yasunaga. 1979. Study of kinetics of adsorption-desorption of Pb^{2+} on γ-Al_2O_3 surface by means of relaxation techniques. *J. Phys. Chem.* 83:1866-1871.

Hayes, K.F., and J.O. Leckie. 1986. Mechanisms of lead ion adsorption at the goethite/water interface. pp.141-158. *In* J.A. Davis and K.F. Hayes (ed.) Geochemical processes at mineral surfaces. ACS Symp. 323. Meet. Am. Chem. Soc., Washington, DC.

Hiemstra, T., W.H. Van Riemsdijk, and G.H. Bolt. 1989a. Multisite proton adsorption modeling at the solid/solution interface of (hydr)oxides: A new approach. I. Model description and evaluation of intrinsic reaction constants. *J. Colloid Interface Sci.* 133:91-104.

Hiemstra, T., J.C.M. De Wit, and W.H. Van Riemsdijk. 1989b. Multisite proton adsorption modeling at the solid/solution interface of (hydr)oxides: A new approach. II. Application to various important (hydr)oxides. *J. Colloid Interface Sci.* 133:105-117.

James, R.O., and T.W. Healy. 1972a. Adsorption of hydrolyzable metal ions at the oxide-water interface: II. Charge reversal of SiO_2 and TiO_2 colloids by adsorbed Co(II), La(III), and Th(IV) as model systems. *J. Colloid Interface Sci.* 40:53-65.

James, R.O., and T.W. Healy. 1972b. Adsorption of hydrolyzable metal ions at the oxide-water interface: III. A thermodynamic model of adsorption. *J. Colloid Interface Sci.* 41:65-80.

Johnson, C.A., and Xyla, A.G. 1991. The oxidation of chromium(III) to chromium(VI) on the surface of manganate (γ-MnOOH). *Geochim Cosmochim Acta.* 55:2861-2866.

Kinselev, A.V., and V.I. Lygin. 1975. Infrared spectra of surface compounds. Wiley and Sons, NY.

Krishnan, K.M. 1989. Electron energy-loss spectroscopy. *In* L.M. Coyne, S.McKeever, and D. F. Blake (eds.) Spectroscopic characterization of minerals and their surfaces. pp.54-74. ACS symposium series 415. American Chemical Society, Washington DC.

Kinselev, A.V., and V.I. Lygin. 1975. Infrared spectra of surface compounds. Wiley and Sons, NY.

Makdisi, R.S. 1992. Tannery wastes definition, risk assessment and cleanup option, Berkeley, California. *J. Haz. Mater.* 29:79-96.

Manceau, A.A., and L. Charlet. 1992. X-ray absorption spectroscopic study of the sorption of Cr(III) at the oxide-water interface: II. Adsorption, coprecipitation, and surface precipitation on hydrous ferric oxide. *J. Colloid Interface Sci.* **148**: 443-458.

McBride, M.B. 1989a. Oxidation of dihydroxybenzene in aerated aqueous suspensions of birnessite. *Clays Clay Miner.* 37:341-347.

McBride, M.B. 1989b. Oxidation of 1,2- and 1,4-dihydroxybenzene by birnessite in acidic aqueous suspensions. *Clays Clay Miner.* 37:479-486.

McBride, M.B. 1987. Adsorption and oxidation of phenolic compounds by iron and manganese oxides. *Soil Sci. Soc. Am. J.* 51:1466-1472.

McBride, M.B. 1982. Cu^{2+}-Adsorption characteristics of aluminum hydroxide and oxyhydroxides. *Clays Clay Miner.* **30**:21-28.

McBride, M.B., A.R. Fraser, and W.J. McHardy. 1984. Cu^{2+} interaction with microcrystalline gibbsite. Evidence for oriented chemisorbed copper ions. *Clays Clay Miner.* **32**:12-18.

Murray, J.W., and J.G. Dillard, 1979. The oxidation of cobalt(II) adsorbed on manganese dioxide. *Geochim. Cosmochim. Acta.* 43:781-787.

Pauling, L. 1960. The nature of the electrostatic bond, 3rd ed., Cornell Univ. Press, Ithaca, NY.

Schindler, P.W. 1981. Surface complexes at oxide-water interfaces. pp. 1-49. *In* M.A. Anderson and A.J. Rubin (eds.) Adsorption of inorganics at solid-liquid interfaces. Ann Arbor Science, MI.

Schindler, P.W., and W. Stumm. 1987. The surface chemistry of oxides, hydroxides, and oxide minerals. pp.83-110. *In* W. Stumm (ed.) Aquatic surface chemistry. Wiley and Sons, NY.

Sparks, D.L. 1989. Kinetics of soil chemical processes. Academic Press, New York.

Stone, A.T. 1991. Oxidation and hydrolysis of ionizable organic pollutants at hydrous metal oxide surfaces. pp. 231-254. *In* D.L. Sparks and D.L. Suarez (eds.) Rates of soil chemical processes, Soil Sci. Soc. Am. Special Publication, Soil Sci. Soc. Am., Madison, WI.

Tewari, P.H., and W. Lee. 1975. Adsorption of Co(II) at the oxide-water interface. *J. Colloid Interface Sci.* 52:77-88.

Torrent, J., V. Barron, and U. Schwertmann. 1990. Phosphate adsorption and desorption by goethites differing in crystal morphology. *Soil Sci. Soc. Am. J.* **54**:1007-1012.

Turner, M.A., and R.H. Rust. 1971. Effects of chromium on growth and mineral nutrition of soybeans. Soil Sci. Soc. Am. Proc. **35**:755-758.

Yates, D.E., S. Levine, and T.W. Healy. 1974. Site-binding model of the electric double layer at the oxide/water interface. *J.C.S. Faraday* I. 70:1807-1820.

Zhang, P.C., and D.L. Sparks. 1989. Kinetics and mechanism of molybdate adsorption/desorption at the goethite/water interface using pressure-jump relaxation. *Soil Sci. Soc. Am. J.* 53:1028--1034.

Zhang, P.C., and D.L. Sparks. 1990a. Kinetics and mechanisms of sulfate adsorption/desorption at the goethite/water interface using pressure-jump relaxation. *Soil Sci. Soc. Am. J.* 54: 1266-1273.

Zhang, P.C., and D.L. Sparks. 1990b. Kinetics of selenite and selenate adsorption/desorption at the goethite/water interface using pressure-jump relaxation. *Environ. Sci. Technol.* 24: 1848-1856.

CHAPTER 2

INHIBITORY MECHANISMS of Cr(III) OXIDATION by δ-MnO_2

2.1 Abstract

The oxidation of Cr(III) by Mn-oxides is inhibited at pH values greater than 4. In this chapter, we show that the inhibition is due to the formation of a $Cr(OH)_3$ precipitate on δ-MnO_2. Subsequent to the oxidation of an amount of Cr(III) equal to a monolayer of surface coverage, surface facilitated nucleation of $Cr(OH)_3$ terminates the redox reaction between Mn(IV)/Mn(III) and Cr(III). The $Cr(OH)_3$ phase acts both as a barrier to electron transfer between solution Cr(III) species and Mn(IV)/Mn(III), and as a redox stable sink for Cr(III). This system imposes some unique boundaries on surface precipitation as direct inner-sphere surface complexation of Cr(III) would result in an electron transfer reaction between Cr(III) and Mn(IV)/Mn(III). Therefore, the electrostatic influence of the surface appears to promote the nucleation of this hydrolyzable metal ion.

2.2 Introduction

Redox reactions at mineral interfaces are prevalent in the environment, and often have a dramatic influence on the behavior and hazard of heavy metals. Furthermore, these reactions are also important in catalytic and electrochemical processes. Chromium is one such metal in which two oxidation states are stable under surficial conditions, Cr(III) and Cr(VI). The behavioral and toxicological differences of these oxidation states are dramatic,

and thus it is of great importance to determine processes which may cause or effect changes in the oxidation state of Cr.

While the hazard of Cr(III) is low, the potential for oxidation makes its hazard tantamount to Cr(VI). Manganese oxides are the only known naturally occurring oxidant of Cr(III) (Eary and Rai, 1987). Chromium(III) oxidation by commonly occurring forms of Mn-oxide, birnessite and manganite, has been characterized (Fendorf and Zasoski, 1992; Johnson and Xyla, 1991; Amacher and Baker, 1982) and was limited at higher solution Cr(III) concentrations and pH values.

Recently, static and kinetic studies of Cr(III) oxidation by δ-MnO_2 have been investigated (Fendorf and Zasoski, 1992; Amacher and Baker, 1982). The extent of Cr(III) oxidation by δ-MnO_2, with varying initial Cr(III) concentrations over the pH range of 3 to 5, is presented in Table 2-1. At pH values less than 4, the oxidation reaction proceeds until a reactant (Cr(III) or MnO_2) is limiting. However, as the solution Cr(III) concentrations and pH increased the extent of oxidation decreased. In addition to affecting the extent of the redox reaction, solution Cr(III) concentrations and pH have a large influence on the rates of Cr(III) oxidation. At pH 5, a rapid initial oxidation rate is quickly followed by a sharp rate decline and a cessation of the reaction. In contrast, at pH 3 the reaction rate is much slower, but continues until a reactant is limiting (Fendorf and Zasoski, 1992). Clearly, the oxidation of Cr(III) by δ-MnO_2 does not go to completion as Cr(III) concentrations and pH increase.

The following reaction was hypothesized for the oxidation of Cr(III) by δ-MnO_2 at pH 5,

$$CrOH^{2+} + 1.5\ \delta\text{-}MnO_2 \Leftrightarrow HCrO_4^- + 1.5\ Mn^{2+} \qquad (2.1)$$

A negative ΔG_{rxn} was calculated for the all the reaction conditions employed by Fendorf and Zasoski (1992), which are depicted in Table 2-1. However, for the reaction of solid $Cr(OH)_{3\,(s)}$ and MnO_2, a positive ΔG_{rxn} value was calculated at pH values greater than 3.

Table 2-1. The extent of Cr(III) oxidation by δ-MnO_2 with the associated saturation indices (SI) for $Cr(OH)_{3\,(c)}$ as a function of pH and initial Cr(III) quantities.[a]

$Cr(III)_{initial}$[b]	pH	$Cr(VI)_{produced}$[b]	%Cr oxidized	SI[c]
11.8	3.0	6.33	53.6	-6.98
	4.0	6.34	53.7	-4.09
	4.5	6.12	51.9	-2.75
	5.0	4.80	40.7	-1.58
19.6	3.0	9.94	50.7	-6.75
	4.0	10.1	51.4	-3.84
	4.5	6.25	31.9	-2.51
	5.0	4.24	13.7	-1.34
31.0	3.0	12.5	40.3	-6.57
	4.0	7.85	25.3	-3.67
	4.5	5.38	17.4	-2.34
	5.0	4.13	13.3	-1.17
38.0	3.0	11.3	29.7	-6.47
	4.0	7.59	20.0	-3.57
	4.5	4.84	12.7	-2.24
	5.0	3.83	10.0	-1.07

[a] Data are from Fendorf and Zasoski (1992) using 0.25 mg MnO_2 in a 25 mL matrix of 0.1*M* $NaNO_3$. Further experimental details are given in the *Materials and Methods*.

[b] In units of μmoles.

[c] $SI=\log (IAP/K_{sp})$for $Cr(OH)_{3\,(c)}$. Saturation indices are reported based on solution species calculated from thermodynamic parameters of Rai et al. (1987) and the chemical speciation program MINTEQA2 (Allison et al., 1990).

The solid phase reaction,

$$Cr(OH)_{3\,(s)} + 1.5\ \delta\text{-}MnO_2 + 2\ H^+ \Leftrightarrow HCrO_4^- + 1.5\ Mn^{2+} + 2\ H_2O \qquad (2.2)$$

indicates an inverse relationship with pH and predicts the reaction to be thermodynamically less favorable with increased pH. Thus, the solution speciation does not appear to thermodynamically limit Cr(III) oxidation. However, solid-phase $Cr(OH)_{3\,(s)}$ is redox stable with respect to MnO_2 and would thus act as a potential redox-stable sink for Cr(III).

Amacher and Baker (1982) proposed that Mn(II) liberated from the redox reaction was sorbing on δ-MnO_2, competing with Cr(III), and thus inhibiting further oxidation. The sorption of Cr(VI) was proposed as the limiting factor in Cr(III) oxidation by β-MnO_2 (pyrolusite) (Eary and Rai, 1987). However, the stoichiometric quantities of Mn(II) and Cr(VI) from Reaction (2.1) where found in solution--that is, a solution ratio of 1.5 Mn(II) : 1 Cr(VI) was observed (Fendorf and Zasoski, 1992; Amacher and Baker, 1982). Both Al(III) (400 μ*M* at pH 5) (Fendorf, 1990) and Fe(III) (17.9 m*M* at pH 5.5) (Amacher and Baker, 1982) poison Cr(III) oxidation by δ-MnO_2. It was hypothesized that these metals formed (oxy)hydroxide surface precipitates which masked the surface of the Mn-oxide, and thus inhibited an electron transfer reaction. It was similarly proposed (Fendorf and Zasoski, 1992) that Cr(III) formed a (oxy)hydroxide surface precipitate which inhibited subsequent oxidation. Although surface precipitation may explain Cr(III) oxidation inhibition, it has not been unequivocally proven, and other redox controlling factors cannot be ruled out.

Chromium(III) oxidation by γ-MnOOH (manganite) has also recently been investigated (Johnson and Xyla, 1991). The oxidation reaction rate was first-order with respect to Cr(III) and γ-MnOOH, and second-order overall, at low Cr(III) surface loadings. The reaction was believed to consist of an adsorption step, three separate electron transfer steps, and a desorption step (Johnson and Xyla, 1991). Solution data indicated that for each Cr(III) oxidized, 3 Mn(III) were reduced to Mn(II). However, beyond a critical Cr(III) loading level, oxidation was inhibited. Under conditions where the oxidation reaction was inhibited, the reaction rate was proportional to: $[Cr(III)]_o$ -

[Cr(VI)] • {γ-MnOOH}. Sorption of a Cr-hydroxide phase was also believed to be the source of oxidation inhibition (Johnson and Xyla, 1991).

Various hypotheses have thus been introduced to account for the inhibition in Cr(III) oxidation: (i) sorption of Mn(II) that is released during the oxidation processes, (ii) Cr(VI) sorption on the Mn-oxide, (iii) valence changes of the surface bound Mn species, (iv) surface nucleation or precipitation of Cr-hydroxide, and (v) degradation of structural vacancies in the Mn-oxide. The former two processes appear to be insignificant in Cr(III) oxidation. Valence alterations of surface Mn would not seem to limit the reaction as Mn(III) reacts equally well with Cr(III) as Mn(IV) (Johnson and Xyla, 1991), and solution Mn(II) : Cr(VI) ratios are in agreement with expected reaction stoichiometry indicating that Mn(II) is not appreciably retained after the redox reaction (Fendorf and Zasoski, 1992; Johnson and Xyla, 1991; Amacher and Baker, 1982). The latter hypothesis would not seem reasonable based on the observed oxidation of Cr(III) by Mn-oxides without structural vacancies: β-MnO_2 and γ-MnOOH.

Surface precipitation appears to explain the inhibition in Cr(III) oxidation by Mn-oxides, but direct evidence supporting this hypothesis has not been previously presented. In this study, we give evidence based on various microscopic and spectroscopic techniques that $Cr(OH)_3 \cdot nH_2O$ surface precipitation does occur and appears to be the source of the oxidation inhibition.

Recently, Manceau and Charlet (1992) used extended x-ray absorption fine structure (EXAFS) spectroscopy to study the oxidation process of Cr(III) by various Mn-oxides. They propose that in the presence of multinucleated Cr(III) (aq) species, mono-nuclear Cr(III) diffuses to the lattice vacancies in the Mn-oxide structures and is complexed in these sites subsequent to electron transfer with Mn(IV). It is suggested that the number of vacancies in the lattice structure determines the extent and rate of Cr(III) oxidation. While this study is based on a powerful technique, we do not find the results of Manceau

and Charlet (1992) entirely in agreement with previous studies (Fendorf and Zasoski, 1992; Amacher and Baker, 1982) on Cr(III) oxidation.

If Cr(III) oxidation occurred only with the vacancy filling Cr(III) species, the rate of reaction would be dependent on the number of vacancies. Thus, as stated by Manceau and Charlet (1992), oxidation would increase as the number of vacancies in the lattice structure increase, and therefore the rate of reaction should increase with time. This contradicts the rates of reaction observed by others (Fendorf and Zasoski, 1992; Johnson and Xyla, 1991; Amacher and Baker, 1982) in which the oxidation clearly decreases with time as a function of decreasing surface area. In addition, the oxidizing abilities of the Mn-oxides can be explained by the increase in zero points of charge (ZPC) of the Mn-oxides with a decrease in vacancy site density (Healy et al., 1966) rather than as a direct result of the vacancies being needed for oxidation. Furthermore, expecting Cr(III) to complex only in the vacancy sites of Mn-oxides is inconsistent with the pH dependence of cationic metal sorption observed by numerous researchers. Complete consumption of δ-MnO_2 at $pH < 4$ also contradicts this hypothesis. Here, we propose a mechanism for the source of Cr(III) oxidation inhibition based on previous studies and on direct microscopic and spectroscopic evidence presented in this study.

Determining oxidation and inhibitory mechanisms is important as such information may provide an understanding of redox reaction pathways and may allow them to be controlled. The sorption mechanism of Cr(III) on Mn-oxides appears to be a factor in controlling the extent of oxidation. The Cr(III) sorption processes are expected to be similar to those of other hydrolyzable metal ions on oxide surfaces, although ligand exchange may be slower with hexaqua-Cr(III) (Taube, 1970). Sorption studies involving non-redox reactive systems should thus give insight as to the sorption mechanism of Cr(III) on MnO_2. Conversely, the restriction in having electron transfer follow sorption allows one to gain information that would otherwise be unobtainable.

2.2.1 Sorption Mechanisms

The sorption mechanism of Cr(III) on Mn-oxides is highly influential on the extent and rate of the redox reaction. Many studies of hydrolyzable metal ion sorption on oxide surfaces have resulted in hypothesized models for the sorption processes based strictly on macroscopic data (Hayes and Leckie, 1986; Farley, et al., 1985; Davis et al, 1978; Stumm et al., 1976; Yates et al., 1974; Bowden et al., 1973; James and Healy, 1972). Many of these complexation models describe the sorption of hydrolyzable metal ions on oxide surfaces without considering surface precipitation (Hayes and Leckie, 1986; Davis et al, 1978; Stumm et al., 1976; Yates et al., 1974; Bowden et al., 1973). However, surface precipitation has been observed by various researchers (Charlet and Manceau, 1992; Manceau and Charlet, 1992; Crowther et al., 1983; Tewari and Lee, 1975) and has been used to successfully model the sorption of hydrolyzable metal ions (Farley, et al., 1985; James and Healy, 1972). James and Healy (1972) provided a thermodynamic development which accounted for hydrolyzable metal ion sorption on oxide surfaces based on surface precipitation prior to bulk solution precipitation. In this model the electrostatic effects of the interfacial region are incorporated into the free energy terms, with a lowering of the solubility constant resulting in this region. Farley et al. (1985) also incorporate surface precipitation into a thermodynamic sorption model; their model extends a surface complexation model to account for surface precipitation.

With the advancement in surface probing techniques, direct molecular level information has been obtained for sorption reactions. However, such studies have also led to differing conclusions on sorption mechanisms. Electron paramagnetic resonance (EPR) spectroscopic investigations of Mn(II) sorption on TiO_2 indicated a progression from isolated site binding to the formation of surface clusters with increased Mn(II) concentrations (Bleam and McBride, 1986). The attributes of synchrotron radiation have allowed researchers to conduct X-ray absorption spectroscopy (XAS) studies on metal

sorption reactions *in situ*. Results based on XAS indicate that various hydrolyzable metal ions form polynuclear species, with varying numbers of nuclei, on oxides (Charlet and Manceau, 1992; Manceau and Charlet, 1992; Brown et al., 1989). X-ray photoelectron spectra (XPS) of Co sorbed on MnO_2 indicated the formation of $Co(OH)_2$, thus giving evidence for surface precipitation (Crowther et al., 1983). A recent extensive study of Cr(III) sorption on hydrous ferric oxide (HFO) (Charlet and Manceau, 1992) coupled structural analysis (EXAFS spectroscopy) with macroscopic (thermodynamic) modeling. The surface precipitation model (Farley et al., 1985) was used to interpret adsorption isotherms, the results were in agreement with the EXAFS analysis. Even at low surface coverage (< 10% of the active surface site occupancy) Cr(III) was observed in a surface nucleated state. With increasing surface coverage nucleation became more extensive, distributing over the sorbent surface rather than forming surface clusters. In a continuing progression, further increases in Cr(III) altered the nucleated structure from α-CrOOH to γ-CrOOH--the γ-CrOOH structure was representative of the local structure of pure hydrous chromium oxide [$Cr(OH)_3 \cdot nH_2O$] and had an identical solubility product. Thus, Cr(III) sorbed as a polynuclear species even at low surface coverage and formed a surface precipitate where solution precipitation was not observed (Charlet and Manceau, 1992).

While much knowledge has been gained on sorption mechanisms of hydrolyzable metal ions, both macroscopic and spectroscopic/microscopic studies have led to differing mechanistic conclusions. Furthermore, the phenomena governing these processes are unresolved and may differ in various systems. Therefore, additional studies are necessary to help clarify these important reactions. The intent of this study was to determine: (i) if surface precipitation occurred in systems of Cr-MnO_2, and, if present, the composition of the precipitate, (ii) factors which may govern the precipitation, and (iii) the inhibitory factor in Cr(III) oxidation.

2.3 Materials and Methods

In this study, samples were prepared for HRTEM, energy dispersive x-ray spectroscopy (EDS), and electron energy loss spectroscopy (EELS) by dispersing 0.2 mg of powdered oxide, δ-MnO_2, on a holey carbon film supported by a copper mesh grid. The δ-MnO_2 was synthesized as described by Fendorf and Zasoski (1992), and had a surface area of 223 $m^2\ g^{-1}$. Potentiometric titration and electrokinetic studies indicated the ZPC = 2.7. Reactions were carried out by suspending the oxide coated grid in 10 mL solutions of 400 μ*M* Cr(III) at pH 5, or 1 m*M* Cr(III) at pH 4, in 0.1 *M* $NaNO_3$ at 25°C in an $N_{2\ (g)}$ environment. The resulting solid/solution ratio was 0.02 g L^{-1}. The pH was maintained at the initial pH value throughout the experiment by the addition of reagent grade NaOH. Chromium(III) stock solutions were made from reagent grade nitrate salts with acidified deionized H_2O. The stock solutions were never allowed to age more than 5 days and were stored under acidic conditions to reduce potential polymerization. After a 24 h reaction period the grids were removed from solution, rinsed in deionized water, and air dried at 25°C. Results were consistent between replicates and within each sample; thus, the results do not appear to be artifacts of individual preparations. Micrographs illustrated in this chapter are representative of each treatment. All of the surface characterization techniques used in this study were performed on a JEOL 200 CX transmission electron microscope at 200 kV.

For solution data referenced from Fendorf and Zasoski (1992), static studies were performed using batch methods unless otherwise indicated. Twenty-five mL of solution and 2.5 mg of MnO_2 were placed in polyethylene tubes to yield an initial solid concentration of 0.1 g L^{-1}. Each run consisted of dispensing the oxide in the reaction vessels, adding supporting electrolyte (0.1 *M* $NaNO_3$), hydrating for 24 h, adjusting pH, and finally adding $Cr(NO_3)_3$ solutions. After a 24 h shaking period, the suspensions were

centrifuged, filtered through a 0.45 μm pore membrane filter, and the filtrate analyzed. The reactions were always carried out under a $N_{2\,(g)}$ environment.

2.4 Results

2.4.1 High-Resolution TEM

High-resolution TEM was performed to ascertain whether any alteration in the surface structure of δ-MnO_2 could be detected after reaction with Cr(III). At low magnification, the characteristic spherical clusters of needles in synthetic birnessite can be seen (Fig. 2-1). A dramatic alteration occurs in this system after reacting with Cr(III) (Fig. 2-2). The post-reaction solid phase shows a large alteration in morphology; the birnessite needles are removed and the inner material has fused, resulting in a convoluted mass. Dissolution of the oxide is apparent (particularly in Fig. 2-2b) with the solid material decreasing from a dense mass to a thin film from the center of a particle out. The apparent dissolution may be a Cr-hydroxide precipitate, a re-precipitation of the Mn-oxide, or the dissolution of the original MnO_2. At high magnification, HRTEM images show that the unreacted MnO_2 was partially crystalline (Fig. 2-3). Interspersed with amorphous material, there are layers of parallel atomic planes exhibiting severe bends and twists which in some cases form distinctive needle-shaped protrusions. In the unreacted MnO_2, the needles are prominent and clearly delineated. At high magnification (Fig. 2-4), the dramatic change in the solid phase after MnO_2 was reacted with Cr(III) can be clearly seen. The crystalline MnO_2 needles are no longer prevalent in the surface structure, and a new highly ordered material is now present. The prominent lattice fringes indicate that the new solid phase is crystalline with distinct faceted grains. The new crystalline phase was

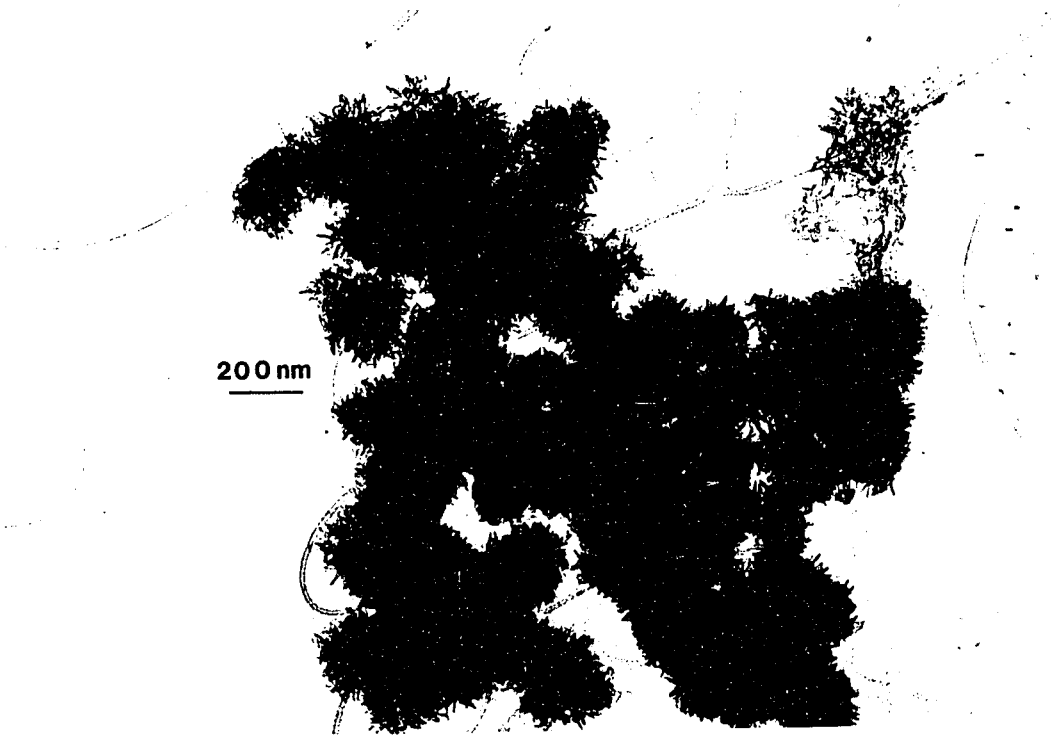

Figure 2-1. Low magnification HRTEM image of unreacted δ-MnO_2 showing spherical clusters of needles characteristic of synthetic birnessite.

deposited at the edge of remnant MnO_2, often extending for hundreds of Å as shown in Fig. 2-4. After reaction with 400 μ*M* Cr(III) at pH 5, extensive deposits of the new crystalline material can be seen (Fig. 2-5a,b).

The electron diffraction (ED) pattern of the new crystalline phase (Fig. 2-6b) was dramatically changed from that of the unreacted MnO_2 (Fig. 2-6a). In the unreacted material, diffuse ring patterns are observed resulting from a dispersion of amorphous material within a matrix of partially crystalline material. The d-spacings from ED are characteristic of birnessite, with low-order values of 1.4, 2.4, 3.5, and about 7.3 Å--in agreement with x-ray diffraction data (Fendorf and Zasoski, 1992). In contrast, the new crystalline phase present in the Cr-MnO_2 systems was highly ordered, and in one case a

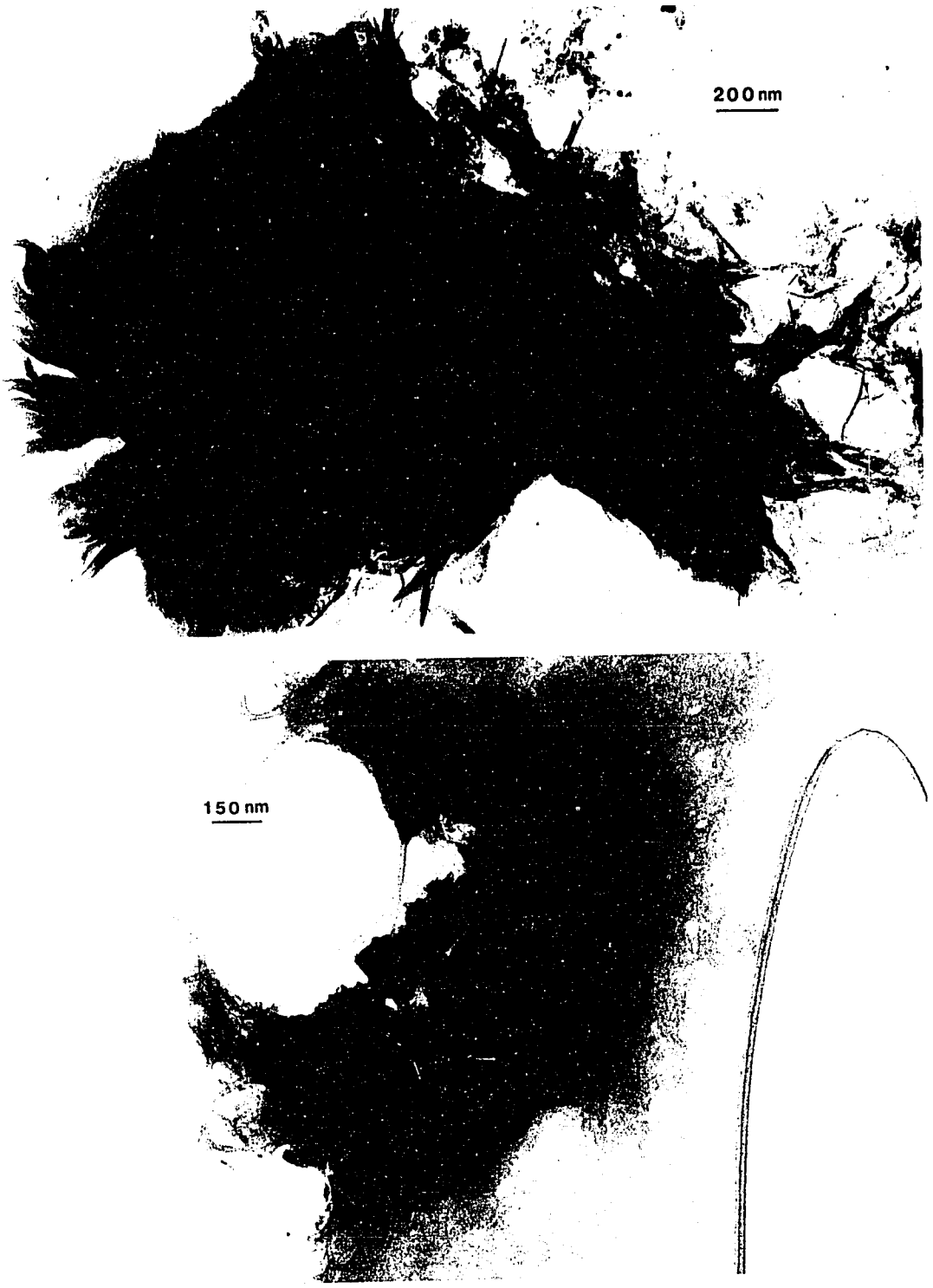

Figure 2-2. Low magnification HRTEM image of δ-MnO_2 after reaction with (a) 1 m*M* Cr(III) at pH 4, and (b) 400 μ*M* Cr(III) at pH 5. The crystalline needles are removed and the inner material has fused resulting in a convoluted mass with the solid material decreasing from a dense mass to a thin film from the center of the particle out (particularly exemplified in image b)

perfectly oriented single crystal pattern was observed (Fig. 2-7). The resulting diffraction pattern exhibited six-fold symmetry, and allowed crystallographic assessment of this solid phase. Indexing the reciprocal lattice gave real lattice parameters in good agreement with the hexagonal structure of $Cr(OH)_3 \cdot nH_2O$ (the γ-CrOOH structure). Thus, the new crystalline phase appears to be $Cr(OH)_3 \cdot nH_2O$ (c).

Figure 2-3. High magnification HRTEM image of δ-MnO_2 depicting the crystalline needles (indicated by the arrow) interspersed with amorphous material.

2.4.2 Energy Dispersive X-ray Spectroscopic (EDS) Analysis

All elements have a defined energy at which core-shell electrons are ejected, which results in a sharp increase in absorption of incident energy. When core holes are filled as the system relaxes to a ground state, x-rays of characteristic energy are emitted. Thus, the

Figure 2-4. High magnification HRTEM image of δ-MnO_2 after reaction with 1 m*M* Cr(III) at pH 4. A new highly ordered material with distinct faceted grains (upper arrow) can be seen deposited on the Mn-oxide (lower arrow).

X-ray emission energy of an element can be used to determine the elemental constituents of a sample. Here, we used an analytical electron microscope (AEM) equipped with an energy dispersive X-ray spectrometer to determine the composition of the solid phase present in Cr-MnO_2 systems. In the scanning transmission (STEM) mode distinct areas of interest can be probed with a finely focused electron beam for analysis of elemental compositions.

The energy dispersive x-ray spectra for the Cr-MnO_2 systems indicated that the reacted solid material was a composite of MnO_2 and $Cr(OH)_3$. A Cr : O ratio of 1 : 3 in the highly crystalline material provides further evidence that this product is $Cr(OH)_3$. In addition, EXAFS indicated the presence of $Cr(OH)_3 \cdot nH_2O$ on the surface of birnessite

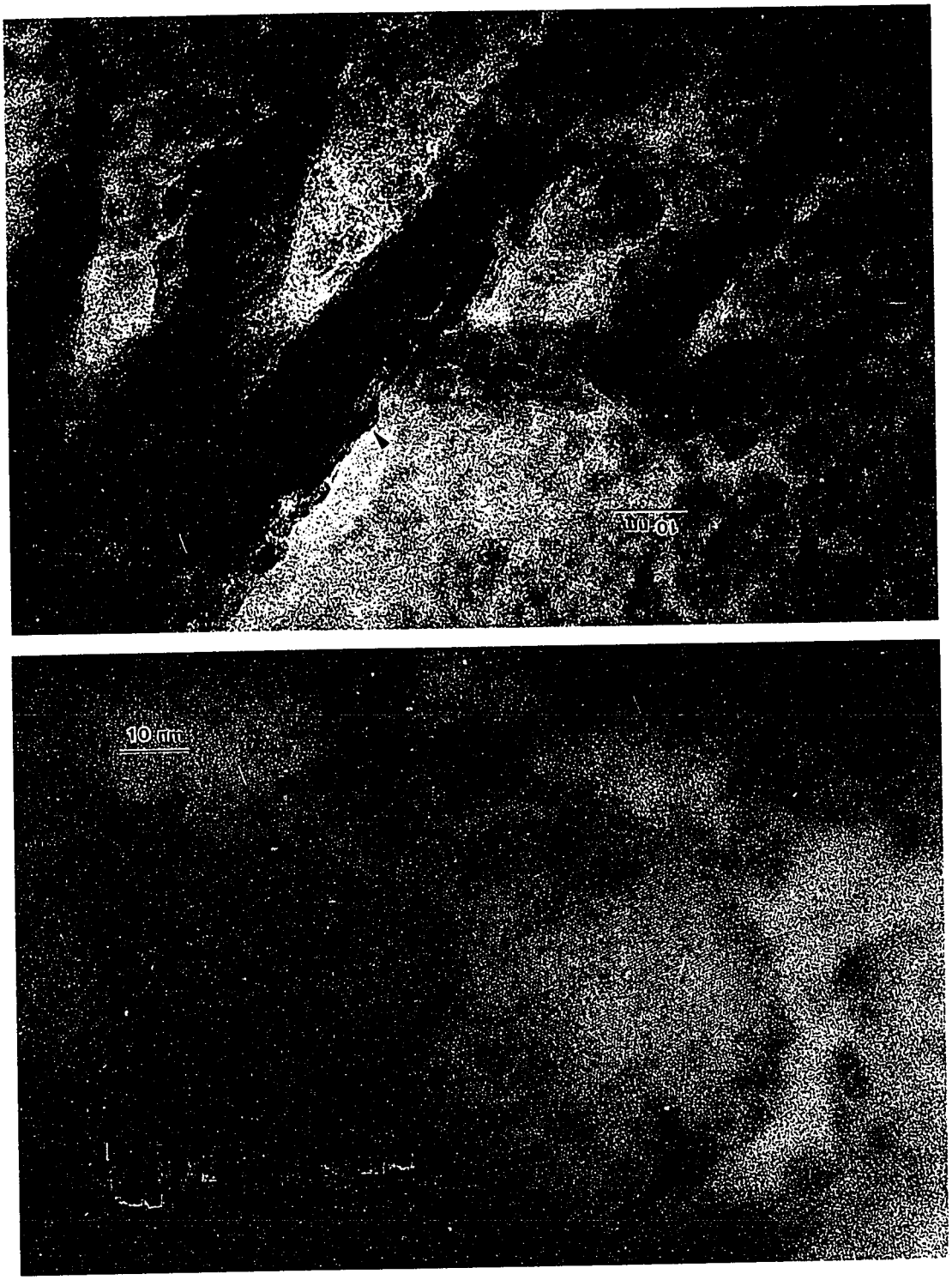

Figure 2-5. High magnification HRTEM images of δ-MnO_2 after reaction with 400 μ*M* Cr(III) at pH 5. Extensive crystalline material is depicted in both micrographs, with (a) showing remnants of the Mn-oxide (marked by the arrow) and (b) the degree of ordering present in the newly deposited material.

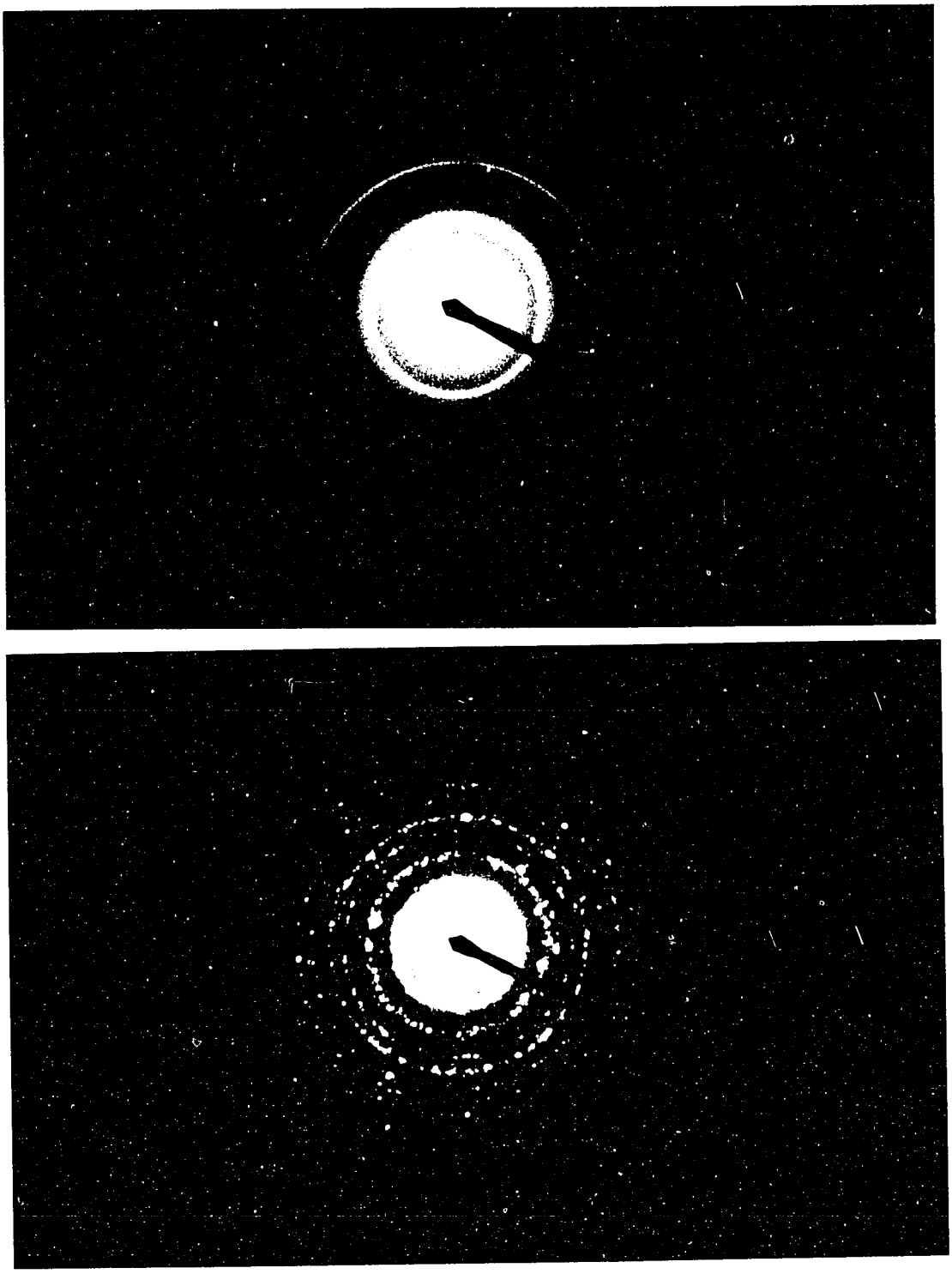

Figure 2-6. Electron diffraction pattern of: (a) unreacted δ-MnO_2 and (b) δ-MnO_2 after reaction with Cr(III). The high degree of crystallinity is apparent after reaction with Cr(III) as shown by the sharp ring patterns (b).

(Manceau and Charlet, 1992). As a result of STEM and HRTEM analysis, it appears that the new $Cr(OH)_3$ material is deposited over the existing MnO_2 and crystal growths of the new material {$Cr(OH)_3 \cdot nH_2O$} protrude into the surrounding media. Probing the carbon surface of the grid indicated that precipitation had not occurred except where colloidal material was present prior to reaction.

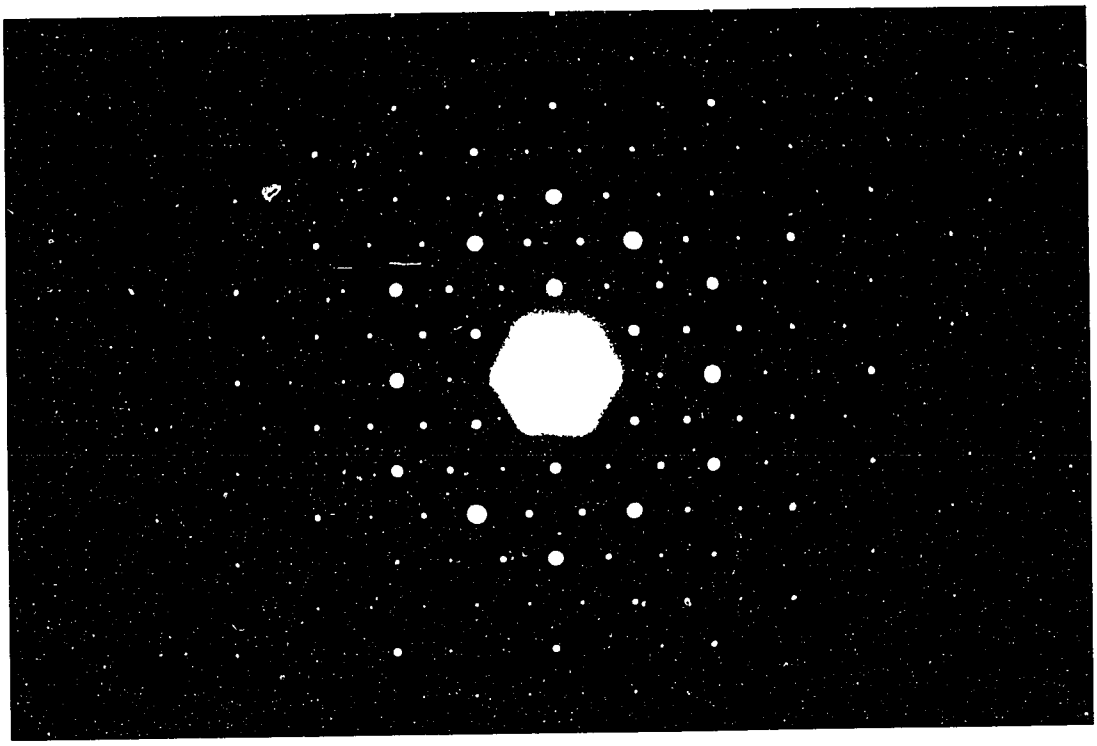

Figure 2-7. A perfectly oriented single crystal pattern of δ-MnO_2 after reaction with Cr(III). The resulting diffraction pattern exhibits six fold symmetry and allowed crystallographic assessment of this solid phase which appeared to be $Cr(OH)_3 \cdot nH_2O$ (the γ-CrOOH structure).

2.4.3 Electron Energy-Loss Spectroscopic (EELS) Investigations

Electron diffraction data and EDS confirm the deposition of $Cr(OH)_3 \cdot nH_2O$ on MnO_2. However, neither of these techniques gives information as to valence alterations in

the MnO_2. As mentioned in the previous section, binding energies of core electrons are a function of the atomic number, allowing the energy absorption edge positions to unequivocally identify the elements present in a sample. Thus, electron energy loss spectroscopy (EELS) can also be used to identify the elemental constituents of a sample. This technique is particularly useful for the identification of the lightest elements, for which the more commonly used EDS technique has an extremely low detection efficiency.

In addition to determining elemental constituents, EELS gives information on the valence state of each species present. For the first row transition metals, the excitation of the L_3 ($2p_{3/2}$) and L_2 ($2p_{1/2}$) levels following the dipole transitions to the unoccupied *d* states results in prominent pre-edge features, termed white lines, in the EELS. The position of the white lines relative to the incident energy, along with the L_2:L_3 peak ratios, form the bases for determining the valence state of the absorbing species. Positive chemical shifts occur as a function of oxidation states; a 1 eV shift occurs for each increase in valence from Mn(II) to Mn(IV) (Krishnan, 1989). Furthermore, previous studies provide a catalogue of L_2/L_3 ratios for Mn in which the ratio changes from 0.25 for Mn(II) to 0.65 for Mn(IV) (Krishnan, 1989). After calibrating the energy scale with that of a known MnO sample, we use this technique to determine alterations in the oxidation state of MnO_2 after reaction with Cr(III).

Based on the high surface area of this mineral {223 $m^2\ g^{-1}$} and an ideal crystalline birnessite structure, greater than one third of the Mn is expected to be surface associated. Thus, although EELS gives the oxidation state of the entire solid-phase Mn, an extensive surface alteration would represent a significant fraction of the total Mn present in the material. Based on the signal/noise and previous results (Krishnan, 1989), EELS should resolve valence changes involving greater than 10% of the total Mn. The EELS spectrum depicted in Fig. 2-8 is of the Cr(III) reacted MnO_2. This spectrum is characteristic of Mn(IV) and gives no indication of Mn(III) or Mn(II) being the dominant surface species

after reaction with Cr(III). The L_2 and L_3 peaks are in the proportions of Mn(IV) (L_2/L_3 = 0.65) and the

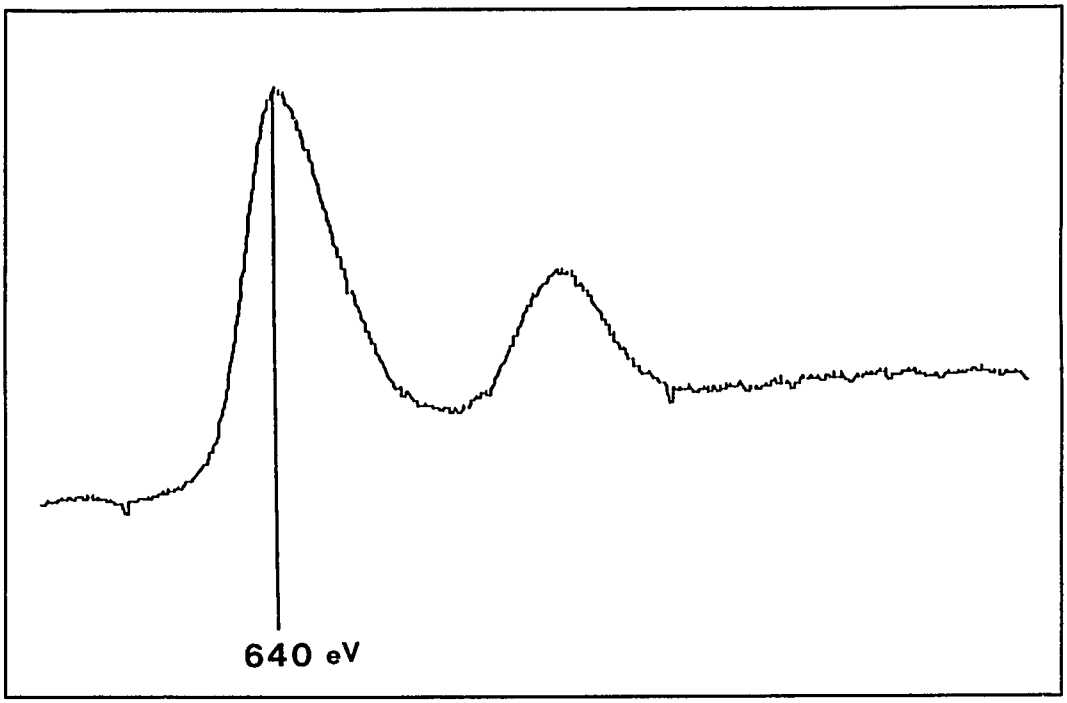

Figure 2-8. Electron energy loss spectrum (EELS) of δ-MnO_2 after reaction with 400 μ*M* Cr(III) at pH 5. The spectrum is characteristic of Mn(IV) and gives no indications of Mn(III) or Mn(II) being the dominant surface species after reaction with Cr(III).

L_3 peak resides at the Mn(IV) position, 640 eV. Because EELS probes the bulk material, Mn(III) {and possibly Mn(II)} may be present in the system as well. However, EELS would easily resolve a valence change of the entire Mn surface from Mn(IV) to Mn(II), which would be necessary to inhibit Cr(III) oxidation. Thus, after a 24 h reaction period with Cr(III), remnant Mn-oxide does not appear to have a valence alteration of the magnitude necessary to inhibit Cr(III) oxidation.

2.5 Discussion

As previously discussed, macroscopic investigations indicate that at pH 5, Cr(III) oxidation by birnessite proceeds according to Reaction (2.1) (Fendorf and Zasoski, 1992). However, oxidation is inhibited when critical Cr(III) loading levels are exceeded (Fendorf and Zasoski, 1992; Amacher and Baker, 1982), but direct evidence for the source of inhibition has not been obtained.

2.5.1 The Mechanism of Cr(III) Oxidation Inhibition

Prior to reaction, birnessite is present as a partially crystalline phase with amorphous material interspersed. After reacting with Cr(III) a dramatic alteration in the solid phase occurs. A large portion of the MnO_2 is eroded due to a reductive dissolution of the original oxide during the reaction with Cr(III). During this process soluble Mn(II) is produced from the electron transfer reaction which thus decreases the solid-phase Mn (Fendorf and Zasoski, 1992; Johnson and Xyla, 1991; Amacher and Baker, 1982). In addition to the reductive dissolution of the MnO_2, a new highly ordered (crystalline) material is deposited at the surface of the remaining MnO_2, which in some cases extended over 100Å out from the original surface. The new crystalline solid material is $Cr(OH)_3 \cdot nH_2O$, as confirmed by EDS and ED. At both pH values employed in this study a large proportion of MnO_2 remains in the system after reaction with Cr(III)--in agreement with previous studies (Fendorf and Zasoski, 1992; Amacher and Baker, 1982). The new crystalline material was always centered around the MnO_2, indicating the formation of a surface-facilitated precipitation reaction.

Steady-state solution data (Fendorf and Zasoski, 1992) indicates that as the saturation indices (SI = log IAP / K_{sp}, where IAP = ion activity product) of $Cr(OH)_{3\,(c)}$ increase, the amount of Cr(III) oxidized by birnessite approaches the amount required to

form a single Cr(III) monolayer of coverage as shown in Fig. 2-9. Figure 2-9 shows that as the SI of $Cr(OH)_{3\,(c)}$ was increased, the quantity of Cr(III) oxidized (or Cr(VI) produced) decreased and began to level off at approximately 3.7 μmoles. Using a hydrated radii of 3.4 Å for Cr(III), this would be the amount needed to form a single monolayer of coverage on the MnO_2 surface. This implies that a quantity of Cr(III) equal to a monolayer of surface coverage initially complexed with the MnO_2 surface, and then underwent subsequent oxidation. During the oxidation time for this first monolayer, Cr(III) species beyond the sorbed monolayer begin to nucleate as Cr-hydroxide. The nucleation process continues toward an equilibrium distribution which is dependent on the solution Cr(III) concentration and pH, Reaction (2.3).

$$Cr^{3+} + 3\,OH^- + nH_2O \leftrightarrow Cr(OH)_3 \bullet nH_2O \qquad (2.3)$$

The new $Cr(OH)_{3\,(c)}$ species is not redox reactive based on a positive ΔG_{rxn} occurring for Reaction (2.2) (Fendorf and Zasoski, 1992) under conditions employed in this study. Hence, $Cr(OH)_{3\,(c)}$ is thermodynamically redox stable and thus inhibits further Cr(III) oxidation in two ways: it acts as a non-redox reactive sink for the Cr(III), and it forms a physical barrier between remnant MnO_2 and solution Cr(III). The micrographs (Figs. 4 and 5) and EDS analysis show the precipitate to be surface associated, but the Cr(III) forming the precipitate can not be in an inner-sphere coordination with the MnO_2 surface as this would result in an electron transfer reaction.

It has been proposed that a possible means of inhibiting the oxidation of Cr(III) would be the production of surface Mn(II)--which would form an energetically unfavorable activated complex (Amacher and Baker, 1982). Manganese(III) would not inhibit the redox reaction as it is redox reactive with Cr(III) (Johnson and Xyla, 1991), and, as will be discussed, is a necessary intermediate in the oxidation of Mn(IV) which was uninhibited at low pH. Solution data indicated Cr(VI) : Mn(II) production in stoichiometric quantities; thus, it does not appear that Mn(II) is retained or readsorbed by the surface. Furthermore,

EELS shows no indication of Mn(II) present in the Mn-oxide after reaction with Cr(III). While a small amount of Mn(II) may be present in the MnO_2, it does not appear to be a significant factor in the oxidation reaction.

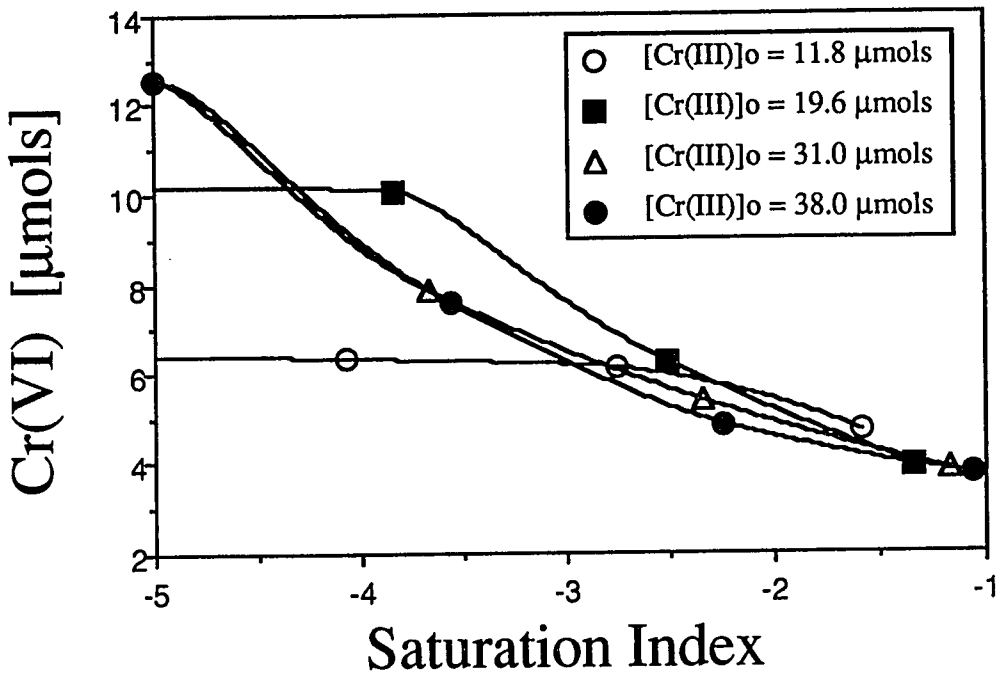

Figure 2-9. The extent of Cr(VI) produced (or Cr(III) oxidized) from the oxidation of Cr(III) by δ-MnO_2 is shown as a function of the $Cr(OH)_3$ (c) saturation index (SI = log IAP/K_{sp}) for various initial Cr(III) levels with 2.5 mg MnO_2 (data from Fendorf and Zasoski, 1992).

The idealized δ-MnO_2 structure has a permanent charge associated with its atomic arrangement, as 1 out of 6 Mn(IV) sites are vacant (Arrhenious, et al., 1979). It has been hypothesized that Cr(III) (Manceau and Charlet, 1992) and other transition metals (Arrhenious, et al., 1979) are sorbed only by these structural vacancies. While based on results using an advanced spectroscopic technique, this hypothesis does not account for the pH dependence, observed by numerous researchers, of metal sorption on δ-MnO_2. We

find no correlation between the oxidation reaction and the structural vacancies. Steady-state solution data (Fendorf and Zasoski, 1992) suggests a monolayer of Cr(III) coverage being oxidized prior to cessation of the reaction; at best, vacancy sites would account for only 1/6 of this amount. Furthermore, actual birnessite has amorphous material intermixed with the crystalline phase (as illustrated by Fig. 2-2) and would thus have even fewer cavity sites than an idealized crystalline structure. In addition, kinetic studies of Cr(III) oxidation by γ-MnOOH revealed that the oxidation reaction had a first-order dependence on Cr(III) concentration and γ-MnOOH surface area, with the reaction being second-order overall, prior to oxidation inhibition (Johnson and Xyla, 1991).

Therefore, our findings indicate that the inhibitory factor in Cr(III) oxidation by birnessite at pH values greater than 4 is due to the formation of a Cr(III)-hydroxide precipitate, Reaction (2.3). The degree of precipitation is dependent on the solution Cr(III) concentration and pH. The precipitate acts both as a sink and barrier for further redox reactions and would appear to form at least a hydrated Cr(III) ion away from the surface (we believe that the precipitation reaction occurs at distances greater than 2.8 Å away from the surface or Cr(III) would be oxidized prior to nucleation).

2.5.2 A Molecular Orbital Theory Approach

Frontier molecular orbital theory (FMOT) has recently provided an elegant explanation for the redox reactions on the pyrite surface (Luther, 1987,1990). In FMOT, for a reaction to be "symmetry allowed" the following criteria must be met: 1) the molecular orbitals must align for good overlap, 2) the lowest unoccupied molecular orbital (LUMO) of the oxidant should be lower than that of the highest occupied molecular orbital (HOMO) of the reductant or within 6 eV, and 3) the bond breaking/forming products must be in agreement with expected products (Luther, 1990).

The frontier molecular orbital theory (FMOT) applied to the Cr(III)-MnO_2 system gives insight into redox reaction pathways and factors controlling the formation of a $Cr(OH)_3$ surface precipitate. The rates of Cr(III) oxidation by δ-MnO_2 (Fendorf and Zasoski, 1992; Amacher and Baker, 1982) and γ-MnOOH (Johnson and Xyla, 1991) suggests an inner-sphere binding mechanism, in agreement with symmetry arguments of MOT. For the redox reaction of Cr(III) and Mn(IV)/Mn(III) (Reaction (2.1)), with both Cr and Mn roughly in octahedral coordination, electrons must be transferred from the t_{2g} states of Cr to the e_g states of Mn--a π to σ^* type process (Fig. 2-10). As illustrated by the simplified frontier orbital projections, Fig. 2-10a, the t_{2g} orbital states of Cr(III) (d_{xz}, d_{yz}, d_{xy}) are not in the same symmetry as the e_g orbital states of the Mn(IV) (d_{z2}, d_{x2-y2}), and thus it is not possible to obtain a significant orbital overlap necessary for an outer-sphere electron transfer mechanism. However, if Cr(III) binds as an inner-sphere complex, the O bridged between Cr(III) and Mn(IV)/Mn(III) will facilitate the electron transfer process (Fig. 2-10a). The filled p orbitals of O^{2-} facilitate the electron transfer by aligning with both the Cr(III) and the Mn(IV) orbitals, allowing for an electron transfer reaction. In the inner-sphere process, the O electrons are transferred to Mn and the Cr(III) electrons to O, with an accompanied O ligand exchange (the O ligand is transferred from Mn to the Cr). Therefore, Cr(III) would necessarily bind as an inner-sphere complex to allow electron transfer--in agreement with the observed reaction rates (Fendorf and Zasoski, 1992; Johnson and Xyla, 1991; Amacher and Baker, 1982).

The electron transfer reaction between Cr(III) and Mn(IV) is disproportionate, 2 Mn(IV) ions must be reduced (one gaining two electrons and another gaining one) for each Cr(VI) produced. Chromium(III) bound to two O (bidentate) atoms, each bridged by two Mn(IV), would undergo a two electron transfer with one Mn (forming Mn(II)) while also undergoing a single electron transfer with a second Mn (forming Mn(III)) (Fig. 2-10b). This binding mechanism is in agreement with EXAFS data which indicate a bidentate inner-sphere complexation of Cr(III) on birnessite (Manceau and Charlet, 1992) and on HFO

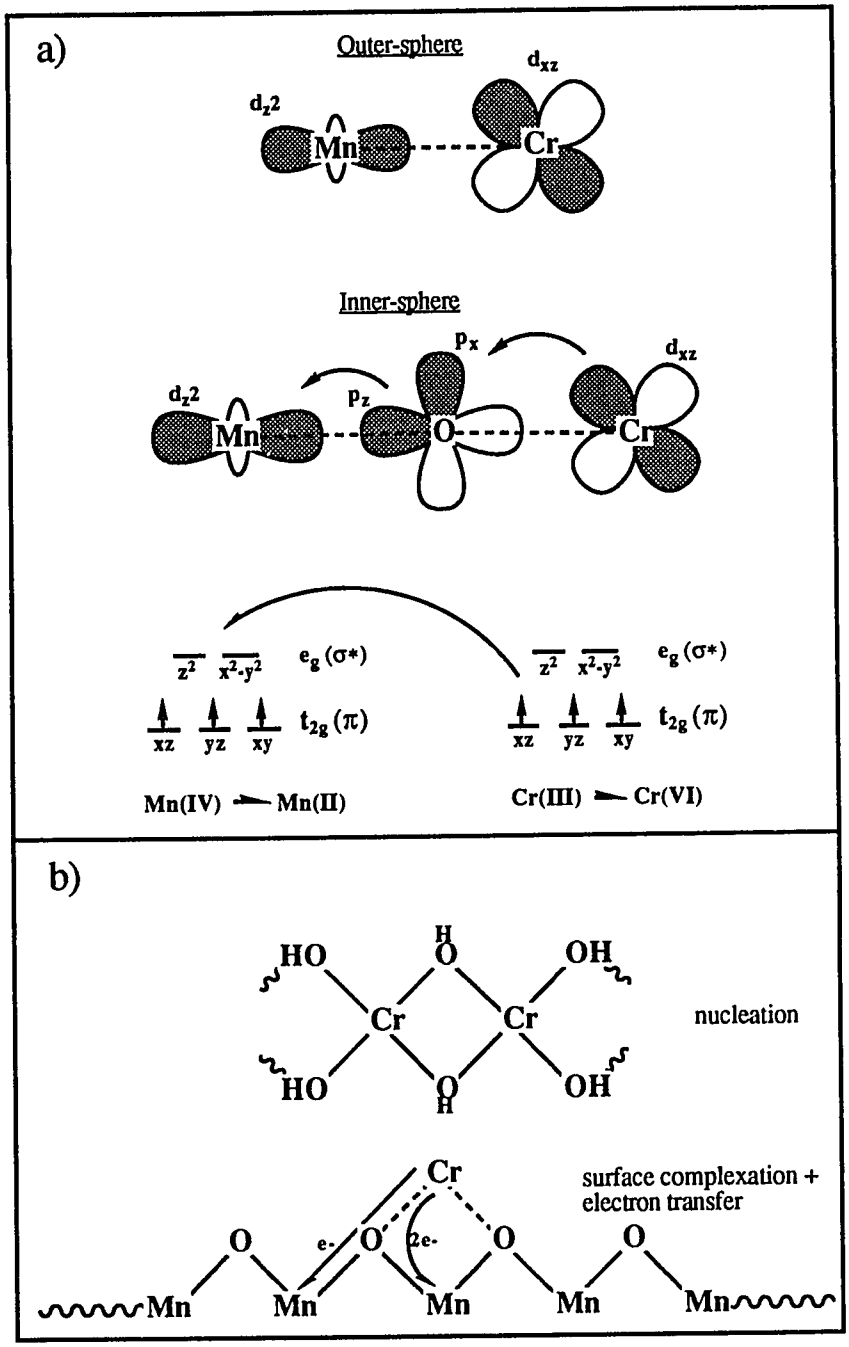

Figure 2-10. Schematic illustration of (a) the MOT diagram for the electron transfer between Cr(III) and Mn(IV)/Mn(III); the simplified orbital depictions show the orbital symmetry is not conducive for an outer-sphere process, but when incorporating an O atom the inner-sphere process is viable. In (b) the Cr(III) surface complex with the electron pathways is shown accompanied by the envisioned nucleation of the Cr-hydroxide which inhibits and ultimately terminates the redox reaction.

(Charlet and Manceau, 1992). The electron transfer would then occur by an inner-sphere π to σ^* type process. As a result, Mn(III) must be present at least as an intermediate prior to reaction with a second Cr(III) species. Both the formation of Mn(II) or Mn(III) would occur by the same FMOT electron transfer path as described above--the only difference being the number of electrons transferred. At steady-state, Mn(III)/Mn(II) may remain on the surface; however, solution data (Fendorf and Zasoski, 1992) indicate that Mn(II) is released to solution in stoichiometric proportion relative to Cr(VI). Therefore, Mn(IV) should predominate in the Mn-oxide after reaction with Cr(III)--in agreement with EELS analysis.

Based on FMOT, Cr(III) would bind in an inner-sphere bidentate coordination with MnO_2 to allow for electron transfer. This is in agreement with observed rapid reaction rates (Fendorf and Zasoski, 1992; Amacher and Baker, 1982) and EXAFS analysis (Manceau and Charlet, 1992). Furthermore, FMOT also agrees with the increase in Cr(III) oxidation rates, prior to cessation, at higher pH values (Fendorf and Zasoski, 1992; Amacher and Baker, 1982). Increased pH values would increase the negative surface charge of the oxide and the hydrolysis products of Cr(III), both of which enhance the complexation of Cr(III) with MnO_2--and thus Cr(III) oxidation. In addition, OH^- ligands of the Cr(III) hydrolysis products would donate electron density to the Cr(III) and increase its reducing power (Luther, 1990), thus increasing the electron transfer rate. Subsequent to electron transfer, Cr(VI) would be desorbed as it predominantly forms anionic species which would be electrostatically repelled from the surface. At pH values greater than 4, Cr(III) oxidation, Reactions (2.1) and precipitation occur simultaneously in the interfacial region. However, after the $Cr(OH)_3$ precipitate has occurred subsequent to a surface monolayer of Cr(III) oxidation, further Cr(III) oxidation is inhibited.

Therefore, the overall reaction for Cr(III) oxidation by δ-MnO_2 at pH > 4 can be summarized as two simultaneous reactions. First Reaction (2.1) occurs in a three step

process: i) a bidentate inner-sphere complexation of Cr(III) with δ-MnO_2, ii) electron transfer, and accompanied O ligand exchange, between Cr(III) and Mn(IV)/Mn(III) forming Cr(VI) and Mn(III)/Mn(II), and iii) desorption of Cr(VI) and Mn(II). Step (ii) is a 3 electron transfer process in which for each Cr(III) oxidized either 2 Mn(IV) are reduced to 1 Mn(III) and 1 Mn(II), or 1 Mn(IV) and 1 Mn(III) are reduced to 2 Mn(II). Simultaneous with Reaction (2.1), Reaction (2.3) proceeds forming $Cr(OH)_3 \cdot nH_2O$ (c) at distances greater than 2.8 Å away from the surface, and consequently subsequent oxidation is inhibited.

2.5.3 Implications of the Surface Precipitation Mechanism

Hydrolyzable metal ion sorption on oxide surfaces may result in surface precipitation reactions. However, the chemical/physical phenomena controlling this process have not been clearly determined. James and Healy (1972) developed a thermodynamic expression which incorporated the electrostatic effects of the interfacial region to describe surface precipitation.

The incorporation of an electrostatic term into the free energies of formation greatly reduced solubility constants; thus, electrostatic influences from the charged surfaces are used to model the decrease in metal-hydroxide solubility constants and the sorption of hydrolyzable metal ions. Under a strong electric field, that would result with a metal-oxide such as δ-MnO_2, solvation energies are greatly reduced, primarily due to a dramatic decrease in the dielectric constant near the surface. The dielectric constant (relative permittivity) may drop to a value as low as 6 in the interfacial region compared to values of 78.5 in the bulk solution (James and Healy, 1972; Murray and Dillard, 1979; Bockris and Reddy, 1970).

It has also been proposed that surface nucleation is facilitated through a decrease in solvation energy when a metal ion complexes with a surface (Stone, 1991). The surface would thus act as an energy barrier reductant--facilitating nucleation of sorbed species. In addition, an accumulation of counter-ions near the surface would increase the number of metal ions present (assuming a negatively charged surface and a cationic metal), and the surface could act as a sink for hydroxyl ions. While a single factor may influence the onset of surface precipitation, it is likely that various factors control this process. The Cr(III)-MnO_2 system imposes some unique boundaries on the surface precipitation mechanism, due to the oxidation of Cr(III) species which enter a direct inner-sphere coordination with the surface.

The $Cr(OH)_3$ precipitate forms in the interfacial region but does not directly incorporate inner-sphere Cr(III) surface complexed on MnO_2, as such species would undergo a redox reaction with Mn as previously described. Therefore, the forces governing these processes must not be associated with the chemical binding of a species to the surface. Rather, it appears that the influences of the surface in the interfacial region facilitate the formation of a Cr-hydroxide precipitate without direct inner-sphere surface complexation. The proposed incorporation of interfacial electrostatics in the free energy terms (James and Healy, 1972) dramatically lowers the solubility of a metal hydroxide species without introducing a complexation factor. This thermodynamic development was used by Dillard and Murray (1979) to explain the precipitation of $Co(OH)_2$ on the mineral birnessite. Based on the surface charge of δ-MnO_2, Dillard and Murray (1979) calculated that the solubility constant was lowered by at least 10^2. The thermodynamic incorporation of surface induced electrostatics is entirely in agreement with our findings on the Cr-MnO_2 system.

Although the solutions of this study were undersaturated with respect to $Cr(OH)_{3(c)}$, and precipitation was not observed in solution, a surface precipitate of $Cr(OH)_3$

occurred on δ-MnO_2. The high surface charge of the δ-MnO_2 would greatly reduce the $Cr(OH)_3$ solubility, thus catalyzing the nucleation of this phase. This study indicates that for Cr(III) the electrostatic influences of the MnO_2 surface induce a catalyzes of Cr-hydroxide precipitation; the precipitation reaction does not appear to be influenced by direct inner-sphere complexation with the MnO_2 surface.

2.6 Summary/Conclusions

Chromium(III) oxidation by birnessite is inhibited at higher solution Cr(III) concentration and pH values. The HRTEM studies reveal the formation of a new crystalline $Cr(OH)_3$ phase which is deposited at the surface of the MnO_2--often extending extensively into the surrounding media. The inhibitory factor is due to the formation of a $Cr(OH)_3$ surface precipitate which acts as both a sink for Cr(III) and as an electron transfer barrier. The MnO_2 surface does not appear to undergo a significant valence change--a possible source of inhibition. Frontier molecular orbital theory predicts the redox reaction to occur via a bidentate inner-sphere electron transfer reaction. Chromium(III) oxidation rates are in agreement with this postulate; outer-sphere complexation would result in a much slower oxidation rate than observed.

Chromium(III) oxidation decreased with increased pH to a quantity necessary to form a monolayer of surface coverage on the MnO_2. During the time for the electron transfer reaction of the first monolayer {sorption of Cr(III), electron transfer, and desorption of Cr(VI)}, $Cr(OH)_3 \cdot nH_2O_{(c)}$ nucleates in the interfacial region and inhibits further Cr(III) oxidation. The precipitation reaction does not appear to directly involve Cr(III) in an inner-sphere coordination with MnO_2. However, the electrostatic influence of the surface in the interfacial region decreases the solubility of the metal-hydroxide. This facilitates nucleation and enhances the rate of precipitation. Once formed, the oxidation of

Cr(III) is dependent on the dissolution of the $Cr(OH)_3$ species and would most likely occur in slight amounts for prolonged periods.

The Cr-MnO_2 system has provided an interesting system for study and has given significant insights on the phenomena governing surface precipitation of hydrolyzable metal ions. For disposal in the environment, higher levels of Cr(III) at elevated pH values would be preferable since they would inhibit oxidation and enhance the formation of a surface precipitate. Following the formation of the $Cr(OH)_3$ precipitate, the release of Cr(III) would be dependent upon the dissolution rate of the hydroxide species.

2.7 References

Allison, J.D., D.S. Brown, and K.J. Novo-Gradac. 1990 MINTEQA2/PRODEFA2, A Geochemical Assessment Model for Environmental Systems: Version 3.0. U.S. Environmental Protection Agency: Athens, GA.

Amacher, M.C., and D.E. Baker. 1982. Redox reactions involving chromium, plutonium, and manganese in soils. DE-AS08-77DPO4515. Inst. for Res. on Land and Water Res., Penn State Univ, PA.

Arrhenius, G., K. Cheung, S. Crane, M. Fisk, J. Frazer, J. Korkisch, T. Mellin, S. Nakao, A. Tsai, and G. Wolf. 1979. Counterions in marine manganates. *Colloques Internationaux du C.N.R.S.* **298**: 333-356.

Bleam, W.F., and M.B. McBride. 1986. The chemistry of adsorbed Cu(II) and Mn(II) in aqueous titanium dioxide suspensions. *J. Colloid Interface Sci.* **110**: 335-346.

Bockris, J.O., and A.K.N. Reddy. 1970. Modern Electrochemistry. Plenum, NY.

Bowden, J.W., M.C.A. Bolland, A.M. Posner, and J.P. Quirk. 1973. Generalized model for anion and cation adsorption at oxide surfaces. *Nature* **245**:81-83.

Charlet, L. and A.A. Mancaeu. 1992. X-ray absorption spectroscopic study of the sorption of Cr(III) at the oxide-water interface: I. Molecular mechanism of Cr(III) oxidation on Mn oxides. *J. Colloid Interface Sci.* **148**: 425-442.

Crowther, D.L., J.G. Dillard, and J.W. Murray. 1983. The mechanism of Co(II) oxidation on synthetic birnessite. *Geochim. Cosmochim. Acta.* **47**:1399-1403.

Davis, J.A., R.O. James, and J.O. Leckie. 1978. Surface ionization and complexation at the oxide/water interface. I.Computation of electrical double layer properties in simple electrolytes. *J. Colloid Interface Sci.* **63**:480-499.

Dzombak, D.A., and F.M.M. Morel. 1990. Sruface complexation modeling-hydrous ferric oxide. Wiley and Sons, NY.

Eary, L.E., and D. Rai. 1987. Kinetics of chromium(III) oxidation to chromium (VI) by reaction with manganese dioxide. *Environ. Sci. Technol.* **21**:547-552.

Farley, K.J., Dzombak, D.A., and F.M.M. Morel. 1985. A surface precipitation model for the sorption of cations on metal oxides. *J. Colloid Interface Sci.* **106**:226-242.

Fendorf, S.E. 1990. Metal ion influences on chromium oxidation by manganese dioxide. M.S. Thesis, University of California, Davis.

Fendorf, S.E., and R.J. Zasoski. 1992. Chromium(III) oxidation by δ-MnO_2. I: Characterization. *Environ. Sci. Technol.* **26**: 79-85.

Hayes, K.F., and J.O. Leckie. 1986. Mechanisms of lead ion adsorption at the goethite/water interface. pp.141-158. *In* J.A. Davis and K.F. Hayes (ed.) Geochemical processes at mineral surfaces. ACS Symp. 323. Meet. Am. Chem. Soc., Washington, DC.

Healy, T.W., A.P. Herring, and D.W. Furstenau. 1966. The effect of crystal structure on the surface properties of a series of manganese dioxides. *J. Colloid Interface Sci.* **21**:435-444.

James, R.O., and T.W. Healy. 1972. Adsorption of hydrolyzable metal ions at the oxide-water interface: II. Charge reversal of SiO_2 and TiO_2 colloids by adsorbed Co(II), La(III), and Th(IV) as model systems. *J. Colloid Interface Sci.* **40**:53-65.

Johnson, C.A., and Xyla, A.G. 1991. The oxidation of chromium(III) to chromium(VI) on the surface of manganate (γ-MnOOH). *Geochim Cosmochim Acta.* **55**:2861-2866.

Krishnan, K.M. 1989. Electron energy-loss spectroscopy. *In* L.M. Coyne, S.McKeever, and D. F. Blake (eds.) Spectroscopic characterization of minerals and their surfaces. pp.54-74. ACS symposium series 415. American Chemical Society, Washington DC.

Luther, G.W., III. 1990. The frontier-molecular-orbital theory approach in geochemical processes. pp.193-198. *In* W. Stumm (ed.) Aquatic chemical kinetics. Wiley and Sons, NY.

Luther, G.W., III. 1987. Pyrite oxidation and reduction: Molecular orbital theory considerations. *Geochim. Cosmochim. Acta.* **51**:3193-3199.

Manceau, A.A., and L. Charlet. 1992. X-ray absorption spectroscopic study of the sorption of Cr(III) at the oxide-water interface: II. Adsorption, coprecipitation, and surface precipitation on hydrous ferric oxide. *J. Colloid Interface Sci.* **148**: 443-458.

Murray, J.W., and J.G. Dillard, 1979. The oxidation of cobalt(II) adsorbed on manganese dioxide. *Geochim. Cosmochim. Acta.* **43**:781-787.

Rai, D., B.M. Sass, and D.A. Moore. 1987. Chromium(III) hydrolysis constants and solubility of chromium(III) hydroxide. *Inorg. Chem.* **26**:345-349.

Stone, A.T. 1991. Oxidation and hydrolysis of ionizable organic pollutants at hydrous metal oxide surfaces. pp. 231-254. *In* D.L. Sparks and D.L. Suarez (eds.) Rates of soil chemical processes, Soil Sci. Soc. Am. Special Publication. Soil Sci. Soc. Am., Madison, WI.

Stumm, W., H. Hohl, and F. Dalang. 1976. Interaction of metal ions with hydrous oxide surfaces. *Croat. Chim. Acta.* **48**:491-504.

Taube, H. 1970. Electron Transfer Reactions of Complex Ions in Solution. Academic Press, New York.

Tewari, P.H., and W. Lee. 1975. Adsorption of Co(II) at the oxide-water interface. *J. Colloid Interface Sci.* **52**:77-88.

Yates, D.E., Levine, S., and T.W. Healy. 1974. Site-binding model of the electric double layer at the oxide/water interface. *J.C.S. Faraday* I. **70**:1807-1820.

CHAPTER 3

AN ELECTRON PARAMAGNETIC RESONANCE SPECTROSCOPICALLY MONITORED STOPPED-FLOW (EPR-SF) KINETIC STUDY of Mn(II) SORPTION/DESORPTION on δ-MnO_2

3.1 Abstract

Many important reactions involving colloidal suspensions are rapid. Here, we introduce the application of a technique capable of directly measuring rapid colloidal reactions (within 20 ms after the reaction initiation) *in situ*: an electron paramagnetic resonance spectroscopically monitored stopped-flow method (EPR-SF). The utility of this technique is demonstrated by investigating the sorption of Mn(II) on δ-MnO_2. The sorption reaction was complete in less than 1 s, with greater than 80% of the Mn(II) being sorbed within 200 ms. A first-order rate dependence on Mn(II) was observed. Measurement of the initial reaction rate allowed the forward (sorption) rate constant to be determined ($k_f' = 3.74 \times 10^{-3}$ s^{-1}), and the reverse (desorption) rate constant was determined using an integrated reversible first-order rate expression ($k_r' = 3.08 \times 10^{-4}$ s^{-1}). Using these rate constants, the predicted time dependence of Mn(II) sorption was in good agreement with the measured sorption rate. The results indicate that chemical kinetics are being measured which allows for determination of precise reaction rates and confirmation of postulated reaction mechanisms.

3.2 Introduction

Determining reaction rates and mechanisms is essential for understanding chemical processes (Sparks, 1989). Advances in methodologies have allowed investigation of many rapid reactions in gas, solution, and solid phases. Few methods exist, however, for measurement of rapid reactions in colloidal suspensions. Many techniques that are currently used to study colloidal suspensions measure both physical (i.e., transport or diffusion) and chemical phenomena simultaneously, which greatly complicates the measurement of elementary reactions or chemical rate-controlling processes. Moreover, apparent rate laws and parameters are measured. Measuring chemical kinetics allows one to ascertain reaction rates and mechanisms, knowledge of which is necessary to understand, predict, and control reaction pathways. Reactions of colloidal suspensions are of interest to scientists in an array of fields: catalysis, electrochemistry, and environmental and soil chemistry. Therefore, it is important to develop methods which are capable of measuring chemical kinetics in such systems. In this study, we demonstrate the application of an electron paramagnetic resonance spectroscopically monitored stopped-flow (EPR-SF) kinetic technique which, for an EPR-active metal species, enables the rapid and direct *in situ* detection of reactions in a colloidal suspension.

To obtain chemical kinetic information, a technique must be able to monitor a reaction over the time frame in which it occurs while minimizing the effects of diffusion on the reaction rate. However, many soil chemical processes are rapid, precluding the use of traditional batch or flow techniques (Sparks, 1989). Filtration of suspensions prior to analysis has been extensively used to monitor the solution components of suspensions, but the time for filtration itself often limits the study of rapid reactions. Chemical relaxation techniques have been used to investigate suspension reactions by monitoring a system parameter related to a species concentration (e.g., electrical conductivity) which is not adversely affected by the presence of colloidal material (Ikeda et al., 1983; Ikeda et al.,

1984; Hayes and Leckie, 1986; Zhang and Sparks, 1990). However, with many of these techniques the reaction must be fully reversible, reactant species are not directly measured, and rate constants are determined from linearized rate equations that often are dependent on equilibrium parameters. Since the stopped-flow mixing can be carried out in less than 20 ms (and EPR signal digitized within a few μs), the EPR-SF technique eliminates the conventional limitations of measuring colloidal reactions, allowing for rapid direct measurement of a reactant species *in situ*..

Stopped-flow kinetic methods have found limited use in colloidal chemistry (Ikeda et al., 1984). However, they have been employed to study biochemical reactions, and EPR spectroscopically measured stopped-flow kinetics has been applied to the study of biological solution chemistry (Klimes et al., 1980; Stach et al., 1985). Klimes et al. (1980) found the time-limiting factor in EPR-SF was the mixing rate of the stopped-flow cell. The time resolution of stopped-flow mixing is generally less than 20 ms with mixing efficiency of 90% or greater (Klimes et al., 1980; Ikeda et al., 1984), and has been reduced to 1 ms for an electromagnetic driven accelerated-flow system (Stach et al., 1985). Therefore, EPR-SF is capable of monitoring reactions with a half-life greater than 20 ms.

The EPR-SF technique offers many advantages for studying sorption reactions which have an EPR detectable constituent of interest. Many organic molecules (especially free radicals), in addition to Mn(II) and Cu(II), are EPR active and of interest to soil and environmental scientists; a host of other constituents are EPR active and of possible interest in other chemical fields. For an EPR active (paramagnetic) species, the unpaired electron spin moment interacts with a magnetic field which gives rise to different energy states; this in turn allows energy in the microwave frequency to be absorbed by the species which can then be measured (Drago, 1977). A species which is EPR active in solution often may not be EPR active when it is in a sorbed state due to rapid spin relaxation pathways, or the spectra may be broadened to the point where they contribute insignificantly to the signal

intensity (McBride, 1982; Bleam and McBride, 1986). Consequently, the sorption of an EPR active species can be monitored by the reduction in signal intensity, which allows one to determine sorption kinetics. In addition, desorption kinetics can also be measured by monitoring the signal intensity after a sudden decrease in the sorptive concentration of the suspension (i.e., after the solution concentration undergoes a perturbation and is decreased the system re-adjusts to the new equilibrium by desorbing surface bound species, which can thus be measured as a function of time). Electron paramagnetic resonance spectroscopy has been extensively used to investigate sorption and oxidation reactions on soil constituents (Clementz et al., 1973; McBride, 1982; Bleam and McBride, 1986; McBride, 1987; McBride, 1989). However, EPR spectroscopy has not been applied to kinetic investigations of colloidal materials.

The binding of solution species to solid surfaces present in soil and water systems is a primary determinant in the behavior of many substances. Such processes can tie up plant nutrients, remove hazardous contaminants, and modify mineral surfaces. Manganese(II) is a model EPR active species; hence, for reactions in which this ion is involved, EPR-SF kinetics is ideal. The intent of this study was to develop a stopped-flow kinetic technique monitored by EPR spectroscopy which could directly measure rapid reaction rates. Here, we use Mn(II) sorption on δ-MnO_2 to demonstrate the utility of this technique for the study of colloidal reactions, but this technique is suitable for any EPR active species. In addition to monitoring sorption/desorption reactions, this technique is also capable of measuring redox reactions involving Mn-oxides, as Mn(II) is liberated during such processes.

3.3 Materials and Methods

A schematic diagram of the instrumental set-up is shown in Fig. 3-1. Dual 2 mL in-port syringes feed an EPR-SF mixing cell (Hi-Tech Scientific Limited, Salisbury, England). The mixing cell (Wilmad, model wg-385-b, a variable temperature aqueous mixing cell) is located in the EPR spectrometer, allowing EPR detection of the cell contents. A single outflow-port is fitted with a 2 mL effluent collection syringe equipped with a triggering switch. The triggering switch activates the data acquisition system (Microstar Electronics, Redmind, Washington, model DAP 2400 data acquisition processor board mounted in an IBM-AT). Each run consists of filling the in-port syringes with the desired reactants, flushing the system with the reactants several times, and finally initiating and monitoring the reaction. Consecutive runs can be conducted with the same reactants simply by repeating this procedure.

To obtain quantitative information on Mn(II), the EPR cell was filled with a known concentration of Mn(II) (in the absence of colloidal material). The magnetic field was then swept, resulting in the Mn(II) hyperfine sextet structure (inset in Fig. 3-2). The magnetic field was centered at the down field peak for quantitative measurement of the Mn(II) present in solution. Known solution concentrations of Mn(II) were used to relate the EPR signal with the Mn(II) concentration. Figure 3-2 shows the linear relationship between the EPR signal and Mn(II) concentration within the range of 5 to 500 μM Mn(II) (in this paper brackets will be used to denote concentration units).

For the sorption reaction we used 50 or 80 μM Mn(II) in reactant syringe I, and 1 g/L MnO_2 (synthetic birnessite) in reactant syringe II. The Mn(II) solutions were made from their nitrate salts with $N_{2\,(g)}$ saturated deionized water. The properties of the oxide are given elsewhere (Fendorf and Zasoski, 1992). Equal volumes from each syringe are injected into the mixing cell yielding initial reactant concentrations of 25 and 40 μM Mn(II) and 0.5 g/L MnO_2. At least 4 runs were signal averaged to yield the final data presented in

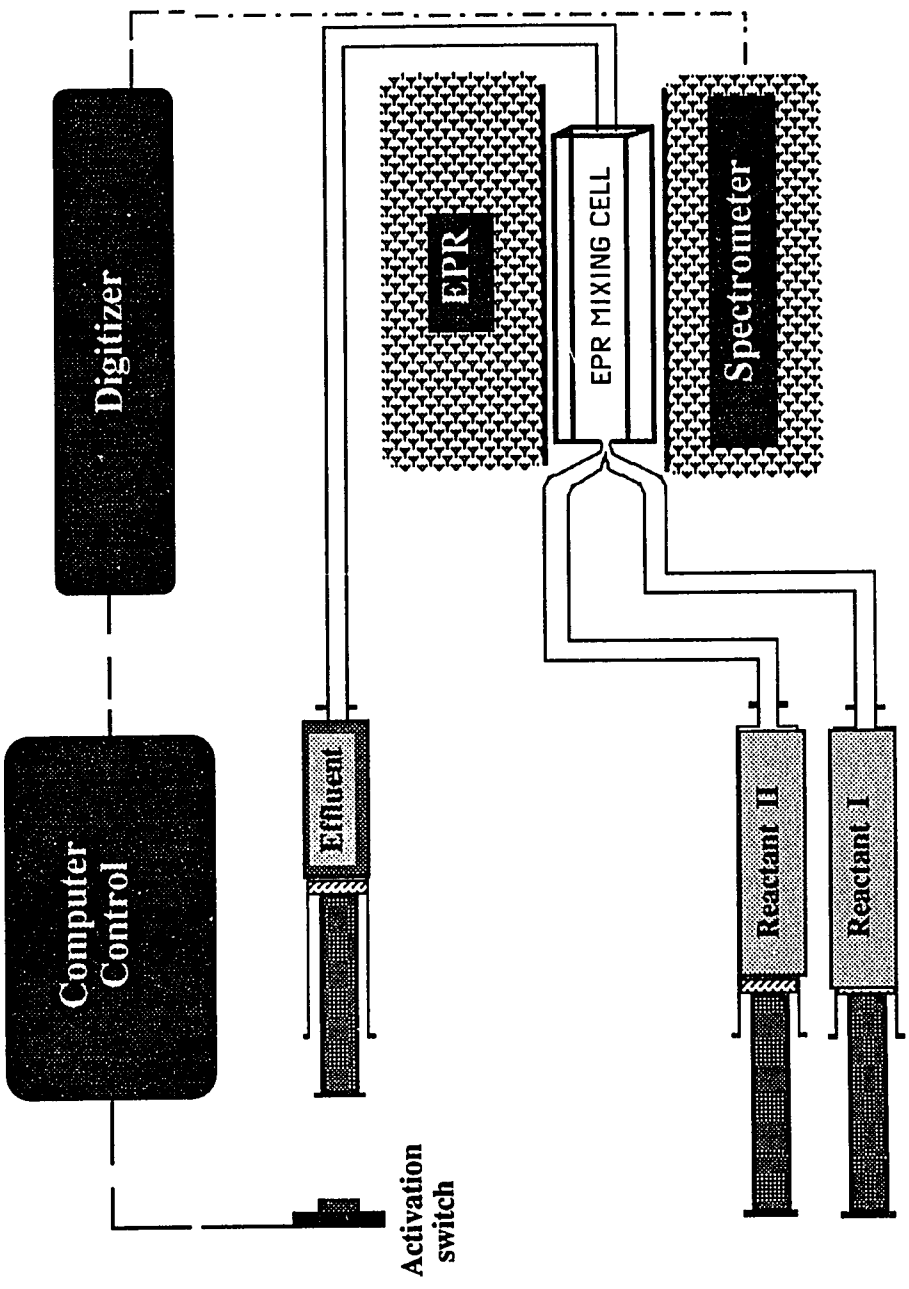

Figure 3-1. Schematic illustration of the electron paramagnetic resonance spectroscopically monitored stopped-flow (EPR-SF) apparatus.

this research. The reactions were carried out at pH 5.0 in 0.001*M* $NaNO_3$, and pH was maintained constant with a 0.001*M* acetate buffer (experimental runs were conducted with and without the acetate buffer and did not differ appreciably). The particle size of the oxide was < 2 μm and a stable suspension was formed at this ionic strength for times well exceeding the experimental run time.

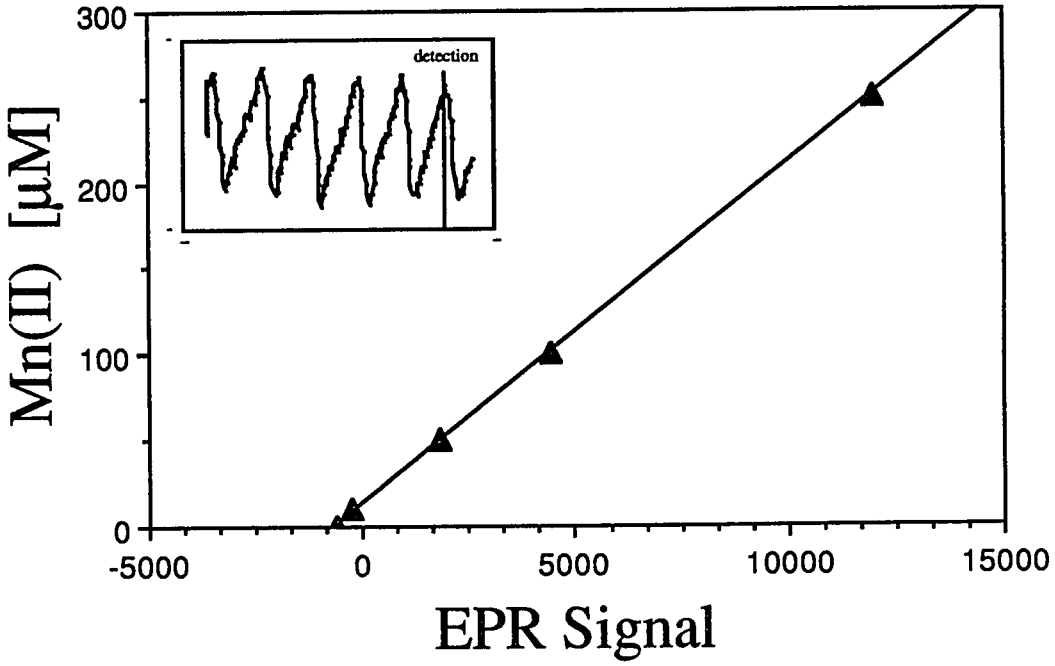

Figure 3-2. The standard curve relating signal intensity of the down field hyperfine peak to solution Mn(II) concentration. An excellent linear relation was consistently obtained between signal intensity and [Mn(II)]--the correlation coefficient was never less than one, to three significant digits. Inset, the sextet hyperfine structure of Mn(II) aqueous.

3.4 Results and Discussion

Chemical kinetics gives mechanistic information about a reaction by allowing one to hypothesize a reaction mechanism that can be tested with experimental data. At pH 5, the following complexation reaction of Mn(II) on δ-MnO_2 is suggested for low Mn(II) surface loading (the basis for this hypothesis is discussed below):

$$Mn^{2+} + \text{S-} \underset{k_r}{\overset{k_f}{\rightleftharpoons}} \text{S-Mn} + H^+ \qquad (3.1)$$

Where Mn^{2+} is the solution concentration of Mn(II) ([Mn^{2+}]), S- is the surface site, S-Mn is the complexed (sorbed) Mn(II), k_f is the forward (sorption) rate constant, and k_r is the reverse (desorption) rate constant. Recently, Hiemstra et al. (1989a,b) have used surface structural crystallographic consideration to determine proton affinities of oxides. Three primary surface site 'types' were evaluated of which the O(H) surface group is either: singly, doubly, or triply coordinated by the central cation of the oxide. The proton affinities of these sites are dramatically different due to their differing coordination environments. For MnO_2, in which Mn (the central cation) is coordinated by six O, two surface types are reactive under normal pH ranges: singly coordinated O(H) and doubly coordinated O(H) groups. At pH 5, based on the ZPC of this oxide (ZPC = 2.8; Fendorf and Zasoski, 1992) and known proton affinities (Balistrieri and Murray, 1982; Hiemstra et al., 1989b), the singly coordinated groups are protonated and the doubly coordinated groups are deprotonated (oxo), as depicted in the following protonation reactions:

$$Mn\text{-}OH_2^{+2/3} \leftrightarrow Mn\text{-}OH^{-1/3} + H^+ \qquad pK \approx 3.3 \qquad (3.2)$$

$$Mn_2\text{-}OH^{+1/3} \leftrightarrow Mn_2\text{-}O^{-2/3} + H^+ \qquad pK \approx 2.3 \qquad (3.3)$$

(i.e., at pH 5, the surface species on the product side of Eqs. (3.2) and (3.3) would predominate, Mn-$OH^{-1/3}$ and Mn_2-$O^{-2/3}$). On the dominant (010) surface plane of δ-MnO_2,

these two 'types' of sites are adjacent to one another (Arrhenius et al., 1979; Potter and Rossman, 1979). Therefore, at pH 5, bidentate complexation of Mn(II) (Balistrieri and Murray, 1982; Morgan and Stumm, 1964) would displace one proton--in agreement with empirical observations (Morgan and Stumm, 1964). Figure 3-3 illustrates the surface structure of the (010) plane and the hypothesized Mn(II) complexation reactions. At higher pH values (pH > 6.4), greater than one proton is released for each Mn(II) sorbed. The increased proton release can be explained by a polymerization of Mn(II)-hydroxide, which may form surface clusters similar to those observed on TiO_2 (Bleam and McBride, 1986). However, under the reaction conditions employed in this study, cluster formation would not be expected. Charge balance in this system would be maintained by the background electrolyte (Na^+ and NO_3^-), which were maintained in large excess to simplify reaction conditions. Hence, in our representation **S-** would represent these two functional groups as a single site and charge balance would be maintained by the unrepresented background electrolyte.

In the overall sorption reaction, one proton is thus released for each Mn(II) sorbed at pH 5 after steady state conditions have been reached (Morgan and Stumm, 1964). The forward (sorption) reaction would thus not be influenced by H^+, provided the surface functional groups are not altered. By maintaining a constant pH, the H^+ term in the reverse (desorption) rate expression can be incorporated into the reaction coefficient. This was the case in our experiments. In addition, the release of surface H^+ is often considered to be a slow structural rearrangement of the solid phase (Dzombak and Morel, 1990), and thus would not enter into the rapid sorption mechanism investigated in this research. Furthermore, the reaction rate was not influenced by further increases in solution pH to pH 6. Thus, the forward reaction should be dependent on $[Mn^{2+}]$ and [S-]; being first order in $[Mn^{2+}]$ and [S-], and second order overall if it is an elementary reaction. The reverse reaction would be dependent on the amount of Mn(II) complexed, [S-Mn], and $[H^+]$.

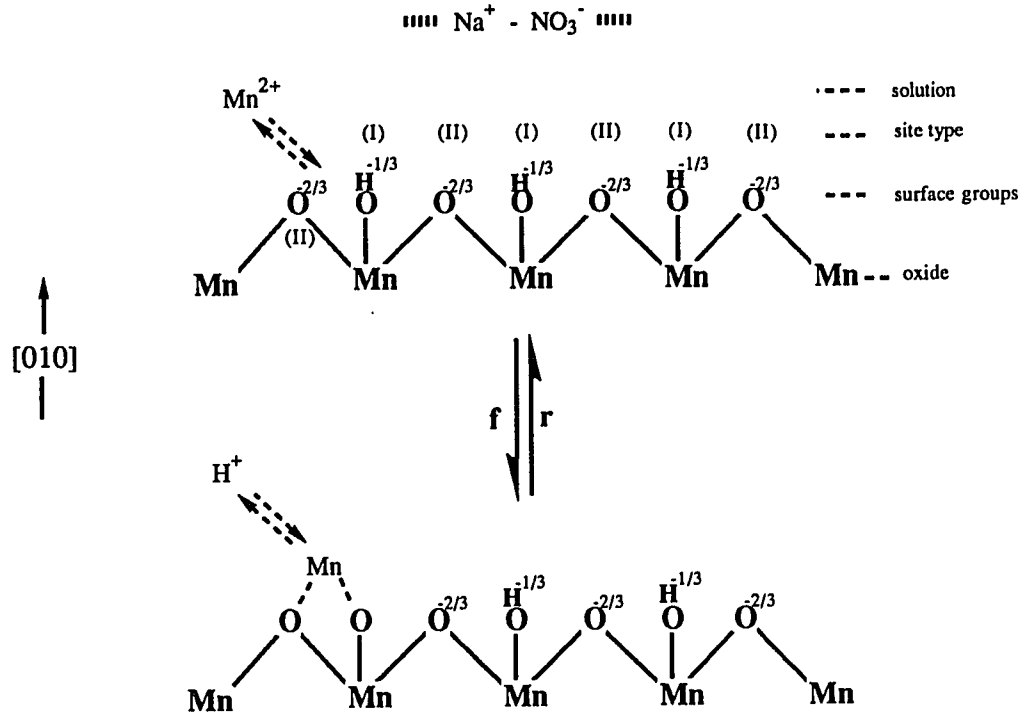

Figure 3-3. A depiction of the (010) surface plane of δ-MnO_2 with the surface functional groups represented at pH 5. Singly (site type I) and doubly (site type II) coordinated O(H) groups are shown, which are adjacent to each other, along with the bidentate complexation of Mn(II).

Reaction (3.1) is of the type, A + B <==> C + D, and leads to the following second-order reversible rate expression,

$$d[Mn^{2+}]/dt = -k_f[Mn^{2+}][\mathbf{S}\text{-}] + k_r[\mathbf{S}\text{-}Mn][H^+] \qquad (3.4)$$

where t is time. However, by ensuring a large excess of sorbent over sorptive ([S-] >> $[Mn^{2+}]$), and maintaining a constant pH, the overall reaction should be pseudo first-order depending only on $[Mn^{2+}]$. Thus, under the reaction parameters employed in this study, the rate expression would be simplified to a pseudo first-order reaction.

$$d[Mn^{2+}]/dt = -k_f'[Mn^{2+}] + k_r'[\mathbf{S}\text{-}Mn] \qquad (3.5)$$

where $k_f' = k_f [S\text{-}]$ and $k_r' = k_r [H^+]$. Integration of the above simplified reversible first-order rate expression, Eq.(3.5), leads to Eq. (3.6).

$$\ln\{[1 + (k_r' / k_f')] ([Mn^{2+}] / [Mn^{2+}]_o) - (k_r' / k_f')\} = - (k_f' + k_r') t \qquad (3.6)$$

Unfortunately, k_f' and k_r' cannot be independently determined solely from rate information on the sorption of Mn(II) (one equation, two unknowns) without a further simplifying assumption. If one assumes that at the onset of the reaction the initial reaction rate will be dominated by the forward reaction, and the initial reaction rate can be accurately measured, then the forward rate constant can be ascertained using a first-order non-reversible analysis (in which k_f' can be determined from the time dependent Mn(II) sorption data). The reverse reaction rate constant, k_r', can then be calculated using k_f' and the integrated expression for a reversible first-order reaction (Eq. (3.6)).

The following discussion uses this approach to determine the forward and reverse rate constants for Mn(II) sorption on δ-MnO_2. With a knowledge of k_f' and k_r', a rearrangement of Eq. (3.6) allows one to calculate the Mn(II) sorption as a function of time. Thus, once the rate constants are determined, the validity of the above approach can be verified by predicting the time dependence of Mn(II) sorption and comparing the predicted trends with those that are measured.

Because the forward rate is much greater at the onset of the reaction, measuring initial reaction rates should allow one to measure only the forward (sorption) rate constant, k_f. For the system parameters defined previously and a site density of 6 sites/nm^2 (Morgan and Stumm, 1964), the number of sorption sites would be at least two orders of magnitude greater (>100x) than the number of Mn(II) ions present, even at the highest Mn(II) concentration.

The following reaction is hypothesized to represent the contributing species of Reaction (3.1) for the sorption of Mn(II) by MnO_2 (i.e., for the initial reaction rate and conditions employed in this study):

$$Mn^{2+} \text{ ---> } \mathbf{S}\text{-}Mn \tag{3.7}$$

Reaction (3.7) is valid far from equilibrium where $R_{sorption} >> R_{desorption}$ (where R is the reaction rate, $-d\,[Mn^{2+}] / d\,t$); thus, $k_f[Mn^{2+}] - k_r[Mn\text{-}\mathbf{S}] \approx k_f[Mn^{2+}]$. The rate dependence can be described as:

$$R = -d\,[Mn^{2+}] / d\,t = k_f'\,[Mn^{2+}] \tag{3.8}$$

The first-order dependence of $[Mn^{2+}]$ can be evaluated using the integrated form of Eq. (3.8) (Sparks, 1989):

$$\log [Mn^{2+}]_t = \log [Mn^{2+}]_o - \frac{k\,t}{2.303} \tag{3.9}$$

Under pseudo-first order conditions for $[Mn^{2+}]$, the time dependence of $[Mn^{2+}]$ is thus given by the Eq. (3.9). Therefore, if the reaction is assumed to be non-reversible (which should be the case at the onset of the sorption reaction) and first-order in $[Mn^{2+}]$, a semilog plot of $[Mn]_t$ versus t should result in a straight line with the slope = k / 2.303, and log $[Mn^{2+}]_o$ being the intercept.

However, obtaining a linear plot based on Eq. (3.9) is necessary but not definitive proof that the reaction is first-order (Sparks, 1989). If the reaction is truly first-order the rate constant should not vary with the concentration of Mn(II). This provides a good test for a proposed reaction order; if the reaction is first-order the slope of the semilog plot should remain unchanged with varying $[Mn^{2+}]$.

In order to deduce mechanistic information on the sorption of Mn(II) on δ-MnO_2 and to confirm the reaction order, two initial concentrations of Mn(II) were used, 40 and 25

μM. Figure 4 illustrates the typically observed decay of solution Mn(II) as a function of time. Here, data were taken every 50 μs and 100 points were averaged to give the time-dependent sorption of Mn(II) as shown (Fig. 3-4). Although not shown, greater than 80% of the sorption reactions were complete for both initial Mn(II) concentration within 200 ms.

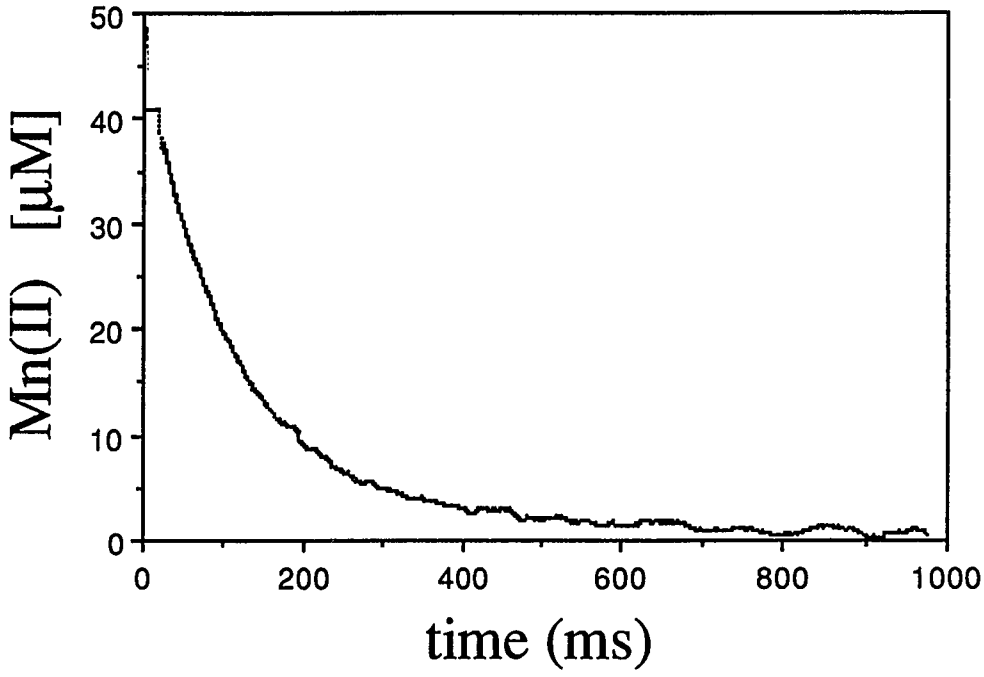

Figure 3-4. A typical rate curve of Mn(II) sorption on δ-MnO_2 (40 μ*M* initial Mn(II) is depicted).

If Eq. (3.7) is correct and elementary, a linear semilog plot of $[Mn^{2+}]$ as a function of time should result which is independent of $[Mn^{2+}]$ (Fig. 3-5). The correlation coefficient indicates the plots are quite linear as they should be for a first-order reaction, and the slopes of the two concentration plots are in good agreement--the higher Mn(II) concentration sorption resulted in a slightly higher slope. The rate constants obtained for the first-order reaction mechanism are 3.73×10^{-3} s^{-1} and 3.75×10^{-3} s^{-1} for 25 μ*M* and

40 μM $[Mn^{2+}]_o$, respectively, with an averaged $k_f' = 3.74 \times 10^{-3} \pm 0.1 \times 10^{-4}$ s^{-1}. In addition to the k_f' values being similar, the semilog plot should also yield an intercept value equal to the log $[Mn^{2+}]_o$; indeed the intercept values are in close agreement with the known

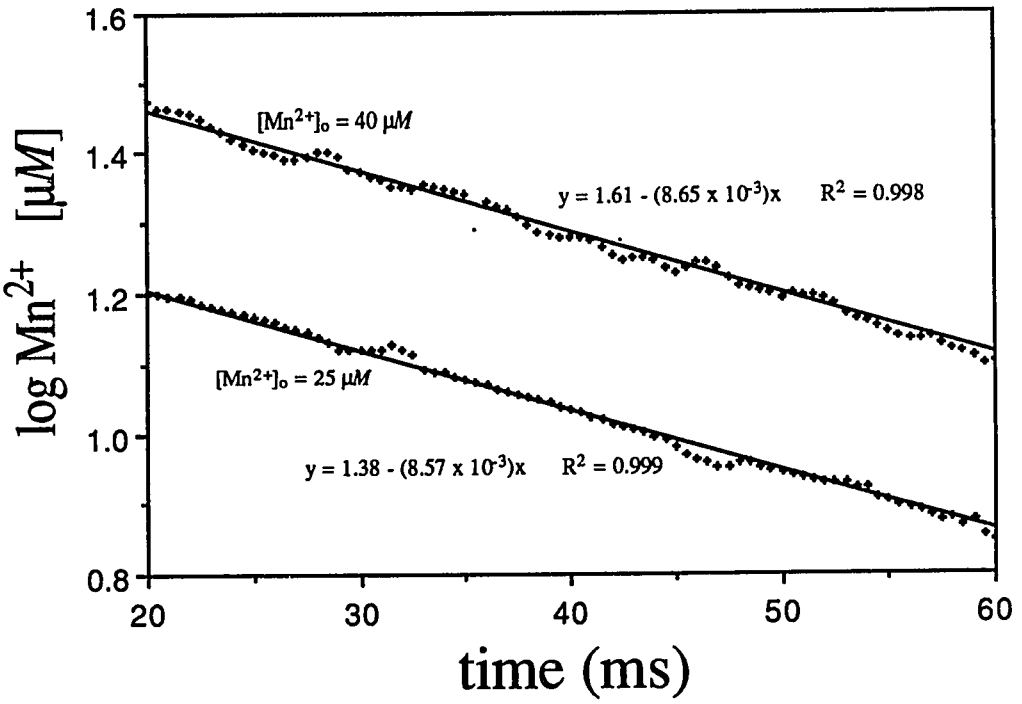

Figure 3-5. Initial reaction rates depicting the first-order dependence of Mn(II) sorption as a function of time for initial $[Mn^{2+}]$ of 25 and 40 μM.

$[Mn^{2+}]_o$: 24 μM and 41 μM. Consequently, Eq (3.7) appears to be valid for the experimental conditions invoked here.

The measured k_f' was then used in combination with Eq. (3.6) and the known reaction parameters to calculate k_r'; the calculated k_r' was 3.04×10^{-4} s^{-1}. After determining the k_f' and k_r', one can predict the time dependence of Mn(II) sorption, and for further validation of the rate constants compare the calculated values to those measured

experimentally. Rearranging Eq. 4 allows the time dependence of Mn(II) sorption to be predicted.

$$[Mn^{2+}]_t = [Mn^{2+}]_o\{k_r' + k_f' \exp -(k_f' + k_r')t \;/\; k_f' + k_r'\} \qquad (3.10)$$

Figure 3-6 illustrates the measured and predicted time dependence of Mn(II) sorption on δ-MnO_2. The predicted trends of Mn(II) sorption were in good agreement with those measured, validating the accuracy of the forward and reverse rate constants.

The validation of reaction (3.7) as a first-order elementary reaction indicates that chemical kinetics were measured; thus, transport phenomena were not rate-limiting. If diffusion processes were influencing the reaction rate, or if an incorrect reaction order was assumed, then a deviation from linearity in the semilog plot depicted in Fig. 3-4 would occur (the reaction would not conform solely to a first-order dependence on $[Mn^{2+}]$) and there would be poor conformity between measured and predicted Mn(II) sorption on δ-MnO_2 with time (Bunnett, 1986).

Determining reaction mechanisms and rates are essential to understanding, predicting, and possibly controlling chemical processes. The EPR-SF kinetic technique has shown great utility in measuring rapid reaction rates in colloidal suspensions. Moreover, the results presented here indicate that the apparatus measures chemical kinetics, devoid of transport rate limiting phenomena. This technique is ideally suited for sorption reactions involving colloidal material as the need for filtration is eliminated, thus allowing rapid data acquisition of reaction constituents. The rate parameters can be used to evaluate the time scale of reactions, and to ascertain reaction mechanisms. Utilizing the rapid measurements capable with this technique one can measure reactions at sufficiently early times so as to determine k_f values. With a knowledge of k_f values, integrated rate expressions can be used to calculate k_r. Furthermore, since chemical kinetic are being determined, equilibrium constants (K_{eq}^{kin}) can be ascertained from the ratio of k_f / k_r. The

Figure 3-6. The predicted time dependence of Mn(II) sorption on δ-MnO_2 compared to the measured sorption rate curves for initial [Mn^{2+}] of 25 μ*M* (a), and 40 μ*M* (b).

a)

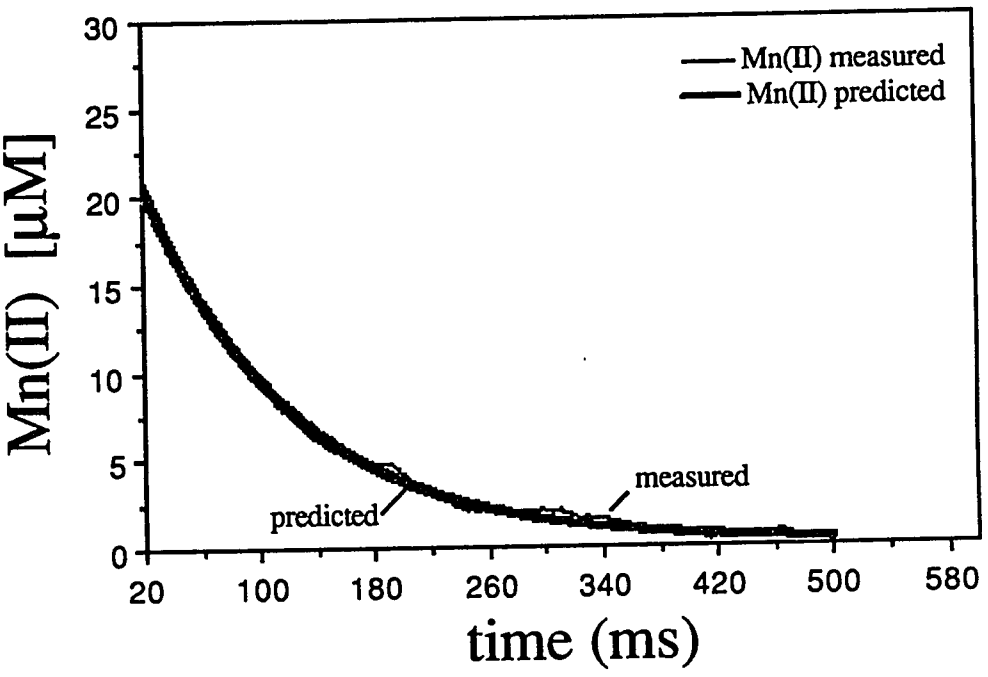
Mn(II) measured
Mn(II) predicted
Mn(II) [µM]
30
25
20
15
10
5
0
predicted
measured
20
100
180
260
340
420
500
580
time (ms)

b)

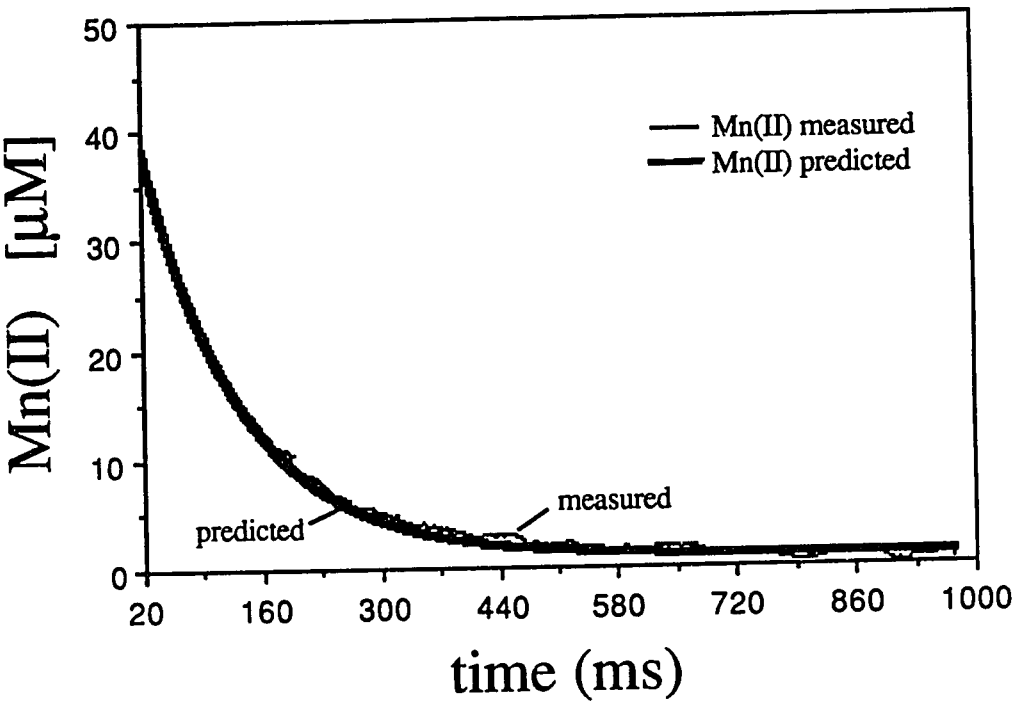
Mn(II) [μM]
50
40
30
20
10
0
20
160
300
440
580
720
860
1000
time (ms)
Mn(II) measured
Mn(II) predicted
predicted
measured

K_{eq}^{kin} values may then be compared to equilibrium constants (K_{eq}) determined via traditional equilibrium approaches (Sparks, 1989).

Although the EPR-SF technique is limited to paramagnetic species, there are many agriculturally and environmentally significant species which are EPR active. The EPR-SF technique provides many advantages for studying soil chemical reactions: (i) it allows direct measurement of surface reactions involving EPR-active ions, (ii) rate constants and equilibria are thus accurately determined from direct measurements, and (iii) reaction mechanisms, necessary to determine the fate of environmental constituents, can be elucidated. Therefore, we feel that this simple yet elegant kinetic technique has great potential for studying many soil and colloidal surface reactions.

In this study, we use EPR spectroscopy only to quantitatively measure solution Mn(II), but, depending on one's objectives, EPR spectroscopy can also be used to obtain surface information. The time necessary for a complete magnetic sweep would be prohibitive for rapid reaction measurements; thus, reducing the extent of time dependent surface information gleaned for such reactions (although slower reaction may be monitored continually with complete EPR spectra). However, spectra can be taken prior to reaction and at a steady state after reaction, giving information on surface structural alterations induced by the reaction being investigated. Such information would greatly complement many kinetic investigations.

3.5 References

Arrhenius, G., K. Cheung, S. Crane, M. Fisk, J. Frazer, J. Korkisch, T. Mellin, S. Nakao, A. Tsai, and G. Wolf. 1979. Counterions in marine manganates. *Colloques Internationaux du C.N.R.S.* **298**: 333-356.

Balistrieri, L.S., and J.W. Murray. 1982. The surface chemistry of δMnO_2 in major ion seawater. *Geochim. Cosmochim. Acta.* **46**: 1041-1052.

Bleam, W.F, and M.B. McBride. 1986. The chemistry of adsorbed Cu(II) and Mn(II) in aqueous titanium dioxide suspensions. *J. Colloid Interface Sci.* **110**: 335-346.

Bunnett, J.F. 1986. Kinetics in Solution. pp. 171-250. *In* C.F. Bernasconi (ed.) Investigations of rates and mechanisms of reactions, 4th ed. Wiley and Sons, New York.

Clementz, D.M., T.J. Pinnavaia, and M.M. Mortland. 1973. Stereochemistry of hydrated copper(II) ions on the interlamellar surfaces of layer silicates. An electron spin resonance study. *J. Phys. Chem.* **77**, 196-200.

Drago, R.S. 1977. Physical methods in chemistry. Saunders College Publishing, Orlando, FL.

Dzombak, D.A., and M.M. Morel. 1990. Surface Complexation Modeling. Wiley, New York.

Fendorf, S.E., and R.J. Zasoski. 1992. Chromium(III) oxidation by δ-MnO_2. I: Characterization. *Environ. Sci. Technol.* **26:** 79-85.

Hayes, K.M., and J.O. Leckie. 1986. Mechanism of lead ion adsorption at the goethite-water interface. pp. 114-141. *In* J.A. Davis and K.M. Hayes (eds.) Geochemical processes at mineral surfaces. ACS publications, Washington, D.C.

Hiemstra, T., W.H. Van Riemsdijk, and G.H. Bolt. 1989a. Multisite proton adsorption modeling at the solid/solution interface of (hydr)oxides: A new approach. I. Model description and evaluation of intrinsic reaction constants. *J. Colloid Interface Sci.* **133**: 91-104.

Hiemstra, T., J.C.M. De Witt, and W.H. Van Riemsdijk. 1989b. Multisite proton adsorption modeling at the solid/solution interface of (hydr)oxides: A new approach. II. Application to various important (hydr)oxides. *J. Colloid Interface Sci.* **133**: 105-117.

Ikeda, T., M. Sasaki, and T. Yasunaga. 1983. Kinetic studies of ion exchange of alkylammonium ion for sodium ion in aqueous suspensions of zeolite 4A using the pressure-jump method. *J. Phys. Chem.* **87**: 745-749.

Ikeda, T., J. Nakahara, M. Sasaki, and T. Yasunaga. 1984. Kinetic behavior of alkali metal ion on zeolite 4A surface using the stopped-flow method. *J. Colloid Interface Sci.* **97**: 278-283.

Klimes, N., G. Lassmann, and B. Ebert. 1980. Time-resolved EPR spectroscopy. Stopped-flow EPR apparatus for biological application. J. Mag. Res. 37: 53-59.

McBride, M.B. 1982. Hydrolysis and dehydration reactions of exchangeable Cu^{2+} on hectorite. *Clays & Clay Minerals.* **30**: 200-206.

McBride, M.B. 1987. Adsorption and oxidation of phenolic compounds by iron and manganese oxides. *Soil Sci. Soc. Amer. J.* **51**: 1466-1472.

McBride, M.B. 1989. Oxidation of dihydroxybenzenes in aerated aqueous suspensions of birnessite. *Clays & Clay Minerals.* **37**: 341-347.

Morgan, J.J., and W. Stumm. 1964. Colloid-chemical properties of manganese dioxide. *J. Colloid Sci.* **19**: 347-359.

Potter, R.M., and G.R. Rossman. 1979. The tetravalent manganese oxides: Identification, hydration, and structural relationships by infrared spectroscopy. *Am. Mineral.* **64**: 1199-1218.

Sparks, D.L. 1989. Kinetics of soil chemical processes. Academic Press, New York.

Stach, J., R. Kirmse, W. Dietzsch, G. Lassmann, V.K. Belyaeva, and I.N. Marov. 1985. Ligand exchange reactions between copper(II)- and nickel(II)-chelates of different sulfur- and selenium-containing ligands. VI [1]. Kinetics of ligand exchange reactions studied by stopped-flow ESR. *Inorgan. Chim. Acta.* 96: 55-59.

Zhang, P.C., and D.L. Sparks. 1990. Kinetics of selenate and selenite adsorption/desorption at the goethite/water interface. *Environ. Sci. Technol.* **24**, 1848-1856.

CHAPTER 4

KINETICS AND MECHANISMS OF CHROMIUM(III) OXIDATION by δ-MnO_2

4.1 Abstract

Determining reaction rates and mechanisms is necessary to understand environmental processes. However, investigating reactions in colloidal suspensions has been problematic, particularly the study of rapid reactions. The redox reaction between Cr(III) and Mn-oxides is of environmental significance as the more toxic and mobile Cr(VI) is formed, and Mn(II) is liberated with an accompanying degradation of the oxide. In this study, we employed an electron paramagnetic resonance spectroscopically monitored stopped-flow (EPR-SF) kinetic technique to determine the reaction rate and mechanism of the redox reaction between Cr(III) and δ-MnO_2. The results of the EPR-SF technique were compared to those obtained using a stirred-flow reactor, which allowed for a comparison between the rate of Cr(VI) and Mn(II) released to solution. At pH 3, the release of both Mn(II) and Cr(VI) indicated a second-order reaction mechanism--dependent on Cr(III) and δ-MnO_2 concentrations. At higher pH values, the release of Mn(II) was retarded while Cr(VI) was accelerated. The rate coefficient for the release of Mn(II) was approximately 1.5 times greater than that for Cr(VI). A three step reaction mechanism was postulated for the oxidation of Cr(III) by δ-MnO_2, and the rate constants for each reaction step were ascertained from the measured product release rate coefficients.

4.2 Introduction

As the environment becomes increasingly sensitive to anthropogenic effects, a knowledge of pollutant reactions in soils and waters is increasingly important. Pollutant reactions with colloidal material are one of the primary determinants in the fate of these potentially harmful substances. In natural systems, meta-stable conditions predominate, and thus kinetic constraints rather than thermodynamic ones often determine a reaction pathway. Therefore, it is important for researchers to study kinetic reactions in environmental systems.

Oxidation/reduction reactions affect the behavior, mobility, and toxicity of many metal ions in the environment. Chromium is one such metal in which two oxidation states are stable under surface conditions, Cr(III) and Cr(VI). The difference in behavior of these two oxidation states is profound, necessitating the importance of knowing which state is present and the potential for transformation in a given system. If the potential for oxidation exists, then the hazard of Cr(III) is tantamount to that of Cr(VI). Manganese oxides are one of the strongest oxidants present in surface environments, and they have a strong affinity for various metal ions. Thus, Mn-oxides have pronounced effects on both redox and sorption reactions. Furthermore, Mn-oxides appear to be the only naturally occurring oxidant of Cr(III) in surficial systems (Eary and Rai, 1987). It is therefore important to characterize Cr(III) oxidation and to determine factors which influence the oxidation process. In addition, an important consideration in the oxidation of many substances by Mn-oxides is the degradation of the oxide and an accompanied release of Mn(II). In this study we employed an electron paramagnetic resonance spectroscopically monitored stopped-flow (EPR-SF) kinetics to investigate the reductive dissolution rate of δ-MnO_2 by Cr(III). The rate of Mn(II) released was compared to that of Cr(VI), allowing for greater insight on the reaction mechanism.

Coupling EPR monitoring with a stopped-flow kinetic technique (EPR-SF) allows one to directly measure an EPR active constituent on a millisecond time scale without any complications induced by the presence of colloidal material. While EPR-SF kinetics is limited to reactions involving an EPR active species, many organic molecules (especially free radicals), in addition to Mn(II) and Cu(II), are EPR active and of interest to soil and environmental scientists. A host of other constituents are also EPR active and of possible interest in other chemical fields. McBride and co-workers (McBride, 1989; McBride, 1987; Bleam and McBride, 1986, McBride, 1982) have utilized electron paramagnetic resonance (EPR) spectroscopy for investigating reactions involving EPR active constituents, e.g., Mn(II) and Cu(II), but kinetic investigations were not been conducted.

A species which is EPR active in solution often will not be when it is in a sorbed state due to rapid spin relaxation pathways, or the spectra may be broadened to the point where they contribute insignificantly to the signal intensity (Bleam and McBride, 1986; McBride, 1982). Consequently, the sorption of an EPR active species can be monitored by the decrease in signal intensity or the desorption by the increase in signal intensity. In addition to monitoring sorption/desorption reactions, the kinetic technique presented in this Chapter can be used to monitor dissolution/precipitation reactions and is particularly advantageous for measuring redox reactions involving Mn-oxides, as the reductive dissolution liberates Mn(II).

Stopped-flow kinetic investigations have been prevalent in the study of solution reactions. The rapid initial mixing and coupling of flow cells with various analytical instruments makes this technique well suited for investigating a variety of solution reactions. Furthermore, the versatility of stopped-flow kinetics for studying dramatically different reaction time scales, and its ease of employment, has added to its popularity. With the use of rapid injectors, millisecond time scales are obtainable (Stach et al., 1985), while conventional syringe injectors allow for measurement of time scales >20 ms (Klimes

et al., 1980); the maximum length of measurement time is only determined by the physical constraints of a given system. However, stopped-flow kinetics has only found limited application in the study of colloidal reactions due to analytical problems associated with the colloidal material.

Two experimental approaches may be used to employ stopped-flow kinetics: initiating the reaction with subsequent monitoring, or a chemical relaxation. Chemical relaxation is used with stopped-flow kinetics by inducing a small change in a reactant concentration, i.e., a concentration-jump, resulting in a small perturbation of the system. The approach to a new equilibrium is monitored with a method that is sensitive to small changes in concentration (Bernasconi, 1976). Electrical conductivity (EC) has been employed to measure the chemical relaxation induced by small concentration jumps in colloidal suspensions; however, EC only monitors the reaction indirectly. Ikeda et al. (1984) employed stopped-flow kinetics, using a chemical relaxation approach, to investigate metal reactions on zeolites. Such an approach avoids the analytical difficulties associated with colloidal material, but it is limited by the restrictions of chemical relaxation techniques. With relaxation approaches the reaction must be fully reversible, reactant species are not usually measured directly (e.g., with EC), and rate constants are determined from linearized rate equations that are often dependent on equilibrium parameters.

The indirect monitoring along with the necessity of a fully reversible reaction and dependence on equilibrium parameters with chemical relaxation approaches often makes them too restrictive for studying many reactions. A more direct approach is to monitor a reaction after its initiation. When coupled with a method which directly monitors a reactant species, the researcher is provided with a powerful kinetic technique which may greatly simplify the evaluation of chemical kinetics. Moreover, it allows for the measurement of a wide range of reaction time scales. In addition, the reaction need not be reversible as direct measurement of a reactant species removes the restrictions of chemical relaxation

techniques. These advantages are offset somewhat, however, since the simplifying assets of chemical-relaxation approaches, e.g., linearization of reactions regardless of molecularity or order, cannot be utilized.

Reactions involving colloidal suspensions are important in an array of disciplines including metal supported catalysis, electrochemistry, and soil and water chemistry. Therefore, it is important for researchers to have means available for studying these reactions. A variety of reactions can be studied due to the ease with which stopped-flow cells may be coupled with various analytical techniques, such as EPR. In addition, the versatility offered by stopped-flow kinetics for investigating a broad range of reaction time scales increases its applicability to many systems in colloidal research. Investigating the reductive dissolution rate of Mn-oxides by oxidants present in surface waters or soils may be particularly well suited for EPR-SF kinetics and is of great environmental importance.

The oxidation of Cr(III) to Cr(VI) poses a severe environmental hazard, but this reaction mechanism has not been resolved. A rapid initial reaction is followed by a sharp decrease in the reaction rate at higher pH values. In Chapter 2 we found that the inhibition resulted from the formation of a $Cr(OH)_3 \cdot nH_2O$ surface precipitate on δ-MnO_2, which inhibited subsequent oxidation. Manceau and Charlet (1992) hypothesized that the redox reaction was dependent on surface diffusion of Cr(III) ions into structural vacancies of the δ-MnO_2. The decrease in reaction rate with increased pH would thus arise due to the increase polymerization of solution Cr(III), which would sterically restrict it from entering cavity sites. These authors further postulated that the rate limiting step in Cr(III) oxidation was the electron transfer. However, their hypotheses do not agree with various factors observed by other researchers. Firstly, their hypotheses would indicate an increased reaction rate with oxidation; this is clearly refuted by experimental evidence (Fendorf and Zasoski, 1992; Johnson and Xyla, 1991; Eary and Rai, 1987; Amacher and Baker, 1982). Secondly, Cr(III) oxidation occurs on Mn-oxides without structural vacancies, e.g., γ-

MnOOH and β–MnO_2 (Johnson and Xyla, 1991; Eary and Rai, 1987). Thirdly, the initial reaction rate increased with increased pH (Fendorf and Zasoski, 1992; Amacher and Baker, 1982). Fourthly, solution polymerization at millimolar Cr(III) concentration (or less) between pH 2-7 is minimal (Rai et al., 1987). Finally, the sorption of non-oxidizable metals on δ-MnO_2 show a pH dependency which does not correlate with sorption only at site vacancies (Zasoski and Burau, 1988; Balistrieri and Murray, 1982; Murray, 1974), and the inner-sphere complexation of Cr(III) with Mn-oxides provides a pathway for the redox reaction (Chapter 2).

Accordingly, we investigated the redox reaction kinetics at pH 3 to minimize complicating reactions and to deduce the oxidation mechanism (e.g., precipitation or retention reactions); thus, information on the redox process was gleaned. Subsequently we evaluated the reaction rate at higher pH values to assess the role of congruent reactions on the redox process. A comparison between the rate of Mn(II) released to that of Cr(VI) produced was made to determine the rate limiting step.

4.3 Materials and Methods

The reductive dissolution rate of MnO_2 by Cr(III) was measured by employing the EPR-SF technique and monitoring the release of Mn(II). Details on this technique can be found in Chapter 3. To obtain quantitative information on Mn(II), the EPR cell was filled with a known concentration of Mn(II) (in the absence of colloidal material). The magnetic field was then swept, resulting in the Mn(II) hyperfine sextet structure. The magnetic field was centered at the downfield Mn(II) hyperfine peak for quantitative measurement of the Mn(II) present in solution. A linear relationship between the EPR signal and Mn(II) concentration resulted within the range of 5 to 500 μM Mn(II). The reductive dissolution rates of δ-MnO_2 by Cr(III) were measured at pH 3, 4, and 5, with initial Cr(III)

concentrations, $[Cr(III)]_o$, ranging from 77 to 770 μM, and 0.10, 0.25, 0.5, and 1.0 g L^{-1} MnO_2. Although Mn(II) is liberated at pH 3 in the absence of Cr(III) (Murray, 1974), we did not detect Mn(II) with EPR spectroscopy over the duration of these experiments (< 30 min). The initial rates were determined by collecting EPR signals every 1 ms, and averaging 500 signals to give data points every 0.5 s. Three individual runs were signal averaged to produce the analyzed data.

The Cr(VI) data evaluated in this study were from Fendorf and Zasoski (1992), and were determined using a stirred-flow technique. Chromium(VI) was measured using the s-diphenyl carbazide method (Bartlett and James, 1979). The reaction was initiated by injecting 1 ml of 2.5 g L^{-1} MnO_2 into the stirred-flow chamber, yielding a final suspension density of 0.1 g L^{-1}. In the stirred-flow experiments, $[Cr(III)]_o$ = 77 or 770 μM, $\{MnO_2\}_o$ = 0.1 g L^{-1} and pH = 3.0.

The zero point of charge (ZPC) and surface area of the δ-MnO_2 were 2.7 and 223 m^2 g^{-1}, respectively (Fendorf and Zasoski, 1992). The suspension density of MnO_2 was converted to [(moles of sites) / L] using a site density of 6 sites nm^{-2} (Morgan and Stumm, 1964) and a bidentate surface Cr(III) complex (Chapter 2 and Manceau and Charlet, 1992). Chromium solutions were made from reagent grade nitrate salts, and pH was adjusted with 1.0 M HNO_3 or 1.0 M NaOH. All reactions were conducted in a 0.1 M $NaNO_3$ matrix at 25°C and 1 atm pressure.

4.4 Results and Discussion

At pH 3, the redox reaction between Cr(III) and δ-MnO_2 proceeds until a reactant is limiting (Fendorf and Zasoski, 1992). The reaction between Cr(III) and δ-MnO_2 can be expressed as:

$$Cr(OH)^{2+} + 1.5\ MnO_2 \rightarrow HCrO_4^- + 1.5\ Mn^{2+} \qquad (4.1)$$

Thus, the redox reaction produces Cr(VI) and Mn^{2+}, making detection of either product a viable means of following the reaction. However, detection of the products in solution may not be an accurate representation of the redox reaction rate since they may be retained on the oxide subsequent to formation. Furthermore, the rate of Cr(VI) released to solution may not be proportional to the rate of Mn(II) released. It has been proposed that Mn(II) formed during Cr(III) oxidation by Mn-oxides may bind to the surface and compete with Cr(III) for sorption sites at pH > 4 (Amacher and Baker, 1982); in contrast, anionic Cr(VI) should be repelled from the negatively charged surface.

Manganese oxides have a strong affinity for Mn(II) (Murray, 1975; Morgan and Stumm, 1964), and the sorption process on δ-MnO_2 is very rapid--being complete in less than 1 s (Chapter 3). However, steady state data indicated that the ratio of [Cr(VI)] : [Mn^{2+}] was in the expected stoichiometric proportions, 1 : 1.5 (Fendorf and Zasoski, 1992) and little Mn(II) sorption would be expected at pH 3. However, this does not necessarily imply that the rate of Mn(II) released is proportional to that of Cr(VI), but only that at a steady-state their quantities are in the expected stoichiometric amounts.

The molecularity expressed in Reaction (4.1) is 1.5 MnO_2 to 1 Cr(III). However, Cr(III) binds to the MnO_2 surface in an inner-sphere bidentate mechanism (Chapter 2 and Manceau and Charlet, 1992). The single complexation reaction would allow 1 Cr(III) to oxidize 1.5 Mn(IV) as the molecularity of Reaction (4.1) suggests. Therefore, to deduce a rate expression it is necessary to depict the reaction as 1 Cr(III) complexing with a single bidentate MnO_2 surface site, **-S**.

$$Cr(OH)^{2+} + \text{-}\mathbf{S} \rightarrow HCrO_4^- + 1.5\ Mn^{2+} \qquad (4.2)$$

4.3.1 Reductive Dissolution Rate of δ-MnO_2

A typical EPR-SF kinetic curve for the Cr(III) induced reductive dissolution of MnO_2 at pH 3 is shown in Fig. 4-1. The rapid detection with EPR-SF provided abundant data at the onset of the reaction and permitted the use of an initial rate method for evaluation of the redox reaction. A reaction order with respect to a single constituent was determined by varying the concentration of one constituent while keeping all other constituents constant and measuring the initial reaction rate. The initial reaction rate should not be affected by the build-up of products or secondary reactions (Steinfeld et al., 1989; Walker et al., 1988; Atkinson, 1985; Lasaga, 1981). In a plot of log rate versus log reactant concentration, the slope of the resulting curve represents the reaction order, **n**, with respect to that reactant (denoted by the superscript/subscript symbols: c= Cr(III) and m = MnO_2). The initial release of Mn(II) would yield the following expression.

$$d[Mn^{2+}]/dt = k_m \{\text{-S}\}^{\mathbf{n}_m} [Cr(III)]^{\mathbf{n}_c} \qquad (4.3.1)$$

Employing logarithms allows one to graphically evaluate **n** and k , where k is the rate coefficient,

$$\log\{d[Mn^{2+}]/dt\} = \log k_m + \mathbf{n}_m \log\{\text{-S}\} + \mathbf{n}_c \log[Cr(III)] \qquad (4.3.2)$$

The reaction order of both reactants in Eq. (4.2) were evaluated in this manner with the EPR-SF technique at pH 3. Keeping [Cr(III)] constant and varying {-S}, Eq. (4.3.2) reduces to,

$$\log\{d[Mn^{2+}]/dt\} = \log k_m' + \mathbf{n}_{MnO_2} \log\{\text{-S}\} \qquad (4.4)$$

where $k_m' = k_m[Cr(III)]_o$; keeping {-S} constant while varying [Cr(III)] yields

$$\log\{d[Mn^{2+}]/dt\} = \log k_m'' + \mathbf{n}_{Cr} \log[Cr(III)] \qquad (4.5)$$

where $k_m'' = k_m\{\text{-S}\}_o$. The rate coefficients defined in Reactions [3-5] are observed (or apparent) coefficients representative of the overall-reaction, not an elementary reaction, and

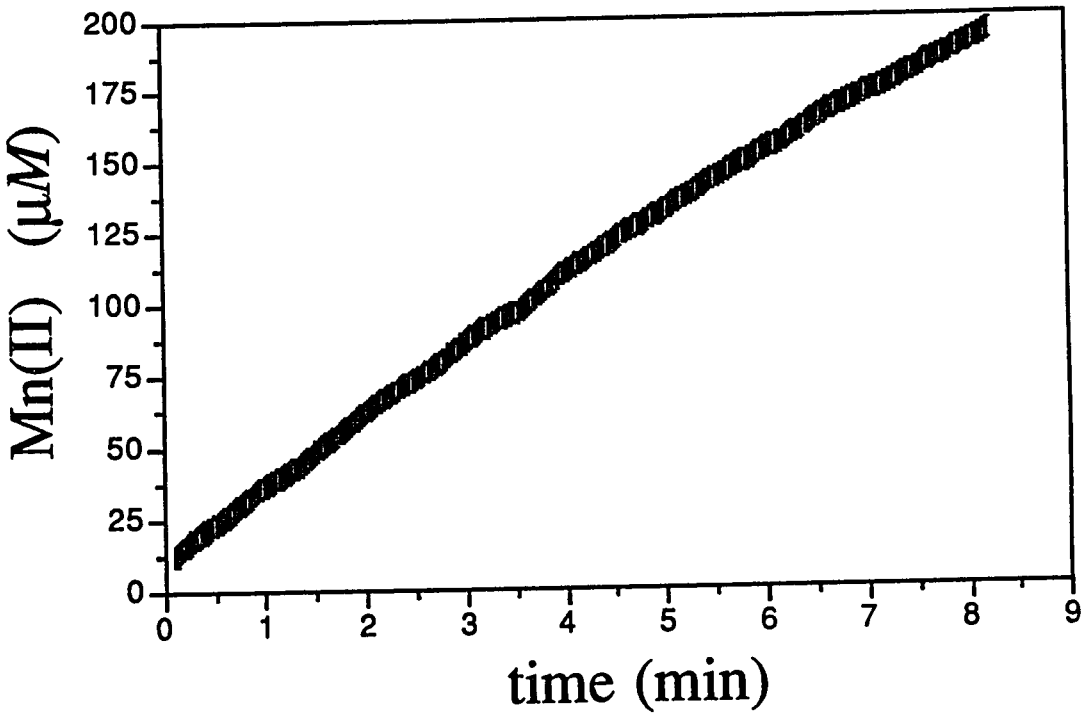

Figure 4-1. A typical EPR-SF kinetic curve for δ-MnO_2 reductive dissolution by Cr(III) at pH 3 ($[Cr(III)]_o$ = 400 μ*M* and $\{MnO_2\}_o = 0.25\ g\ L^{-1}$).

thus they differ for the release of Cr(VI) and Mn(II). Accordingly, we use subscripts to denote the rate coefficient for the release of each product.

The rate of Mn(II) released, ($d[Mn^{2+}]/dt$), as a function of $[Cr(III)]_o$ is depicted in Fig. 4-2, with $\{\text{-S}\}_o = 1.11$ m*M*. A first-order rate, $d[Mn^{2+}]/dt$, dependence on $[Cr(III)]_o$ was observed ($n_{Cr} = 1$). A first-order dependence on the surface site density, $\{\text{-S}\}_o$, was also determined for the rate of Mn(II) released (Fig. 4-3). Therefore, at pH 3, a first-order

dependence on both reactants, Cr(III) and {-S}, was observed giving the following second-order overall reaction rate expression based on the release of Mn(II) to solution.

$$d\,[Mn^{2+}] / d\,t = k_m\,[Cr(III)]\,\{-S\} \qquad (4.6)$$

The rate coefficient was determined by assuming the initial concentration of the non-varied reactant remained constant over the time of measurement. The anti-log of the intercepts in Figs. 4-2 and 4-3 resulted in $k_m' = 1.05 \times 10^{-3}\ s^{-1}$, and $k_m'' = 1.62 \times 10^{-3}\ s^{-1}$. Accounting for the concentration of the non-varied reactant, as described by Eqs. 4-4 and 4-5, yielded an average k_m value of $1.42 \times 10^{-6} \pm 0.04 \times 10^{-6}\ \mu M^{-1}\ s^{-1}$.

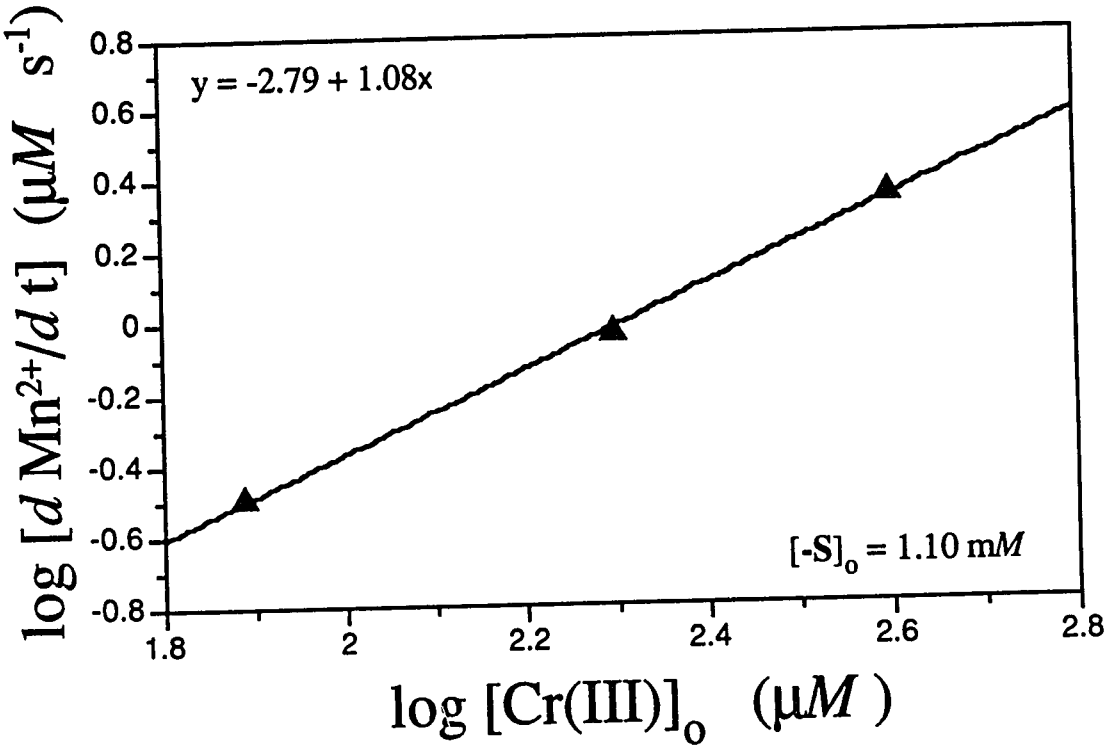

Figure 4-2. The reaction rate, $d\,[Mn^{2+}]/dt$, as a function of initial Cr(III) concentration, $[Cr(III)]_o$, with $\{MnO_2\}_o = 1\ g\ L^{-1}$, depicting the first-order rate dependence on [Cr(III)].

4.4.2 The Rate of Cr(VI) Released to Solution

The rate of Cr(VI) produced was also measured at pH 3 using a stirred-flow reactor. Two initial concentrations of Cr(III) were investigated, 77 and 770 μM, and a initial $\{MnO_2\}_o$ level of 0.1 g L^{-1} was employed ($\{\text{-S}\}_o = 111\ \mu M$). With the 77 μM Cr(III) concentration both $[Cr(III)]_o$ and $\{\text{-S}\}_o$ should contribute to the rate equation, necessitating the employment of a second-order analysis. This can be expressed using Eq. (4.7) (Steinfeld et al., 1989).

$$k_c\, t = 1/([Cr(III)]_o - \{\text{-S}\}_o) \times \ln([Cr(III)]_t\{\text{-S}\}_o/[Cr(III)]_o\{\text{-S}\}_t) \qquad (4.7)$$

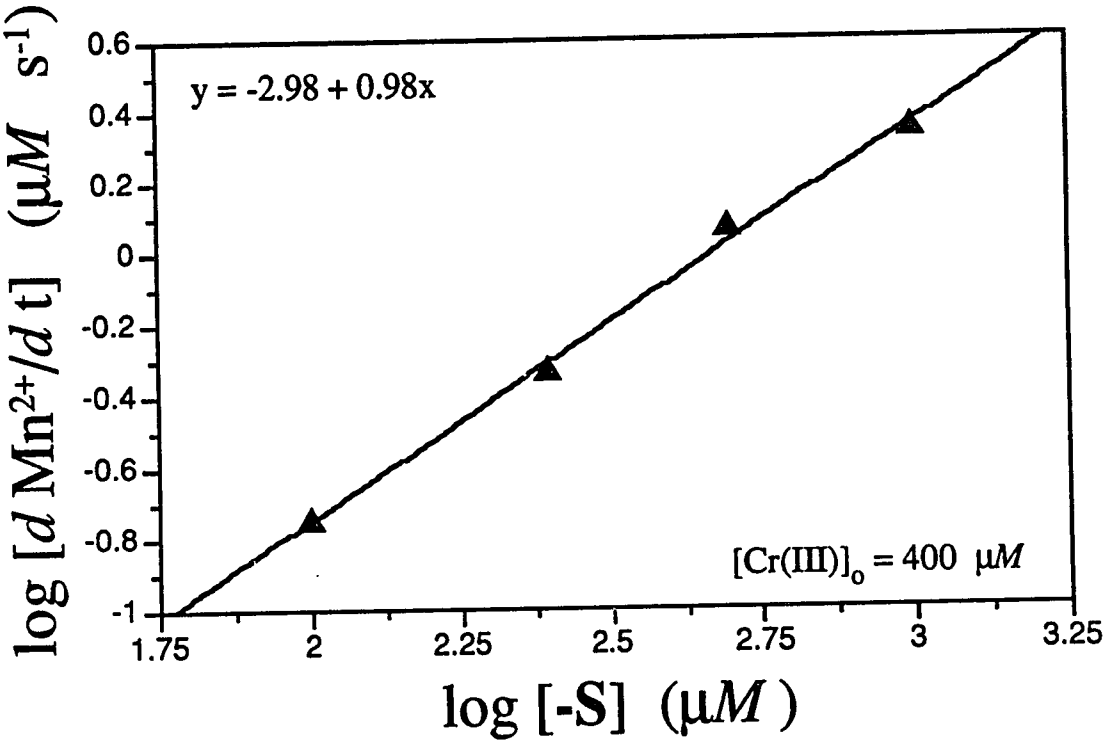

Figure 4-3. The reaction rate dependence, $d\,[Mn^{2+}]/dt$, with respect to $\{MnO_2\}_o$, with $[Cr(III)]_o = 200$ μM. A first-order reaction dependence on the initial level of MnO_2 is illustrated.

Figure 4-4 depicts the second-order expression and the conformity of the data to this rate law. The observed rate coefficient for the production of solution Cr(VI), k_c, was 5.53 x 10^{-5} μM^{-1} s^{-1}. Therefore, both the rate of Cr(VI) and the rate of Mn(II) entering solution indicated that a second-order reaction mechanism was operational at pH 3 for the redox reaction between Cr(III) and δ-MnO_2. A second-order overall reaction rate expression was also derived for Cr(III) oxidation by γ-MnOOH based on the production of Cr(VI) at pH < 4.5. The overall reaction was first-order with respect to both $[Cr(III)]_o$ and $\{MnO_2\}_o$ (Johnson and Xyla, 1991).

Under reaction conditions of 770 μM $[Cr(III)]_o$ pseudo-first order conditions should prevail as Cr(III) is in excess of the surface site density {-S}. Under these conditions the reaction rate should be dependent only on {-S},

$$d\,[Cr(VI)] / d\,t = k'_c' \{-S\} \qquad (4.8.1)$$

where $k' = k_c\,[Cr(III)]_o$ and thus the reaction should be zero-order with respect to Cr concentration.

$$d\,([Cr]_o - [Cr]_t) / d\,t = k_c'' \qquad (4.8.2)$$

where $k_c'' = k_c\,[Cr(III)]_o\,\{-S\}_o$.

Although it is more orthodox to conduct a pseudo-first order analysis, a zero-order representation (Eq. 8b) was used in this study due to analytical constraints. In the stirred-flow reactor higher suspension densities could not be employed because flow was obstructed. In addition, low Cr(III) concentrations resulted in too little oxidation for accurate detection. Therefore, when measuring Cr(VI) with this apparatus one cannot achieve pseudo-first order conditions with respect to Cr(III).

Nonetheless, by measuring Cr(VI) one can obtain the rate coefficient from a zero-order rate expression. Figure 4-5 depicts the change in Cr speciation as a function of time. Good conformity to zero-order kinetics was observed and the rate coefficients from both the second-order (k_c = 8.71 x 10^{-7} μM^{-1} s^{-1}) and pseudo zero-order (k_c = 7.83 x 10 μM^{-1} s^{-1} μM^{-1} s^{-1}) conditions are in good agreement , k_c = 8.27 x 10^{-7} ± 0.44 x 10^{-7} μM s^{-1}.

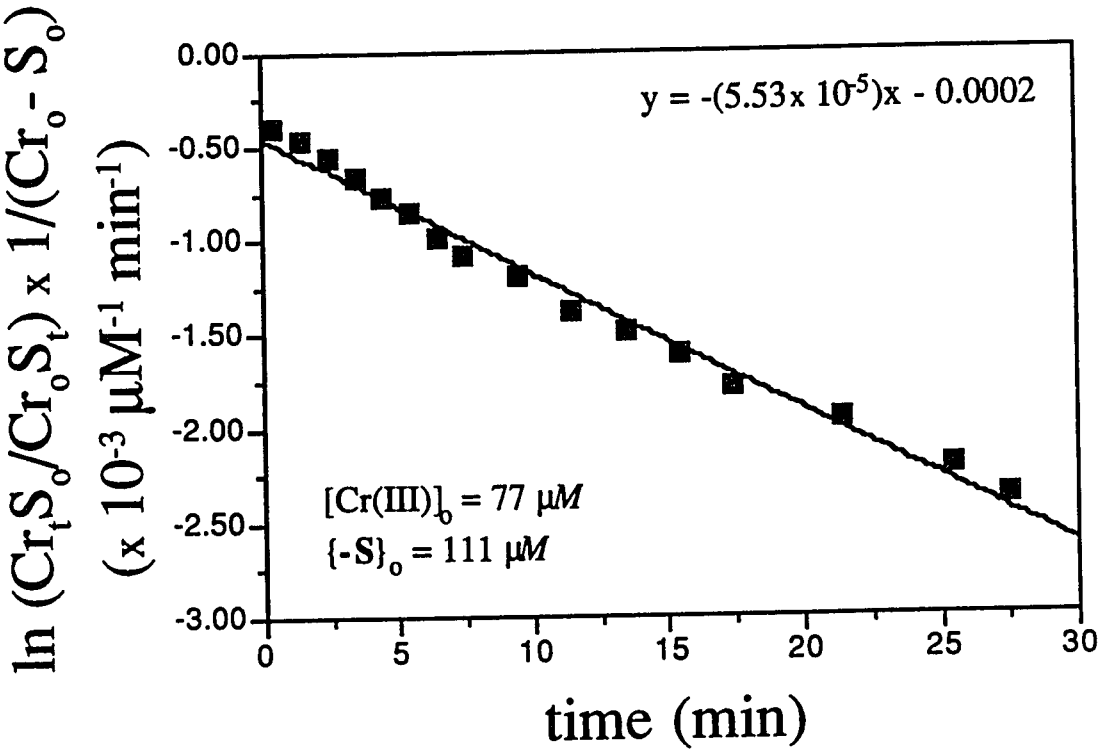

Figure 4-4. The rate of Cr(VI) released to solution expressed as a second-order reaction.

To further evaluate and verify the pseudo zero-order conditions, Reaction (4.8), the rate of solution Mn(II) formation was measured under various Mn-oxide concentrations with the EPR-SF technique. In contrast to the first-order $[Cr(III)]_o$ dependence on $[Mn^{2+}]$ released that was observed at high suspension densities, fractional order $[Cr(III)]_o$

dependencies were discerned with lower -S concentrations (Fig. 4-6). With a continued decrease in surface site density, $\{-S\}_o$, an eventual zero-order dependency on [Cr(III)] occurs (i.e., as $\{-S\}_o \rightarrow 0$, $n_{Cr} \rightarrow 0$, where n_{Cr} is the reaction order with respect to [Cr(III)]). The progression toward $n_{Cr} = 0$ on $d[Mn^{2+}]/dt$ indicates a (pseudo) site saturation of the surface (Steinfeld et al., 1989). The results of the EPR-SF system verify that a first-order dependence, $n_{Cr} = 1$, was not operational when the Cr(III) concentration exceeds the surface site density, verifying the validity of the pseudo zero-order reaction analysis presented earlier.

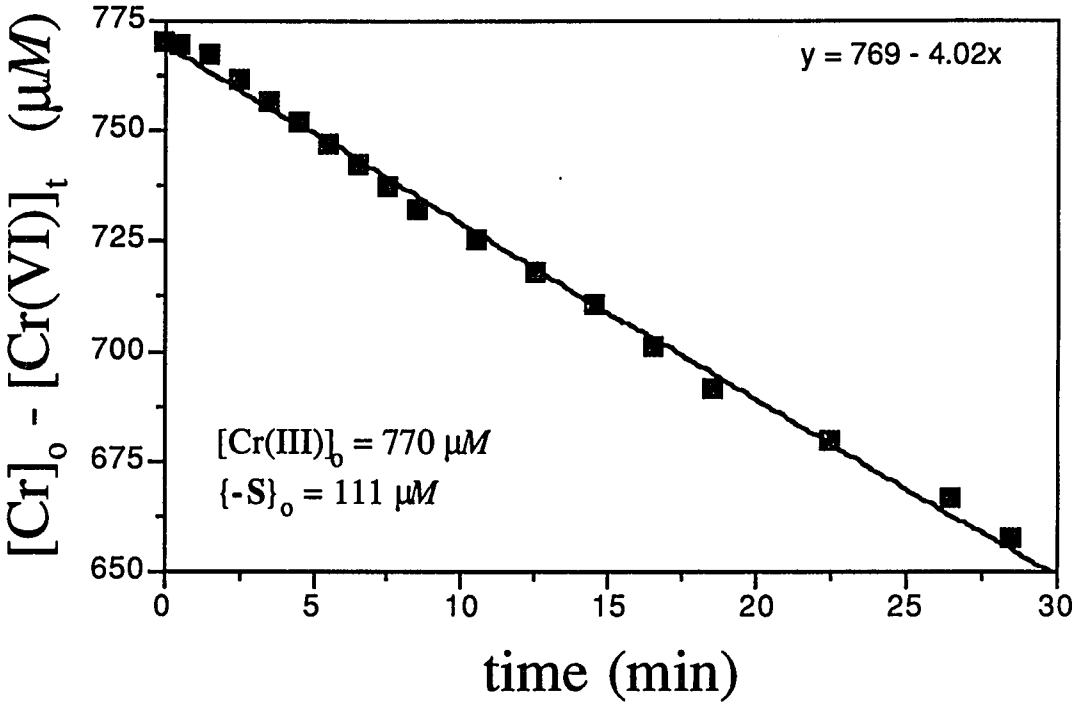

Figure 4-5. Chromium(VI) production from Cr(III) oxidation by δ-MnO_2 at pH 3 ($[Cr(III)]_o = 770\ \mu M$ and $\{MnO_2\}_o = 0.1\ g\ L^{-1}$).

The rates of Mn(II) and Cr(VI) released to solution are slightly different at pH 3; the observed rate of Mn(II) released being ≈1.7 time greater than that for Cr(VI). At pH 3

the oxide surface has only a slight negative charge, and retention of Mn(II) at this pH was minimal (Fendorf and Zasoski, 1992). One would therefore expect that the release of Mn(II) to solution would not be retarded by readsorption on the oxide. This is supported by the rate data as the expected stoichiometry between the observed product release rate was maintained.

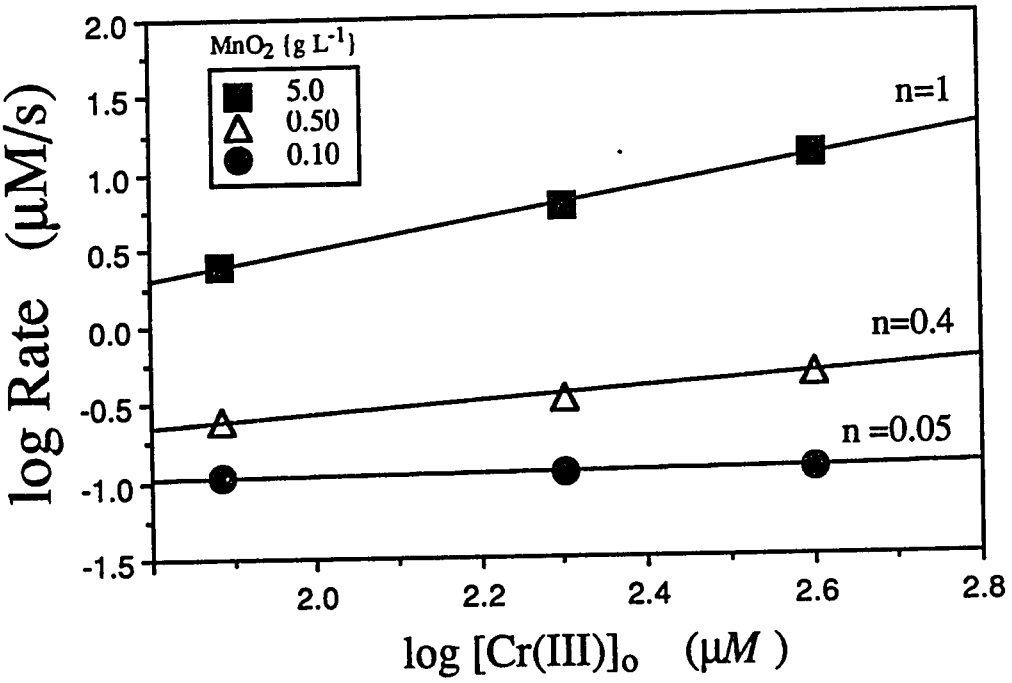

Figure 4-6. Suspension density effects on the [Cr(III)] reaction order (n_{Cr}); as the suspension density decreases, n_{Cr} decreases and approaches a zero-order dependence.

4.4.3 pH Effects on the Redox Reaction Rate

Although the solution production rate of Mn(II) and Cr(VI) correlated well with their stoichiometric proportions, Fendorf and Zasoski (1992) observed that as pH increased the rate of Cr(VI) released to solution increased while the results of this study indicate that Mn(II) entered solution more slowly with increased pH (Fig. 4-7). Furthermore, the

trends in the release of Mn(II) and Cr(VI) differ significantly. Chromium(VI) is initially released very rapidly to solution, followed by a sharp decline in the reaction rate and subsequent cessation of the reaction. In contrast, Mn(II) is released only slowly to solution (relative to lower pH values), but the release continued at a constant rate. However, at a steady-state the proportion of Cr(VI) to Mn(II) is as expected (Fendorf and Zasoski, 1992; Amacher and Baker, 1982). The rate dependence in both cases is convoluted by the presence of a $Cr(OH)_3 \cdot nH_2O$ surface precipitate (Chapter 2). In addition, the initial reaction rate exceeds the detection limits of the stirred-flow system employed.

The EPR-SF technique is capable of measure rapid reactions (> 20 ms); however, the release of Mn(II) does not appear to represent the redox reaction rate at pH 5 as noted by the dramatic differences in the rate of Mn(II) versus Cr(VI) entering solution. The release of Mn(II) may be retarded by both the higher negative surface charge on the oxide and the formation of a $Cr(OH)_3$ surface precipitate. Johnson and Xyla (1991) observed that the rate of Cr(III) oxidation by γ-MnOOH at pH > 4.5 was dependent on levels of [Cr(III)], $\{MnO_2\}$, and sorbed Cr(III). The sorbed Cr(III) term was necessary to describe the redox inhibition, which occurred at pH values greater than 4.5. Unfortunately, the time dependency of Cr(III) sorption was not measurable with either of the techniques employed in this study. The rate of Cr(III) sorption exceeds the detection limits of the stirred-flow apparatus and while stopped-flow kinetics should resolve the reaction rate, the Cr(III) EPR signal intensity was not sufficient to allow for quantitative measurement of this species.

Nonetheless, important qualitative observations can be made. While at a steady-state the solution quantities of Mn(II) and Cr(VI) are in their expected stoichiometries; the rate of products released have opposing trends with increased pH. It appears that the increased surface charge and surface precipitation, resulting from an increased pH, retards the rate of Mn(II) released but does not inhibit it. Thus, after prolonged reaction the Mn(II) generated from the redox reaction enters the aqueous environment. It is possible that the increased negative surface charge accelerates the desorption of Cr(VI) which thus exits the

interfacial region during the early stages of Cr-hydroxide polymerization. However, the release of Mn(II) may be retarded by the electrostatic attraction to the surface, allowing for more extensive nucleation of Cr(III)-hydroxide to develop. This may further obstruct the desorption of Mn(II).

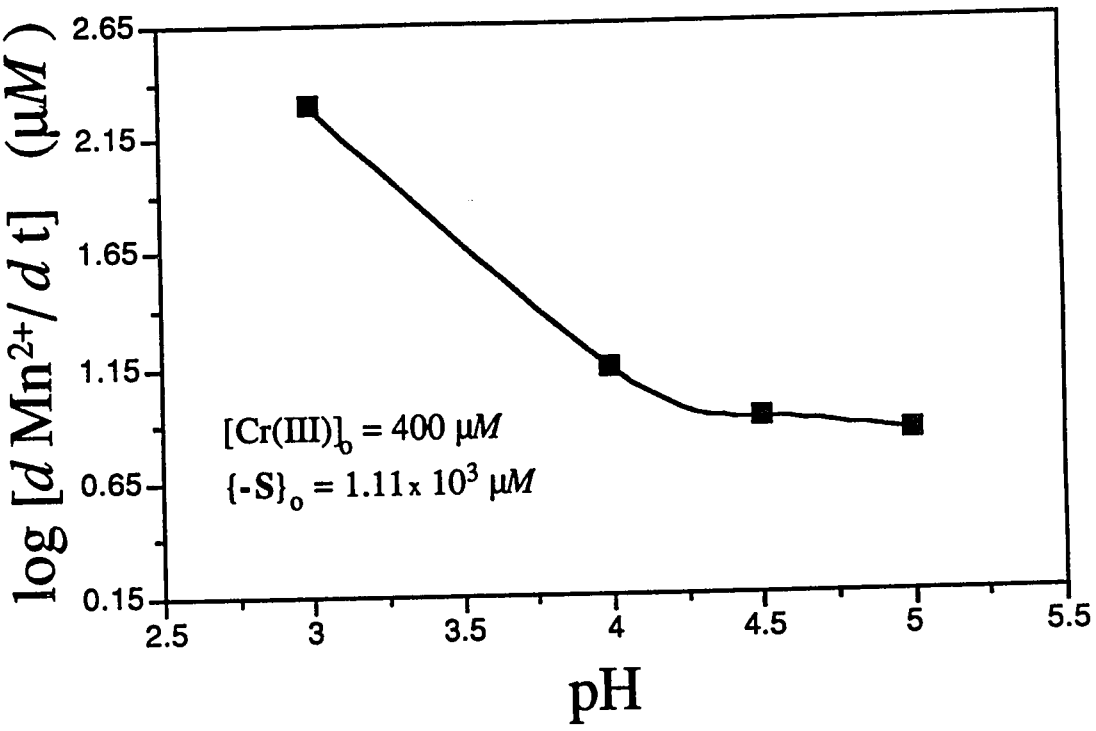

Figure 4-7. The effect of pH on the rate of Mn(II) release to solution, $\{MnO_2\}_o = 0.25$ g L^{-1} and $[Cr(III)]_o = 400$ μM.

4.4.4 Redox Reaction Mechanism

In the Cr(III) oxidation process, a multi-step reaction occurs which consists of: (i) solution Cr(III) migration to the negatively charged MnO_2 surface, (ii) bidentate complexation of Cr(III) with the surface functional groups, (iii) electron transfer between Cr(III) and Mn(IV)/Mn(III), (iv) ligand exchange (i.e., surface oxygen are exchanged to

the newly formed Cr(VI) species), and (v) surface complex bonds are broken releasing the products Mn(II) and Cr(VI) in a stoichiometry of 1.5 : 1 (Chapter 2). The chemical reaction can be described by three steps if one models the electron transfer and ligand exchange reaction as a single process. Thus the Cr(III) oxidation process by δ-MnO_2 would be represented by the following series of reactions. Steps **b** and **c** are depicted as

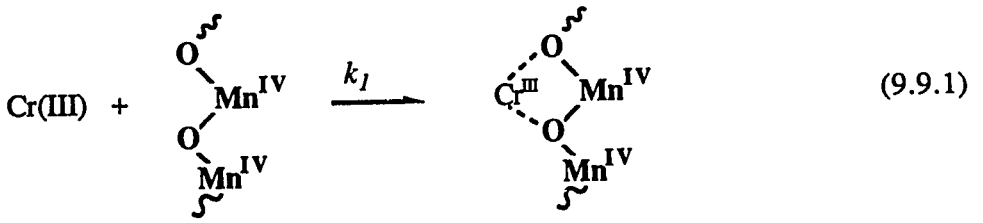

(9.9.1)

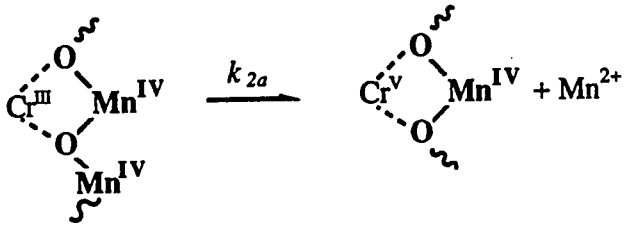

(9.9.2)

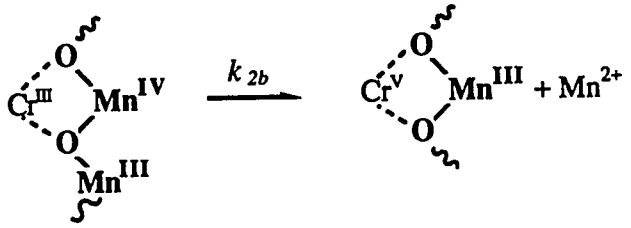

(9.9.3)

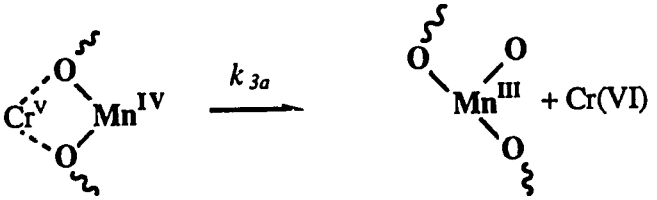

(9.9.4)

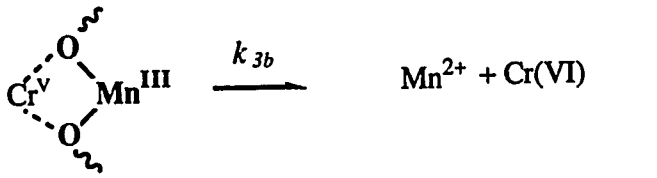

(9.9.5)

two reactions in which (9.9.2) and (9.9.4) would represent the oxide with two adjacent Mn(VI) atoms while (9.9.3) and (9.9.5) would represent a Mn(IV) and Mn(III) adjacent two each other. Thus, a further assumption is that reaction 2 Mn(IV) and 1 Mn(IV) + 1 Mn(III) would react in a similar manner, which would seem valid based on a single electron transfer occurring in the final reaction step--Reaction (9.9.4) and (9.9.5).

Using this reaction sequence (Reaction 9.9), the observed rate coefficients for the release of Mn(II) and Cr(VI) would be composed of multiple reaction steps:

$$d\,[\mathrm{Cr(VI)}] / d\,t = k_3\,\{\mathrm{Cr^{V}\text{-}S}\} \tag{9.10.1}$$

$$= k_2 k_3 \{\mathrm{Cr^{III}\text{-}S}\} \tag{9.10.2}$$

$$= k_1 k_2 k_3 [\mathrm{Cr(III)}]\,\{\mathrm{\text{-}S}\} \tag{9.10.3}$$

$$d\,[\mathrm{Mn^{2+}}] / d\,t = k_2\,\{\mathrm{Cr^{III}\text{-}S}\} + k_3\,\{\mathrm{Cr^{V}\text{-}S}\} \tag{9.11.1}$$

$$= k_1 k_2\,[\mathrm{Cr(III)}]\,[\mathrm{\text{-}S}] + k_1 k_2 k_3 [\mathrm{Cr(III)}][\mathrm{\text{-}S}] \tag{9.11.2}$$

and thus $k_m = k_1 k_2 + k_1 k_2 k_3$, and $k_c = k_1 k_2 k_3$. Because the observed release of Mn(II) was approximately 1.5 greater than for Cr(VI) (i.e., $d\,[\mathrm{Mn^{2+}}] / d\,t = 1.5\, d\,\mathrm{Cr(VI)} / d\,t$) it appears that k_3 is not rate-limiting (i.e., the expected rate proportions for the overall reaction were observed indicating that the rate constant k_3 must not have been appreciably influential or the rates would have deviated from those predicted by the overall reaction stoichiometry). Therefore, a simplifying assumption results from $k_3 >> k_1$ or k_2, which reduces the dependency of the observed release rate coefficients to $k_m = k_1 k_2 + k_1 k_2$ and $k_c = k_1 k_2$. Solving for the individual rate constants yields k_1 and k_2 values of 7.66×10^{-7} and 9.27×10^{-1} μM^{-1} s^{-1}, respectively. Therefore, it appears that the rate limiting step in Cr(III) oxidation by δ-MnO_2 is the surface complexation reaction.

The proposed reaction mechanism for Cr(III) oxidation by δ-MnO_2 and the associated rate constants differ from those hypothesized by Johnson and Xyla (1991) for

Cr(III) oxidation by γ-MnOOH. With a Mn-oxide composed of Mn(III), three electron transfer steps are necessary for the production of Cr(VI) and these authors believed that the rate-limiting step in the redox reaction was the conversion of Cr(IV) to Cr(V)--due to the instability of Cr(IV). However, since Mn(IV) is the predominant species in MnO_2, Cr(III) would undergo an initial two electron transfer step, thus bypassing the intermediate formation of Cr(IV). Therefore, it would be expected that a different reaction mechanism operates with a Mn(IV) containing oxide than one with solely Mn(III). Our results indicate the rate limiting step is the complexation of Cr(III) with δ-MnO_2. This finding contrasts the hypothesis of Manceau and Charlet (1992) that the rate limiting step may have been the electron transfer. It is supported, however, by the well documented slow ligand exchange reactions of Cr(III) (Taube, 1970). Increased pH would facilitate adsorption, in agreement with observed initial oxidation rates (Fendorf and Zasoski, 1992), by increasing the hydrolysis products of Cr(III) (which are known to enhance cationic metal sorption; Schindler and Stumm, 1987) and increased negative surface charge.

Manceau and Charlet (1992) indicated that Cr was coordinated by 4 Mn(VI) atoms. Their conclusions are based on the observed interatomic distances determined by XAFS. However, in conducting XAFS experiments the Cr(III)-MnO_2 systems were quenched by cooling to 77 K; hence, it is possible that intermediate oxidation states, i.e., Cr(IV) or Cr(V), may be present in their systems. The interatomic distances of these species would be shorter than those for Cr(III) and may therefore result in the distances observed by Manceau and Charlet (1992). The results presented in this Chapter do not support the 'molecular mechanism' proposed by these authors for Cr(III) oxidation by δ-MnO_2. They are, however, consistent with the findings reported in Chapter 2 and with data from other investigations on Cr(III) oxidation by Mn-oxides (Fendorf and Zasoski, 1992; Johnson and Xyla, 1991; Eary and Rai, 1987; Amacher and Baker, 1982).

4.5 Conclusions

In this study, we have utilized an EPR-SF technique to investigate the oxidation of Cr(III) by δ-MnO_2. The redox reaction proceeded via a second-order reaction mechanism which was dependent on Cr(III) and MnO_2. The EPR-SF technique allows one to investigate an array of reactions due to the versatile time scale that can be measured. This technique is well suited for a host of reactions involving EPR active constituents and it offers great utility in measuring the reductive dissolution of Mn-oxides. Redox reactions involving Mn-oxides are of great environmental importance because they often affect the speciation and the hazard of many compounds.

4.6 References

Amacher, M.C., and D.E. Baker. 1982. Redox reactions involving chromium, plutonium, and manganese in soils. DE-AS08-77DPO4515. Inst. for Res. on Land and Water Res., Penn State Univ, PA.

Atkinson, P.W. 1985. Physical chemistry. Freeman and Company, New York.

Balistrieri, L.S., and J.W. Murray. 1982. The surface chemistry of δMnO_2 in major ion seawater. *Geochim. Cosmochim. Acta.* **46**: 1041-1052.

Bartlett R.J., and B. James. 1979. Behavior of chromium in soils: III. Oxidation. *J. Environ. Qual.* **8**:31-35.

Bernasconi, C.F. 1976. Relaxation kinetics. Academic Press, New York.

Bleam, W.F, and M.B. McBride. 1986. The chemistry of adsorbed Cu(II) and Mn(II) in aqueous titanium dioxide suspensions. *J. Colloid Interface Sci.* **110**:335-346.

Eary, L.E., and D. Rai. 1987. Kinetics of chromium(III) oxidation to chromium(VI) by reaction with manganese dioxide. *Environ. Sci. Technol.* **21**:1187-1193.

Fendorf, S.E., and R.J. Zasoski. 1992. Chromium(III) oxidation by δ-MnO_2. I: Characterization. *Environ. Sci. Technol.* **26**: 79-85.

Ikeda, T., J. Nakahara, M. Sasaki, and T. Yasunaga. 1984. Kinetic behavior of alkali metal ion on a zeolite 4A surface using the stopped-flow method. *J. Colloid Interface Sci.* **97**: 278-283.

Johnson, C.A., and Xyla, A.G. 1991. The oxidation of chromium(III) to chromium(VI) on the surface of manganate (γ-MnOOH). *Geochim Cosmochim Acta.* **55**:2861-2866.

Klimes, N., G. Lassmann, and B. Ebert. 1980. Time-resolved EPR spectroscopy. Stopped-flow EPR apparatus for biological application. *J. Mag. Res.* **37**:53-59.

Lasaga, A.C. 1981. Rate laws of chemical reactions. pp. 1-68. *In* A.C. Lasaga and R.J. Kirkpatrick (eds.) Kinetics of geochemical processes. Reviews in mineralogy, Vol. 8. Mineral. Soc. Am., Washington D.C.

Manceau, A.A., and L. Charlet. 1992. X-ray absorption spectroscopic study of the sorption of Cr(III) at the oxide-water interface: II. Adsorption, coprecipitation, and surface precipitation on hydrous ferric oxide. *J. Colloid Interface Sci.* **148**: 443-458.

McBride, M.B. 1989. Oxidation of dihydroxybenzenes in aerated aqueous suspensions of birnessite. *Clays Clay Miner* **37**:341-347.

McBride, M.B. 1987. Adsorption and oxidation of phenolic compounds by iron and manganese oxides. *Soil Sci. Soc. Am. J.* **51**:1466-1472.

McBride, M.B. 1982. Hydrolysis and dehydration reactions of exchangeable Cu^{2+} on hectorite. *Clays Clay Miner.* **30**:200-206.

Morgan, J.J., and W. Stumm. 1964. Colloid-chemical properties of manganese dioxide. *J. Colloid Sci.* **19**:347-359.

Murray, J.W. 1974. The surface chemistry of hydrous manganese dioxide. J. Colloid Interface Sci. **46**:357-371.

Murray, J.W. 1975. The interaction of metal ions at the manganese dioxide-solution interface. *Geochim. Cosmochim. Acta* **30**:505-519.

Rai, D., B.M. Sass, and D.A. Moore. 1987. Chromium(III) hydrolysis constants and solubility of chromium(III) hydroxide. *Inorg. Chem.* **26**:345-349.

Schindler, P.W., and W. Stumm. 1987. The surface chemistry of oxides, hydroxides, and oxide minerals. pp.83-110. *In* W. Stumm (ed.) Aquatic surface chemistry. Wiley and Sons, NY.

Stach, J., R. Kirmse, W. Dietzsch, G. Lassmann, V.K. Belyaeva, and I.N. Marov. 1985. Ligand exchange reactions between copper(II)- and nickel(II)-chelates of different sulfur- and selenium-containing ligands. VI [1]. Kinetics of ligand exchange reactions studied by stopped-flow ESR. *Inorgan. Chim. Acta.* **96**:55-59.

Steinfeld, J.E., J.S. Francisco, and W.L. Hase. 1989. Chemical kinetics and dynamics. Prentice Hall, New Jersey.

Taube, H. 1970. Electron transfer reactions of complex ions in solution. Academic Press, New York.

Walker, W.J., C.S. Cronan, H.H. Patterson. 1988. A kinetic study of aluminum adsorption by aluminosilicate clay minerals. *Geochim. Cosmochim. Acta.* **52**:55-62.

Zasoski, R.J., and R.G. Burau. 1988. Sorption and sorptive interactions of cadmium and zinc on hydrous manganese dioxide. *Soil. Sci. Soc. Am. J.* **52**:81-87.

CHAPTER 5

SURFACE PRECIPITATION REACTIONS on OXIDES

5.1 Abstract

Retention of heavy metal ions on solid surfaces is an important process for many catalytic and electrochemical reactions, and for maintaining environmental quality. Determining reaction mechanisms are essential for understanding such processes. However, various mechanisms have been proposed for the sorption of cationic heavy metals on oxide surfaces. In this study, we provide direct evidence using high resolution transmission electron microscopy (HRTEM) for the formation of a surface precipitate prior to bulk solution precipitation. Furthermore, the type of surface present influenced the onset of surface precipitation. At pH 5 and 400 μM Al(III), a surface precipitate was observed on MnO_2 (the birnessite phase), but was not apparent on TiO_2 (the rutile phase). Thus, surface precipitation reactions must be considered in modeling the sorption mechanisms of hydrolyzable metal ions on oxide surfaces.

5.2 Introduction

In the previous chapters the redox reaction between Cr(III) and δ-MnO_2 was investigated, including the novel application of a kinetic technique capable of measuring rapid sorption/desorption and redox reactions. In addition to redox reactions, retention of metal ions at the solid/solution interface is an integral part of colloidal systems which dramatically influences the mobility and toxicity of these species. Furthermore, metal

reactions at surfaces can alter the properties of the sorbent thereby influencing subsequent retention reactions. An example of the importance of such reactions resides in the potential for Cr(III) oxidation by Mn-oxides. If Cr(III) sorbs on a non-redox reactive surface, the potential for oxidation will decrease due to the inability of Cr(III) and Mn(IV)/Mn(II) to complex. Oxidation will also be inhibited if a competing sorptive (e.g., another metal ion or an organic molecule) can bind on the Mn-oxide in a manner which inhibits Cr(III) complexation with the Mn surface. Therefore, it is essential for researchers to determine metal sorption mechanisms to allow an accurate determination of metal speciation and mobility in surficial systems. Accordingly, this and the following chapters will investigate the sorption mechanism of hydrolyzable metal ions on oxide materials and the surface modifications invoked by these processes.

The mechanisms of metal ion retention on colloidal particles are of great interest to colloidal and environmental scientists. The reactivity, high surface area, and coating ability of oxide materials make them very influential in the sorption of metal ions. Numerous thermodynamic approaches have been used in describing metal sorption processes on oxides (Schindler and Stumm, 1987; Hayes and Leckie, 1986; Farley et al., 1985; Davis et al, 1978; Yates et al., 1974; Bowden et al., 1973; James and Healy, 1972a,b; Burube and De Bruyn, 1968a,b). However, these macroscopic approaches do not give direct evidence for the mechanisms of sorption reactions. Spectroscopic studies have also indicated various mechanisms for the sorption of metal ions. Here, we provide direct experimental evidence, using an advanced structure analysis technique, high-resolution transmission electron microscopy (HRTEM), that surface precipitation can occur prior to bulk solution precipitation and is influenced by the type of surface. Consequently, such phenomena need to be considered in catalytic and environmental processes. Mechanistic models proposed to describe cationic metal ion sorption reactions should incorporate surface precipitation reactions rather than modeling the total sorption process as just an isolated-site binding mechanism.

5.3 Materials and Methods

In this study, samples were prepared for HRTEM examination by dispersing powdered oxide, MnO_2 (the birnessite phase) and TiO_2 (the rutile phase), on a holey carbon film supported by a copper mesh grid. The surface areas of the oxides were determined by an EGME method (Heilman et al., 1965) and were 223 $m^2 g^{-1}$ for MnO_2 and 44 $m^2 g^{-1}$ for TiO_2. To have similar surface areas of each oxide, 1 mg TiO_2 and 0.2 mg MnO_2 were dispensed on the grids--at 10 mL solution volumes this resulted in 0.1 g L^{-1} TiO_2 and 0.02 g L^{-1} MnO_2. Reactions were carried out by suspending the oxide-containing grid in a 10 ml solution of 0.1 *M* $NaNO_3$ and 400 μM Al(III) at pH 5, 20°C, and 1 atm pressure. After a 24 h reaction period the grids were removed from solution, rinsed in deionized water, and air dried at 20°C. Results were consistent between replicates and within each sample; thus, the results do not appear to be artifacts of individual preparations. Micrographs illustrated in this paper are representative of each treatment. Further details on the HRTEM imaging technique are given in Chapter 2.

5.4 Results and Discussion

High-resolution TEM images show that the unreacted δ-MnO_2 was partially crystalline (Fig. 5-1a). The characteristic balls of needles of synthetic birnessite are depicted (McKenzie, 1977). Interspersed with amorphous material, there are layers of parallel atomic planes exhibiting severe bends and twists which in some cases form distinctive needle-shaped protrusions. In the unreacted MnO_2, the needles are prominent and clearly delineated. After reaction with Al(III), the basic structure of the δ-MnO_2 appears to be unchanged (Fig. 5-1b). However, under closer inspection a structural alteration of the colloid can be discerned. The characteristic needles are still present, but are no longer as sharply defined as in the unreacted material. An amorphous layer can be seen along the

edges of the MnO_2 particles, filling in between the needles as well as coating the edges. In addition, an overall loss of detail in the image is apparent. This persisted over a range of focus settings bracketing the optimum value, indicating that the electron beam has passed through an incoherently scattering (non-crystalline) layer in addition to the material that was previously being imaged. Therefore, we conclude that an amorphous layer developed after reaction with Al(III) and completely enveloped the MnO_2 surface. The amorphous material is expected to be a precipitate of $Al(OH)_x$, where x denotes molecularity of hydroxyl species associated with each Al; x may vary depending upon the bonding arrangement of Al with the OH groups and with the surface.

The rutile polymorph of TiO_2 is depicted in Fig. 5-2a prior to reaction with Al(III). The micrograph shows that this material is polycrystalline, with distinctly faceted grains of fairly uniform size. Atomic planes are visible within many of the grains, and allow orientation differences between grains to be observed directly. After reacting with Al(III) (Fig. 5-2b), the TiO_2 appears to be unaltered. Even very close inspection of the images does not reveal the formation of a surface precipitate; the crystalline structure remains unchanged, and no amorphous material is present.

The MnO_2 and TiO_2 surfaces differ in their ability to induce surface precipitation in systems of 400 μM Al(III) at pH 5. At pH 5, the MnO_2 (zero point of charge, ZPC =2.8) (Fendorf and Zasoski, 1992) surface was strongly negatively charged while TiO_2 (ZPC=6.7) was positively charged. While the net charge of the TiO_2 is positive, singly coordinated surface function groups should be negatively charged (Hiemstra et al., 1989). The absence of a precipitate on the surface of the TiO_2 discounts the possibility that a colloid acts only as a nucleation site for the formation of a precipitate. The enhancement of precipitation in between the needles of the MnO_2 may be due to electrostatic effects, which are increased due to the close proximity of the charged surfaces, rather than simply an abundance of nucleation sites. Hence, the lack of precipitation in the TiO_2-Al(III) system

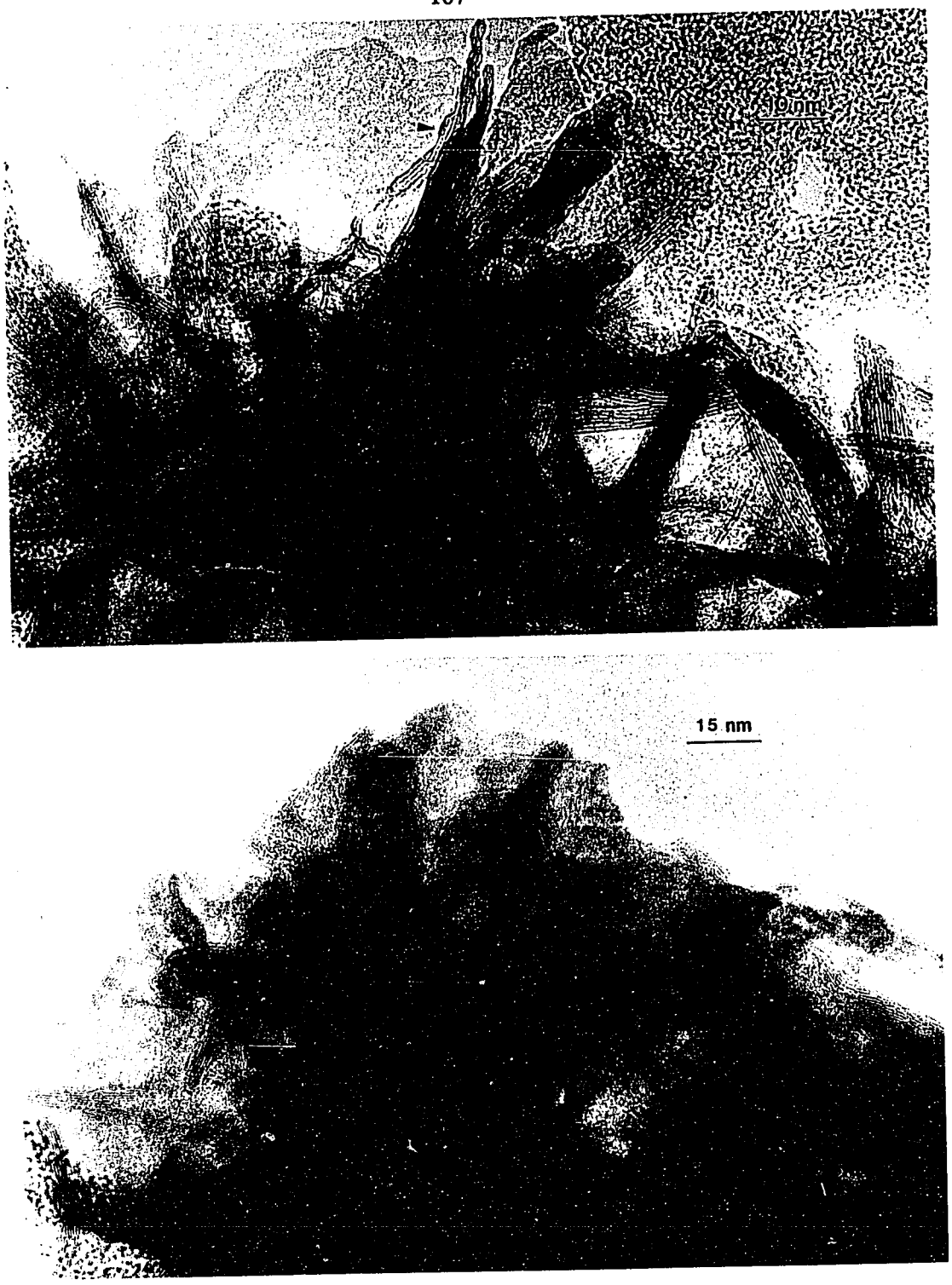

Figure 5-1. High-resolution TEM image of (a) unreacted δ-MnO_2 (birnessite phase) and (b) MnO_2 after reaction with 400 μ*M* Al(III) at pH 5. After MnO_2 was reacted with Al(III), an amorphous layer has enveloped the MnO_2 surface, which is shown by the amorphous material deposited at the edges of the needle structures and a resulting overall loss of detail in the image.

charged. While the net charge of the TiO_2 is positive, singly coordinated surface function groups should be negatively charged (Hiemstra et al., 1989). The absence of a precipitate on the surface of the TiO_2 discounts the possibility that a colloid acts only as a nucleation site for the formation of a precipitate. The enhancement of precipitation in between the needles of the MnO_2 may be due to electrostatic effects, which are increased due to the close proximity of the charged surfaces, rather than simply an abundance of nucleation sites. Hence, the lack of precipitation in the TiO_2-Al(III) system substantiates: (i) that surface precipitation can occur prior to bulk solution precipitation (as exemplified by the MnO_2 system in this study), and (ii) that the properties of the surface do affect the formation of a surface precipitate.

Hypothesized mechanisms for cationic metal sorption on oxide surfaces include: adsorption of the free ion or hydrolysis products (Schindler and Stumm, 1987; Davis et al., 1978; Bowden et al., 1973; Burube and De Bruyn, 1968), adsorption of polymerized species (Brown et al, 1989; Alvarez and Sparks, 1985), surface cluster formation (Bleam and McBride, 1986), and the formation of a surface precipitate (Farley et al., 1985; Crowther et al., 1983; Murray and Dillard, 1979; Tewari and Lee, 1975; James and Healy, 1972). The multi-nuclear metal species observed at lower surface coverage by spectroscopic techniques (Brown et al., 1989; Bleam and McBride, 1986) may be a precursor to the formation of a surface precipitate. The mass action balance proposed by Bleam and McBride (1986) to explain the progression from isolated-site binding to the formation of multi-nuclear sorbed clusters with increases in solution metal concentration may explain the formation of a surface precipitate at the even greater solution metal ion concentrations used in this study. Direct evidence has also been obtained using X-ray photoelectron spectroscopy (XPS) for the formation of a Co(II) surface precipitate on oxide surfaces (Crowther et al., 1983; Tewari and Lee, 1975). Crowther et al. (1983) observed XPS spectra characteristic of $Co(OH)_2$ on the surface of a synthetic birnessite when critical

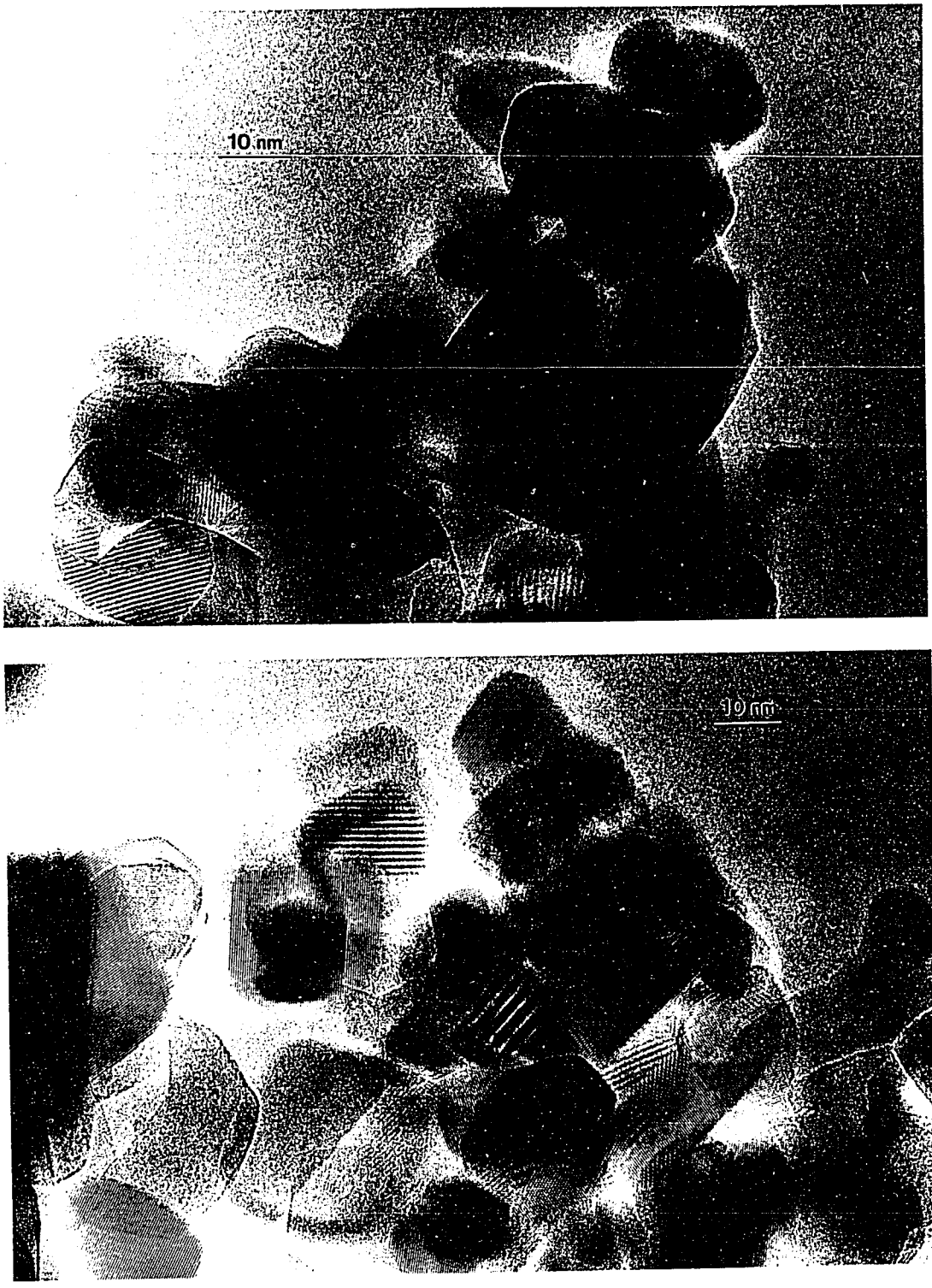

Figure 5-2. High-resolution TEM image of (a) unreacted TiO_2 and (b) TiO_2 after reaction with 400 μM Al(III) at pH 5. The TiO_2 structure appears to be unaltered after reacting with Al(III); no amorphous material is seen on the surface.

pH and Co(II) concentrations were exceeded. However, the results of the XPS studies have been questioned (Brown et al., 1989). As demonstrated here, HRTEM provides a tool for obtaining direct evidence for the formation of a surface precipitate. Clearly, the MnO_2 surface structure underwent an alteration, while the TiO_2 surface appeared unaltered.

The formation of a surface metal precipitate prior to bulk solution precipitation has important implications for environmental quality and catalytic processes. Surface precipitation represents a means of metal removal from solution which will remove greater quantities of the metal ion from the aqueous environment and only dissolution of the precipitate will release the metal to solution. Moreover, the surface precipitate will mask the properties of the original sorbent and only the surface properties of the metal hydroxide will be exhibited by the resulting conglomerated colloid.

5.5 Conclusions

Surface precipitation of Al(III) on δ-MnO_2 was discerned while no surface alteration was observed on TiO_2 at pH 5. The results of this study indicate the need for obtaining direct evidence on surface reactions, and the consideration of sorption mechanisms other than just specific site complexation. The surface structural alterations induced by Al on Mn-oxides may affect potential redox reactions, e.g., Cr(III) oxidation. The redox reactivity of an Al-hydroxide coated Mn-oxide are unknown; in the following chapter the effect of Al on Cr(III) oxidation will be investigated.

5.6 References

Alvarez, R., and D.L. Sparks. 1985. Polymerization of silicate anions in solution at low concentrations. *Nature* **318**:649-651.

Bleam, W.F., and M.B. McBride. 1986. The chemistry of adsorbed Cu(II) and Mn(II) in aqueous titanium dioxide suspensions. *J. Colloid Interface Sci.* **110**: 335-346.

Bowden, J.W., M.C.A. Bolland, A.M. Posner, and J.P. Quirk. 1973. Generalized model for anion and cation adsorption at oxide surfaces. *Nature* **245**:81-83.

Brown, G.E. Jr., G.A. Parks, and C.J. Chisholm-Brause. 1989. In-situ x-ray absorption spectroscopic studies of ions at oxide-water interfaces. *Chimia.* **43**:248-256.

Burube, Y.G., and P.L. De Bruyn. 1968a. Adsorption at the rutile-solution interface. I: Thermodynamic and experimental study. *J. Colloid Interface Sci.* **27**:305-316.

Burube, Y.G., and P.L. De Bruyn. 1968b. Adsorption at the rutile-solution interface. II: Model of the electrochemical double layer. *J. Colloid Interface Sci.* **28**:92-105.

Crowther, D.L., J.G. Dillard, and J.W. Murray. 1983. The mechanism of Co(II) oxidation on synthetic birnessite. *Geochim. Cosmochim. Acta.* **47**:1399-1403.

Davis, J.A., R.O. James, and J.O. Leckie. 1978. Surface ionization and complexation at the oxide/water interface. I.Computation of electrical double layer properties in simple electrolytes. *J. Colloid Interface Sci.* **63**:480-499.

Farley, K.J., D.A. Dzombak, and F.M.M. Morel. 1985. A surface precipitation model for the sorption of cations on metal oxides. *J. Colloid Interface Sci.* **106**:226-242.

Fendorf, S.E., and R.J. Zasoski. 1992. Chromium(III) oxidation by δ-MnO_2. I: Characterization. *Environ. Sci. Technol.* **26**:79-85.

Hayes, K.F., and J.O. Leckie. 1986. Mechanisms of lead ion adsorption at the goethite/water interface. pp.141-158. *In* J.A. Davis and K.F. Hayes (ed.) Geochemical processes at mineral surfaces. ACS Symp. 323. Meet. Am. Chem. Soc., Washington, DC.

Heilman, M.C., D.L. Carter, and C.L. Gonzalez. 1965. The ethylene glycol monoethyl ether (EGME) technique for determing soil-surface area. *Soil Science.* **100**:409-413.

Hiemstra, T., J.C.M. De Wit, and W.H. Van Riemsdijk. 1989. Multisite proton adsorption modeling at the solid/solution interface of (hydr)oxides: A new approach. II. Application to various important (hydr)oxides. *J. Colloid Interface Sci.* **133**:105-117.

James, R.O., and T.W. Healy. 1972a. Adsorption of hydrolyzable metal ions at the oxide-water interface: II. Charge reversal of SiO_2 and TiO_2 colloids by adsorbed Co(II), La(III), and Th(IV) as model systems. *J. Colloid Interface Sci.* **40**:53-65.

James, R.O., and T.W. Healy. 1972b. Adsorption of hydrolyzable metal ions at the oxide-water interface: III. A thermodynamic model of adsorption. *J. Colloid Interface Sci.* 41:65-80.3.

Murray, J.W., and J.G. Dillard, 1979. The oxidation of cobalt(II) adsorbed on manganese dioxide. *Geochim. Cosmochim. Acta.* **43**:781-787.

McKenzie, 1977. Manganese oxides and hydroxides. pp. 181-193. *In* J.B. Dixon (ed.) Minerals in the Soil Environment. Soil Sci. Soc. Am, Madison WI.

Schindler, P.W., and W. Stumm. 1987. The surface chemistry of oxides, hydroxides, and oxide minerals. pp.83-110 *In* W. Stumm (ed.) Aquatic surface chemistry. Wiley and Sons, NY.

Tewari, P.H., and W. Lee. 1975. Adsorption of Co(II) at the oxide-water interface. *J. Colloid Interface Sci.* **52**:77-88.

Yates, D.E., Levine, S., and T.W. Healy. 1974. Site-binding model of the electric double layer at the oxide/water interface. *J.C.S. Faraday* I. **70**:1807-1820.

CHAPTER 6

COMPETING METAL ION INFLUENCES on Cr(III) OXIDATION by δ-MnO_2

6.1 Abstract

The oxidation of Cr(III) to Cr(VI) represents a significant environmental hazard due to the much greater mobility and toxicity of Cr(VI). Despite the importance of Cr(III) oxidation, many factors influencing this important chemical process in soils and waters remain unknown. In this study we investigate the sorption mechanisms of Al, La, Co(II), Cr(VI), and Mn(II) on δ-MnO_2 and their effects on Cr(III) oxidation. Only Al affected the extent of Cr(III) oxidation at pH ≥ 4, and at pH 5 the presence of Al, with 2.84 μmoles Cr(III) initially present, decreased oxidation from 2.80 to 0.28 μmoles Cr(VI). None of the competing ions influenced the degree of oxidation at pH 3. Neither of the oxidation reaction products, Mn(II) and Cr(VI), affected the extent of oxidation. High-resolution transmission electron microscopy (HRTEM) revealed that Al-hydroxide surface clusters formed on δ-MnO_2 at pH 4, thus accounting for the observed sorption and electrophoretic mobility trends and Cr(III) oxidation inhibition. The amorphous $Al(OH)_{3\ (am)}$ surface precipitate occurred at an ion activity product 10^3 times lower than where precipitation in bulk solution occurred. Subsequent to the Al-MnO_2 reaction, introduction of Cr(III) resulted in a semicrystalline Cr-hydroxide phase on the Al reacted δ-MnO_2. The resulting colloid was composed of three distinct metal-(hydr)oxides: δ-MnO_2, Al-, and Cr-hydroxide.

6.2 Introduction

Oxidation-reduction reactions dramatically affect the hazard of many compounds in the environment. Oxide/solution interfaces often influence redox reactions by allowing accelerated redox pathways, e.g., the oxygenation of metal ions (Davies and Morgan, 1989; Wehrli and Stumm, 1989) or by acting as an oxidant or reductant of a species present in soils and waters, e.g., the oxidation of small organic molecules (Stone, 1991; McBride, 1987).

Chromium is a redox reactive metal ion utilized in a variety of industrial processes, which has two stable oxidation states in the surface environment: Cr(III) and Cr(VI). Redox reactions affect the mobility and toxicity of Cr in soils and waters due to the lower toxicity and mobility of Cr(III) than Cr(VI). Chromium(VI) readily penetrates plant and animal cell membranes and is toxic as an oxidizing agent; consequently, the drinking water standard maximum for Cr is 10^{-6} *M* (U.S. EPA, 1984). Concentrations as low as 5 ppm Cr(VI) in soils can be toxic to plants (Turner and Rust, 1971). Furthermore, anionic forms of Cr(VI) predominate under surficial environments, resulting in a greater mobility of this species than Cr(III) due to the abundance of negatively charged surfaces in soils and the low hydroxide solubility of the Cr(III). In contrast to Cr(VI), Cr(III) is not known to be toxic to plants and is essential in human nutrition (Bartlett and James, 1988). However, while Cr(III) was once considered relatively harmless in the environment, the potential for Cr(III) oxidation makes its hazard tantamount to that of Cr(VI).

Manganese oxides are one of the most reactive inorganic species present in surface environments, having pronounced effects on the redox status of soils or sediments (Bartlett, 1986). These oxides are the only known naturally occurring oxidant of Cr(III) at pH < 9 (Eary and Rai, 1987), and readily oxidize this species (Fendorf and Zasoski, 1992; Eary and Rai, 1987; Amacher and Baker, 1982; Bartlett and James, 1979). While recent

investigations have thoroughly assessed Cr(III) oxidation by Mn-oxides in simple systems (Chapter 2; Manceau and Charlet, 1992; Johnson and Xyla, 1991; Eary and Rai, 1987), influences induced by the complex matrices of soils and waters have not been investigated. A knowledge of reaction conditions which affect Cr(III) oxidation is imperative for predicting the fate of Cr in soil and water systems, allowing one to determine conditions which facilitate or retard the formation of Cr(VI).

Although Cr(III) oxidation by Mn-oxides readily occurs, reaction inhibitions have been observed (Fendorf and Zasoski, 1992; Manceau and Charlet; 1992; Johnson and Xyla, 1991; Eary and Rai, 1987; Amacher and Baker, 1982). Determining the source of reaction inhibition is needed to evaluate the hazard of Cr under specific site conditions and could result in the development of a safe disposal or containment method for Cr.

Eary and Rai (1987) found that the solution concentration of Cr(VI) described the rate-limiting factor in Cr(III) oxidation by β-MnO_2 (pyrolusite). At pH values greater than 5, the rate dependence of Cr(III) oxidation by γ-MnOOH was described by the formation of a Cr-hydroxide surface phase which limited the extent and rate of the reaction (Johnson and Xyla, 1991). Amacher and Baker (1982) observed a limitation in Cr(III) oxidation by δ-MnO_2 (birnessite), and hypothesized that Mn(II) produced in the reaction was readsorbing to the surface, thus inhibiting Cr(III) sorption and subsequent oxidation.

Fendorf and Zasoski (1992) also found limited Cr(III) oxidation by δ-MnO_2 at initial Cr(III) concentrations exceeding 77 μM and pH values greater than 4. Thermodynamic calculations based on solution species indicated that the reaction should have proceeded under conditions where it was inhibited. The initial oxidation rate was faster at higher pH values; however, after a rapid initial oxidation rate a dramatic rate decrease occurred, followed by negligible oxidation. A charge reversal of the δ-MnO_2, as determined from electrophoretic mobility (EM), occurred under reaction conditions which inhibited Cr(III) oxidation. Based on our results (Chapter 2) and those of Manceau and

Charlet (1992) the inhibitory mechanism in Cr(III) oxidation by δ-MnO_2 was the formation of a $Cr(OH)_3 \cdot nH_2O$ surface precipitate. The $Cr(OH)_3$ surface precipitate inhibits Cr(III) oxidation by acting as a redox stable sink for Cr(III) and as a physical barrier between solution Cr(III) species and the oxidative Mn surface.

Bidentate inner-sphere complexation of Cr(III) on Mn-oxides is the initial step in the redox reaction. Hence, if a competing sorbate can inhibit Cr(III) complexation on Mn-oxides, the oxidation process may be hindered. Even in a system composed initially only of Cr(III) and MnO_2, at least three solution metal species exist after the conception of the redox reaction: Cr(III), Cr(VI), and Mn(II). Competition from Cr(VI) or Mn(II) could possibly influence the sorption of Cr(III), and hence its oxidation. While Mn-oxides have a strong affinity for various metal ions (Balistrieri, and Murray, 1982; Loganathan et al., 1977; Murray, 1974; Loganathan and Burau, 1973; Morgan and Stumm, 1964), they exhibit competitive sorption among metals (Zasoski and Burau, 1988; Traina and Doner, 1985; Loganathan and Burau, 1973). Thus, in the complex matrices of soil and water systems, various other species may be present which influence Cr(III) oxidation.

Since Cr(III) surface precipitation on Mn-oxides limits the oxidation of this species (Fendorf et al., 1992; Manceau and Charlet, 1992), other hydrolyzable metal ions may also limit oxidation. In addition, metal ions (Me), particularly Al, may form a solid solution with Cr(III)--as observed for Cr(III) and Fe(III) (Sass and Rai, 1987). The formation of a Cr,Me-hydroxide precipitate would limit the aqueous Cr(III) concentration, and if surface associated would form a physical barrier between redox reactive Cr(III) and Mn(IV)/(III) species. This limitation in oxidation may be important in determining the potential for Cr(VI) production from Cr(III), and thus for decreasing the potential hazard of Cr.

Aluminum is common in many soil and water systems and its behavior in the surface environment is similar to that of Cr(III) (Bartlett and James, 1988, 1979). Thus, its effects on Cr(III) oxidation may have significant environmental implications.

Furthermore, another trivalent ion, Fe(III), was observed to completely inhibit Cr(III) oxidation by δ-MnO_2 (Amacher and Baker, 1982).

Because of the potential formation of a solid solution and competitive sorption between Cr(III) and Al, the influences of Al on Cr(III) oxidation were investigated in this study. In addition, to gain further information on the chemical/physical aspects of competitive metal ion sorption on Cr(III) oxidation, a trivalent ion with much different hydrolysis properties than Al, Fe(III), or Cr(III) was studied. Lanthanum has different hydrolysis properties, hydroxide solubility, and ionic radius than either Al, Fe(III), or Cr(III), and thus the influence of La on Cr(III) oxidation was investigated. The first hydrolysis constant ($Me^{3+} + H_2O <--> MeOH^{2+} + H^+$) for La is at least 10^5 times smaller than that of Cr(III), Fe(III), or Al(III) (log $K_{1_{Fe}}$ = -3.05, log $K_{1_{Al}}$ = -4.97, log $K_{1_{Cr}}$ = -4.01, log $K_{1_{La}}$ = -9.06; Baes and Mesmer, 1976). In addition, La is an important simulant for radioactive metals, e.g., Ce, and thus assessing its behavior is of environmental importance.

Determining inhibitory factors in Cr(III) oxidation will enable a more comprehensive assessment of Cr hazards under specified conditions and may allow for the development of a safe disposal technique for Cr. Accordingly, the objectives of this research were to: (i) determine the effects of competing metal ions on Cr(III) oxidation, (ii) assess the inhibitory effects of oxidation products [Cr(VI) and Mn(II)], and (iii) when present, to determine the mechanism of oxidation inhibition.

6.3 Materials and Methods

The mineral birnessite (δ-MnO_2) was prepared by the method of Buser et al. (1954). The specific surface area and zero point of charge (ZPC) were 223 x 10^3 m^2 kg^{-1} and 2.7, respectively. X-ray diffraction studies of the Mn-oxide, using a random powder

mount, produced four broad peaks at 0.73, 0.36, 0.24, and 0.14 nm. These values are characteristic of δ-MnO_2 and are in good agreement with those observed by others (Loganathan and Burau, 1973; Loganathan et al., 1977; Zasoski and Burau, 1988). Electron diffraction patterns confirmed the d spacings obtained from X-ray diffraction, and transmission electron micrographs (TEM) are representative of a synthetic birnessite. All chemicals that were used were reagent grade, and metal solutions were made from their nitrate salts. The MnO_2 was suspended in either 0.1*M* $NaNO_3$ or 0.001*M* $NaNO_3$ at the desired pH value, which was maintained by addition of NaOH or HNO_3.

Chromium(VI) was analyzed by the s-diphenyl carbazide method (Bartlett and James, 1979). Aluminum, Co, La, and total Cr were analyzed using a sequential ICP-optical emission spectrophotometer. Solution Mn was determined by conventional atomic absorption methods using a Perkin Elmer 508 spectrophotometer with an air-acetylene flame. Matrices of standards were matched to equilibrium solutions with either 0.1 or 0.001*M* $NaNO_3$. The sorption and EM measurements were reported earlier (Fendorf, 1990), but are summarized here with a mechanistic evaluation and are supported with direct molecular level information.

6.3.1 Batch Studies

Batch methods were used to obtain steady state data. Supporting electrolytes were 0.1 *M* $NaNO_3$. Twenty five ml of solution and 2.5 mg MnO_2 were placed in 50 ml polyethylene tubes to yield an initial solid concentration of 0.1 g L^{-1}. In noncompetitive sorption studies, the oxide was dispensed to the reaction vessel with the supporting electrolyte, and allowed to hydrate for 24 h. After pH adjustment, the metal ion of interest was added with initial metal concentrations of 303 μ*M*, and the total volume brought to 25

ml. The system was then mixed on a reciprocating shaker for 24 h, filtered through a 0.45 μm pore membrane filter and the effluent was analyzed.

In competitive studies, the competing metal ion was added at an initial concentration of 290 μ*M* to the oxide and supporting electrolyte after hydration. The system was allowed to react for 4 h prior to the addition of Cr(III); Cr(III) was then added and the sample was shaken for 24 h, filtered, and the effluent analyzed. All investigations were carried out over the pH range of 3 to 5 at 25 ±4 °C. A $N_{2\,(g)}$ environment was maintained by initially bubbling $N_{2\,(g)}$ through the suspension and then keeping samples under a $N_{2\,(g)}$ stream. A portion of the final solid material in both competitive and non-competitive studies was removed for TEM analysis.

6.3.2 Electrokinetic Investigations

The electrophoretic mobility (EM) of the MnO_2 particles was measured by conventional procedures using a Ranks Brothers apparatus. Constant ionic strength and adequate current flow were established with 0.1 *M* $NaNO_3$, and a 0.01 *M* Na acetate buffer maintained the pH at the desired level. The acetate buffer did not significantly alter the reactions, using the conditions employed in this study. Samples were prepared for EM measurement using techniques similar to those employed in the non-competitive batch studies, except the EM was measured prior to sample filtration.

6.3.3 Electron Microscopy

High-resolution transmission electron microscopy (HRTEM) was performed on the solid material from systems of Al-MnO_2 and Al-Cr-MnO_2. In this study, micrographs of MnO_2 reacted with 400 μ*M* Al at pH 4 are shown in addition to a series of micrographs of

the Al-Cr-MnO_2 systems. After the batch reactions, electron microscopy was performed by dispensing 0.25 ml of the suspension on a holey carbon film supported by a copper mesh grid. The oxide coated grids were then rinsed with deionized water and air dried in a glass chamber. Following this procedure HRTEM was performed on the specimens at 300 KeV with a Hitachi 9000NAR transmission electron microscope.

6.4 Results

6.4.1 Sorption and Electrokinetics Studies

The sorption of Al, La, and Mn(II) on δ-MnO_2, normalized to the surface area, are shown in Fig. 6-1 with solution pH ranging from 3 to 5. The amount of sorption on δ-MnO_2 decreased in the order: Al > Mn(II) > La. The difference in sorption trends of La and Mn(II) may result from differences in their hydrated ionic radii, valencies, or from the greater intrinsic (chemical) or structural (steric) compatibility of Mn(II) with δ-MnO_2. Neither La nor Mn(II) hydrolyze to an appreciable extent at the pH values employed in this study, but δ-MnO_2 has shown to have a high affinity for its own divalent cation (Morgan and Stumm, 1964). Chromium(VI) predominantly forms the anionic $HCrO_4^-$ species in the pH range studied and very little sorption of Cr(VI) occurred on δ-MnO_2 (Fig. 6-1).

The EM of δ-MnO_2 was measured in the presence of 290 μ*M* Al, La, and Mn(II), added individually in a 0.1*M* $NaNO_3$ solution (Fig. 6-2). Charge reversal of the oxide was induced by all three of these metal ions; however, the trends in EM with and without Mn(II) were very similar. Manganese(II) induced a positive EM on δ-MnO_2 only at the two lowest pH values and the EM became more negative with increased pH.

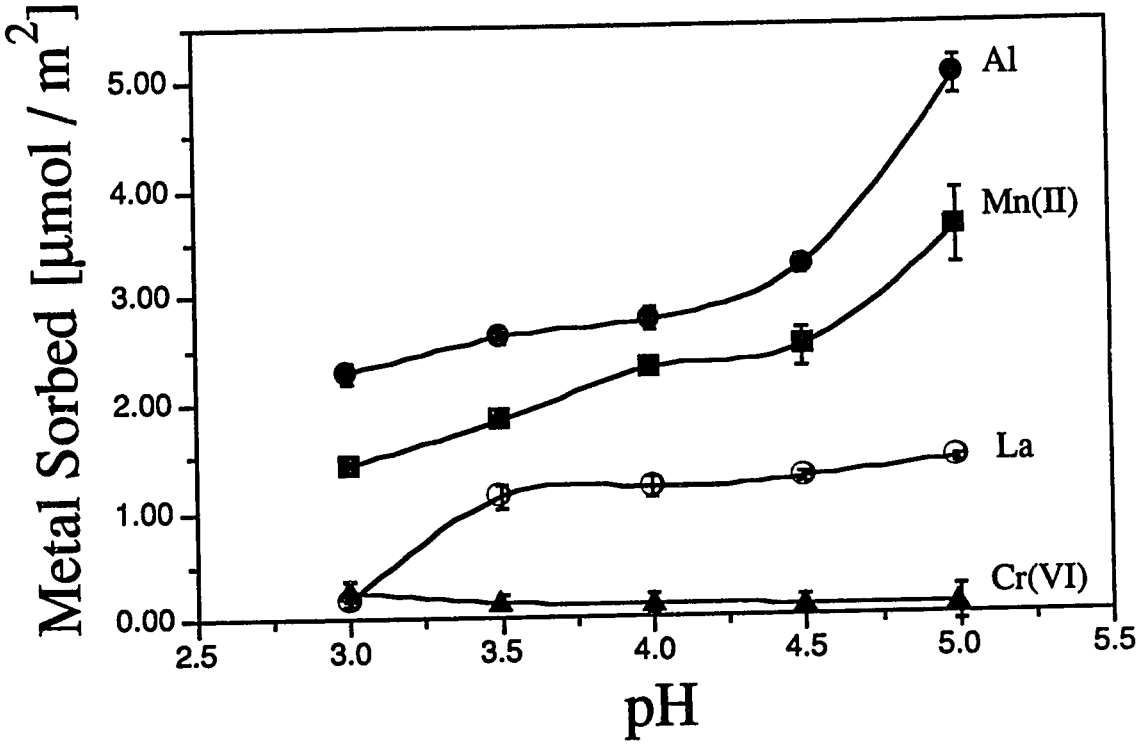

Figure 6-1. The sorption of Al, La, Mn(II), and Cr(VI) on δ-MnO_2 at initial concentrations of 303 μ*M* in a matrix of 0.1 *M* $NaNO_3$ (data from Fendorf, 1990).

Aluminum induced a positive EM on δ-MnO_2 throughout the pH range studied (Fig. 6-2). From pH 3 to 5, there are two relatively linear sections of the pH vs. EM data for the Al-MnO_2 system, similar to the EM of MnO_2 after reaction with Cr(III) (Fendorf and Zasoski, 1992). At pH 4, the positive slope of the EM vs. pH curve dramatically increased in the presence of Al. The point where the slope changes appears to represent the onset of a process which largely alters the surface properties of δ-MnO_2 and possibly a change in the sorption mechanism of Al. Electron micrographs of the MnO_2 surface prior to reaction and after reaction with 400 μ*M* Al at pH 4 indicate a change in the surface structure of the oxide (Fig. 6-3).

The MnO_2 micrographs show that the unreacted material (Fig. 6-3a) was partially crystalline, with the characteristic balls of needles of synthetic birnessite depicted

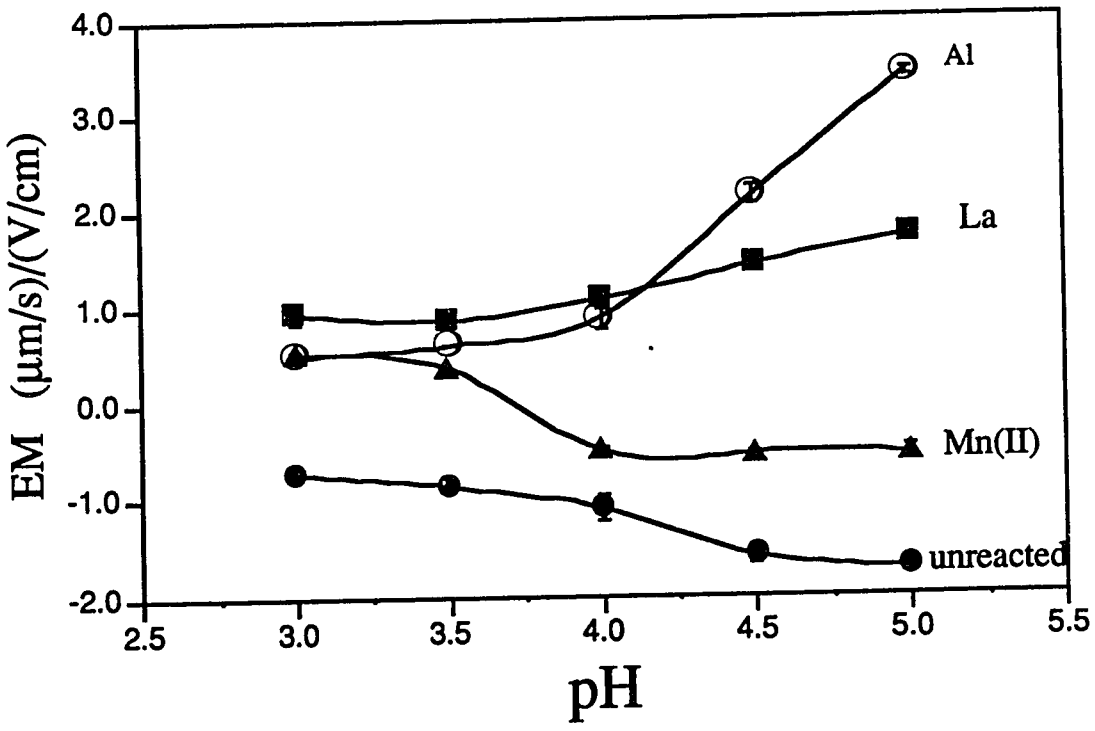

Figure 6-2. Electrophoretic mobility (EM) of δ-MnO_2 after reaction with Al, La, and Mn(II) as a function of solution pH. The initial metal concentration was 303 μ*M* (data from Fendorf, 1990).

(McKenzie, 1977). Interspersed with amorphous material, a crystalline needle-like morphology is characterized by layers of parallel atomic planes exhibiting severe bends and twist forming a dense inner mass with needle shape protrusions. In the unreacted images, the needles are clearly delineated with no amorphous deposition. However, after reacting with Al at pH 4 a distinct change in the surface structure can be discerned. The needle-like morphology is still apparent, but no longer are the crystalline needles clearly delineated and an amorphous layer can be seen on the edges of the δ-MnO_2 particles. Furthermore, a

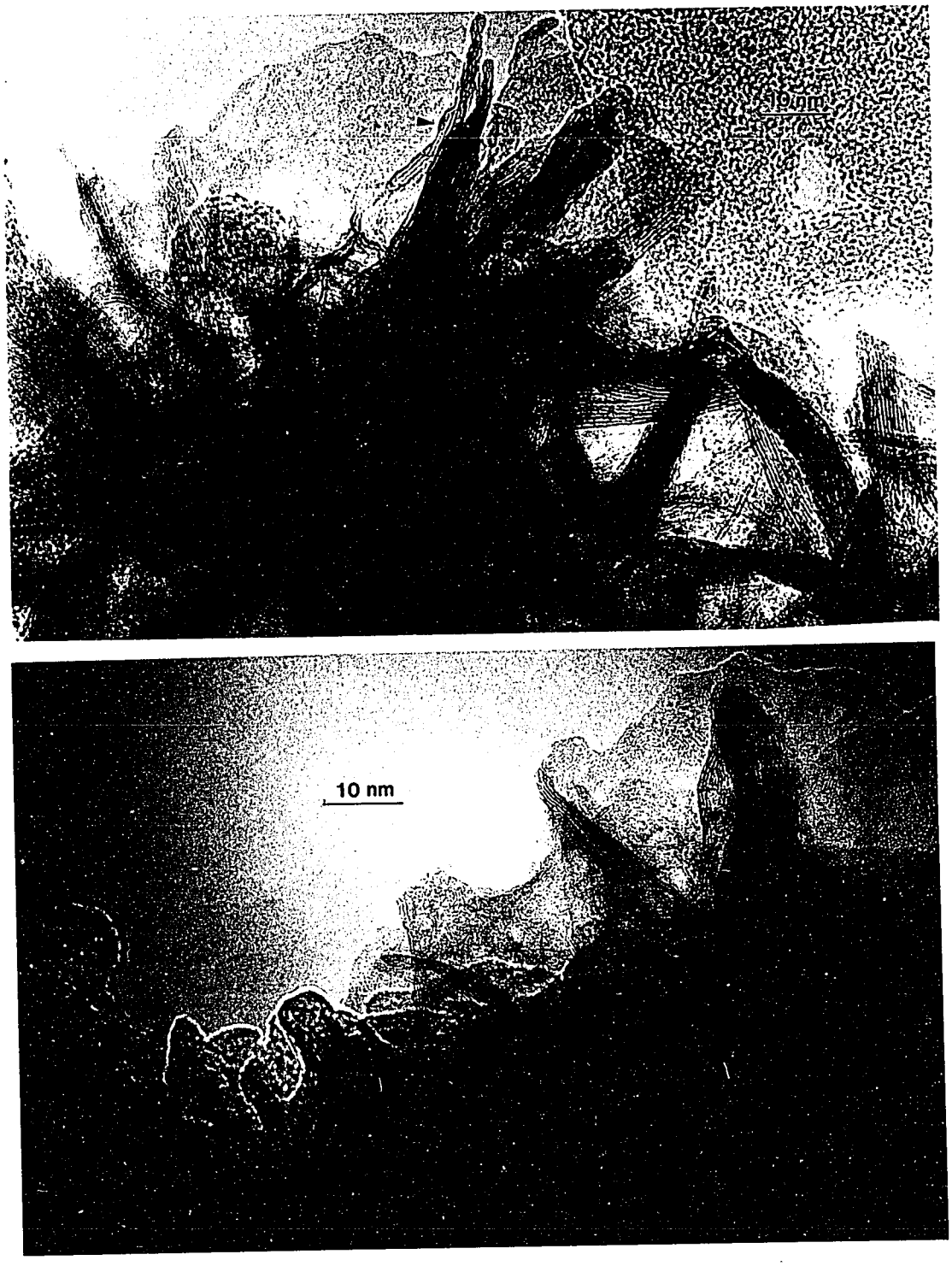

Figure 6-3. High-resolution electron micrograph of δ-MnO_2 (a) prior to reaction and (b) after reaction with 400 μ*M* Al at pH 4. After reaction (b), amorphous deposition of Al-hydroxide is observed.

decrease in the clarity of the image occurred which persisted over a range of focus values bracketing the optimum value indicting that the electron beam was incoherently scattered by an amorphous layer. Although a surface alteration is clearly discerned on the δ-MnO_2 surface at pH 4 (400 μM Al), there are areas in the micrograph which remain clear and do not have amorphous material at their edges. Thus, amorphous $Al(OH)_3$ formed discrete surface deposits (clusters) on the δ-MnO_2 at pH 4. Below pH 4 no surface modification was observed, and at pH 5 (400 μM Al) a more extensive surface deposition was observed in which the δ-MnO_2 surface was entirely enveloped (Chapter 5). Therefore, HRTEM provides direct evidence that at an initial Al concentration of 400 μM, Al-hydroxide surface clusters occur at pH 4 which expand at pH 5 to form a surface precipitate completely enveloping the Mn-oxide.

Lanthanum also induced a positive EM throughout the pH range investigated. However, the La-MnO_2 EM did not undergo an abrupt slope change over the pH range studied. Although the EM of La-MnO_2 was more positive than Al-MnO_2 at pH values below 4 , the EM of Al-MnO_2 significantly surpassed that of La-MnO_2 at pH values greater than 4. Thus, it appears that while the Al sorption mechanism may be altered over the pH range of 3 to 5, the sorption mechanism of La remains consistent throughout the pH range investigated. This would suggest that La binds in an isolated site adsorption mechanism while Al initially adsorbs but begins to nucleate and forms a surface precipitate on δ-MnO_2 with increased pH over the pH range of 3 to 5.

6.4.2 Competing Metal Ion Effects on Cr(III) Oxidation

Previously, the competitive sorption effects of 290 μM Al, La, Co(II), Mn(II) and Cr(VI) on the oxidation of Cr(III) were examined at pH 3 and 5 by reacting these metals with the oxide prior to Cr(III) additions. The results are summarized in Table 6-1.

Table 6-1. Competitive ion effects on Cr(III) oxidation by δ-MnO_2 at pH 3 and 5. The initial concentration of the competing ions was 290 μ*M* (data from Fendorf, 1990).

pH	$Cr(III)_o$[a]	Competing Ion	Cr(VI)[b]	%Oxidation
3	1.83	none	1.69 ± 0.08	92.3
		Mn(II)	1.72 ± 0.05	94.0
		Cr(VI)	1.71 ± 0.28	93.4
		Al(III)	1.70 ± 0.12	93.1
		La(III)	1.68 ± 0.09	91.8
		Co(II)	1.71 ± 0.10	93.8
	15.38	none	9.24 ± 0.50	60.1
		Mn(II)	9.12 ± 0.11	59.3
		Cr(VI)	8.04 ± 0.22	52.3
		Al(III)	9.06 ± 0.65	58.9
		La(III)	8.79 ± 0.37	57.2
		Co(II)	8.58 ± 0.55	55.8
5	1.83	none	1.74 ± 0.029	95.0
		Mn(II)	1.72 ± 0.071	94.0
		Cr(VI)	1.71 ± 0.13	93.2
		Al(III)	0.273 ± 0.020	14.9
		La(III)	1.79 ± 0.093	97.5
		Co(II)	1.70 ± 0.10	93.1
	15.38	none	2.15 ± 0.12	14.0
		Mn(II)	1.74 ± 0.074	11.3
		Cr(VI)	1.83 ± 0.33	11.9
		Al(III)	0.61 ± 0.018	3.98
		La(III)	1.89 ± 0.11	12.3
		Co(II)	1.86 ± 0.062	12.1

[a] Initial Cr(III) level (μmols)
[b] μmols

At pH 3, none of the competing ions affected Cr(III) oxidation, and only Al influenced the degree of oxidation at pH 5. At pH 5, the effect of Al on Cr(III) oxidation was dramatic. Without competing ions present, and at an initial Cr(III) concentration of 73.3 μ*M*, greater than 1.80 μmoles of the initial 1.84 μmoles Cr(III) were oxidized (95%), but only 0.28 μmoles (15%) were oxidized when the Mn-oxide was previously reacted with 290 μ*M* Al. At added Cr(III) concentrations of 615 μ*M* (19.7 μmoles), prior reaction with

290 μM Al decreased the extent of oxidation from 2.76 µmoles (14%) to less than 0.74 µmoles (4%). The chemical equilibrium program MINTEQA2 (Allison et al., 1990) predicted that 290 μM Al would be slightly over-saturated with respect to $Al(OH)_{3\ (am)}$ at pH 5, yet sorption trends (Fig. 6-1) do not shift where precipitation is predicted. Furthermore, solution precipitation was never observed in identical solutions without δ-MnO_2 present. Neither of the reaction products, Mn(II) nor Cr(VI), added prior to Cr(III), affected the extent of oxidation.

To further evaluate the effects of Al on Cr(III) oxidation by MnO_2, more extensive concentration and pH values were investigated. Figure 6-4 illustrates the effects of Al over the pH range of 3 to 5 with Al concentrations of 40, 200, and 400 μM. In Fig. 6-4, the extent of Cr(III) oxidation is shown by the amount of Cr(VI) produced as a function of the saturation index ($SI = \log IAP/K_{sp}$, where IAP is the ion activity product) for $Al(OH)_{3\ (am)}$, calculated using MINTEQA2. Although the formation of crystalline $Al(OH)_3$ phases (e.g., diaspore, boehmite, or gibbsite) would be more thermodynamically favorable, an amorphous surface precipitate was discerned with HRTEM--necessitating employment of $SI_{Al(OH)_{3\ (am)}}$. Although it would be thermodynamically more favorable to form crystalline phases, kinetic constraints often are the controlling factor in precipitation reactions and appear to be the govern the reaction under these conditions.

As the $SI_{Al(OH)_{3\ (am)}}$ increased the extent of oxidation decreased, and as saturation with respect to $Al(OH)_{3\ (am)}$ was approached oxidation became almost negligible (Fig. 6-4). The formation of an Al-hydroxide surface precipitate coincided with Al induced Cr(III) oxidation inhibition (Fig. 6-3); complete Al-hydroxide surface coverage at pH 5 (observed in Chapter 5) almost totally inhibits Cr(III) oxidation. Therefore, $Al(OH)_3$ surface nucleation inhibits Cr(III) oxidation and may explain the sorption and EM of Al.

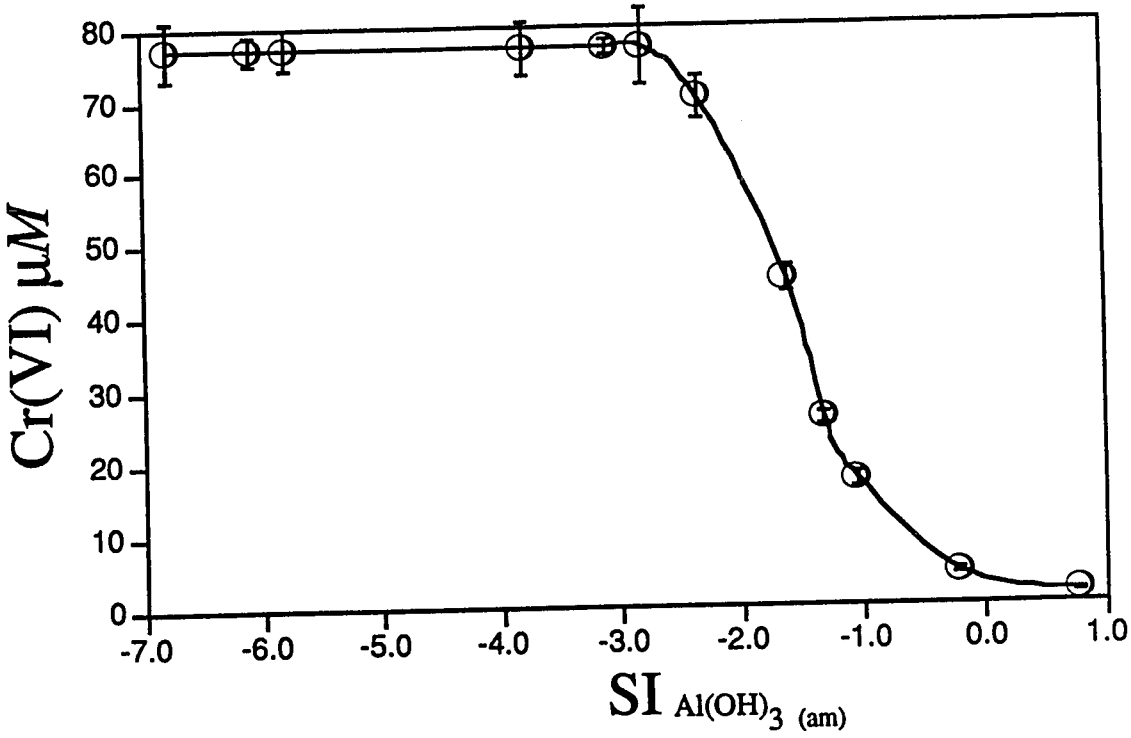

Figure 6-4. The effect of Al on Cr(III) oxidation by δ-MnO_2 expressed by the Cr(VI) production as a function of the saturation index (SI) for $Al(OH)_3$ (am). Reactions were carried out at initial Al concentrations of 40, 200, and 400 μ*M* at pH 3.0, 4.0, 4.5, and 5.0 with 77 μ*M* Cr(III).

6.5 Discussion

6.5.1 Influences of Competing Metal Ions

The oxidation of Cr(III) by δ-MnO_2 is limited at pH ≥ 4 when Cr(III) concentrations exceed 77 μ*M* (Fendorf and Zasoski, 1992). Of the competing ions studied, only Al, at pH ≥ 4, influenced the extent of Cr(III) oxidation, yet at lower pH values Al had no effect (Table 6-1). Thus, Cr(III) and Al induce a limiting factor in the oxidation process which operates only at higher pH values--surface precipitation.

Although colloidal δ-MnO_2 has a strong negative charge in an indifferent electrolyte (e.g., $NaNO_3$), La and Al additions induce a charge reversal (Fig. 6-2) which becomes more positive with increased pH and trivalent metal ion concentrations, as was observed with Cr(III) (Fendorf and Zasoski, 1992). The EM of δ-MnO_2 after reacting with Cr(III) may result from Cr(III), Mn(II), or Cr(VI) (Fendorf and Zasoski, 1992). However, individual studies of Mn(II) and Cr(VI) effects on the EM of δ-MnO_2 (Fig. 6-2) indicate that the trends observed after reaction with Cr(III) are not due to either Mn(II) or Cr(VI). Therefore, Cr(III) rather than oxidation products must be the cause of the EM alteration observed by Fendorf and Zasoski (1992) after δ-MnO_2 was reacted with Cr(III).

The d_3 electron configuration of Cr(III) results in a high ligand stability, with relatively slow ligand exchange reactions, (Taube, 1970) and thus should allow Cr(III) to form the strongest complex with Mn-oxide. This is confirmed by the lack of influence of Al on oxidation at low pH values and by the other metal ions at all pH values studied. Therefore, neither Mn(II) nor La should affect the oxidation of Cr(III) by MnO_2 to any appreciable extent. The results shown in Table 6-1 indicate that indeed this was observed--Cr(III) oxidation was not affected by prior reaction of δ-MnO_2 with Mn(II), Co(II), or La. This conclusion differs from the hypothesis that Mn(II) formed during the oxidation process may compete with Cr(III) for sorption sites. However, it is in agreement with the expected amount of Mn(II) found in solution, and with results from a stirred-flow study (Fendorf and Zasoski, 1992). Since Mn(II) does sorb on δ-MnO_2 (Fig. 6-1), it seems likely that Cr(III) competes with Mn(II) sorption (i.e., Cr(III) displaces Mn(II) from the surface) because the requisite Mn(II) is found in solution following Cr(III) oxidation (Fendorf and Zasoski, 1992; Amacher and Baker, 1982). The lack of competing ion adsorption effects on Cr(III) oxidation further discounts the possibility that Cr(III) must bind in site vacancies to be oxidized. If a competing ion was retained in a site vacancy (and both Mn(II) and Al should be sterically suitable for these sites), it is doubtful that Cr(III) could displace an ion in such a strong coordination environment.

Chromium(VI) forms anionic species under the conditions employed in this study (predominantly $HCrO_4^-$). Unless Cr(VI) is specifically adsorbed to the surface, electrostatic interactions would result in very little adsorption of $HCrO_4^-$. As solution pH increases above the ZPC, the surface becomes more negatively charged. Therefore, neglecting chemical interactions, those based on electrostatics should result in little sorption of Cr(VI) over the pH range of this study. This hypothesis was corroborated as sorption of Cr(VI) was low throughout the pH range studied (Fig. 6-1). Moreover, reacting Cr(VI) with δ-MnO_2 prior to the addition of Cr(III) did not affect the extent of oxidation (Table 6-1).

6.5.2 Inhibitory Mechanisms

Aluminum invoked a strong charge reversal on δ-MnO_2 at pH values greater than 4, as was observed with Cr(III) (Fendorf and Zasoski, 1992). A dramatic change in the slope of the EM vs. pH curve occurred over the pH range of 3 to 5 in the presence of Al. Although La also produced a significant charge reversal, the EM trends did not dramatically shift over the pH range investigated and the extent of Cr(III) oxidation was not altered. The discrepancy between Al and La, that both produced positive EM but had opposite effects on Cr(III) oxidation, may be explained by their differing hydrolysis constants and thus their retention mechanisms.

At higher pH values (pH > 4), the hydrolysis products of either Al or Cr(III) may bind to the oxide surface in a manner which inhibits the redox reaction of MnO_2 and Cr(III). It is well established that the hydrolysis of metal ions relates to their sorption (Schindler and Stumm, 1987), but the results of this study impart another criterion for sorbed Al and Cr(III) at higher pH values: the resulting surface species formed in a manner which limited the redox reaction of Cr(III)-MnO_2. The first hydrolysis constants of Cr(III) and Al are similar while La is smaller by at least 10^5. Chromium(III) oxidation was

correlated with and decreased as conditions favoring the hydrolysis of Al or Cr(III) increased. Table 6-2 lists the proportions of monomeric hydrolysis species present in solution for the various metal ions used, as calculated by MINTEQA2. One should recognize that in the electrified solid/solution interface, solution hydrolysis constants may not be representative of interfacial hydrolysis reactions (James and Healy, 1972). Furthermore, the Me-hydroxide solubility of Al and Cr(III) are much lower than the other metal ions investigated, thus saturation conditions were approached or exceeded for Al- or $Cr(OH)_3$ at the higher pH levels of this study. Although precipitation was never observed in solution under these reaction conditions, Al or Cr-hydroxide surface precipitation may be expected due to surficial influences (due to the lowering of solvation energies resulting from the electrified interface or surface complex). The higher hydroxide solubility of the other metal ions would limit their surface precipitation.

The polymerization of Al species may occur at the higher Al concentrations and pH values investigated; however, we did not attempt to quantitatively address polymerization as free energy of formation data are not known or reliable. In addition, Cr(III) polymerization has been suggested, but recent evidence indicates polynuclear Cr(III) species are insignificant under conditions employed in this study (Rai et al., 1987). Here, MINTEQA2 was used only to predict the proportions of monomeric hydrolysis species. This was conducted to exemplify the correlation between the hydrolysis products and sorption and EM (Table 6-2).

Various researchers have indicated that surface precipitation occurred prior to bulk precipitation (Charlet and Manceau, 1992; Crowther et al., 1982; Murray and Dillard, 1979; Tewari and Lee, 1975; James and Healy, 1972). James and Healy (1972) theorized that incorporating electric field effects imparted by oxide surfaces into the free energies of reaction greatly reduces the Me-hydroxide's solubility in the interfacial region. Based on the surface charge of δ-MnO_2, Murray and Dillard (1979) used the model developed by

James and Healy (1972) and calculated that the solubility of Me-hydroxides was reduced by at least 10^2 in the interfacial region. In this study, it also is apparent that while Cr(III) and Al did not precipitate in solution, surface catalyzed nucleation did occur. Neither La nor Mn(II), however, formed surface precipitates under conditions employed in this study due to their much higher hydroxide solubility.

Table 6-2. Speciation of solution components as a function of pH, calculated by the computer program MINTEQA2.

Component	pH	Percent Species
Al(III)	3	97.4 Al^{3+}
		2.6 $Al(OH)^{+2}$
	4	60.1 Al^{3+}
		39.9 $Al(OH)^{+2}$
	5	7.1 Al^{3+}
		64.2 $Al(OH)^{+2}$
		28.7 $Al(OH)_2^{+}$
La(III)	3-5	100 La^{+3}
Mn(II)	3-5	100 Mn^{+2}
Cr(III)	3	92.3 Cr^{+3}
		7.7 $Cr(OH)^{+2}$
	4	53.9 Cr^{+3}
		45.1 $Cr(OH)^{+2}$
	5	8.9 Cr^{+3}
		74.8 $Cr(OH)^{+2}$
		16.1 $Cr(OH)_2^{+}$
Cr(VI)	3	99.7 $HCrO_4^{-}$
	4	99.4 $HCrO_4^{-}$
	5	96.5 $HCrO_4^{-}$
		3.5 CrO_4^{2-}

Our results (Chapter 2) and those of Manceau and Charlet (1992) indicate that $Cr(OH)_3 \cdot nH_2O$ formed on δ-MnO_2 at pH $\geq$4 and solution Cr(III) concentrations exceeding 400 μM Cr(III). Precipitation was not observed in solution; therefore, the precipitation reaction must have been surface catalyzed. Inner-sphere surface complexation of the Cr(III) forming the surface precipitate would be restricted as oxidation of Cr(III) would occur prior to nucleation. Thus, $Cr(OH)_3$ nucleation must have occurred in the interfacial region but at a distance great enough to prohibit electron transfer between surface Mn(IV)/Mn(III) and interfacial Cr(III). This indicates that electrostatic effects catalyzed the precipitation reactions. Surface precipitation reactions involving Al may be similar to Cr(III) because of similar hydrolysis constants and hydroxide solubility. This postulate is supported by the HRTEM results which show that a surface precipitate of $Al(OH)_3$ also occurred on δ-MnO_2.

The formation of a surface nucleated Me-hydroxide phase would explain the inhibition in Cr(III) oxidation. At higher additions, sorbed Cr and Al were calculated using their hydrated radii and were sufficient to approach and exceed a monolayer coverage. The sharp increase in EM induced by Al (Fig. 6-2) and Cr(III) (Fendorf and Zasoski, 1992) at a critical pH value would represent the onset of Al- or $Cr(OH)_3$ nucleation and resulted in a surface precipitate. The precipitated Al- or $Cr(OH)_3$ would mask the properties of the δ-MnO_2 and inhibit subsequent Cr(III) oxidation. This would account for the changes in the EM and oxidation inhibition induced by Al on δ-MnO_2.

The change in slope of the Al-MnO_2 EM vs. pH curve may be due to a change in the sorption mechanism of Al on δ-MnO_2. Below pH 4, Al may bind at isolated sites, near pH 4, multinuclear species may begin to form with a progression to complete surface precipitation with increased pH values. Bleam and McBride (1986) noted a progression from isolated site binding to the formation of metal-hydroxide surface clusters of Mn(II), and postulated that mass action balance governed the sorption mechanism. Farley et al.

(1985) have thermodynamically modeled the progression from isolated site binding to the formation of surface precipitates. Recent extended X-ray absorption fine structure (EXAFS) spectroscopic studies indicated that Pb(II) and Co(II) form multinuclear species on oxide surfaces at about 10% surface coverage (Brown et al., 1989), and Cr(HI) also forms multinuclear species on hydrous ferric oxide (Charlet and Manceau, 1992) and δ-MnO_2 (Manceau and Charlet, 1992). At pH 5, a surface precipitate of Al-hydroxide has been observed (Chapter 5) and surface clusters were observed in this study at pH 4; therefore, it seems plausible that a progression from isolated site binding at low pH values (pH < 4) to multinuclear species (pH 4) and finally surface precipitation at higher pH values (pH > 4) may occur. The sorption mechanism seems to correlate with the SI for $Al(OH)_{3\ (am)}$ and would account for the observed EM trends and effects on Cr(III) oxidation that were induced by Al. The other ions investigated appear to maintain an isolated site adsorption mechanism throughout the conditions of this study.

Surface precipitation would not be expected to occur at the lowest pH values that were studied, which explains the absence of an Al effect on Cr(III) oxidation at pH < 4 (Table 6-1 and Fig. 6-4). These trends would not be observed for ions which did not form surface precipitates under these reaction conditions. Consequently, of the metal ions investigated, it appears that surface nucleation is necessary to inhibit Cr(III) oxidation as adsorption did not influence the extent of Cr(VI) formation.

6.5.3 Surface Effects of Sorbed Al

Of the metal ions investigated only Al affected the extent of Cr(III) oxidation; the source of inhibition was the formation of an $Al(OH)_{3\ (am)}$ surface precipitate on δ-MnO_2. To further explore the conditions under which this important oxidation inhibition mechanism occurs, and to determine surface modifications induced by this reaction,

HRTEM and energy dispersive X-ray spectroscopy (EDS) were performed on those reaction systems which are depicted in Fig. 6-4.

Competitive adsorption of Al with Cr(III) does not appear to influence the production of Cr(VI), as shown by the lack of influence of Al at lower pH values. Because Al surface precipitation appears to be the controlling factor influencing the oxidation reaction, the production of Cr(VI) as a function of the SI for $Al(OH)_3$ should be useful for ascertaining conditions which invoke surface precipitation. The extent of oxidation began decreasing at a SI of -3 (Fig. 6-4) with a sharp sigmoidal decrease in Cr(VI) production continuing until negligible oxidation occurred at a SI of approximately -0.3. Therefore, it appears that metal-hydroxide nucleation occurred at an IAP 10^3 times lower (SI = -3.0) than would be predicted for $Al(OH)_{3\ (am)}$ in bulk solution. As previously discussed, Murray and Dillard (1979) calculated that solubility constants would be lowered by at least 10^2 in the interfacial region. The macroscopic data (Fig. 6-4) fully agree with the results of Murray and Dillard (1979) and indicate that solubility constants are lowered by as much as 10^3 in the interfacial region of δ-MnO_2.

The dramatic decrease in Al solubility at the solid/solution interface may result from a coprecipitated $Al,Cr(OH)_3$ phase rather than from a pure $Al(OH)_{3\ (am)}$ phase. Sass and Rai (1987) found that $Fe,Cr(OH)_3$ phases readily precipitate and decreased the solubility of Fe by the amount of Cr present, i.e., the hydroxide solubility of Fe(III) is then governed by an IAP which is a function of Fe(III), OH, and Cr(III) activities. However, in the systems which are described in Fig. 6-4, Al was reacted with the δ-MnO_2 prior to the addition of Cr(III). Thus the potential for a Al-Cr solid solution would decrease. Nonetheless, one cannot rule out the possible formation of a coprecipitate, nor can one definitively confirm the presence of a surface precipitate using only a macroscopic analysis. Accordingly, to further examine the previously defined systems we employed electron

microscopy/spectroscopy to explore whether the precipitation of a surface $Al(OH)_{3\ (am)}$ phase at an SI of -3 resulted, and to determine if a coprecipitate of Al-Cr occurred.

At a SI of less than -3.1, HRTEM analysis indicated that no alteration of the δ-MnO_2 surface occurred (Fig. 6-3a). However, as the SI increased above -3.0 a surface alteration can be discerned which progressively becomes more extensive at higher SI values (Fig. 6-5). In the reacted systems (Fig. 6-5), the deposition of an amorphous-microcrystalline layer can be seen at the edges of the crystalline MnO_2 needles. At SI -2.32 (Fig. 6-5a), the deposited material is predominantly amorphous, although there are areas shown which do indicate partial ordering (microcrystalline). The amorphous deposits ranged from less than 1 to greater than 10 nm in thickness. The amorphous material is not uniformly distributed on the Mn-oxides and there are areas which have extensive coverage (layer depths > 10 nm), thus being completely insulated from the solution. Other areas have little amorphous material and would appear to possibly remain reactive with the solution. This would explain the degree of oxidation depicted in Fig. 6-4; oxidation was decreased but still occurred in appreciable amounts. The heavily deposited areas would not be redox reactive with Cr(III), in contrast to the high reactivity of the exposed portions of Mn-oxide.

The HRTEM analysis showed that further increases in SI enhanced the deposition of the new solid phase. Figure 6-5b illustrates that under conditions which represent approximately the half height point (SI = -1.32) on the SI vs Cr(VI) sigmoidal curve (Fig. 6-4) extensive growths of the new material are observed at the MnO_2 edges. In addition, a further decrease in the clarity of the image occurred, but areas remain which have relatively

Figure 6-5. Solid-phase alteration on δ-MnO_2 induced by reaction with 77 μM Cr(III) and (a) 200 μM Al, pH 4 (SI = -2.32), (b) 40 μM Al, pH 4.5 (SI = -1.32), and (c) 400 μM Al, pH 5 (SI = 0.78).


10 nm

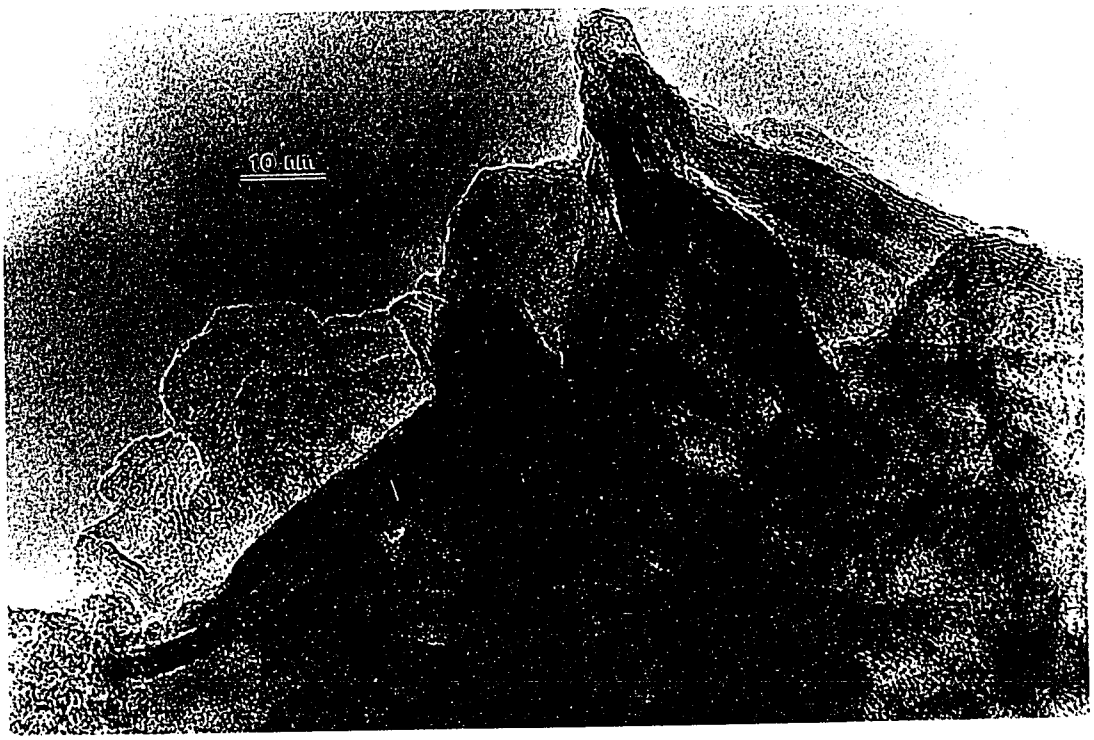
10 nm

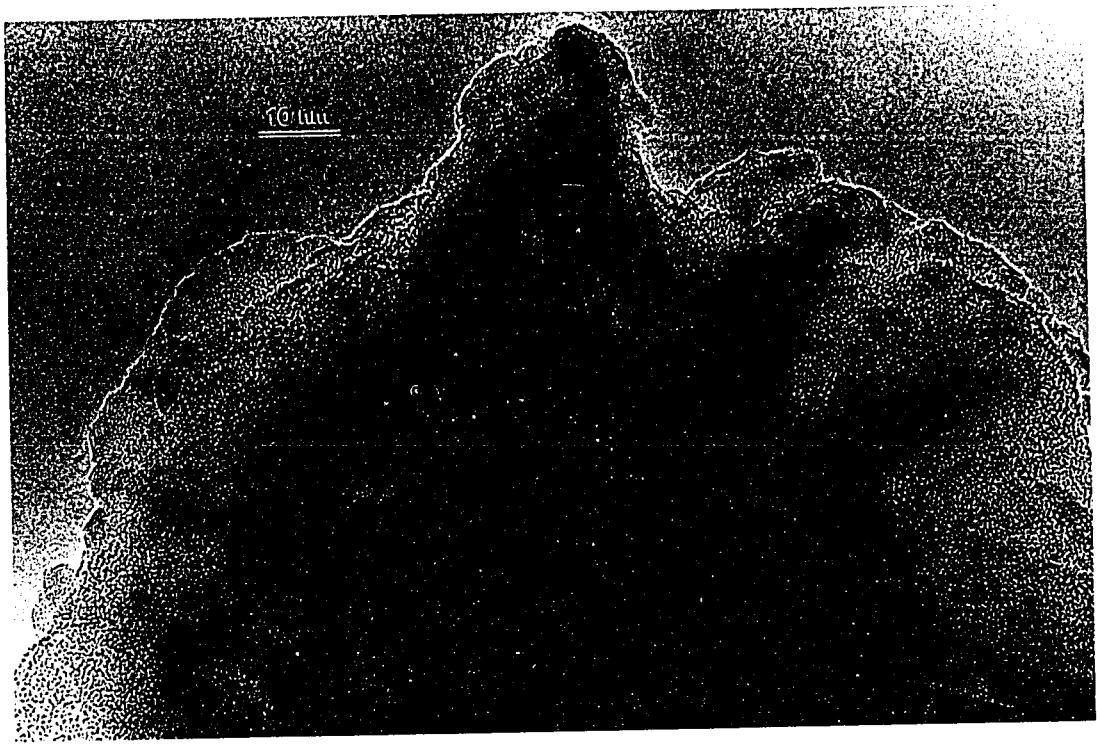
10 μm

Figure 6-6. Low magnification HRTEM image of δ-MnO_2 after reaction with 400 μ*M* Al and 77 μ*M* Cr(III).

little coatings. In contrast, at SI of 0.78 (Fig. 6-5c) a gross change in the particle occurred. The remnant δ-MnO_2 is only partially imaged and there is a vast amount of a newly formed phase which completely encapsulated the original MnO_2. The newly formed amorphous/microcrystalline phase is extensive enough to largely inhibit the imaging of the crystalline MnO_2 needles and would mask its properties from the surrounding solution. Even low magnification images (Fig 6-6) reveal a dramatic alteration in the particle morphology.

The newly deposited material is predominantly amorphous; however, in all of the micrographs there are areas which exhibited atomic ordering (crystallinity). Isolating an area of the solid material depicted in Fig. 6-5b (SI = - 1.32) along with EDS analysis provided evidence for the observed microcrystallinity (Fig. 6-7). In Fig. 6-7 partial atomic

ordering can be clearly seen in the outer 5 nm. A distinct phase boundary occurs between 10 and 20 nm from the surface with the interior phase being almost exclusively amorphous (crystalline MnO_2 needles are out of the plane of view but would reside just below the bottom of the depicted image). Analyzing this phase boundary with a 8 Å EDS probe indicated that the outer semicrystalline area is composed of Cr-hydroxide while the inner band is Al-hydroxide. Therefore, it would appear that other semicrystalline areas of these solids would be due to the deposition of Cr-hydroxide on an Al-hydroxide phase which had

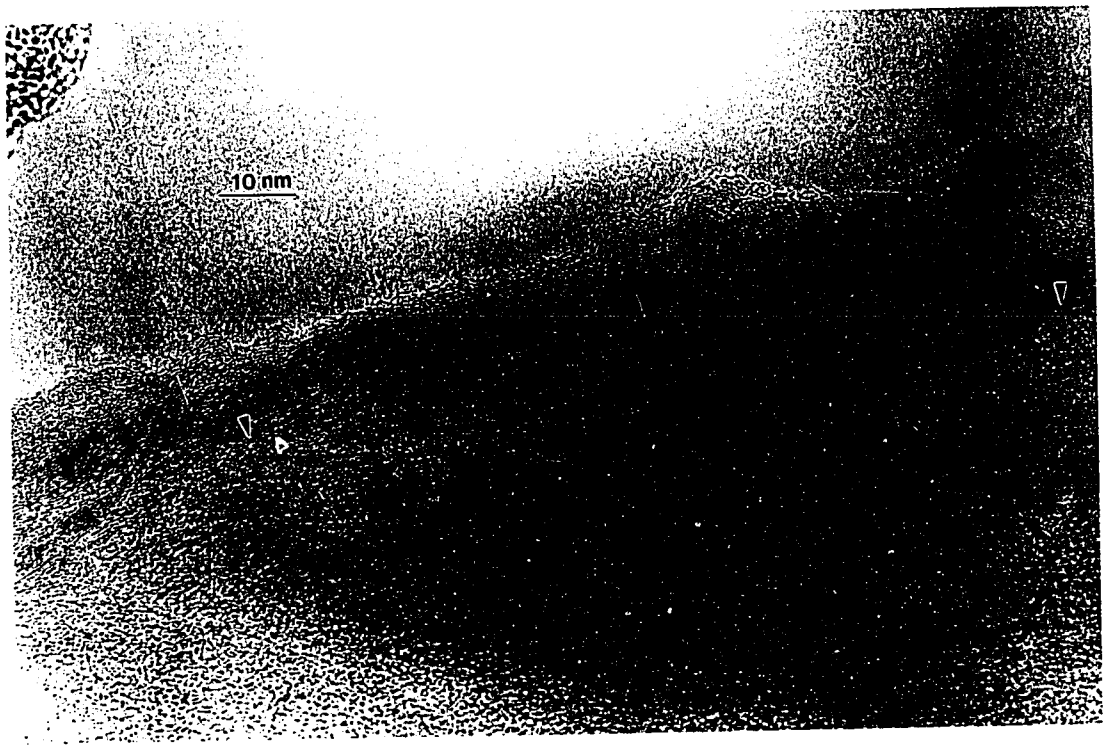

Figure 6-7. Phase boundary (marked by arrows) between the deposited $Al(OH)_3$ (am) material and $Cr(OH)_3 \cdot nH_2O$. The δ-MnO_2 phase is out of the plane of view, but resides slightly below the imaged material.

previously formed. The Cr-hydroxide would thus also account for the areas of microcrystallinity depicted throughout Fig. 6-5.

Although slight amounts of an Al,Cr-hydroxide coprecipitate may have formed, single metal hydroxides appear to be the main materials present in these systems--with distinct phase boundaries separating them. That is not to say that an Al,Cr-hydroxide solid-solution is not possible (or even probable under the appropriate reaction conditions), but rather, the reaction of Al with MnO_2 prior to the introduction of Cr(III) promoted the formation of separate solid phases. Consequently, surface precipitation of Al was possible without the influences of Cr(III). This was followed by the introduction of Cr(III) which formed a second surface precipitate on the Al-hydroxide. This was clearly exemplified by the HRTEM and EDS analyses.

The results of the HRTEM analysis confirm the hypothesis based on the macroscopic trends illustrated in Fig. 6-4. Surface precipitation of $Al(OH)_{3\ (am)}$ occurs at an IAP 10^3 times lower than would be expected for this reaction in solution. In addition, a second surface precipitate composed of a semicrystalline Cr-hydroxide formed on the Al-hydroxide. Thus, the resulting conglomerated colloid is composed of three distinct metal-(hydr)oxide phases: MnO_2, $Al(OH)_{3\ (am)}$, and $Cr(OH)_3 \cdot nH_2O$, with possibly slight amounts of an Al,Cr coprecipitate. At the lower SI where precipitation occurred, the solution would experience physical/chemical attributes of all three phases, while at higher SI properties exerted by the Cr and Al-hydroxides would influence interfacial processes.

6.6 References

Allison, J.D., D.S. Brown, D.S., and K.J. Novo-Gradac. 1990. MINTEQA2/PRODEFA2, A Geochemical Assessment Model for Environmental Systems: Version 3.0. U.S. Environmental Protection Agency: Athens, Georgia.

Amacher, M.C., and D.A. Baker. 1982. Redox reactions involving chromium, plutonium, and manganese in soils, Final report DE-ASO8-77DPO4515; Institute for Research on Land & Water Resources: Penn. State University.

Baes, C.F., and B.E. Mesmer. 1976. The hydrolysis of cations. Wiley and Sons, New York.

Balistrieri, L.S., and J.W. Murray. 1982. The surface chemistry of δMnO_2 in major ion seawater. *Geochim. Cosmochim. Acta.* **46**: 1041-1052.

Bartlett, R.J. 1986. Soil redox behavior. pp. 179-207. *In* D.L. Sparks (ed.) Soil physical chemistry. CRC Press, Boca Raton, FL.

Bartlett, R.J., and J.M. Kimble. 1976. Behavior of chromium in soils: I. Trivalent forms. *J. Environ. Qual.* **5**: 379-382.

Bartlett, R.J., and B.R. James. 1988. Mobility and bioavalability of chromium in soils. pp. 267-303. *In* J.O. Nraigu and E. Nieborer (eds.) Chromium in the Natural and human environments. Wiley and Sons, New York.

Bartlett R.J., and B. James. 1979. Behavior of chromium in soils: III. Oxidation. *J. Environ. Qual.* **8**: 31-35.

Bleam, W.F., and M.B. McBride. 1986. The chemistry of adsorbed Cu(II) and Mn(II) in aqueous titanium dioxide suspensions. *J. Colloid Interface Sci.* **103**: 124-132.

Blok, C., and J.E. DE Bruyn. 1970. The ionic double layer at the Zn/O solution interface: I. Thermodynamic and experimental study. *J. Colloid Interface Sci.* **32**: 518-525.

Brown, G.E., Jr., G.A. Parks, and C.J. Chisholm-Brause. 1989. In-situ x-ray absorption spectroscopic studies of ions at oxide-water interfaces. *Chimia.* **43**: 248-256.

Buser, W., P. Graf, and W. Feitknecht. 1954. Beitrag zur kenntis der mangen (II)-manganit und des δ-MnO_2. Helv. *Chim. Acta.* **37**: 2322-2333.

Charlet, L. and A.A. Manceau. 1992. X-ray absorption spectroscopic study of the sorption of Cr(III) at the oxide-water interface: I. Molecular mechanism of Cr(III) oxidation on Mn oxides. *J. Colloid Interface Sci.* **148**: 425-442.

Crowther, D.L., J.G. Dillard, and J.W. Murray. 1983. The mechanism of Co(II) oxidation on synthetic birnessite. *Geochim. Cosmochim. Acta.* **47**: 1399-1403.

Davies, S.H.R., and J.J. Morgan. 1989. Manganese(II) oxidation kinetics on oxide surfaces. *J. Colloid Interface Sci.* **129**: 63-77.

Eary, L.E., and D. Rai. 1987. Kinetics of chromium(III) oxidation to chromium(VI) by reaction with manganese dioxide. *Environ. Sci. Technol.* **21**:1187-1193.

Farley, K.J., D.A. Dzombak, and F.M.M. Morel. 1985. A surface precipitation model for the sorption of cations on metal oxides. *J. Colloid Interface Sci.* **106**:226-242.

Fendorf, S.E. 1990. Metal ion influences on chromium oxidation by manganese dioxide. M.S. Thesis, University of California, Davis.

Fendorf, S.E., and R.J. Zasoski. 1992. Chromium(III) oxidation by δ-MnO_2: I. Characterization. *Environ. Sci. Technol.* **26**:79-85.

James, R.O., and T.W. Healy. 1972. Adsorption of hydrolyzable metal ions at the oxide-water interface: II. Charge reversal of SiO_2 and TiO_2 colloids by adsorbed Co(II), La, and Th(IV) as model systems. *J. Colloid Interface Sci.* **40**:53-64.

Johnson, C.A., and A.G. Xyla 1991. The oxidation of chromium(III) to chromium(VI) on the surface of manganate (γ-MnOOH). *Geochim Cosmochim Acta.* **55**:2861-2866.

Loganathan, P., and R.G. Burau. 1973. Sorption of heavy metal ions by a hydrous manganese oxide. *Geochim. Cosmochim. Acta.* **37**:1277-1294.

Loganathan, P., R.G. Burau, and D.W. Furstenau. 1977. Influences of pH on the sorption of Co^{2+}, Zn^{2+} and Ca^{2+} by a hydrous manganese oxide. *Soil Sci. Soc. Am. J.* **41**: 57-62.

Manceau, A.A., and L. Charlet. 1992. X-ray absorption spectroscopic study of the sorption of Cr(III) at the oxide-water interface: II. Adsorption, coprecipitation, and surface precipitation on hydrous ferric oxide. *J. Colloid Interface Sci.* **148**: 443-458.

McBride, M.B. 1987. Adsorption and oxidation of phenolic compounds by iron and manganese oxides. *Soil Sci. Soc. Am. J.* **51**: 1466-1472.

McKenzie, 1977. Manganese oxides and hydroxides. pp. 181-193. *In* J.B. Dixon (ed.) Minerals in the soil environment. Soil Sci. Soc. Am, Madison WI.

Morgan, J.J., and W. Stumm. 1964. Colloid-chemical properties of manganese dioxide. *J. Colloid Sci.* **19**:347-359.

Murray, J.W. 1974. The surface chemistry of hydrous manganese oxide. *J. Colloid Interface Sci.* **46**:357-371.

Murray, J.W., and J.G. Dillard. 1979. The oxidation of cobalt(II) adsorbed on manganese dioxide. *Geochim. Cosmochim. Acta.* **43**:781-787.

Rai, D., B.M. Sass, and D.A. Moore. 1987. Chromium(III) hydrolysis constants and solubility of chromium(III) hydroxide. *Inorg. Chem.* **26**:345-349.

Sass, B.M., and D. Rai. 1987. Solubility of amorphous chromium(III)-iron(III) hydroxide solid solutions. *Inorg. Chem.* **26**:2228-2232.

Schindler, P.W., and W. Stumm. 1987. The surface chemistry of oxides, hydroxides, and oxide minerals. pp. 83-110. *In* W. Stumm (ed.) aquatic surface chemistry. Wiley and Sons, New York.

Stone, A.T. 1991. Oxidation and hydrolysis of ionizable organic pollutants at hydrous metal oxide surfaces. pp. 231-254. *In* D.L. Sparks and D.L. Suarez (eds.) Rates of soil chemical processes. Soil Sci. Soc. Am. Special Publication, Madison, WI.

Taube, H. 1970. Electron transfer reactions of complex ions in solution. Academic Press, New York.

Tewari, P.H., and W.J. Lee. 1975. Adsorption of Co(II) at the oxide-water interface. *J. Colloid Interface Sci.* **52**:77-88.

Traina S.J., and H.W. Doner. 1985. Heavy metal induced release of manganese(II) from a hydrous manganese dioxide. *Soil Sci. Soc. Am. J.* **49**:307-313.

Turner, M.A., and R.H. Rust. 1971. Effects of chromium on growth and mineral nutrition of soybeans. Soil Sci. Soc. Am. Proc. **35**:755-758.

U.S. EPA. 1984. Code of federal regulations Title 40, national interim primary drinking water regulations, Part 141. U.S. EPA, Washington, D.C.

Wehrli, B., and W. Stumm. 1989. Vanadyl in natural waters: adsorption and hydrolysis promoted oxygenation. *Geochim. Cosmochim. Acta.* **53**: 69-77.

Zasoski, R.J., and R.G. Burau. 1988. Sorption and sorptive interactions of cadmium and zinc on hydrous manganese dioxide. *Soil. Sci. Soc. Am. J.* **52**:81-87.

CHAPTER 7

X-RAY ABSORPTION FINE STRUCTURE SPECTROSCOPY

7.1 Abstract

Determining the local chemical environment of a species is often necessary to evaluate its reactivity in the environment. However, obtaining direct molecular level information is often problematic and may be possible only with severely invasive techniques, or not possible at all. In this Chapter, a technique is described which is ideally suited for ascertaining the local chemical environment of a particular element in soil, water, or other environmental systems, without the need to subject the sample to a foreign environment: X-ray absorption fine structure spectroscopy (XAFS). Details on the chemical/physical principles of XAFS are given in addition to potential applications of this powerful spectroscopic technique in soil systems.

7.2 Introduction

Determining the behavior of potentially hazardous substances is becoming increasingly important due to concerns over the deterioration of our environment. Reactions at the solid/solution interface are one of the primary determinants in the fate of many hazardous substances. Therefore, determining the chemical state and speciation of solution, surface bound, or solid-state constituents allows one to assess their behavior in the environment. Traditionally, macroscopic approaches have been employed to study

most soil chemical reactions. Although important and meaningful information has been obtained from macroscopic approaches, direct atomic level probing techniques must be utilized to accurately and thoroughly deduce many soil chemical reactions. Furthermore, atomic level information is necessary to determine reaction mechanisms, which are essential for modeling and thus predicting soil chemical reactions. Knowledge of reaction mechanisms may also allow reaction pathways to be controlled, thus facilitating remediation methods and thereby decreasing the potential for environmental deterioration.

Sorption reactions at solid/solution interfaces are important in a variety of processes including soil and water, electrochemical, corrosion, and catalytic. However, despite the importance of these reactions, metal sorption mechanisms remain unresolved. Nevertheless, mechanistic models have been postulated based largely on macroscopic data which attempt to give microscopic representations of the interfacial regions. While differing in their physical conception of the interfacial region, many of these models are mathematically equivalent (Westall and Hohl, 1980). Incorporating direct molecular level evidence into models is needed to accurately represent and predict reactions at the solid/solution interface.

Speciation of solution components and the local chemical environment of solid-state constituents often dictates their reactivity. However, for many systems this information has been difficult to obtain. Fortunately, advancements in atomic level probing techniques are beginning to resolve previous difficulties and offer a promising area of future research in soil chemistry.

An abundance of atomic level probing techniques are currently available. However, many of these techniques are invasive and cause severe damage to a sample since experiments must be performed under adverse conditions (e.g., desiccation, high vacuum, heating, or particle bombardment). Such conditions may yield data that are erroneous due to experimental artifacts or may even preclude experimental analysis. Recent advancements

in surface spectroscopic/microscopic methods have increased one's ability to obtain surface information *in situ*, thus removing artifacts induced by sample preparation or the experimental environment. In addition, more extensive structural and chemical information can be obtained with many of these techniques.

Magnetic and vibrational spectroscopies, such as electron paramagnetic resonance (EPR), nuclear magnetic resonance (NMR), infrared (IR), and Raman spectroscopies, have been prevalent for some time and offer surface and solid state information obtainable under non-invasive sample conditions. Atomic force (AFM) and scanning tunneling microscopies (STM) have recently been developed and offer a host of unique features for investigating surface reactions.

One of the most powerful spectroscopic techniques which has recently been applied to study the atomic structure of natural materials is X-ray absorption fine structure spectroscopy (XAFS). X-ray absorption fine structure spectroscopy allows one to ascertain an array of valuable information on the local chemical/physical environment of an element of interest which includes: valence, chemical state, and structural information on the X-ray absorbing element. With XAFS the local environment of an element is probed allowing its application to the study of materials without long-range order (e.g., solution species or amorphous material).

X-ray absorption spectroscopy has been conducted in the fields of physics, solid-state chemistry, metal supported catalysis, electrochemistry, and a variety of other disciplines for some time. In addition, research utilizing XAFS on earth and marine materials is well established (Calas et al., 1983; Crane, 1981; Arrenhius et al., 1979). Recently, XAFS has been applied to aqueous systems to investigate metal ion reactions at solid/solution interfaces (Charlet and Manceau, 1992; Manceau and Charlet, 1992; Chisholm-Brause et al., 1990a,b; Brown and Parks, 1989; Combes et al., 1989a,b; Hayes et al., 1987).

The utilization of XAFS to soils science will provide a valuable means for obtaining information on the chemical and structural state of soil and water constituents. In fact, the recognition by soils chemists of the many attributes of XAFS has led to the development of a regional committee (NCR 174) for obtaining a dedicated facility at the Advanced Photon Source (Argonne National Laboratory) for soil chemical and mineralogical research with XAFS.

Because XAFS offers a vast amount of information on the chemical and structural environment of species present in soil and water systems, a discussion of its attributes, as well as its limitations, and application in soil chemistry would be useful. Accordingly, it is the objective of this Chapter to familiarize soil chemists with this powerful atomic level probing technique by: (i) giving background theory on the physical/chemical principles of XAFS, (ii) describing experimental details of XAFS, and (iii) showing the application of XAFS in the study of soil chemical reactions.

7.2.1 Atomic Structure

X-ray absorption fine structure spectroscopy involves the interaction of X-ray photons with the core electrons of an atom. Figure 7-1 gives a generic illustration of the electron shells present in an atom. The most inner-shell electron, and the most tightly bound, are the 1s electrons which compose the K shell . Ejection of a 1s electron requires the highest level of energy and leads to K-line emissions, or the X-ray absorption K-edge. The K-edge has been commonly used in the study of first row transition metals. The 2s electrons, L_I shell, are beyond the K shell; L_I-edges are seldom used in XAFS because of the close energy proximity between the L_I and L_{II} edges, as will be further discussed. The 2p orbitals are next in the electron shell build-up, and are split in energy due to differences

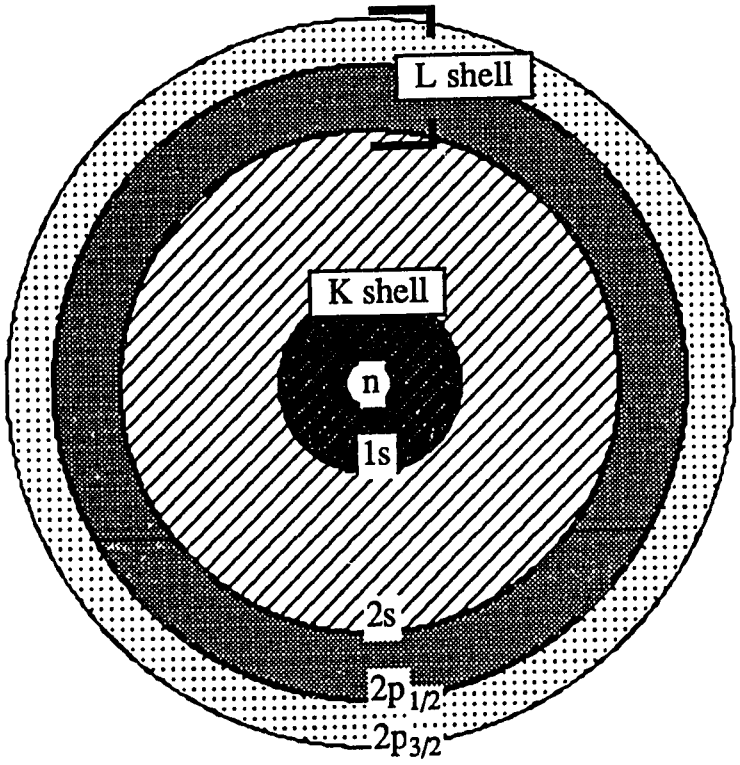

Figure 7-1. A simplified Bohr atom depiction of the inner atomic shells (core electron levels).

in the spin state. The $2p_{1/2}$ followed by the $2p_{3/2}$ electrons occupy the L_{II} and L_{III} shells, respectively. Similar to the L_I-edge, the L_{II}-edge is not frequently used in XAFS. The L_{III}-edge, like the K-edge, is used in XAFS, but primarily for the study of heavier elements in which the energy requirement of 1s electron excitations exceed available energy sources.

7.3 Physical/Chemical Principles of X-ray Absorption

X-rays are highly penetrating to material relative to charged particles due to their low cross-sectional absorption, allowing them to penetrate sample environments commonly

found under natural conditions, e.g., aqueous environments. The extreme intensity of synchrotron X-ray sources (greater than 10^6 times the intensity of conventional X-ray sources, such as stationary and rotating anode X-ray tubes used in X-ray diffractometers) allows experiments to be conducted in an aqueous environment while still obtaining good signal to noise ratios in a relatively short time period--XAFS experiments take minutes instead of days. Thus, XAFS is an *in situ* technique capable of detecting relatively low elemental concentrations necessary for most environmental (soil) samples. However, deep sample penetration makes XAFS inherently non-surface sensitive and resulting data are the average of all atoms of an absorber in the material analyzed (i.e., except under special experimental conditions, XAFS is a bulk analyzing technique). Surface sensitivity can be obtained either by limiting the X-rays to the surface region, e.g., a glancing angle set-up, or by limiting the absorbing species to the surface region.

X-ray absorption spectroscopy is based on the interaction of X-rays with the core electrons of an element. In contrast to other X-ray spectroscopies, such as X-ray photoelectron spectroscopy (XPS), the incident energy is varied with XAFS. When X-ray photons penetrate a sample their energy is consumed by both elastic and inelastic scattering processes. The transmitted intensity, I, is proportional to the original intensity, I_o, and the material thickness, x. The resulting equation relates the exponential intensity loss to the thickness of the material being penetrated:

$$I / I_o = \exp(-\mu x) \tag{7.1}$$

with the proportionality constant μ being the absorption coefficient of the material. The logarithm of Eq. (7.1) is a typical way to display the absorption of X-rays, and it is used in transmission XAFS experiments. The absorption coefficient, μ, describes the ability of the material to absorb X-ray intensity at a particular energy, and it is a function of energy. The absorption coefficient, μ, may also be expressed by a mass absorption coefficient, μ/ρ, to account for the quantity of matter traveled by the photon beam simply by dividing μ by the

material density, ρ. Absorption coefficients are additive, and therefore a material's absorption coefficient is simply the summation of the absorption coefficients of its constituents: $(\mu/\rho)_j = \Sigma (\mu/\rho)_i$.

In order for an atom to absorb the energy of an incident X-ray photon, the atom's electrons must have an empty energy state to occupy after gaining the energy of the photon, or the energy must be great enough to eject the core electron from the atom (Fig. 7-2). Only discrete (quantized) energies are possible for excitation below the binding energy of the electron, while a continuum of states exists for ejected electrons. Electrons which enter vacant valence orbitals (bound states) often give rise to distinct features in the X-ray absorption spectra, thus allowing valence information to be deduced about the absorbing atom. An electron ejected from the atom into the continuum of states is termed a photoelectron. The photon energy required to create a photoelectron is refereed to as the threshold energy (binding energy), and is equal to the absolute value of the binding energy of the electron (Fig 7-2). Thus, as the energy of the incident photons is gradually increased, the absorption (absorption coefficient, μ) generally decreases until a certain critical energy is reached, the binding energy. At the critical energy level absorption (absorption coefficient) abruptly increases by several-fold.

The energy required to eject electrons from core shells decreases with increasing principle quantum number of the shell. That is, the greatest energy is required to eject a K shell (1s) core electron. When sufficient to excite an electron, all the energy of an incident photon is transferred to the absorbing atom; thus, continued increases in the incident energy beyond the binding energy leads to higher photoelectron kinetic energies. The binding energy is determined by the atomic structure and is thus characteristic of an element, which permits element selectivity with XAFS. Values for all elements are tabulated in standard chemistry and physics handbooks. Thus, choosing an appropriate energy window for experiments makes XAFS an inherently element-specific analytical

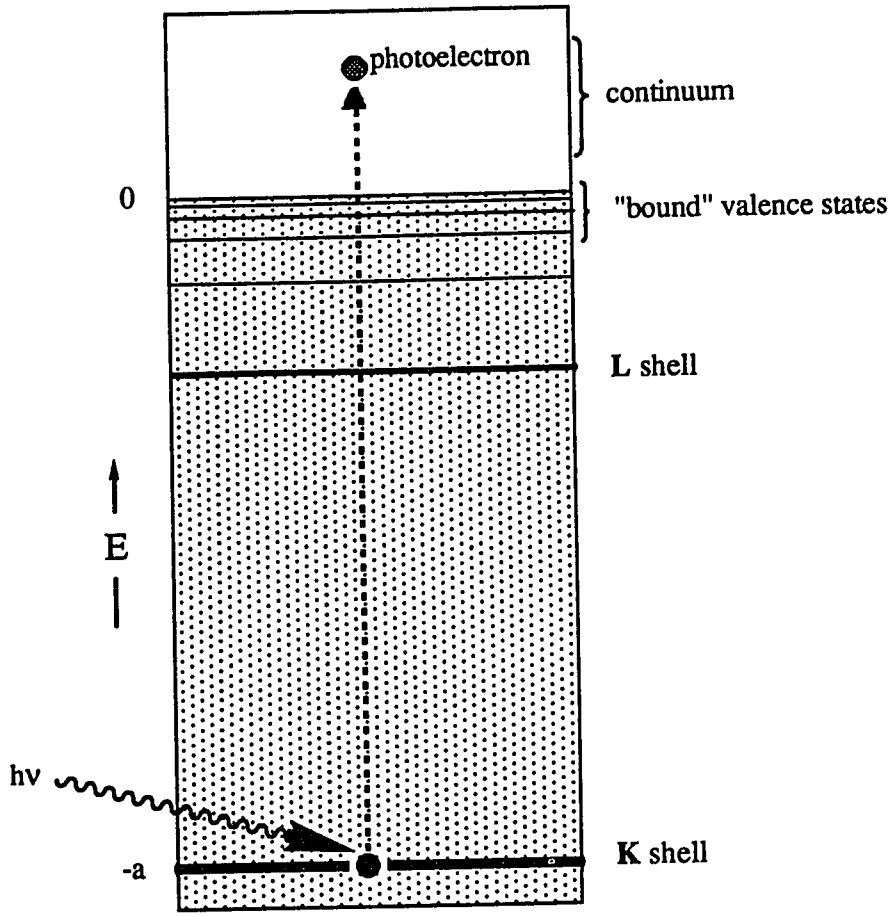

Figure 7-2. Electron shell energy level diagram illustrating a photon (hν) induced excitation of a K shell electron into the continuum--the production of a photoelectron.

technique which allows an element of interest to be selected in a complex matrix--provided other elements do not cause an interference.

Embodied in the X-ray absorption spectrum is both chemical and structural information on the absorbing element. Figure 7-3 illustrates an X-ray absorption spectrum. The fine structure in the X-ray absorption spectrum at energies less than ≈50 eV above the edge is denoted as the X-ray absorption near edge structure (XANES). The XANES features arise from a multitude of chemical and physical phenomena which are starting to be

quantified. These phenomena include multiple scattering, many body interactions, distortion of the excited state wavefunction by the Coulombic field, and other processes. Although an abundance of information resides in the near edge spectra, the underlying phenomena, and consequently a detailed analysis, of this region is much more complex than with EXAFS. Nonetheless, the information contained in XANES has permitted the valence and site coordination of elements present in glasses and minerals to be evaluated

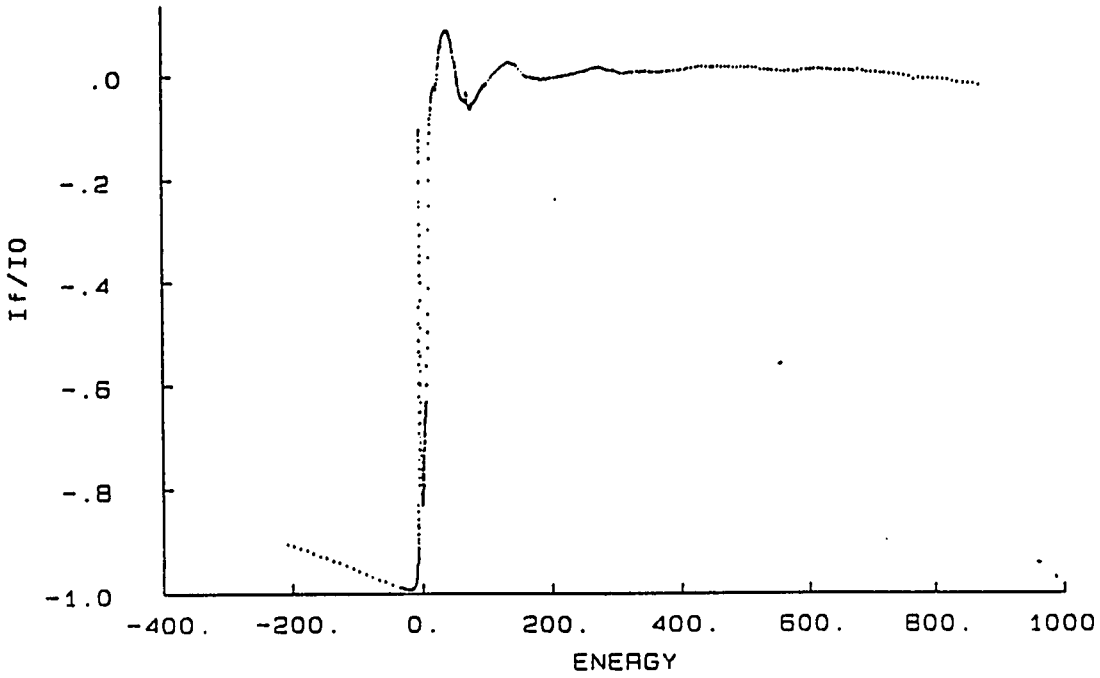

Figure 7-3. The fluorescence X-ray absorption spectrum of $K_2Cr_2O_7$ showing a sharp pre-edge peak (white line) resulting from the s->d transition which results from p-d orbital mixing.

(Waychunas, 1987). In addition, the XANES region often gives a useful 'finger print' of the absorbing elements' chemical state. Thus, a major advantage of XANES is the ability to qualitatively determine the species present, which is especially useful for determining

valences of solid state constituents. Advancements in extracting the wealth of information from XANES are being made, and it appears that future research will benefit significantly from such developments (Durham, 1988).

Beyond the near edge structure is the extended X-ray absorption fine structure (EXAFS). The EXAFS region occurs at energies greater than 50 to 1000 eV above the absorption edge and is characterized by small wiggles or oscillations which provide detailed information as to the number of nearest neighbors (coordination number) and their distances from the absorber (central atom). The oscillations are produced from the interaction (scattering) of the photoelectron wave with the neighboring atoms of the central absorber. Hence, encoded in these oscillations is a detailed mapping of the type and location of the neighboring atoms surrounding the absorbing element, thus giving the local structural environment of the material.

The oscillatory function in EXAFS arises from the dependence of X-ray absorption on the final state of the photoelectron. In quantum theory, the photoelectron can be represented by a spherical wave pattern. The probability of an X-ray photon absorbing a core electron depends on the initial and final state of the electron. The initial state is the localized core level corresponding to the absorption edge. For the elements heavier than He, the initial energy state is not appreciably influenced by the location of the atom--whether it is isolated or coordinated by other atoms. The final state is the ejected photoelectron, which can be represented as an outgoing spherical wave originating from the X-ray absorbing atom. When the atom is present in a structural environment, a neighboring atom will back-scatter the outgoing photoelectron, thus producing an

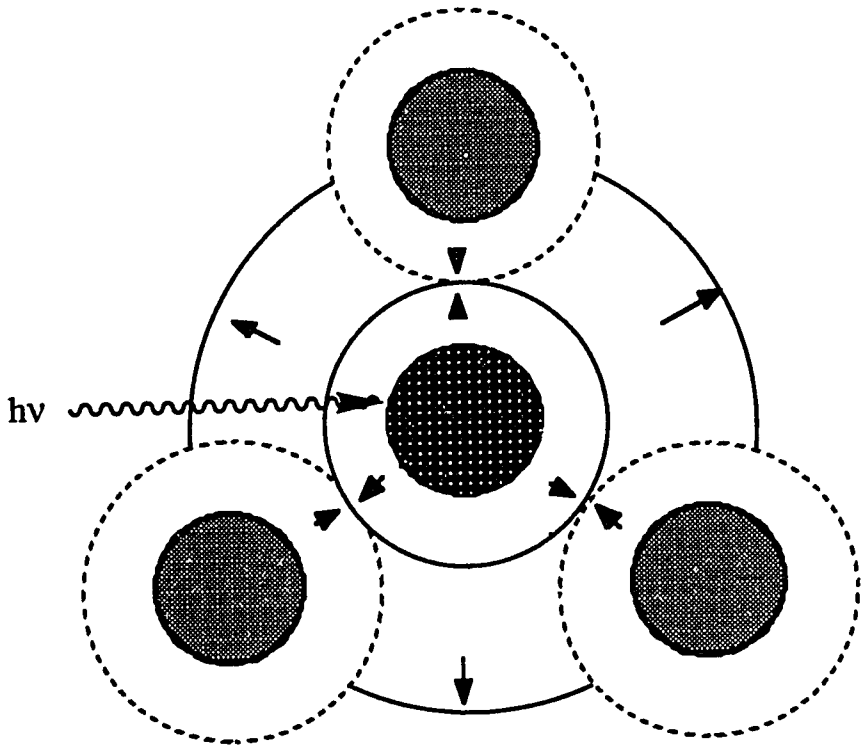

Figure 7-4. Interference effects resulting from the photon generated excitation of the absorber atom (outgoing wave, solid line) and the backscattering from neighboring atoms (incoming wave, dashed line). The interference effects on final state wave function give rise to the EXAFS.

incoming electron wave. The resulting final state is then the sum of the outgoing and all incoming waves from each neighboring atom (Fig. 7-4). This interference between the outgoing and incoming wave produces the sinusoidal variation of the X-ray absorption coefficient, μ, as a function of energy.

Therefore, X-ray absorption is a function of the binding energy and the outward-moving spherical waves interference effects with neighboring atoms. An increase in the electron wave amplitude increases absorption, while a decrease in amplitude reduces absorption of the incident X-rays, producing the oscillations observed in the EXAFS

region (Stern, 1974). Thus, while EXAFS is designated a spectroscopy, the primary structural information arises from scattering phenomena. The final state interference effects involving the scattering of the outgoing photoelectrons from neighboring atoms produces the extended X-ray absorption fine structure (EXAFS).

The simplified representation of the phenomena yielding EXAFS has resulted in the *short-range single-electron single-scattering theory* (Stern, 1974). Unlike the XANES region, single scattering of the wave function dominates the final state function which allows one to relatively easily de-convolute the sinusoidal oscillations of EXAFS into useful structural information. Single scattering processes dominate in the EXAFS region because at these energies the mean free path of the photoelectron (IMFP) decreases with increased energy, resulting in the survival of only singly scattered electrons in the final state function. Multiple scattering is apparent in the XANES region due to longer IMFP for the electrons of these energies.

The amplitude of the sinusoidal modulation of μ depends on the type of neighboring atoms and the bonding mechanism. The frequency of the oscillation is related to the distance between the absorbing atom and the neighboring atoms (Sayers et al., 1971). Generally, the multiple- and single-scattering processes are restricted to maximum path lengths of < 1 nm in solids and liquids; therefore, limiting the information to the local environment of the X-ray absorbing atom.

The modulation of the absorption rate in the EXAFS region can be expressed as:

$$\chi(E) = [\mu(E) - \mu_o(E)] / \mu_o(E) \qquad (7.2)$$

normalized to the background absorption rate (μ_o), for energies greater than ≈50 eV. Equation (7.2) expresses the function $\chi(E)$, referred to as the chi function, in terms of the measured $\mu(E)$ (which would be $[I_f/I_o]$ in fluorescence, or $[\ln I_o/I]$ in transmission) for the absorber in the material and $\mu_o(E)$ which physically represents μ for an isolated absorber

atom (i.e., the absorber without any neighboring atoms to invoke scattering of the photoelectron wave). The energy, E, of the χ function must then be converted into the photoelectron wavevector, k, to obtain structural information,

$$k = [(2m / \bar{h}^2) (E-E_0)]^{1/2} \tag{7.3}$$

where $\bar{h}$ is Plank's constant divided by 2π, and m is the mass of an electron. Transforming χ into k space results in $\chi(k)$ and gives rise to the structural information embodied in the EXAFS spectra;

$$\chi(k) = \sum_i (Ni\ S_i(k)\ F_j(k) [\exp(-2\sigma_j^2 k^2)][\exp(-2r_j / \lambda_j] * \left\{ \frac{\sin(2kr_j + \phi_{ij}(k)}{k\, r_j^2} \right\} \tag{7.4}$$

where Ni is the effective coordination number (CN) of the absorber in the i^{th} shell. An EXAFS function in k space is illustrated in Fig. 7-5a. The sum of Eq. (7.4) is taken over the atoms at a distance r_i for the absorbing atom, and thus one wishes to separate the contributions from each shell i which contribute to this function. The total phase shift, $\phi_{ij}(k)$, is due to twice the coulombic interaction of the absorber and once from that of the backscattering atom. This is due to the photoelectron experiencing the central atom phase shift twice, once going out and once coming back. However, it only experiences the neighboring atom phase shift once by propagating from the absorbing atom to the neighboring atoms and back to the absorber. The k dependence of the neighboring atom backscattering amplitude is represented by $F_j(k)$ which is determined by the potential of the backscattering atom.

In addition to the production of a photoelectron, X-ray absorption can also excite collective electron excitation processes. The corresponding energy dependent amplitude reduction factor, $S_i(k)$, accounts for these multiple electron excitation processes. This term is the only EXAFS amplitude term which is particularly dependent on the absorber; a

more extensive discussion on its effect on the EXAFS envelope is given by Stern et al. (1980). A second amplitude reduction factor , exp ($-2r_j / \lambda_j$), accounts for inelastic losses in the scattering process. This reduction factor results from the excited state having a finite lifetime, which occurs from the photoelectron giving up energy to other processes (e.g., plasmon oscillation and Auger electrons) and from the core-hole decay. If the core-hole decays before the return of the photoelectron, coherent interference of the reflected wave with the outgoing wave will be prevented. The Debye-Waller factor, σ_j , accounts for thermal harmonic vibrations and static disorder, and is usually treated with a Gaussian pair distribution. Each EXAFS wave is thus determined by the back scattering amplitude ($N_j F_j(k)$), modified by the reduction factors $S_i(k)$, exp ($-2\sigma_j^2 k^2$), and exp($-2r_j / \lambda_j$), the $1/k\, r_j^2$ distance dependence, the sinusoidal oscillation which is a function of interatomic distances ($2k\, r_j$), and the phase shift $\phi_{ij}(k)$ (Stern, 1988).

The sinusoidal oscillations in an EXAFS spectra are caused by the interference $\sin(2k\, r)$ term with a frequency of 2r in k space. The higher the oscillation frequency, the larger the distance r. The EXAFS amplitude is reduced by ($1 / r^2$), implying that the larger the distance, the weaker the signal (assuming all other parameters are constant). The phase shifts are unique only if the threshold energy, E_o, is specified. Changing E_o will change the momentum k and thus the phase shift function, $\phi(k)$. For fitting experimental data based on an empirical E_o with theoretical phase shifts, or those derived from model compounds, E_o must be allowed to vary. This also adds to the removal of small but significant bonding effects resulting from electronic configurations and atomic charges (Lee and Beni, 1977).

Multiple scattering is significant if atoms are in a collinear array and is a prominent contributor in the XANES region. Here, the outgoing photoelectron is 'forward-scattered' by the intervening atom, enhancing the amplitude. However, the *single-electron single-scattering* theory of EXAFS uses the fact that in most cases multiple scattering is not

important at the higher energies of the EXAFS region where electron mean free paths decrease (Sayers et al., 1971). Generally, multiple scattering processes can be described by adding all scattering paths that originate and terminate at the absorbing atom. These processes are described by sin ($2k\,r_{eff}$), with $2r_{eff}$ being the total scattering path length which is much larger than that of the direct backscattering from the nearest neighbors. Therefore, multiple scattering will give rise to rapidly oscillatory waves in k space which tend to cancel. In addition, these waves are significantly attenuated by the large scattering path lengths, making it relatively noninfluential compared to direct backscattering.

Once an atomic excitation has occurred, two paths are possible for atomic relaxation: production of fluorescence X-rays or Auger electrons. The decay of a higher shell electron to the core hole results in X-ray fluorescence. The energy of the fluorescent radiation is simply the energy difference between the shells and is characteristic of the absorbing atom. The fluorescence yield (the probability of radiative emission) increases monotonically as a function of the atomic number (Z), and is more dominant for K-line emissions than higher line emissions (e.g., L emissions). Thus, while measuring the transmitted X-ray beam is one means for conducting XAFS, it is also possible to monitor a phenomenon related to the absorption of the incident energy.

Detection of the fluorescence X-rays or Auger electrons, resulting from the production of core holes, is a viable means for measuring X-ray absorption, but fluorescence intensity is proportional to μ only when the material has dilute concentrations of the absorber . Because many of the elements of interest in soils are at relatively low concentrations and certainly not in a homogenous chemical state, monitoring the fluorescence X-ray production results in far better signal/noise (S/N) than simply the transmitted beam would produce. This results because in fluorescence the undesirable comparison of two large numbers is avoided (i.e., when the absorbance is low I and I_o

may be almost equal), which enhances signal to noise ratios (S/N) relative to transmission experiments (Heald, 1988).

The fluorescence X-rays are related to the core hole production by

$$I_f / I_o = \mu x \tag{7.5}$$

where I_f is the resulting fluorescence X-ray intensity. While the fluorescence intensity is related to the X-ray absorption, it is a consequence of the core hole production and therefore the exponential decay term is not present in Eq. (7.5). In contrast to transmission mode, in fluorescence detection μ increases above and below the absorption edge with increasing energy.

An X-ray absorption spectrum measured in fluorescence mode is illustrated in Figure 7-3. Two general regions of the spectra are important to note, the pre- and post-edge. The pre-edge is dominated by a relatively smooth change in increase in μ. However, as the energy increases and nears the core electron binding energy, excitation of the core electron by transitions to bound empty orbital states may occur. This results in pronounced pre-edge and edge peaks which are often termed 'white lines' in reference to early studies in which these intense transitions resulted in white lines on the film recorder. Such transitions give information as to the valence state and site environment of the absorber. Figure 3 exemplifies such a feature for Cr(VI); in contrast, no such pre-edge feature is observed for Cr(III) materials. The sharp pre-edge peak arises from the 1s->3d transition, and is a finger print for the presence of Cr(VI). Although the 1s->3d transition is dipole forbidden, mixing of d-p states in tetrahedral coordinated Cr(VI) results in the observed transition. Thus, white line intensities give electronic information on the valence and electron symmetries; the lower symmetry (tetrahedral) and higher valence of Cr(VI), as opposed to Cr(III), result in the intense white lines that are present. Reference compounds can be used to qualitatively deduce the valence state of an unknown sample, which in some

cases may be sufficiently resolved to allow for quantitative measurements of oxidation states.

The edge-position results from the excitation of a core electron and gives the energy threshold, E_0, which is the minimum energy required to eject the core electron--a characteristic feature identifying an element. Removal of valence electrons, an increased valence state, results in a shift in the core electron energy levels. To compensate for the removal of the valence electrons, the core electrons are drawn closer to the positively charged nucleus, resulting in a greater energy necessary for their excitation. This phenomenon is apparent in the energy position of the absorption edge, which shifts to higher energies with increased valences of the absorbing atom--usually about 2 eV for each gain in valence.

Defining an edge-position remains somewhat arbitrary, and no simple way to determine E_0 is available. In practice, the edge position may be taken as the onset of an edge, the inflection point, the edge peak, or some characteristically identifiable feature in the edge spectrum. However a reference E_0 (the true E_0 is not definable) is chosen, the key thing is to be consistent between samples and standards. The jump height at the absorption edge is a direct consequence of the number of atoms being exited by the X-rays and the ability to experimentally obtain a signal. When analyzing the spectra, the jump height is usually normalized to unity.

7.4 Experimental Considerations

The absorption edge is characteristic of a specific element and a particular core electron level. The K and L_{III} edges have been predominantly used in EXAFS studies. With currently available synchrotron light sources, the binding energy of a core electron must be greater than approximately 5 KeV in order to conduct XAFS analysis *in situ*. In

addition, the energy selection for a core level excitation should preferably be such that another excitation energy is not present within 1 KeV higher (or the EXAFS spectra will be convoluted by the second excitation), and the excitation energy selected should be optimized to allow the greatest energy possible to reside between that excitation edge and any which may reside at lower energies. Consequently, for elements between Ca and Te (Z = 20-52), energies needed to excite the K shell electrons (1s) are usually bracketed. For elements with Z greater than Te (Z>52), the L_{III} ($2p_{3/2}$) electron excitation energy is bracketed. Currently, the energy range needed to conduct XAFS *in situ* is its primary limitation to applications in soils. Elements with atomic number < Ca remain difficult to study with XAFS except under vacuum condition. This limits the study of many important elements present in soils (e.g., Al, Si, Na, S, C, B, etc.).

7.4.1 Transmission Detection

In transmission mode the primary (incident) X-ray beam passes through a detector, usually an ionization chamber, after being monochromatized, and impinges on the sample. The sample is oriented perpendicular to the beam; the beam exits the sample and enters a second detector. The absorption of the X-rays can thus be determined as a function of the incident energy by measuring the incoming X-ray intensity, Io, and the exiting X-ray intensity, I, with the integrated form of Eq. (7.1)

$$\text{Absorption} = \mu x = \ln (Io / I) \qquad (7.6)$$

Currently, one limitation in conducting XAFS studies is the availability of synchrotron facilities (beam time). Therefore, one must optimize the available time. Accordingly, it is beneficial to determine the probable signal output of a sample prior to conducting an experiment, allowing one to optimize sample preparation and decide what is potentially

feasible. By rearranging Eq. (7.6) the probable absorption of a given sample can be determined.

$$\mu x = \Sigma \mu_i x = \Sigma \mu/\rho_i \bullet \rho x = \Sigma \mu/\rho \, W_i \bullet q/A \qquad (7.7)$$

where, W_i is the weight percent of the absorber in the sample, q is the weight of the sample, and A is the sample area exposed to the beam. In Eq. (7.7) W_i, q, and A are all known experimental parameters, and μ/ρ values have been determined and are available in the literature (McMaster et al., 1969).

Transmission experiments directly measure the absorption of the incident X-rays, but are usually not the best choice for dilute samples. Transmission is however a common means for measuring model compounds or primary minerals with a large quantity of the absorbing element (fluorescence is proportional to absorption only for dilute samples). A thin wafer of the material is usually used for these experiments.

7.4.2 Fluorescence Experiments

Fluorescence detection is commonly used for dilute elements in solids of environmental interest for reasons previously addressed. With fluorescence one must be particularly careful to note excitation levels near the fluorescence energy. If an excitation edge, possibly from another element in the sample, is present within ≈1000 eV below the fluorescence energy, considerable measurable signal will be lost to this excitation (i.e., it will not reach the detector, but rather will be adsorbed by this electron excitation). For example, examining Cr on TiO_2 would not be desirable in fluorescence mode as the Cr K_α fluorescence radiation at 5414 eV is absorbed by the Ti 1s excitation, which occurs at 4965 eV, resulting in very little Cr fluorescence intensity.

Another consideration when in fluorescence mode is the selection of a suitable filter. Because the primary X-ray beam may be elastically scattered, in addition to being absorbed by the sample, these photons may reach the fluorescence detector resulting in a high background signal. A filter which absorbs the incident energy but not the fluorescent energy, i.e., having an absorption edge between the two energies, can help to reduce the scattered photons reaching the fluorescence chamber. For K-edges, Z-1 element filters are the common choice, but the Z-1 rule only holds for $23<Z<44$ elements; above Z=44, Z-2 filters are appropriate (Lytle et al., 1984). For Cr analysis in fluorescence mode, V would be the best filter. The incident X-ray energy will vary from 5789 eV (200 eV below the Cr K-edge which occurs at 5989 eV) upward, while the fluorescence energy for detection will result at 5414 eV. The V K-edge is present at 5465, thus being capable of absorbing the elastically scattered $\geq$ 5789 eV incident energy, but not the 5414 fluorescence energy.

Experimental designs for fluorescence detection are somewhat more complex than transmission experiments; however, the increase in signal intensity needed for dilute samples is well worth the effort. In the fluorescence mode the energy deposited by the incident X-rays is remitted monochromatically at a lower energy. Similar to transmission designs, the incoming X-ray intensity, I_o, is detected, but the production of fluorescence X-ray intensity, I_f, is monitored with a second ionization chamber located in front of the sample. This experimental design is usually accomplished by placing the sample at a 45° angle to the beam with the fluorescence detector also located at a 45° angle to the specimen--the fluorescence detector is thus normal to the incident beam. Fluorescence X-rays are emitted approximately equally in all directions; hence, a large angle detector, e.g., a Lytle detector, is employed to optimize obtaining fluoresced X-rays with accompanying Soller slits to reduce scattered primary beam reaching the detector.

The increased signal that results from fluorescence is in part due to total consumption of the incoming X-rays. Consequently, unlike transmission experiments, the

sample should be sufficiently thick to absorb all of the incoming photons. The thickness necessary for total absorption of the incident photons can be ascertained from Eq. (7.7) by rearranging, setting μ equal to 0, and solving for x (sample thickness). Determining the approximate signal which should result from a given sample is slightly more complex than in transmission, and the fluorescence signal is highly dependent on the experimental parameters, e.g., the detector gain, detection efficiency, etc. Here, the attenuation of the incoming X-rays and outgoing fluorescence X-rays must be determined for the sample depth that is probed. Equation (7.8) gives the relation of the incoming incident energy X-rays along with the production and attenuation of the fluorescence X-rays to the final intensity:

$$\frac{I_f}{I_o} = \int_0^{\infty} \mu_j \left(\frac{\mu_i}{\mu_j}\right) (FY)\,(D)\,\{\exp(-a-b)x\}\,dx \qquad (7.8.1)$$

which upon integration yields,

$$\frac{I_f}{I_o} = \left[\frac{F_t \exp(-a-b)x}{-a-b}\right]_0^{\infty} = \frac{F_t}{a+b} \qquad (7.8.2)$$

where,
$a = \mu_j / \cos\theta$
$b = \mu_b / \cos\phi$
θ = the angle of Io to the surface normal (45°)
ϕ= the angle of the detector to the surface normal (45°)
μ = absorption coefficient
μ_i = μ of absorber at incident energy
μ_j = μ of total material at the incident energy
μ_b = μ of total material at fluorescence energy
FY = fluorescence yield
D = the fraction of FY detected (= 4π * fraction aimed at detector)
$F_t = \mu_j * (\mu_i / \mu_j) * FY * D$
x = distance

7.5 Data Collection

The ultimate goal of any experiment is to derive usable information, and while background information and experimental considerations are a necessary part of conducting an experiment, in XAFS one must know what to do with the resulting data. However, first one must optimize data collection so as to facilitate data analysis.

The absorption of X-rays is not monatomic and the spectra may have regions which one wishes to emphasize. Hence, the spectra are not usually collected in equal weighting. That is, the steps between energies along with the integration time at each energy is varied to optimize the desired signal while maintaining the greatest efficiency of photon utilization (because beam time is precious, excess counting time is not a luxury one usually has in conducting XAFS experiments). Typically, the early pre-edge portion are largely spaced and have short integration times. Nearing the edge, the stepping rate is decreased so as to permit resolution of XANES features. With a continued increase in energy the EXAFS oscillations move to longer wavelengths but have less amplitude, resulting in the employment of larger step sizes but also longer integration times.

7.6 EXAFS Data Analysis and Extraction of Structural Parameters

The first steps in data analysis have already been eluded to in the EXAFS section; the $\chi(k)$ function (Eq. (7.5)) must be obtained from the measured absorption data, $\mu(E)$. The absorbance is measured as either $[I_f/I_o]$ or $[\ln I_o/I]$ depending on whether fluorescence or transmission experiments, respectively, were conducted and the spectra is normalized to a unit jump height. The designation for a reference E_o point is then made by taking the inflection point of the absorption edge, which is achieved by noting the edge peak in the derivative spectra. However, this is not the true Eo (zero energy), which remains an unknown quantity.

The next step in the data reduction is to remove the background by fitting the pre-edge region with a polynomial, a line, or a constant which is extrapolated beyond the edge; the fit is then subtracted from the spectra. Next, the absorption coefficient of an isolated absorber atom must be determined--often assumed to be the smooth part of the measured $\mu(E)$ (Lytle et al., 1974) which approximates $\mu_0(E)$ and is subtracted from the spectra to yield a $\Delta\mu(E)$ curve. Generally, a polynomial or combination of polynomials is used to describe the smooth atomic-like absorption beyond the edge. Finally, the spectra are converted from E to k space, Eq (7.4), resulting in the $\chi(k)$ function. The $\chi(k)$ functions amplitude decays with increasing energy above an absorption edge; multiplied (weighting) by some power of k will help to equate the loss in amplitude. This is necessary to prevent the larger amplitude oscillation from dominating smaller ones in determining interatomic distances, which depend on the frequency not the amplitude. Unless one wishes to emphasize a particular region of the XAFS spectrum, obtaining approximately equal amplitude in the spectra is typically most appropriate. Weighting schemes of k^n, with n equal to 1, 2, or 3 have been suggested for backscattering elements with Z>57, Z=36-56, and Z<36, respectively (Teo and Lee, 1979).

Various approaches have traditionally been used for data analysis, e.g., Fourier transform (a theory independent approach) and curve fitting (a theory dependent approach) methods. Presently, all acceptable data analysis approaches use a fitting process of the Fourier filtered spectra. Fourier transformation of the frequency spectrum yields a real space radial structure function (RSF). The peak maxima correspond to atomic distances but are shifted from real values due to the phase shift. Back transforming the spectra into frequency spectrum produces a Fourier filtered spectra. Individual peaks (shells) in the Fourier transformed spectra can be selected and backtransformed to isolate the contribution of single components in the coordination environment of the absorber. The Fourier transformed spectra are then fit by adjusting coordination number (N_i), nearest neighbor distance (R_i), and Debye-Waller factor (σ_i) until the best agreement is obtained between

the predicted and experimental spectra. Phase shift and amplitude parameters necessary in the fitting procedure are either derived from theory or experimentally (i.e., using model compounds).

An alternative approach for data analysis resides in a combination of experimental and theory approaches by combining these to derived parameters in the EXAFS function, a semi-empirical approach. In the following Chapter such an approach was used. Phase shifts are initially calculated from (approximately) first principles, then refined with empirical standard compounds, and finally compared with other reference compounds of similar elemental constituents. The ability to obtain structural information using the semi-empirical approach is dependent upon the transferability of phase shifts. Because core potentials dominate the scattering process, phase shifts are chemically transferable allowing phase shifts from one system to be used in another with the same elemental constituents (Citrin et al., 1976). Structural parameters can determined using a curve fitting approach in k-space, $\chi(k)$, with the previously obtained phase shifts. This method allows the accuracy of phase shifts to be determined in addition to other anomalies which may arise in the data analysis. Furthermore, individual shells can be isolated for structural analysis of more complex species.

For initially calculating the phase shifts the charge density of each atom is calculated, assuming that the charge density remains unchanged from the free atom, using the Hartree-Fock approximation with linearly overlapping wave functions. The potential is assumed to have spherical symmetry about each atom without overlap. Each atom is considered to be separated by a region of constant potential where the electron is represented by a free wave--'a muffin tin approximation' (Pendry, 1974). Two components comprise the potential: a real electrostatic part due to the total charge density, and a second imaginary part which represents the interaction of the photoelectron with the atoms in the material and other electrons. Finally, the absorber is usually represented by a

Z+1 ionic wavefunction. The accuracy of the phase shifts is then checked by substituting them into different reference compounds which possessed the same absorber and backscatterer.

Successive shells in the EXAFS spectrum can be isolated and analyzed to determine the type, number, and distance of the backscatterer. After the chi function has been Fourier transformed, the first nearest neighbor shell (i.e., the atoms residing closest to the absorber) are selected and that portion of the function is isolated. The function is then back transformed into k space, $\chi(k)$, which is denoted as a Fourier filtered chi function. The Fourier filter extensively smoothes experimental data. Consequently one should always present experimental spectra in addition to Fourier filtered chi functions. Figure 7-5 illustrates chi functions for Cr before and after the filtering process and Fourier transformed spectra. The back transformed chi function is fit by an iterative process to yield the N_i , R_i, and σ_i . Successive coordination shells can be selected in the Fourier transformation process to determine the structural parameters of the absorber. Thus, for the unknown compound R_i N_i , and σ_i are varied while the phase shift and amplitude parameters are fixed to the values obtained from the model compounds. Under the most favorable circumstances the resulting distances are generally accurate within less than ±0.02 Å, and the coordination number within 20%. If the differences in back scattering amplitudes and/or phase shifts of alternative atoms in the neighbor shell are sufficient, the identities of the atom can be ascertained by substituting various possible atoms during the fitting procedure.

For the data analysis reported in this dissertation (Chapter 8), a computer program, EXCURVE (Gurman et al., 1984), was employed which is based on the original theory of Lee and Pendry (1975) and utilizes a curved wave description of the photoelectron wave. The curved wave description allows a lower energy analysis of the spectrum then a simpler

Figure 7-5. Experimental chi function for Cr(III) sorbed on silica and the Fourier filtering of the first shell. In (a) the experimental chi function is depicted and the Fourier transform (FT) in (b). The dashed lines in (b) isolating first shell (the large peak) for Fourier filtering are shown. Isolating this portion of the spectra results in the FT of (c). The first-shell portion of the FT is then backtransformed into k-space to represent the first shell contribution of the chi function, (d).

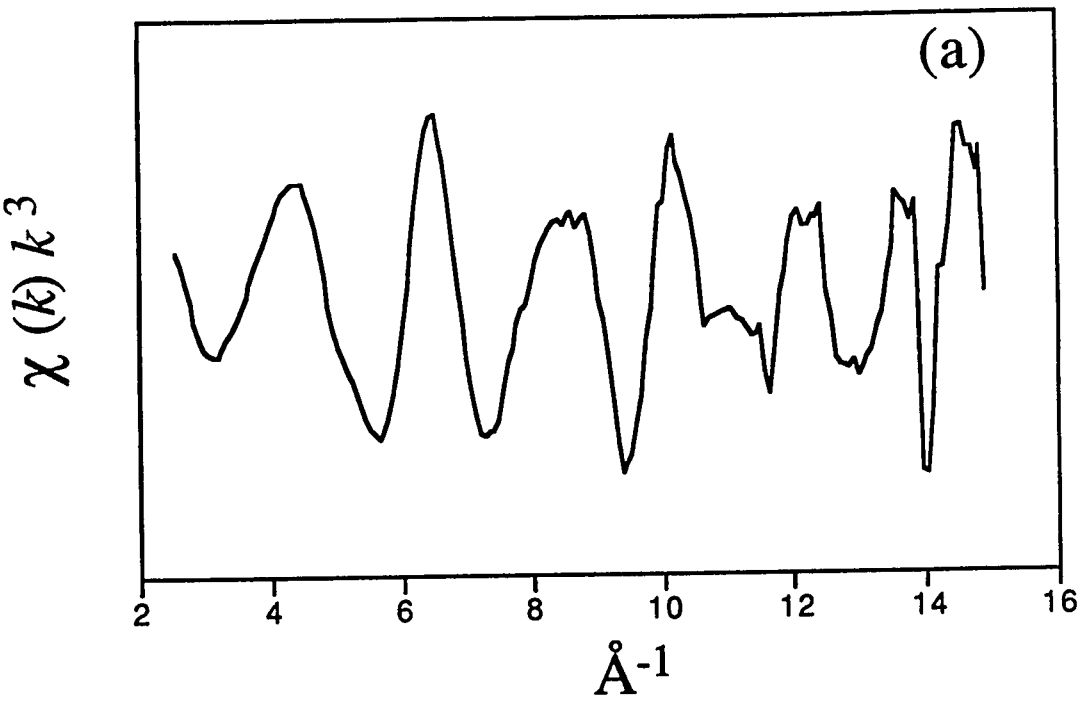
(a)
χ (k) k 3
2
4
6
8
10
12
14
16
Å-1

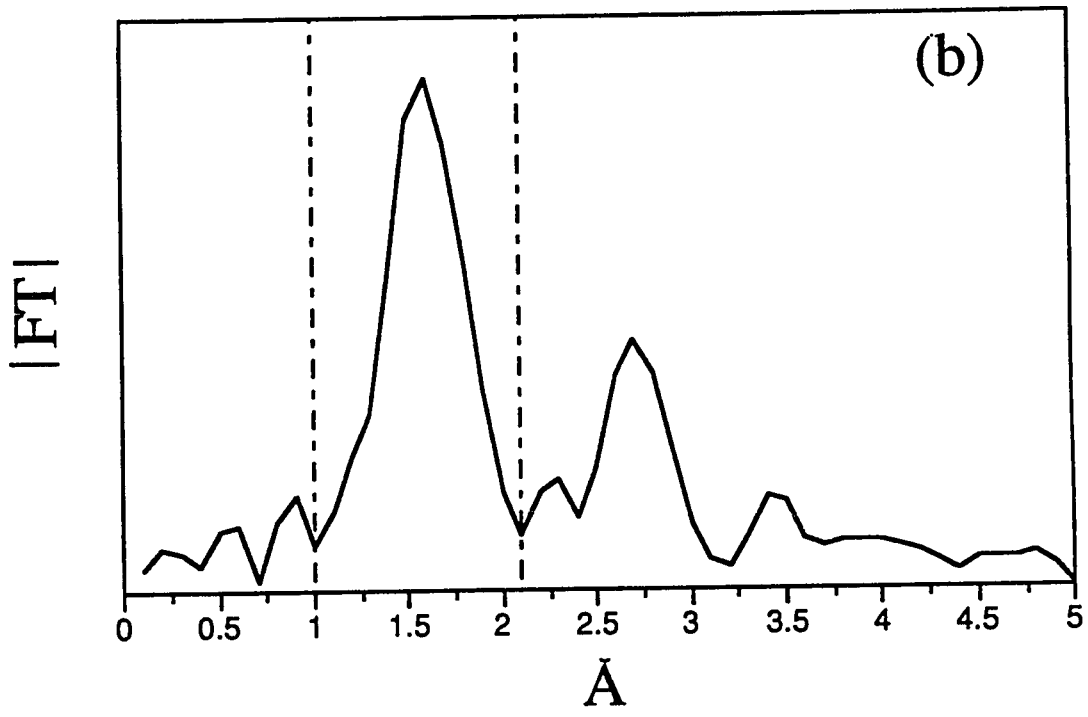
(b)
|FT|
0
0.5
1
1.5
2
2.5
3
3.5
4
4.5
5
Å

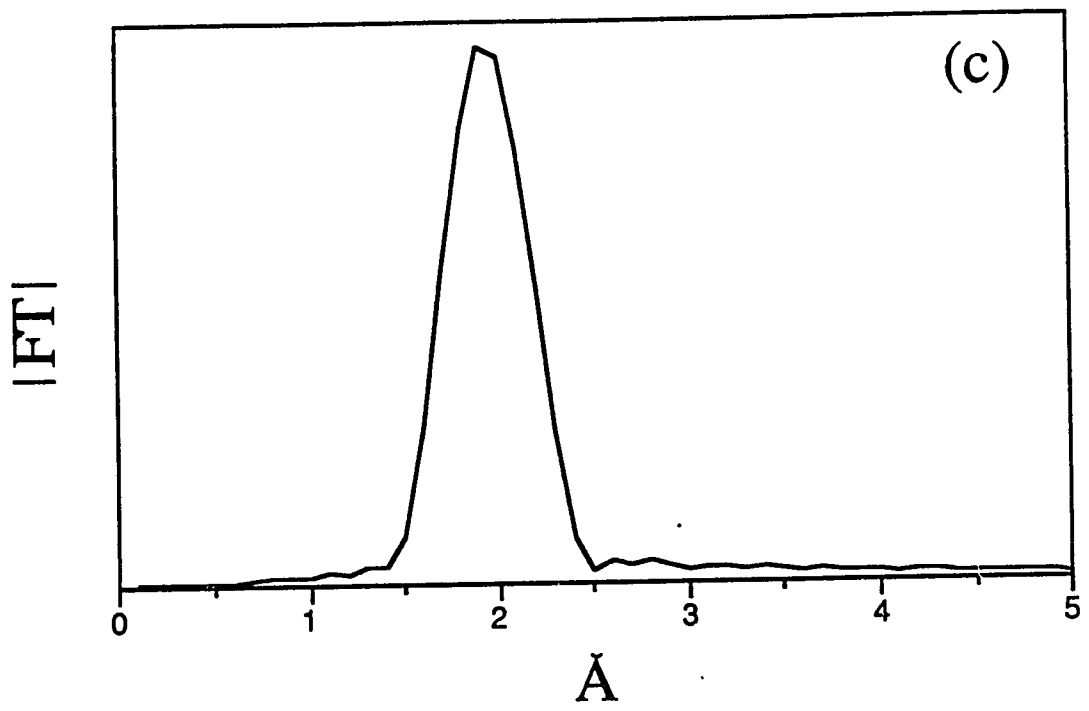
(c)
|FT|
0
1
2
3
4
5
Å

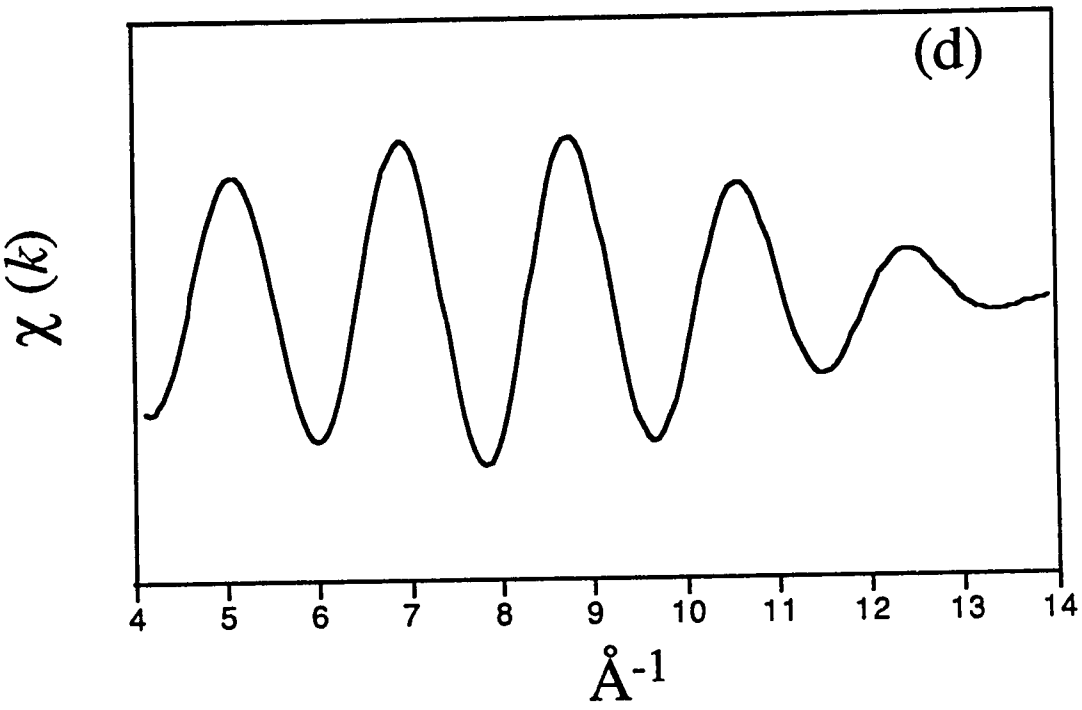
(d)
χ (k)
4
5
6
7
8
9
10
11
12
13
14
Å-1

plane wave approximation, thus extending the spectrum range analyzed and permitting the analysis of weak scatterers which only contribute to the low energy part of the spectrum.

7.7 Application of XAFS to the Soil Environment

X-ray absorption spectroscopy offers many advantages for obtaining information on the local chemical/physical environment of a particular element in soil systems. However, one should not be led to believe that XAFS is all inclusive and that the need for other experimental techniques is eliminated. On the contrary, XAFS has many limitations and employing it in conjunction with other techniques and studies allows one to obtain a more thorough and accurate depiction of a given system. X-ray absorption spectroscopy probes the local chemical and structural environment of a single element; thus, while giving important information about that element it does not facilitate the study of long-range order, as would be determined with X-ray diffraction, nor does it give composite information on a system (i.e., it only probes a single species rather than giving information on the system as a whole). In addition, *in situ* XAFS is limited to the study of heavier elements and its use may be restricted in complex matrices because of complicating absorbencies of the incident or measured energies. Furthermore, because the availability of synchrotron sources remains limited, a thorough knowledge of a system prior to conducting XAFS is essential to ensure that meaningful information is obtained.

The XANES features represent a fingerprint of the chemical state of the absorber. Hence, known model compounds can be used to generally identify the state of a species within a given sample. This is a particularly useful technique for investigating unknown heterogeneous samples in which the state of an absorber cannot be determined by other means. Because the XANES features represent the environment of the absorber,

qualitative structural information can also be gained. Furthermore, the XANES features give important bonding and electronic information about an absorbing species. Wayachunas and co-workers (Waychunas, 1987; Waychunas et al., 1983) have used XANES spectra to determine chemical and structural aspects of Fe and Ti in minerals. Quantitative information on bond angle and first neighbor distances of silica glasses (Marcelli et al., 1985) and zincblende (Sainctavit et al., 1987) have been resolved using this portion of the X-ray absorption spectra. Petiau et al. (1987) and Petiau and Calas (1985) give further details on quantitative aspects of the XANES spectra utilized in these mineralogical systems.

More detailed structural information on an absorber can be ascertained with the EXAFS region of XAFS. The attributes of EXAFS in the study of environmental systems are many: element specificity, the local nature of the structure, the ability to gain directional information due to polarization dependence on single crystals, sensitivity to relatively low elemental concentrations, and applicability to earth materials in various forms (crystalline or amorphous solids, liquids, suspensions) (Brown et al., 1988). EXAFS can be carried out *in situ* yielding direct measurements of interatomic distances between sorbed ions and its first, second, and sometimes third neighbors. Average coordination number and atomic identities in each of these shells are also obtained.

EXAFS has been employed for determining the structures of minerals and surface bound species. The complex structure of various Mn-oxides was accurately determined utilizing EXAFS in one of the first applications of this spectroscopy to natural materials (Arrenhius et al., 1979); the site vacancies present in many Mn-oxides were determined as was the structural environment of interlayer cations (e.g., Cu and Zn). The precipitation of Fe-(hydr)oxide gels and their transformation into crystalline (hydr)oxides is an important factor affecting soil chemical reactions. However, details of these reactions are difficult to obtain even in simple systems. By employing EXAFS spectroscopy to these 'neat'

systems, *in situ* investigations were conducted on the structure of the amorphous Fe-(hydr)oxide gels and their progressive development into crystalline forms (Combes et al., 1989a,b).

Although XAFS is inherently not surface sensitive (unless a more complex experimental setup is used), various studies have been conducted on metal ion sorption in colloidal suspensions. A great advantage of XAFS for investigating metal ion sorption is that experiments can be conducted in an unaltered state, *in situ*. This has allowed the complexation structure of SeO_4^{2-} and SeO_3^{2-} on goethite (Hayes et al., 1987) to be determined in addition to cationic metals on various oxides and clay minerals (Charlet and Manceau; Corker et al., 1991; Chisholm-Brause et al., 1990a,b). Direct structural details on metal ion surface nucleation and precipitation reactions were ascertained with this method (Charlet and Manceau, 1992; Chisholm-Brause et al., 1990b). The oxidation of Cr(III) by Mn-oxides has also been investigated with XAFS (Manceau and Charlet, 1992); the production of Cr(VI) was determined from the 'white line' feature in XANES while EXAFS allowed the structure of the sorbed Cr(III) to be ascertained. Manceau and Charlet (1992) determined the structures of the sorbed species by considering characteristic metal-metal octahedral bond lengths--a 'polyhedral approach'. This approach was implemented in an earlier study for the characterization of Fe- and Mn-oxides (Manceau and Combes, 1988).

The attributes and applications of XAFS are many. However, one should quickly realize from the above discussion that the study of an element in a complex matrix may be problematic and thus most current EXAFS studies have been conducted in simple (relative to natural soil environments) systems. Unfortunately, complex matrices may impede EXAFS analysis due to the composite of chemical environments in which the absorber resides. In addition, the experiments may also be hindered by incident or fluorescent X-ray intensity losses due to their absorbance by other elements in the material. Currently,

the finger print utility of XANES has offer the most applicability to complex natural systems.

Many environmentally important constituents of soil or water systems are in relatively low total concentration. Analysis of these dilute elements can be difficult with XAFS since the total sample is probed rather than a certain region. This problem is exemplified in the study of surface species in which the sorbate only constitutes a small fraction of the total material. Fluorescence detection has provided reasonable sensitivity for some systems; however, much improvement is often needed for EXAFS analysis of dilute environmental constituents. We have recently employed a focusing crystal (Lamble and Heald, 1991) which has vastly improved our elemental sensitivity by increasing the incident X-ray flux 2-4 times between the energies of 6-10 KeV. In addition, new highly sensitive detectors (multi-channel detectors) are being employed which dramatically improve one's ability to study very dilute systems.

While the employment of EXAFS to complex soil systems remains an arduous task, the information gained from such studies makes attempts at extracting structural information from these systems well worth the effort. By first investigating elements of interest in a single structural environment and progressively moving to more complex multi-site systems one may begin to resolve EXAFS structural information on natural soils. We are currently using such an approach by first investigating Cr(III) complexation on Si-oxides (Chapter 8), then progressing to alumino-silicate clay minerals and primary minerals, and finally toward real soil systems. With this approach, the results of each step provides reference data for the next more complex environment. Furthermore, the Cr K-edge energy is sufficiently greater than other elements present in these systems such that neither the incident nor the fluorescent X-ray intensities are sacrificed and no other absorption edge complicates the Cr XAFS spectrum. As continued research is conducted with XAFS on soil components the utility of this technique for investigating the complexity

encountered in real soils will vastly improve. Because of the abundant detailed information obtained with this technique from an unaltered experimental environment, employing this technique in remediation measures appears to be a promising area. However, one must be aware of the difficulties arising in conducting EXAFS on complex heterogeneous systems, particularly when the absorbing atom resides in multiple structural or chemical environments.

The structural information obtained with EXAFS in simple (relatively homogeneous) systems can also be used to quantitate other spectroscopic techniques which may not directly give such precise structures. Once quantitated, the other spectroscopies (e.g., vibrational or magnetic spectroscopies) can be employed to investigate unknown systems. The other techniques may have more advantageous qualities for investigating heterogeneous samples and may be more accessible to a user. Furthermore, conducting other spectroscopic/microscopic studies with XAFS may help to substantiate one's findings and often can add additional complimentary information. For example, XRD or transmission electron microscopy can be used to determine a sample's long range order (crystallinity) while XAFS examines the local order of a particular element in the sample. Microscopic techniques can also compliment XAFS experiments by providing visual information on structural alterations of the sample and the spatial locality of these changes.

Determining the chemical state of solid phase constituents is important as such information reflects the potential for solubilization and the potential behavior of a species entering the aqueous environment. Selective dissolution experiments or simply total dissolution of solids has often been employed to ascertain information on a solid-state species; however, with such measures one cannot be sure that the results are not affected by such procedures. In this area of research, XAFS provides a very easy and accurate means for determining the chemical state of solid phases. The edge position and XANES features give important qualitative, and in some case quantitative information as to the

valence and chemical state of the absorber. Consequently, using XAFS, one could relate structural and chemical changes occurring in the solid phase to solution components during a selective dissolution. The results obtained by XAFS differ from those of XRD in that only the local environment of the X-ray absorbing element is probed rather than the structure of the solid phase.

7.8 Conclusion

Spectroscopic and microscopic techniques have recently found utility in the investigation of soil systems. Continued studies of these processes using advanced surface probing techniques should eventually allow for the development of accurate mechanistic and predictive models for metal sorption. EXAFS provides a powerful tool for obtaining a wealth of information on interfacial processes, and the construction of third generation synchrotron facilities should facilitate these investigations. These new synchrotron sources will be more assessable to outside users, and will have higher intensity light sources. Although not without limitations, XAFS appears to represent one of the most promising tools for investigating soil chemical reactions.

7.9 References

Arrenhius, G., K. Cheung, S.E. Crane, M. Fisk, J.Z. Frazer, J. Korkisch, T. Mellin, S. Nakao, A. Tsai, and G. Wolf. 1979. Counterions in marine manganates. *In* C. Lalou (ed.) Genese des nodules de manganese. *Coll. Int. du CNRS* **289**:333-356.

Brown, G.E., Jr., and G.A. Parks. 1989. Synchrotron-based X-ray absorption studies of cation envrioments in Earth materials. *Rev. Geophys.* **27**(4):519-533.

Brown, G.E., G. Calas, G.A. Waychunas, and J. Petiau. 1988. X-ray absorption spectroscopy and its applications in mineralogy and geochemistry. pp. 431-521. *In* F. Hawthorne (ed.) Spectroscopic Methods in Mineralogy and Geology. Rev. Mineral. vol. 18. Mineral. Soc. Am., Book Crafters, MI.

Calas, G., and J. Petiau. 1983. Structure of oxide glasses: Spectroscopic studies of local order and crystallochemistry: geo-chemical implications. *Bull. Mineral.* **106**:33-55.

Charlet, L., and A. Manceau. 1992. X-ray absorption spectroscopic study of the sorption of Cr(III) at the oxide-water interface: II. Adsorption, coprecipitation, and surface precipitation on hydrous ferric oxide. *J. Colloid Interface Sci.* **148**:443-458.

Chisholm-Brause, C.J., P.A. O'Day, G.E. Brown, Jr, and G.A. Parks. 1990a. Evidence for multinuclear metal-ion complexes at solid/solution interfaces from X-ray absorption spectroscopy. *Nature.* **348**:528-530.

Chisholm-Brause, C.J., A.L. Row, K.F. Hayes, G.E. Brown Jr., G.A. Parks, and J.O. Leckie. 1990b. XANES and EXAFS study of aqueous Pb(II) adsorbed on oxide surfaces. *Geochim. Cosmochim. Acta.* **54**: 1897-1909.

Citrin, P.H., P. Eisenberger, and R.C. Hewitt. 1976. Transferability of phase shifts in extended X-ray absorption fine structure. *Phy. Rev. Lett.* **36**: 1346-1349.

Combes, J.M., A. Manceau, G. Calas, and J.Y. Bottero. 1989a. Formation of ferric oxides from aqueous solutions: a polyhedral appraoch by X-ray absorption spectroscopy: I. Hydrolysis and formation of ferric gels. *Geochim. Cosmochim. Acta.* **53**: 583-594.

Combes, J.M., A. Manceau, and G. Calas. 1989b. Formation of ferric oxides from aqueous solutions: a polyhedral appraoch by X-ray absorption spectroscopy: II. Hematite and formation of ferric gels. *Geochim. Cosmochim. Acta.* **54**: 1083-1091.

Corker, J.M., J. Evans, and J.M. Rummey. 1991. EXAFS studies of pillard clay catalysts. *Material Chem. Phys.* **29**: 201-209.

Crane, S.E. 1981. Structural chemistry of marine manganate minerals. Ph.D. Dissertation. University of California, San Diego.

Durham, P.J. 1988. Theory of XANES. pp.52-86. *In* D.C. Knoningsberger and R. Prins (eds.) X-ray absorption. principles, applications, techniques of EXAFS, SEXAFS, and XANES. Wiley and Sons, NY.

Gurman, S.J., N. Binsted, and I. Ross. 1984. A rapid exact curved-wave theory for EXAFS calculations. *J. Phys.* C **17**: 143-151.

Hayes, K.F, A.L. Roe, G.E. Brown, K.O. Hodgson, J.O. Leckie, and G.A. Parks. 1987. *In situ* X-ray adsorption study of surface complexes: Selenium oxyanions on α-FeOOH. *Science.* **238**:783-786.

Heald, S.M. 1988. Design of an EXAFS experiment. pp. 87-118. *In* D.C. Knoningsberger and R. Prins (eds.) X-ray Absorption. Principles, applications, techniques of EXAFS, SEXAFS, and XANES. Wiley and Sons, NY.

Lamble, G.M., and S.M. Heald. 1991. Operation of a dynamically bent sagittally focusing double crystal monochromator for XAFS studies. *Rev. Sci. Instrum.* **63**:880-884.

Lee, P.A., and G. Beni. 1977. New Method for the calculation of atomic phase shifts: Application to extended X-ray absorption fine structure (EXAFS) in molecules and crystals. *Phys. Rev.* B **15**: 2862-2883.

Lee, P.A., and J.B. Pendry. 1975. Theory of the extended X-ray absorption fine structure. *Phys. Rev.* B **11**: 2795-2811.

Lytle, F.W., R.B. Greegor, D.R. Sandstrom, E.C. Marques, J. Wong, C.L. Spiro, G.P. Huffman, and F.E. Huggins. 1984. Measurements of soft X-ray absorption spectra with a fluorescent ion chamber detector. *Nucl. Instr. and Meth.* **226**:542-548.

Lytle, F.W., D.E. Sayers, and E.A. Stern. 1975. Extended x-ray absorption fine-structure technique. II. Experimental practice and selected results. *Phys. Rev.* B **15**:4825-4835.

Manceau, A., and L. Charlet. 1992. X-ray absorption spectroscopic study of the sorpiton of Cr(III) at the oxide-water interface: I. Molecular mechanisms of Cr(III) oxidation on Mn oxides. *J. Colloid Interface Sci.* **148**:425-442.

Manceau, A., and J.M. Combes. 1988. Structure of Mn and Fe oxides and oxyhydroxides: A topological approach by EXAFS. *Phy. Chem. Minerals.* **15**:283-295.

Marcelli, A., I. Cavoli, A. Bianconi, J. Garcia, A. Gargano, C.R. Natoli, M Benafatto, P. Chiaradia, M. Fanfoni, E. Fritsch, F. Calas, and J. Petiau. 1985. Local structure in SiO_2 glasses by oxygen K edge XANES. *J. Physique.* **46**, C8:107-112.

McMaster, W.H., N. Kerr del Grande, J.H. Mallet, and J.H. Hubell. 1969. Compilation of X-ray cross sections III. *US Atom. Ener. Comm.* UCRL-50174.

Pendry, J.B. 1974. Low energy electron diffraction. Academic Press, NY.

Petiau, J. and G. Calas. 1985. EXAFS and edge structure; application to nucleation in oxide glasses. *J. Physique.* **46**, C8:41-50.

Petiau, J., G. Calas, and P. Sainctavit. 1987. Recent developments in the experimental studies of XANES. *J. Physique* **48**, C9:1085-1096.

Sainctavit, P., J. Petiau, G. Calas, M. Benfatto, and C.R. Natoli. 1987. XANES study of sulfur and zinc K-edges in zincblende: Experiments and multiple-scattering calculations. *J. Physique* **48**, C9:1109-1112.

Sayers, D.E., and B. Bunker. 1988. Data Analysis. pp. 211-253. *In* D.C. Knoningsberger and R. Prins (eds.) X-ray Absorption. Principles, applications, techniques of EXAFS, SEXAFS, and XANES. Wiley and Sons, NY.

Sayers, D.E., E.A. Stern, and F.W. Lytle. 1971. New techniques for investigation noncrystalline structures: Fourier analysis of the extended X-ray-absorption fine structure. *Phys. Rev. Lett.* **64**:1204-1207.

Stern, E.A. 1974. Theory of extended x-ray absorption fine structure. *Phys. Rev.* B **10**:3027-3037.

Stern, E.A. 1988. Theory of EXAFS. pp.3-51. *In* D.C. Knoningsberger and R. Prins (eds.) X-ray Absorption. Principles, applications, techniques of EXAFS, SEXAFS, and XANES. Wiley and Sons, NY.

Stern, E.A., B.A. Bunker, and S.M. Heald. 1980. Many-body effects on extended X-ray absorption fine structure amplitudes. *Phys. Rev.* B **21**: 5521-5539.

Teo, B.K. 1986. EXAFS: Basic Principles and Data Analysis. Springer-Verlag, New York/Berlin.

Teo, B.K., and P.A. Lee. 1979. Ab Initio calculations of amplitude and phase functions for extended X-ray absorption fine structure spectroscopy. *J. Am. Chem. Soc.* **101**:2815-2832.

Waychunas, G.A. 1987. Synchrotron radiation XANES spectroscopy of Ti in minerals: Effects of Ti bonding distances, Ti valence, and site geometry on absorption edge structure. *Am Mineral.* **72**:89-101.

Waychunas, G.A., M.J. Apted, G.E. Brown, Jr. 1983. X-ray K-edge absorpiton spectra of Fe minerals and model compounds: Near-edge structure. *Phys. Chem. Minerals* **10**:1-9.

Westall, J.C. and H. Hohl. 1980. A comparison of electrostatic models for the oxide/soution interface. pp. 265-294. *In* A.C. Zettlemoyer (ed.) Adv. in Colloid and Interface Science. Elsevier Scientific Publishing Company, Amsterdam.

CHAPTER 8

SORPTION MECHANISM of Cr(III) on SILICA: An ATOMIC LEVEL INVESTIGATION

8.1 Abstract

Sorption reactions of metal ions at the solid/solution interface are important in an array of disciplines and are of environmental significance as such reactions can greatly affect metal toxicity. The structural environment of metals at the solid/water interface determines their potential for remobilization to the aqueous environment and the physical/chemical modifications of the sorbent. In this chapter, the surface structure of Cr(III) on a commonly occurring natural sorbent, amorphous SiO_2 (silica), was investigated. A multitude of atomic level experimental techniques were employed to ascertain the Cr(III) surface structure, allowing for a thorough and accurate depiction of its structural environment. Extended X-ray absorption fine structure (EXAFS) spectroscopy, diffuse reflectance infrared Fourier transform spectroscopy (DRIFT), and high-resolution transmission electron microscopy (HRTEM) were used to discern the structural environment of Cr(III) sorbed on silica. Chromium(III) formed a monodentate surface complex on silica, which with increased Cr(III) levels resulted in a nucleated γ-CrOOH type structure. The initial nucleation expanded on the silica surface, but as nucleation growth progressed rather than distributing over the surface discrete highly-ordered γ-CrOOH surface clusters formed.

8.2 Introduction

Inorganic compounds are potential pollutants which can be particularly problematic due to their stability in the environment (i.e., lack of degradation). Chromium is an environmentally significant metal used in various industrial processes. Two oxidation states of Cr are stable under surficial conditions, Cr(III) and Cr(VI). Chromium(VI) is much more hazardous than Cr(III) because it is mobile through plant and animal membranes, and is toxic to cells due to its strong oxidizing nature. In addition, anionic Cr(VI) species predominantly form in soils and waters and are very mobile in the environment. Due to the toxicity and mobility of Cr(VI), the maximum allowable level of Cr in drinking water is 10^{-6} *M* (U.S. EPA, 1984). It is therefore important to determine reactions which affect the oxidation state of Cr. Chromium(III) oxidation is an important process as the rather benign trivalent species is transformed into the hazardous Cr(VI) species. Fortunately, the only known naturally occurring oxidants of Cr(III) are Mn-oxides (Eary and Rai, 1987).

The oxidation of Cr(III) by Mn-oxides is dependent upon the formation of a Cr(III)-MnO_2 complex; thus, reactions which limit this reaction will decrease the potential for Cr(VI) production. One possible mechanism for retarding Cr(III) oxidation is its retention by other non-redox reactive sorbents present in soils or waters, which would prevent oxidation by inhibiting Cr(III) from complexing with Mn-oxides. An array of studies have investigated the retention of metals by soils and soil components. Permanently charged aluminosilicate clay minerals often are the dominant sorbent in soils; however, oxides and hydroxides can play an important factor in the environmental behavior of metal ions. The influence of oxides is enhanced by the formation of high surface area particles and surface coatings on other soil materials. Silica (SiO_2) is a commonly occurring oxide which readily forms coatings on other solids and it can have a very high surface area; thus, silica often exerts a large influence on sorption reactions.

Moreover, sorption reactions are extremely influential on the hazard of metal ions in the environment since the metals are removed from the mobile aqueous phase. Hence, to determine the hazard of Cr in the environment, knowledge of Cr(III) sorption on non-redox reactive solids is necessary. Accordingly, in this study the retention of Cr(III) by silica was investigated.

Because of the agricultural, environmental, and industrial significance of metal retention reactions on oxides, it is important to obtain a detailed understanding of these reactions. Molecular level information is necessary to accurately deduce reaction mechanisms which are essential for understanding chemical/physical factors affecting metal sorption/desorption processes. Mechanistic models have been developed for metal sorption reactions at the oxide/water interface; however, these models have largely been based on macroscopic data without direct atomic level evidence. Therefore, one cannot be certain that model predictions are an accurate representation of interfacial processes. It is important for researchers to utilize techniques which give direct evidence for reaction mechanisms, allowing for the development of mechanistic models based on an accurate physical conception of surface reactions.

Surface complexation models have predominantly been based on the conception of a homogenous surface with a single 2 pKa site in which the sorbing species bind only at isolated sites (Schindler and Stumm, 1987; Hayes and Leckie, 1986; Davis et al., 1978; Yates et al., 1974; Burube and DeBruyn, 1968). Only a few models have considered surface precipitation reactions (Farley et al., 1985; James and Healy, 1972). Recent experimental evidence has indicated that surface nucleation of metal hydroxides occurs much more frequently than previously believed (Charlet and Manceau, 1992; Chisholm-Brause et al, 1990a,b; Bleam and McBride, 1986). Nucleated metal hydroxides of Pb, Co, and Cr(III) on oxides and aluminosilicate minerals have been discerned with extended X-ray absorption fine structure (EXAFS) spectroscopy (Charlet

and Manceau, 1992; Corker et al., 1991; Chisholm-Brause et al., 1990a,b). The number of nuclei (cluster size) was observed to varying depending on the sorbent. At surface loadings of 1.1-1.2 μmol m^{-2}, Co-hydroxide nucleation was greater on γ-Al_2O_3 than on rutile or kaolinite (Chisholm-Brause et al., 1990a).

Although there is direct evidence for surface nucleation of metal hydroxides, the reaction conditions affecting surface nucleation, e.g., pH, aqueous metal concentration, surface coverage (loading), and sorbent properties, are not clear. It is well known that metal sorption is correlated with hydrolysis reactions of ions (Schindler and Stumm, 1987), which is primarily a function of pH. It remains unknown, however, whether this results from surface complexation or precipitation. The extent of surface coverage necessary for nucleation is also not apparent. In this study, factors influencing the Cr(III) sorption mechanism on silica were investigated.

A host of analytical techniques are available for investigating surface reactions, but no single technique is a panacea for obtaining mechanistic information. Rather, by using a combination of these techniques one can acquire an accurate and thorough depiction of interfacial reactions. Many surface analytical techniques are severely invasive, and thus may be inappropriate for studying environmental processes. Magnetic and vibration spectroscopies have been employed for investigating sorption reactions *in situ* without artifacts induced by the analytical conditions. While both magnetic and vibrational spectroscopies provide important atomic level information, they do not always give a quantitative description of the local structural environment of a sorbed species. Nonetheless, they provide important information which can often be gained with less difficulty than with other techniques. X-ray absorption fine structure (XAFS) spectroscopy provides direct information on the local structure of sorbed (adsorbed or surface precipitated) metals. Unfortunately, *in situ* XAFS studies are limited to elements heavier than Sc, and synchrotron facilities, necessary for *in situ* XAFS, are

usually not readily accessible. Furthermore, XAFS provides the local chemical environment of a particular element, but provides no information on spatial resolution of surface species. In contrast to XAFS, transmission electron microscopy (TEM) provides information on the spatial resolution of surface modifications and the ordering (amorphous or degree of crystallinity) of the sorbed entities.

Determining surface structures is necessary for determining reaction mechanisms, the stability of bound species, and for evaluating the physical/chemical properties of the modified surface. Therefore, the objective of this study was to investigate the surface structure of Cr(III) sorbed on SiO_2 and to determine the surface modification and stability of the bound phase. By employing XAFS, diffuse reflectance infrared Fourier transform (DRIFT) spectroscopy, and high resolution transmission electron microscopy (HRTEM) a composite of information was obtained, which allowed for an accurate and detailed analysis of the Cr(III)-SiO_2 sorption mechanism. The local chemical and structural environment of Cr(III) was ascertained with XAFS, molecular information with DRIFT, and HRTEM provided spatial resolution and information on the surface structural modification of the silica after reaction with Cr(III). The DRIFT spectra were evaluated by comparing vibration modes of 'neat' silica and γ-CrOOH to the Cr-silica systems. The results gleaned with XAFS were compared to the information obtained with DRIFT analysis. This permitted the use of DRIFT for evaluating the effect of an extensive range of reaction parameters on the Cr(III) sorption structure.

8.3 Materials and Methods

8.3.1 Batch Studies

The silica used in this study was a Huber Zeothix® 265 amorphous SiO_2 colloid, synthesized as described by Wason (1978). The oxide was washed in pH 3.5 HNO_3 and

then dialyzed until a stable conductivity resulted for 24 h. The surface area was 221 m^2 g^{-1}, as determined by the ethylene glycol monoethyl ether (EGME) method (Heilman, 1965). The particle size of the oxide was less than 2.0 μm.

Batch studies were performed to determine the amount of Cr(III) sorbed on SiO_2 as a function of pH and initial Cr(III) concentration ($[Cr]_o$). A pH range of 3 to 8 was investigated with initial concentrations of 40, 400, 1000 μ*M* Cr(III). For the batch studies, 0.102 g SiO_2 was dispensed in 50 ml centrifuge vessels with 20 ml of 0.1 *M* $NaNO_3$. A 10 m*M* Cr(III) stock solution was used to obtain the desired Cr(III) concentrations. The stock solutions were made from the nitrate salt, $Cr(NO_3)_3$, with acidified deionized water (pH ≤ 2) and were never allowed to age more than five days to limit potential polymerization.

The oxide was allowed to hydrate for 48 h prior to reaction. After the hydration period, the pH was adjusted, the desired amount of Cr(III) was added and the final volume brought to 30 ml, yielding a suspension density of 3.4 g $liter^{-1}$. The pH was held constant with a pH-stat system; upon reaching a steady pH the vessels were placed in a water bath reciprocating shaker. After a 48 h reaction period the samples were filtered through a 0.22 μm pore membrane and the solution analyzed for Cr with a JY-70 ICP spectrophotometer. The solids from DRIFT and XAFS samples were also digested with 12 *N* HNO_3 and analyzed for total Cr. The solution and total digestion results agreed well (within ± 10%); however, the digested samples had a greater internal deviation due to the dilution necessary for ICP analysis. Therefore, changes in solution concentrations are reported.

All reactions were carried out at 25 ± 0.5 °C at 1 atm pressure in a $N_{2\ (g)}$ environment. The initial solutions were purged with $N_{2\ (g)}$ prior to the addition of the

oxide. Thereafter, a $N_{2\,(g)}$ stream was maintained over the surface of the fluid when the vessels were exposed to the surrounding environment.

Several mechanisms can be operational for the retention of metals on oxides; the term sorption is used to describe general uptake of a sorptive without implying a specific mechanism (e.g., adsorption or precipitation). Various terms have been used to describe the amount of a metal sorbed on an oxide. In this study the data are referenced to the potential surface site occupancy, ϕ,

$$\phi = (\text{moles Cr sorbed})/(\text{moles surface sites}) \qquad [1]$$

One should be aware that this does not imply a site occupancy but only a potential maximum if all sorbed Cr(III) occupy a single site. If nucleation or clustering occurs then a different amount of the surface sites would be occupied, i.e., an amount less than ϕ would be covered. This quantity is employed because it has a physical significance on the sorption mechanism. At less than potential monolayer coverage, isolated site binding can account for the total sorption quantity, but at $\phi > 1$ precipitation is required. A reactive surface site density of 4.6 sites nm^{-1} (Fouad et al., 1991; Hiemstra et al., 1989b) was used to calculate the site density for silica.

8.3.2 XAFS Studies

X-ray absorption fine structure spectroscopy was performed at the National Synchrotron Light Source, Brookhaven National Laboratory, under dedicated running conditions on beam line X-11A. The electron storage ring operated at 2.528 GeV with currents ranging from ≈215 mA immediately after a fill to a refill current of 110 mA.

Samples were prepared by the batch method. Solids were consolidated prior to XAFS analysis to maximize the amount of sorbed material analyzed. The equilibrated

suspensions were passed through a 45 mm diameter 0.22 mm membrane filter. The solid material was then placed in a vial and sealed. The samples remained moist and were never allowed to dry. The filtrate was then placed in the Al block sample holders immediately prior to XAFS analysis.

The Cr K edge (5989 eV) was used for analysis. A Si(111) water cooled double crystal monochromator was employed with a sagitally focused beam (Lamble and Heald, 1991). The focused beam provided an intensity greater than three times that provided by the conventional flat monochromator arrangement. A 0.5 mm monochromator slit width was employed, which was readjusted when the vertical beam position moved more than 0.2 units. Higher-order harmonics were rejected by detuning 30% from the maximum incident intensity (I_0).

The incident X-ray intensity was measured with a 15 cm long $N_{2\,(g)}$ filled ionization chamber. Reference materials were run in transmission mode with the transmitted intensity measured with a second ionization chamber. All Cr(III)-SiO_2 systems were analyzed by fluorescence detection. For fluorescence detection the samples were mounted in a 4 x 6 x 25 mm slot cut in an Al block, which provided good temperature conductance necessary for temperature variation of the samples, and sealed with Kapton® tape. The samples were placed at a 45° angle to the incident beam and a wide angle collector with an ionization chamber, a Lytle detector (EXAFS Company), was located 45° off the sample (i.e., normal to the incident beam). The Lytle detector was filled with $Ar_{(g)}$ for Cr Kα fluorescence detection. A V filter (6 absorption lengths thick) and Soller slits were placed between the sample and the detector to reduce elastically scattered incident X-rays from entering the fluorescence detector. Samples were analyzed at ambient and $N_{2\,(l)}$ temperatures (298 and 77 K); no structural differences were discerned between these temperatures and consequently, the 77 K

spectra are reported due to the reduction in thermal disorder. All samples were run at least in triplicate.

Data analysis was accomplished by the procedures previously described (Chapter 7). Phase shifts for O, Si, and Cr were determined by first principle calculations and then refined using model compounds: Cr using a Cr-metal and α-Cr_2O_3, O with α-Cr_2O_3, and Si with NiSi. The EXCURVE (Gurman et al., 1984) routine was employed for determining the interatomic distances (**r**) and coordination numbers (CN) of the Cr nearest neighbors. Amplitude parameters in EXCURVE were defined based on α-Cr_2O_3. Successive shells were isolated in the Fourier transformed spectra, backtransformed, and the r's, CN's, and Debye-Waller factors (σ) varied until the best fit was obtained between the theoretical and experimental curves. After obtaining the structural information of each successive shell out to 4 Å , the structural parameters were then combined to model the entire spectra. The resulting **r** values for the first coordination shell were accurate to $\pm$0.03 Å and CN to $\pm$20% based on fits to model compounds.

8.3.3 Infrared Analysis

Diffuse reflectance infrared Fourier transform (DRIFT) spectroscopy was performed using a Perkin-Elmer FT-IR 1720X spectrometer with a diffuse reflectance accessory. Samples were prepared using the batch methods described earlier; after reaction the solid material was washed with 100 ml of deionized water and the solids dried at 60°C for 24 h. The dried material was then diluted by 90% (by weight) with KBr to reduce the influences of spectral reflectance. Reported spectra are the average of 200 scans.

In addition to the Cr-SiO_2 samples, reference materials were analyzed for comparison. Reference spectra were obtained for γ-CrOOH and SiO_2. The γ-CrOOH

was precipitated by titrating 20 m*M* Cr(III) to pH 6, with pH maintained at this level for 24 h. This procedure was similar to that used by Charlet and Manceau (1992). EXAFS analysis and electron diffraction patterns confirmed that the precipitated material was γ-CrOOH. The standards were also diluted by 90% (by weight) with KBr prior to DRIFT analysis.

8.3.4 HRTEM Analysis

High-resolution TEM was performed on high surface coverage Cr(III) reacted silica, $\phi = 10$. For HRTEM analysis, 0.25 ml of the reacted suspension was dispersed on a holey carbon film supported by a fine mesh copper grid. The oxide coated grids were then rinsed with 50 ml of deionized water, and dried in a glass chamber. Imaging was then performed on a Hitachi 9000NAR electron microscope. Further details on the electron microscopy procedures can be found in Chapters 2, 5, and 6.

8.3.5 Cr(III) Concentration and Surface Area Effects

To evaluate the effect of the initial Cr(III) concentration and total surface area on the sorption mechanism, a systematic variance of each was conducted. The influence of initial metal concentration was investigated by keeping the total amount of Cr(III) (moles) and SiO_2 (g) constant while varying the volume. At pH 6, complete (100 percent) sorption of Cr(III) occurred at the initial concentration employed in this study. Thus, by keeping the quantity of SiO_2 (0.250 g) and Cr(III) constant (100 μmols), and varying the systems volume, a constant surface loading, $\phi = 0.21$, under varying $[Cr]_o$ was obtained. Chromium(III) concentrations ranging from 40 μ*M* to 1 m*M* were investigated.

Surface coverage effects were evaluated by varying the amount of solid present while keeping $[Cr]_o$ and the volume constant. At low site occupancies ($\phi < 1$), two liter reactant systems having $[Cr]_o$ of 40, 100, and 200 μM were reacted with (i) 0.5 g SiO_2 giving ϕ values of 0.085, 0.21, and 0.42; and (ii) 0.2 g SiO_2 giving ϕ values of 0.22, 0.53, and 1.05. The potential site coverages resulting in these systems were: (i) 0.085, 0.21, and 0.42 and (ii) 0.22, 0.53, and 1.05. To determine the coverage effects at high surface loadings ($\phi > 1$) 0.5 g , 1.0 g, and 1.5 g SiO_2 were reacted with 5 mM $[Cr]_o$ in 30 ml suspension volumes.

8.4 Results

8.4.1 X-ray Absorption Fine Structure Analysis of the Cr(III) on Silica

The extended portion of the XAFS (EXAFS) was utilized to discern the local structural environment of Cr(III) sorbed on silica. A range of initial Cr(III) concentrations (100, 200, 400, and 5 x 10^3 μM) at pH 6 were investigated with 0.500 g SiO_2 present. These initial Cr(III) concentrations correspond to potential site occupancies (ϕ) of 0.21, 0.42, 0.85, and 10. The experimental spectra for the Cr-SiO_2 systems are shown in Fig. 8-1 along with that of hydrous chromium oxide (HCO), $Cr(OH)_3 \cdot nH_2O$, with the γ-CrOOH local structure.

The structural parameters derived from EXAFS analysis are summarized in Table 8-1. In all of the Cr specimens approximately six O were observed at 1.99 Å. In γ-CrOOH, a second shell composed of two Cr at 2.99 Å (edge sharing CrO_6 octahedra) and a third shell of 1.5 Cr at 3.98 Å (corner sharing octahedra) were discerned. These results are in good agreement with the structural parameters determined by others for γ-CrOOH (Manceau and Charlet, 1992; Corker et al., 1991). The first two shells (i.e., six O at 1.99 Å, and two Cr at 2.99 Å) in all the Cr(III)-SiO_2 samples were similar to those of the Cr-

hydroxide, with slight variations in the CN. However, a different third shell resided in these materials: a single Si atom at 3.39 Å (Fig. 8-2). The Si-Cr distance of 3.39 Å represents a monodentate complex, in agreement with the CN, and would necessitate a 137° Cr-O-Si bond angle. Beyond the Si shell another Cr shell occurred; however, the EXAFS intensity of this shell is much weaker than the inner-shells and therefore one must place less confidence in the derived structural values. Nonetheless, these outer shells were isolated and corresponded to 1.5 Cr at 3.82 Å and 1.5 Cr at 3.97 Å (Fig. 8-2)--the latter is characteristic of corner sharing Cr octahedra. The 3.82 Å Cr-Cr distance may represent a distorted corner sharing octahedra, which results from the structural restriction imposed by the silica surface; this will be elaborated on later. Consolidating the structural parameters derived from the isolated shells resulted in good agreement between the predicted and experimental chi functions for the samples (Fig 8-3).

Although Cr-hydroxide nucleation was observed in all of the Cr-SiO_2 systems, the extent of nucleation varied depending on ϕ. Figure 8-4 gives the relative intensities of the atomic shells in the Fourier transformed spectra (the radial structure function, RSF). The second peak composed of edge and corner sharing octahedra is apparent in all of the RSFs. However, as ϕ decreases the second peak becomes skewed to the high energy side and a third peak becomes increasingly prominent. The alteration of the second and third peaks with changes in surface coverage arises from structural changes in the corner sharing octahedra and presence of Si in the structural environment of Cr. With the presence of the Si and the 3.82 Å Cr-Cr distance, the second peak becomes composed of the Cr-Cr edge sharing (2.99 Å) and Si (3.39 Å) shells while the third peak results from a distorted corner sharing octahedra (3.82 Å). A very weak peak is also observed in the Fourier transformed spectra at about 4 Å. This is characteristic for undistorted corner sharing Cr octahedra (3.97 Å). As the surface coverage increases this 4 Å peaks becomes

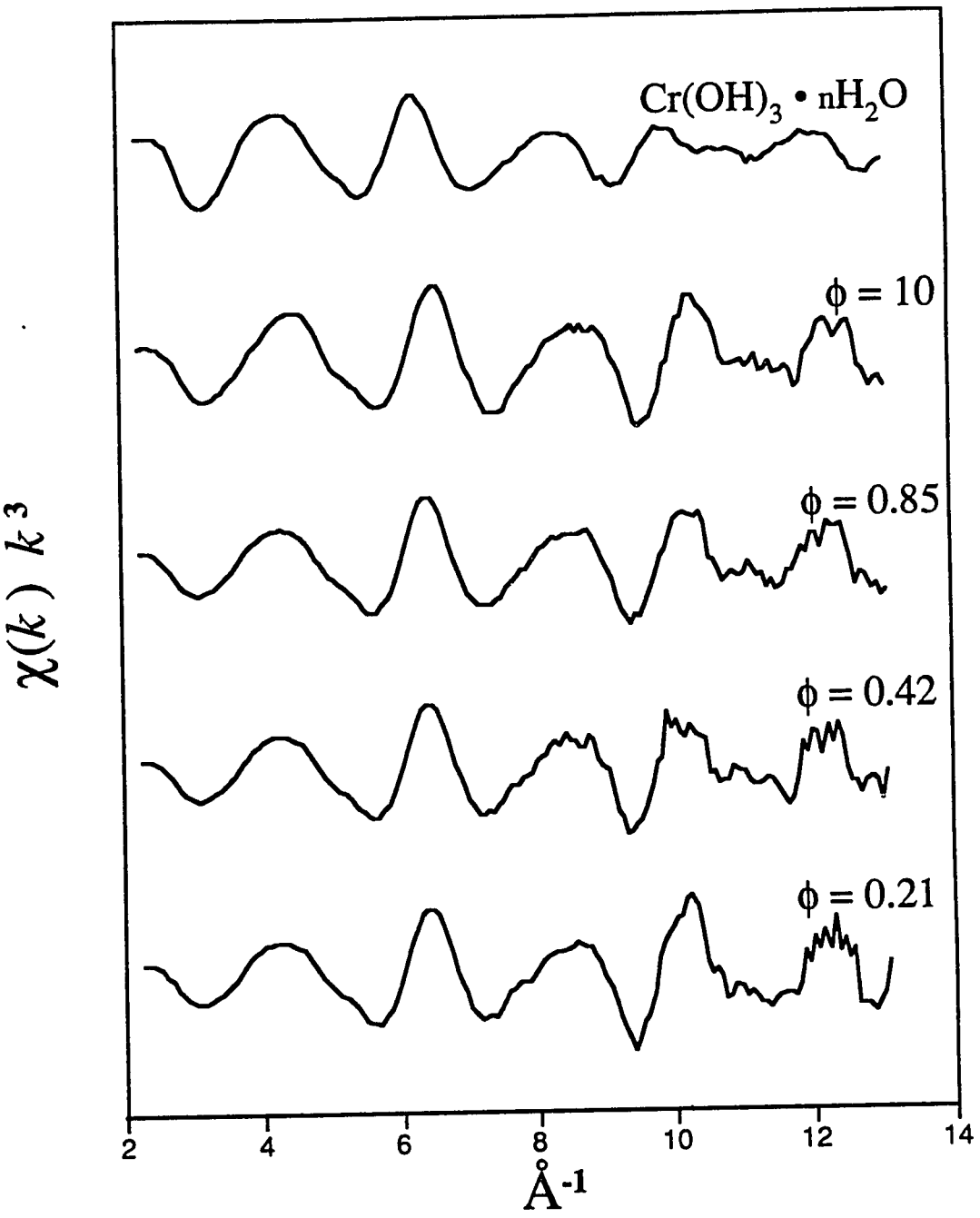

Figure 8-1. Experimental EXAFS spectra of Cr(III) sorbed on silica, multiplied by k^3 to equalize the amplitude over the entire k range.

Table 8-1. Structural information derived from EXAFS analysis: interatomic distances (R), coordination numbers (CN), and the Debye-Waller factors (σ). The edge and corner sharing Cr octahedra distances along with the Cr to Si distances are reported.

	Edge: Cr-Cr			Si-Cr			Corner: Cr-Cr		
	R(Å)	CN	σ (Å)	R(Å)	CN	σ (Å)	R(Å)	CN	σ (Å)
γ-CrOOH	2.98	1.6	0.01				3.96	2.0	0.012
ϕ=10[a]	2.98	2.8	0.013	3.39	1.1	0.004	3.83	1.0	0.011
							3.97	1.8	0.013
ϕ=0.85[a]	2.97	2.7	0.012	3.38	0.9	0.0007	3.81	0.8	0.008
							3.97	1.5	0.011
ϕ=0.42[a]	2.98	2.4	0.009	3.40	1.1	0.002	3.82	1.1	0.002
							3.96	1.4	0.004
ϕ=0.21[a]	2.98	3.0	0.012	3.39	1.1	0.0004	3.83	1.2	0.001
							3.98	1.1	0.001

[a]Potential surface site coverage for Cr(III) sorbed on silica.

more prominent and is most apparent in the hydrous chromium oxide (HCO) precipitate. Thus, the increase in the fourth peak (4 Å), decrease in magnitude of the third peak, and skewing of the second peak with increased surface coverage indicates that as nucleation progressed the structure became increasing similar to that of unstrained γ-CrOOH. Conversely, the influence of silica on the RSF of Cr is definitely shown by the second and third peak variation with changes in ϕ. Figure 8-5 illustrates the Cr-silica surface structure derived from EXAFS analysis. Hence, Cr(III) hydroxide nucleation occurs on silica with a γ-CrOOH type structure, similar to that observed for precipitation on δ-MnO_2 (Chapter 2 and Manceau and Charlet, 1992) and homogeneous solution precipitation. However, a distortion in the corner sharing octahedra of the Cr-hydroxide occurred in the near surface environment; as nucleation progressed the structure 'relaxed' back to that observed for γ-CrOOH.

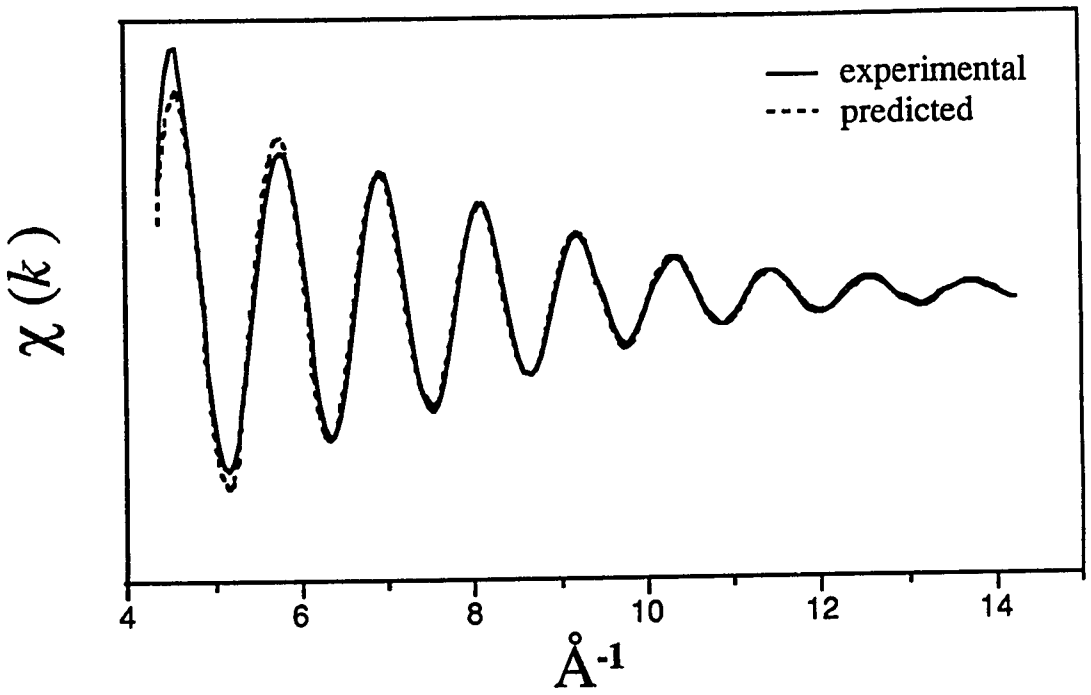

Figure 8-2. The Fourier back-transformed EXAFS function for the isolated second peak of the Fourier transformed spectra. The predicted fit was obtained by incorporating Si and Cr shells.

8.4.2 DRIFT Analysis

The DRIFT spectra for γ-CrOOH are shown in Fig. 8-6. One notes a strong, sharp absorbance at 1385 cm^{-1} and a broader one at 1417 cm^{-1}. These peaks are characteristic of the bending modes for metal oxyhydroxides (Me-OH-Me) with the boehmite type structure (γ-MeOOH) (Ryskin, 1974) and correlate well with the previously defined deformation modes of γ-CrOOH (Snyder and Ibers, 1962). The 1385 cm^{-1} peak is thus assigned to the in-plane (γ-OH) bending mode and the 1417 cm^{-1} to the out-of-plane (δ-OH) mode. The presence of these modes in the Cr-SiO_2 systems may be evidence for the formation of a γ-CrOOH precipitate.

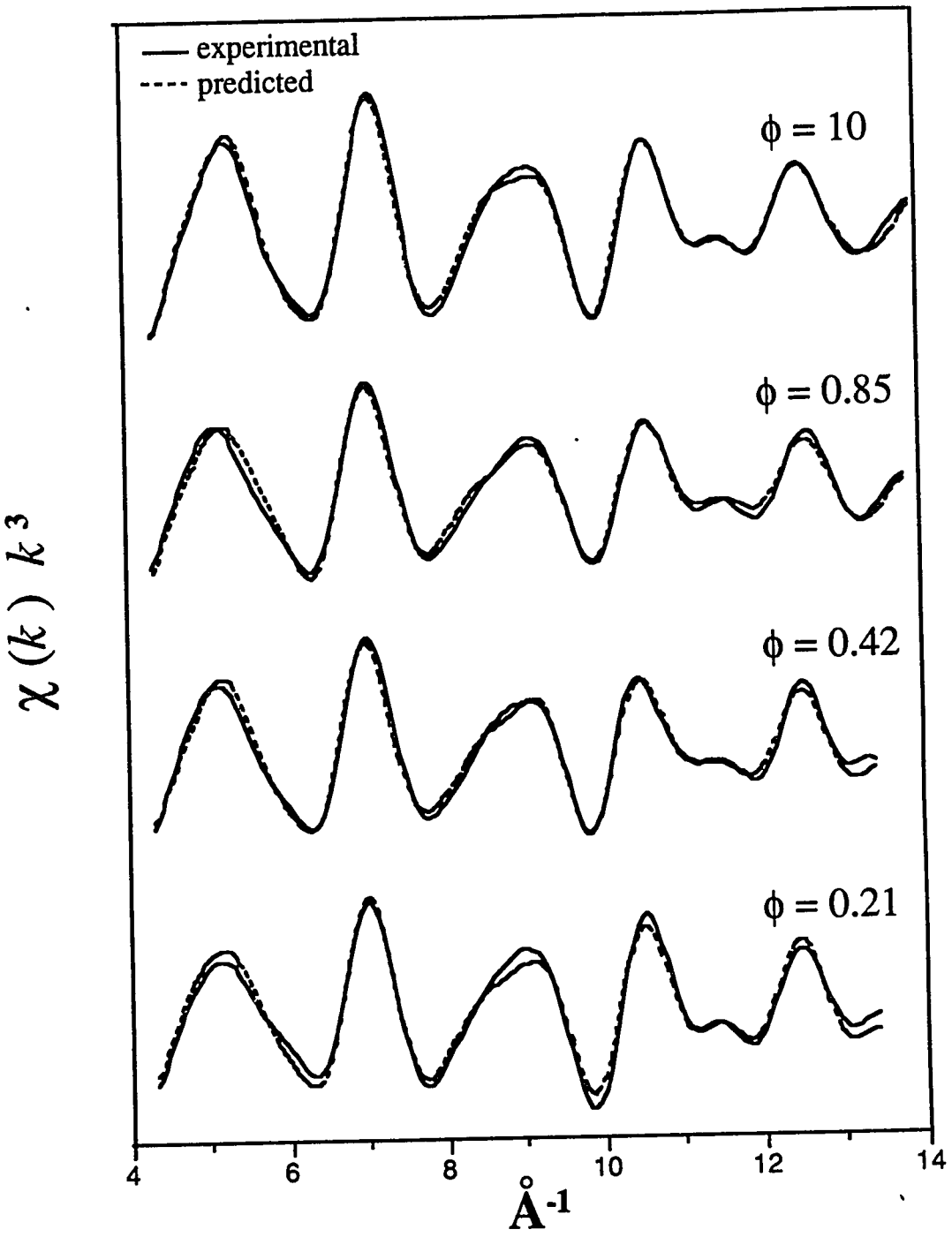

Figure 8-3. The EXAFS function for the Fourier back transformed spectra. The theoretical line was derived with parameters obtained from analysis of the isolated shells.

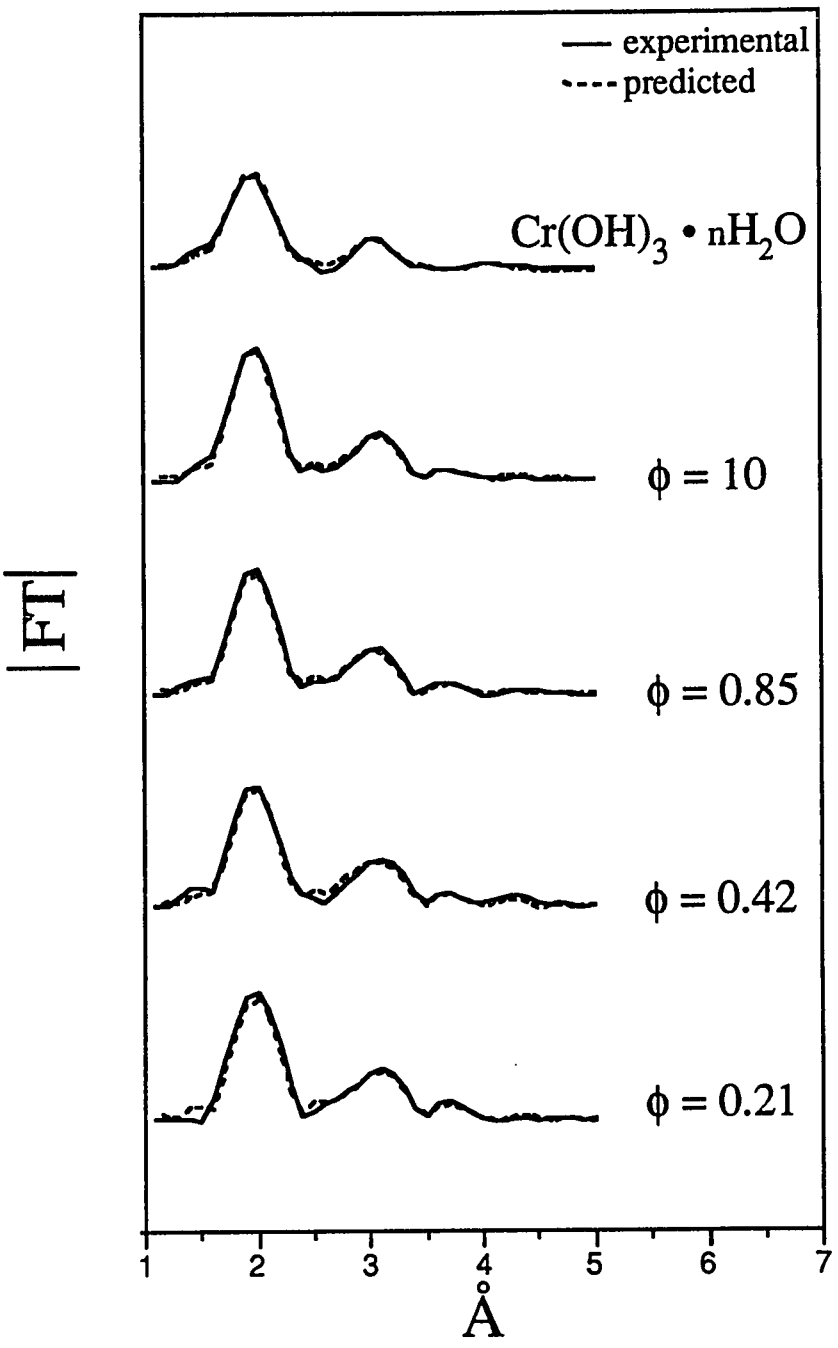

Figure 8-4. Fourier transformed spectra resulting in the radial structure function (RSF) of the inner 4 Å shells: HCO and Cr sorbed on silica are shown. The first peak results from six O at 1.99 Å; the second from Cr at 2.99 Å , and in the absence of Si, another Cr at 3.97. In the presence of Si, the second peak incorporates Si at 3.39 Å, the third and fourth peaks are composed of Cr at 3.82 and 3.97 Å.

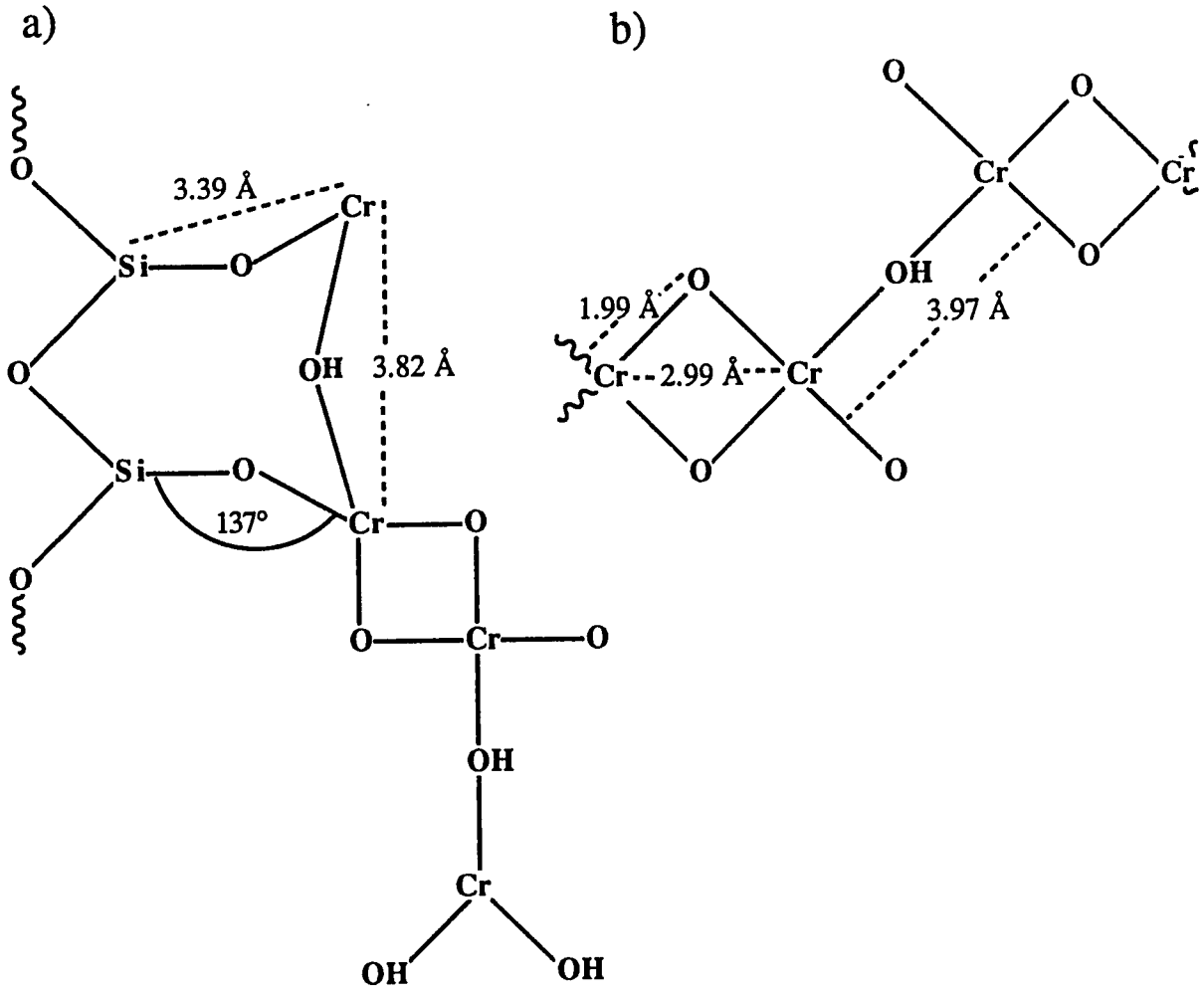

Figure 8-5. A depiction of the surface structure derived by EXAFS analysis (a) showing the interatomic distances for Cr sorbed on silica. The γ-CrOOH type structure is shown forming in (a) and in (b) the interatomic distances of this phase are given.

The DRIFT spectrum of unreacted SiO_2 is also given in Fig. 8-7. The 'neat' silica has a strong characteristic water vibrational band at 1630 cm^{-1}. However, the absorbance in the range of 1350-1600 cm^{-1} is minimal, and thus does not interfere with the prominentbending modes of γ-CrOOH. Consequently, it appears that the 1385 and 1417 cm^{-1} bands in the Cr-SiO_2 spectra should be good evidence for the formation of a γ-

CrOOH surface precipitate, while their absence would suggest that surface precipitation of this phase did not occur.

A third spectrum is shown in Fig. 8-7: Cr(III) sorbed on silica (ϕ = 10). In this spectrum 1385 and 1417 cm^{-1} peaks are visible, but additional absorbances at 1450 and 1550 cm^{-1} are also apparent. The 1385 and 1417 cm^{-1} absorbances are

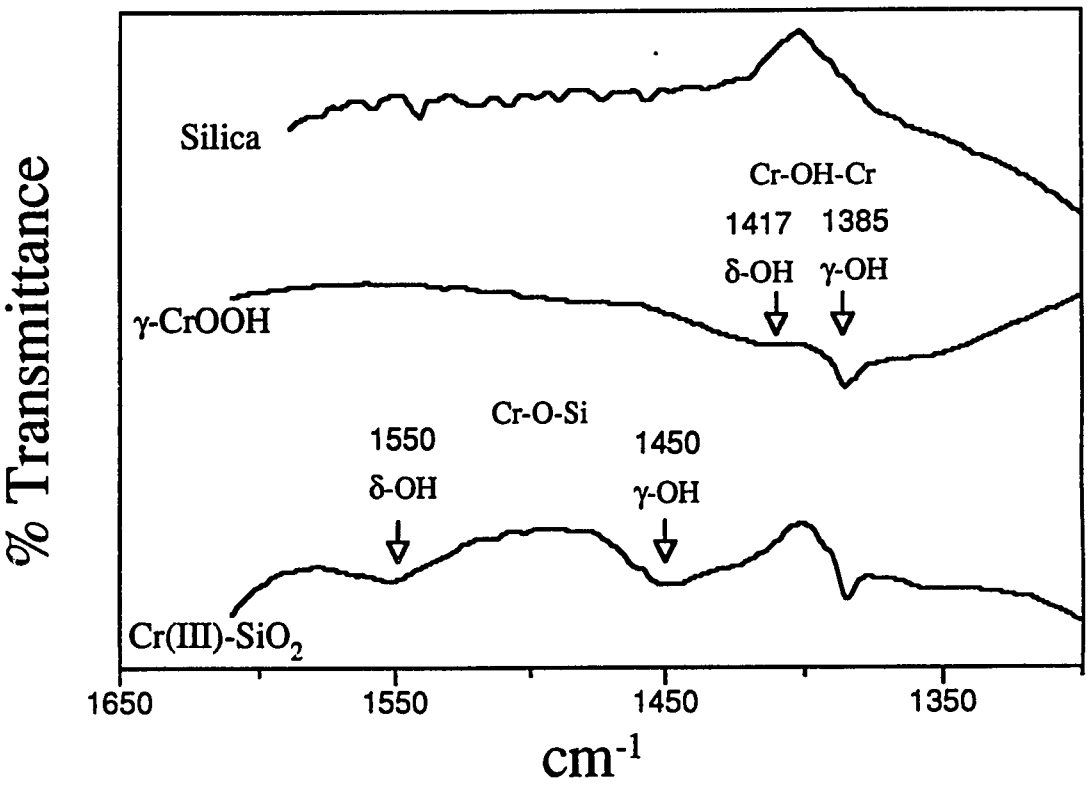

Figure 8-6. The DRIFT spectra for silica, $Cr(OH)_3 \cdot nH_2O$, and for Cr(III) sorbed on silica with ϕ = 10. The peaks at 1385 and 1417 cm^{-1} arise from the Cr-OH-Cr deformations, and the 1450 and 1550 cm^{-1} peaks are due to Cr-O-Si deformation.

identical to those observed for the deformation modes in γ–CrOOH and therefore represent the formation of a surface precipitate. The 1450 and 1550 cm^{-1} peaks are not

found in the Cr-hydroxide spectra; their appearance and magnitude are correlated except under conditions where the 1450 cm^{-1} peak is obstructed by the 1417 cm^{-1} absorbance. These peaks may be representative of a Cr-O-Si interaction. The δ–O and γ-O bending modes in a monodentate Cr-O-Si bond should be shifted to higher energies than for Cr-OH-Cr (Ryskin, 1974). Moreover, the bonding structures deduced from EXAFS suggest a non-linear monodentate Cr-O-Si bonding arrangement yielding two deformation modes. Consequently the 1550 cm^{-1} peak is assigned to the δ–O vibration and the γ–O to the 1450 cm^{-1} vibration in a Cr-O-Si linkage. Table 8-2 presents the assignment of the peaks for the DRIFT spectra of these materials.

With the assignment of the DRIFT peaks in the 1350 to 1600 cm^{-1} region one can identify structural factors arising from the sorption of Cr(III) on silica. In addition, the detection limits of DRIFT for these systems can be determined.

Table 8-2. The assignment of the deformation modes for γ-CrOOH and surface complexed Cr(III) on silica.

frequency (cm^{-1})	bond type	mode
1385	Cr-OH-Cr	γ-OH
1417	Cr-OH-Cr	δ-OH
1450	Cr-O-Si	γ-O
1550	Cr-O-Si	δ-O

8.4.3 DRIFT Analysis with Varying $[Cr]_0$ and Surface Coverage

The DRIFT spectra of 40, 100, 200, 400, and 5 x 10^3 μM $[Cr]_0$ resulting in ϕ values of 0.085, 0.21, 0.43, and 10 are presented in Fig. 8-7. The latter four conditions were identical to those used in the XAFS study permitting a comparison of results from

these two techniques. With $\phi = 0.043$ no alteration from the unreacted SiO_2 spectrum was observed. As ϕ increased to 0.085 relatively broad bands become apparent at 1450 and 1550 cm^{-1}. These broad bands increase in magnitude with further increased ϕ and are the most prominent at the highest coverage ($\phi = 10$) depicted in Fig. 8-7. A sharp peak at 1385 cm^{-1} and a broader band at 1417 cm^{-1} are apparent at $\phi = 0.21$ (100 μM $[Cr]_o$).

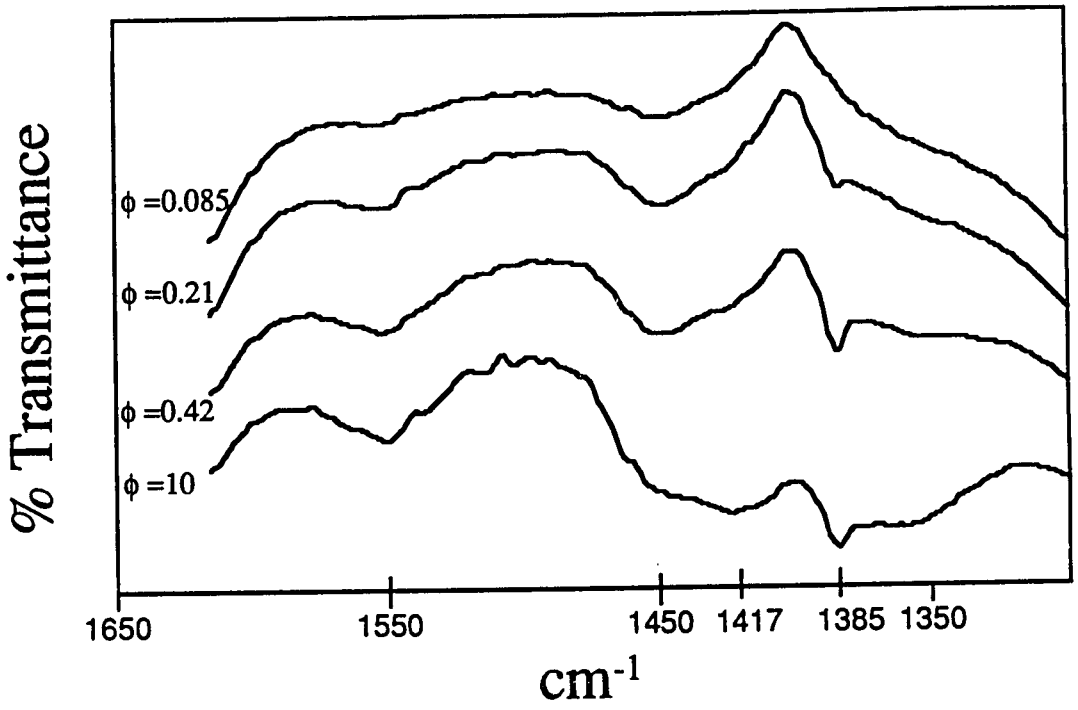

Figure 8-7. DRIFT spectra for Cr(III) sorbed on silica at $[Cr]_o$ of: 40 μM ($\phi = 0.085$), 100 μM ($\phi = 0.21$), 200 μM ($\phi = 0.42$), and 400 μM ($\phi = 0.85$). The peaks at 1385 and 1417 cm^{-1} represent Cr-hydroxide nucleation, while the absorbances at 1450 and 1550 cm^{-1} indicate a monodentate Cr-SiO_2 complex.

The four peaks at 1385, 1417, 1450, and 1550 cm^{-1} all increase with continued increases in surface coverage, but the 1385 and 1417 cm^{-1} peaks clearly begin to dominate this spectral region at higher surface coverage. At $\phi = 10$, the 1450 cm^{-1} becomes only a poorly resolved shoulder on the 1417 cm^{-1} absorbance.

At $\phi = 0.043$ (20 μM $[Cr]_o$), no structural modifications are apparent with DRIFT spectra. However with a two-fold increase in coverage, 0.085, the monodentate surface complex (Cr-O-Si) was observed. Hence the detection for sorbed Cr on silica is between 0.043 and 0.085. The 0.085 coverage spectra do not indicate the presence of nucleated Cr-hydroxide. Nucleation of γ-CrOOH is discerned at 0.21 coverage as noted by the 1385 and 1417 cm^{-1} absorbances. Hence, DRIFT spectra indicate that: the limits of detection reside at ϕ less than 0.085, monodentate surface complexation of Cr on silica occurs at $\phi < 0.20$ (100 μM $[Cr]_o$), and γ-CrOOH nucleation appears at $\phi \geq 0.20$.

8.4.4 Initial Cr(III) Concentration and Surface Coverage Effects

A second set of reaction systems were investigated in which the initial Cr(III) concentration was varied from 20 to 800 μM while the surface loading remained constant. A potential site occupancy (ϕ) of 0.21 was employed in these systems, which would not require nucleation for total sorption. This allowed an assessment of $[Cr]_o$ effects on the surface Cr(III) complexation structure. Under these reaction conditions no appreciable alteration in the sorption mechanism was detected. Absorption bands characteristic of Cr(III) complexed on silica were apparent, with no indication of Cr-hydroxide nucleation (data not shown). Therefore, at low surface coverage the sorption mechanism is affected by ϕ while not influenced by $[Cr]_o$.

The degree of surface coverage was varied by investigating a range of oxide quantities while maintaining $[Cr]_o$ constant. Below monolayer coverage, the extent of surface coverage on the Cr(III) surface structure was dramatic, as illustrated in Fig. 8-8. Under equal $[Cr]_o$, $\phi = 0.085$ resulted in the formation of a monodentate Cr(III) surface complex, as indicated by the absorbances at 1450 and 1550 cm^{-1}, while ϕ of 0.3 gave evidence for γ-CrOOH nucleation. The effects of surface coverage, at fractional

coverage, are further exemplified by the different coverages investigated and shown in Fig. 8-8. In part a , an increase in ϕ from 0.085 to 0.42 resulted in increasing intensities and prominence of the 1450 and 1550 cm^{-1} bands, with the 1385 and 1417 cm^{-1} bands becoming apparent at ϕ of 0.21. This indicates that monodentate Cr(III) surface complexation on silica predominates at ϕ of 0.085 to 0.21, but nucleation of a γ-CrOOH

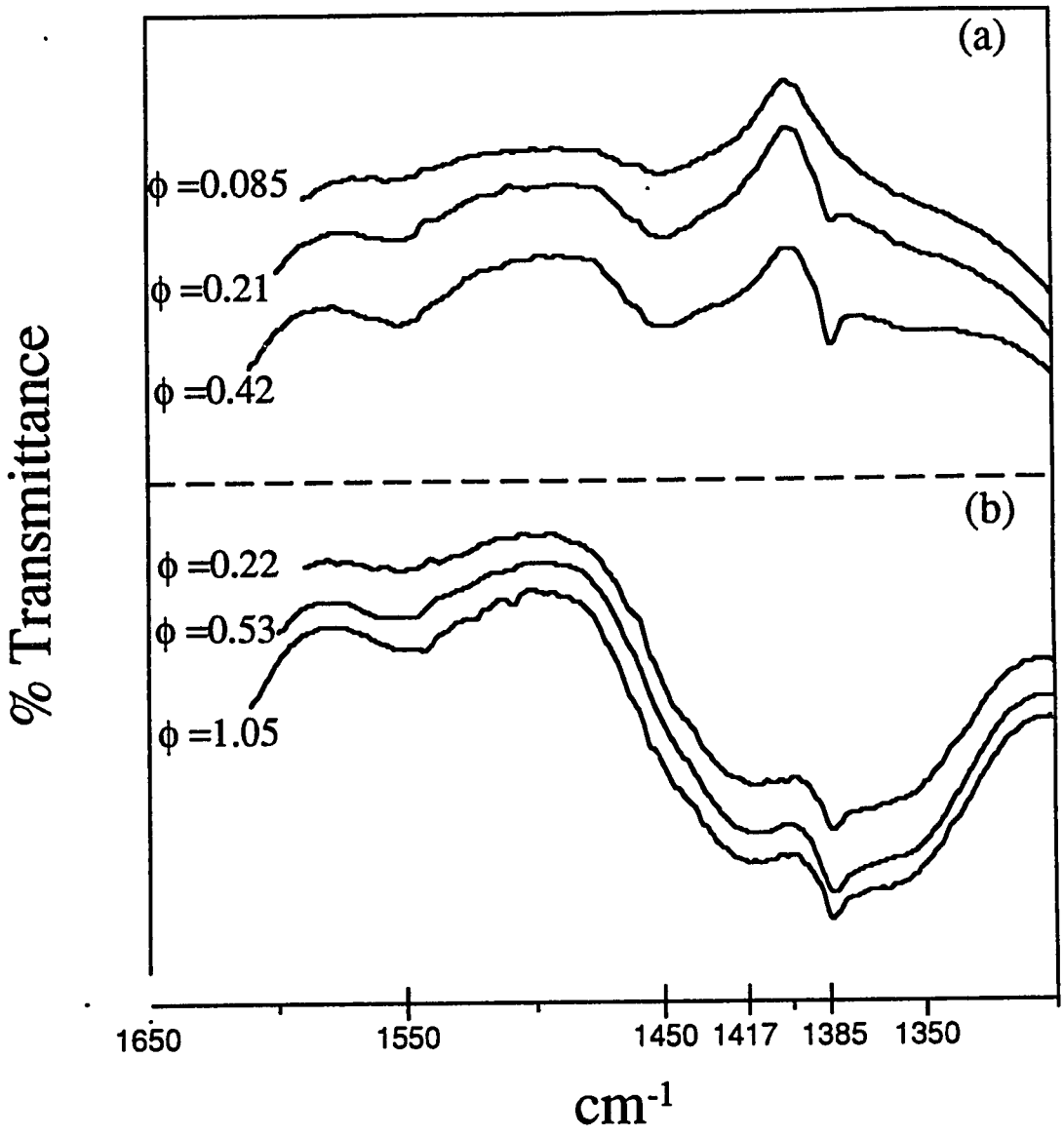

Figure 8-8. The effects of surface coverage at less than potential monolayer coverage (ϕ < 1). Initial Cr(III) concentrations of 40, 100, and 200 μM were reacted with (a) 0.5 g SiO_2 and (b) 0.2 g SiO_2.

type surface species occurs at ϕ values greater than 0.21 and increases at higher values.

With potential site occupancies greater than 1, the surface structure is not influenced by varying ϕ. This is illustrated in Fig. 8-9 in which varying amounts of silica were reacted with equal $[Cr]_o$. In these systems, extensive nucleation was noted with very little difference in the DRIFT spectra for ϕ ranging from 2 to 10.

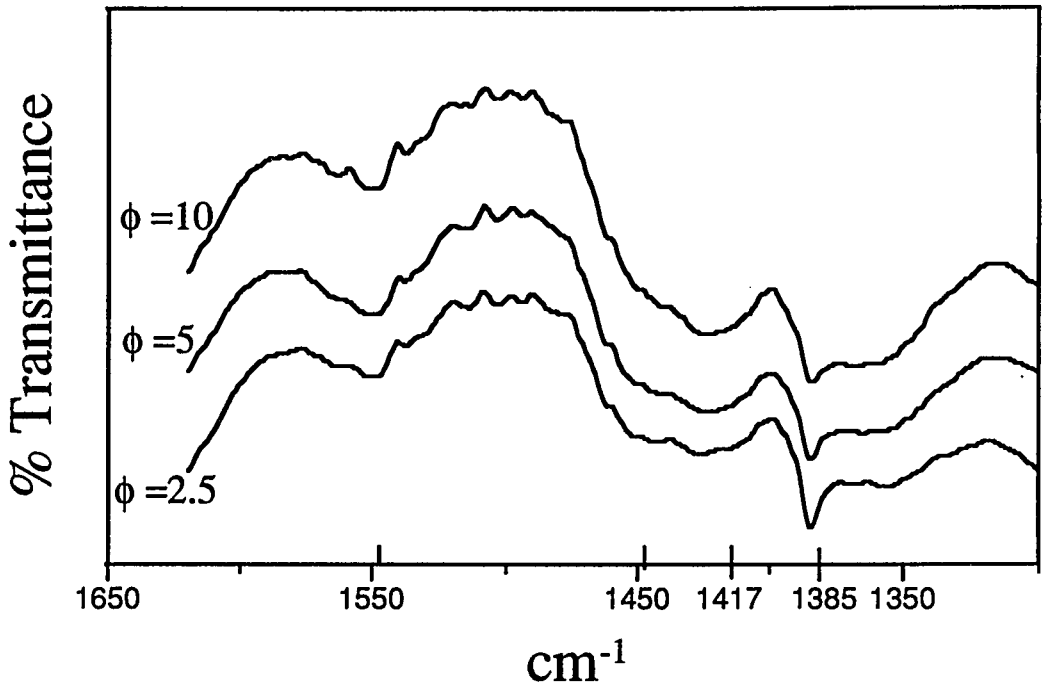

Figure 8-9. Surface coverage effects at greater than monolayer coverage. An initial Cr(III) concentration of 5 m*M* was reacted with 0.5 g (ϕ = 10), 1.0g (ϕ = 5), and 1.5 g (ϕ = 2.5) SiO_2.

8.4.5 pH Effects

Three pH values were investigated to determine the influences of solution pH on the sorption mechanism. However, one should note that pH effects on the surface

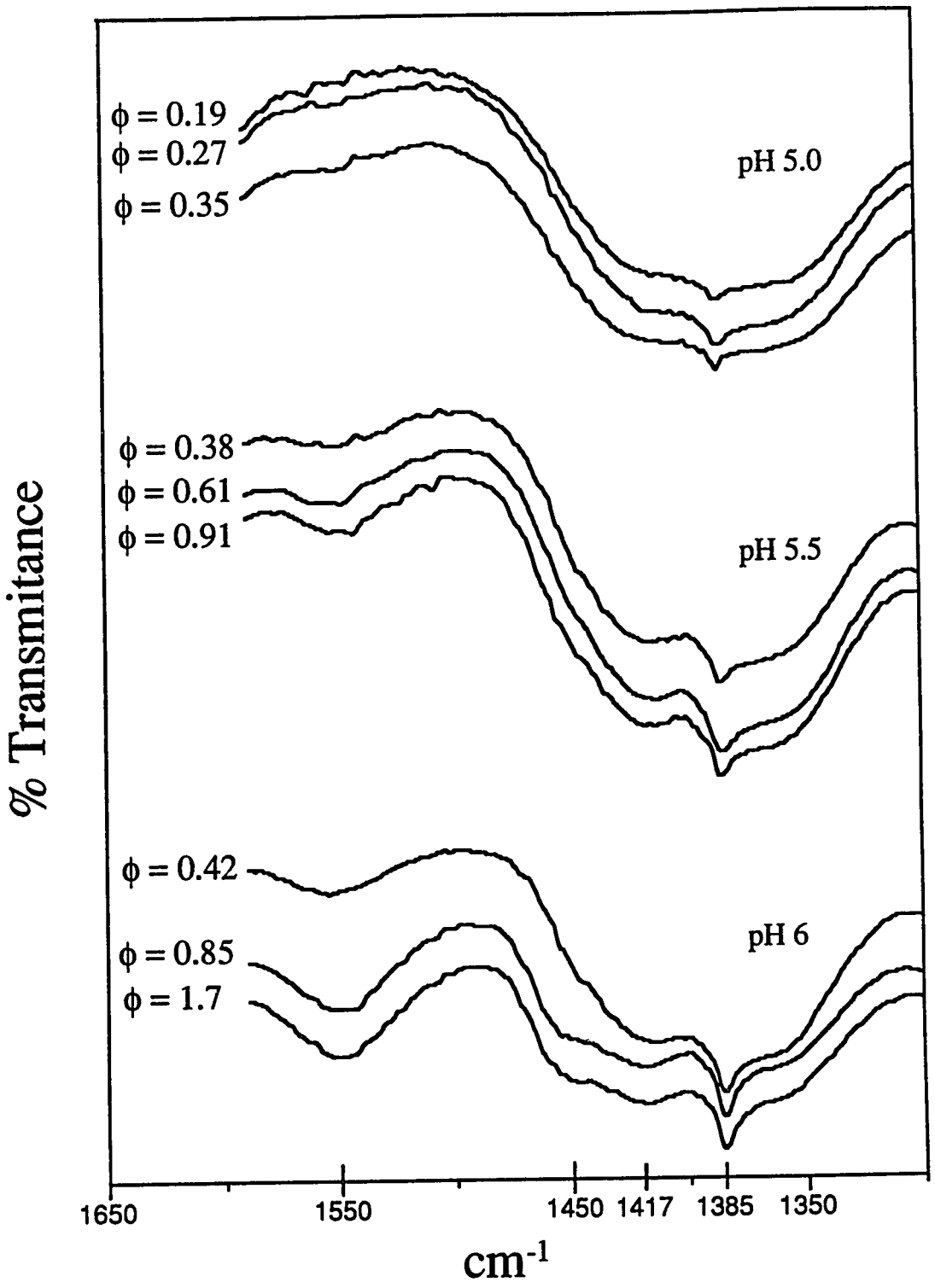

Figure 8-10. DRIFT spectra of Cr(III) sorbed on silica at pH 5.0, 5.5, and 6.0 with 100, 200, and 1000 μM $[Cr]_O$. The potential site occupancy is reported based on changes in solution concentration.

structure probably arise solely from changes in the surface coverage, which is a function of the pH. Figure 8-10 presents the DRIFT spectra of Cr(III) sorbed on silica at pH 5.0, 5.5, and 6.0. At pH 5, very little surface complexation of Cr(III) is observed from the DRIFT spectra (the absence of the 1450 and 1550 cm^{-1} modes). As pH increased to 5.5, more extensive sorption occurs and the Cr-O-Si bond becomes apparent; in addition, γ-CrOOH nucleation was observed (viz., 1417 and 1385 cm^{-1} absorbances). The pH 6 spectra are dominated by absorbances characteristic of γ-CrOOH.

The DRIFT spectra of similar ϕ values correspond well with each other, i.e., a surface loading of ϕ is similar whether the reaction occurred at pH 5, 5.5, or 6. Therefore, it appears that pH has little direct impact on the surface structure, but plays a major role in influencing the extent of sorption. Thus, the predominant role of pH is in determining the amount of sorption, which does affect the surface structure.

8.4.6 HRTEM

Although both EXAFS and DRIFT give important information on the local structural environment of Cr(III), it is difficult to determine the spatial proximity and long-range order of the sorbed material with these two methods. Accordingly, HRTEM was employed to deduce further structural information.

Imaging was performed prior to and after reaction with Cr(III), with ϕ = 10 (Fig. 8-11). The silica was completely amorphous showing no indications of ordering (marked A). After reaction with Cr(III) distinct crystalline areas approximately 20 nm x 20 nm are clearly visible (marked B). The crystalline areas are a γ-CrOOH surface precipitate. The HRTEM images reveal that even when there was greater than ten times the amount of Cr necessary to occupy all the reactive surface sites discrete crystalline particles formed. This finding indicates that Cr-hydroxide nucleation does not progress

over the silica surface but rather formed isolated nucleated areas which, at least with high potential surface coverage, possess long range order (crystalline).

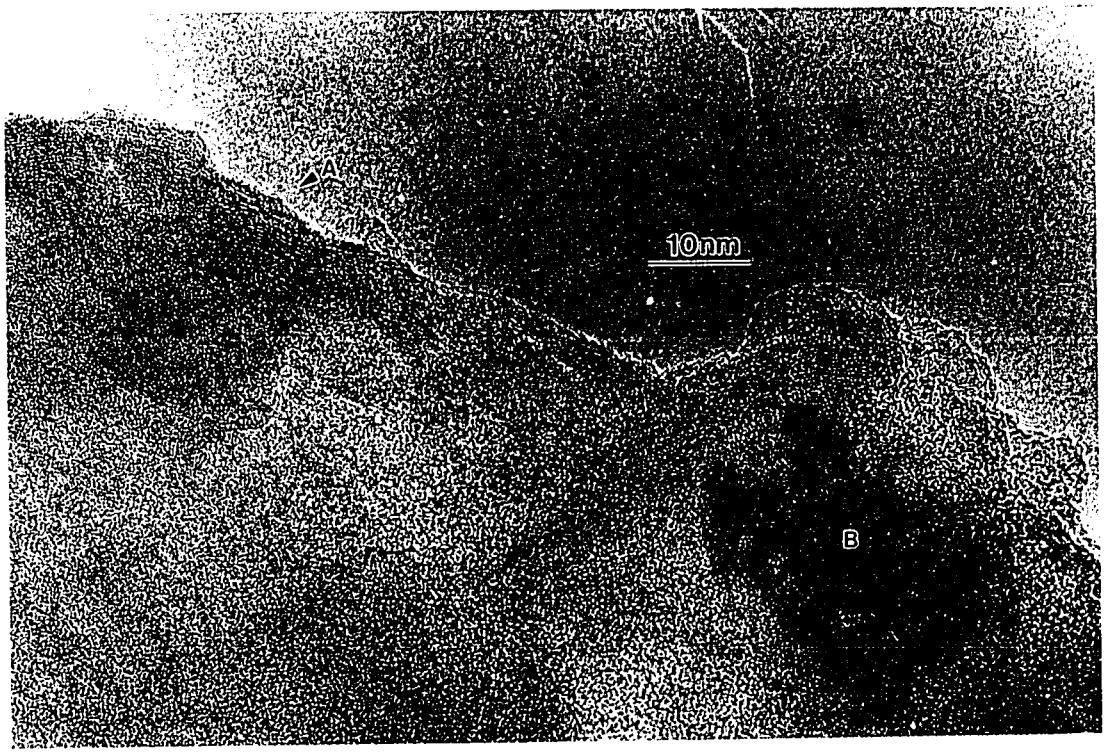

Figure 8-11. High-resolution TEM image of silica after reaction with 5 m*M* Cr(III) at pH 6 (ϕ = 10). A discrete crystalline γ-CrOOH surface precipitate (marked B) has formed on the amorphous silica (marked A).

8.5 Discussion

Both EXAFS and DRIFT analysis indicate that Cr(III) formed an inner-sphere monodentate surface complex on silica. A Si-Cr distance of 3.40 Å was determined; a linear Cr-O-Si arrangement would result in a distance of 3.59 Å and thus a bond angle of 137° is necessary to produce the observed distance. This Cr-Si distance and angle is similar to that observed for Mn in $MnSiO_3$ (Klein and Hurlbut, 1977). Monodentate

coordination with a bond angle of 137° implies that the reactive surface O atoms are singly coordinated by Si. This complexation structure agrees with the multisite surface complexation (MUSIC) model (Hiemstra et al., 1989a,b) which indicates that only the singly coordinated O of SiO_2 are reactive in the pH range of 2 to 10. McBride et al. (1984) and McBride (1982) also observed that Cu^{2+} sorbed only to singley coordinated O(H) groups on Al-oxides. The reactivity of only a single type of surface functional group contrasts with the assumption made by many surface complexation models (Schindler and Stumm, 1987; Hayes and Leckie, 1986; Farley et al., 1985; Davis et al, 1978) that the surface is composed of a homogeneous sites. The results of this study also imply that only singly coordinated surface oxo groups of silica are reactive with Cr(III), and that a 2 pKa protonation reaction is incorrect.

At potential site occupancies (ϕ) below 0.21, only Cr(III) complexed with silica was observed. At coverages equal to and exceeding 0.21, surface nucleation of the γ-CrOOH type structure occurred. A progression from isolated site binding at low coverages to surface hydroxide nucleation of Cu^{2+} on Al-oxides was similary observed (McBride et al., 1984; McBride, 1982). When nucleation of adjacent surface bound Cr(III) species occurs, the structure was distorted due to the shorter bond distances induced by the silica structure; thus, the 3.82 Å Cr-Cr distance formed. Accounting for a 137° bond angle and the O to O distance on silica, the Cr-Cr distance would be expected to be 3.8 Å in good agreement with the observed distance. The hypothesized depiction of the surface complex and nucleation structure is illustrated in Fig. 8-12. Deviation from the homogeneous HCO structure (γ-CrOOH) is thus observed at the silica and goethite (Charlet and Manceau, 1992) interface.

Chromium(III) sorption on α-FeOOH results in a surface precipitate with the α-CrOOH type structure (Charlet and Manceau, 1992); as surface coverage increased nucleation growth expanded over the surface before expanding outward (away from the

surface). Further increases in Cr(III) levels resulted in nucleation progressing outward from the α-FeOOH surface and there was a phase transition to the γ-CrOOH type structure.

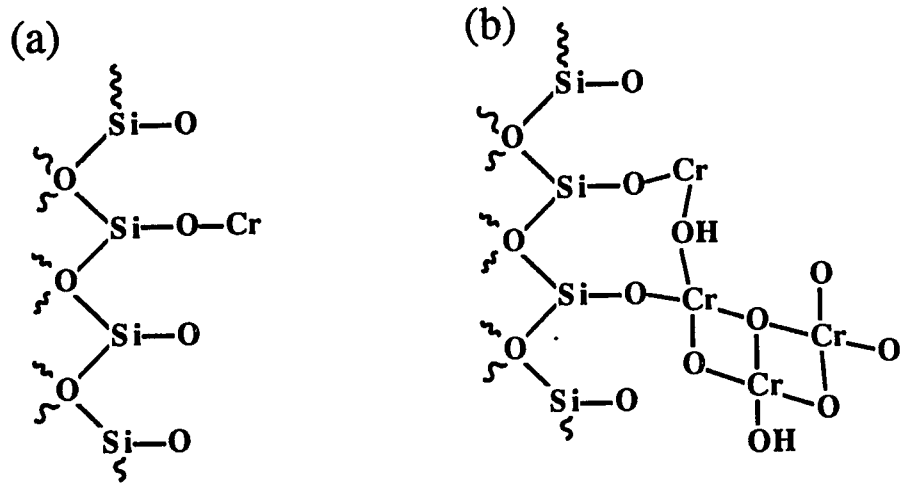

Figure 8-12. Schematic illustration of the envisioned surface structure. The monodentate complexation of Cr(III) on silica is shown in (a). In (b) the nucleation and distorted γ-CrOOH structure is depicted. Note the progressive nucleation away from the surface rather than across it.

Our results indicate somewhat similar phenomena for Cr(III) sorption on silica. A monodentate complex of Cr(III) on silica forms; the complexation continues but nucleation of a γ-CrOOH type phase occurs well before monolayer coverage. The near surface precipitate has a distorted edge-sharing octahedra which resulted in the shorter 3.82 Å Cr-Cr distance. With a continued increase in Cr(III) levels ($\phi > 0.21$) nucleation progressed on the silica surface as noted by increases in Cr-O-Si and Cr-OH-Cr deformation modes (see DRIFT spectra). Further increases in nucleation resulted in the dominance of a 'relaxed' γ-CrOOH precipitate. This is evident in the prominence of the Cr-OH-Cr modes of the DRIFT spectra and the decrease in the third peak intensity and skewing of the second peak in the RSF. High-resolution TEM indicated the formation of

a γ-CrOOH structure, which formed discrete particles on the silica surface even when greater than monolayer coverage was possible ($\phi = 10$).

Therefore, it appears that Cr(III) sorption on silica is similar to that on goethite in that nucleation occurred prior to monolayer coverage (and under conditions where solution precipitation was not observed) and that early in the nucleation process the new phase progressed over the sorbent's surface. In addition, in the near surface environment the nucleation structure was altered from that in the 'free phase' (homogeneous precipitate) due to structural constraints induced by the sorbent. In contrast to sorption on goethite, a monodentate surface complex formed on silica and nucleation of γ-CrOOH was not extensively distributed over the surface but formed isolated clusters.

8.5.1 Reaction Factors Influencing the Sorption Mechanism

Various reaction factors may influence the sorption mechanism: pH, metal concentration, surface coverage, and sorbent type. In this study we evaluated how these four factors affected the surface structure of Cr(III) sorbed on silica. Both pH and metal concentrations are well known to affect the extent of metal sorption. Moreover, the correlation between hydrolysis reactions and sorption of cationic metals is also well established (Schindler and Stumm, 1987). The extent of surface coverage and sorbent type also influence sorption but in a less defined manner. The influences of these parameters on the sorption mechanism and resulting surface structure are not resolved.

In this study, various atomic level experimental techniques were employed over a range of reaction conditions to help clarify the phenomena governing the sorption mechanism. Our findings indicate that solution metal concentrations and pH only indirectly influence the sorption structure by determining the extent of sorption. The dominant reaction factor influencing sorption is the degree of surface coverage.

Isolated site adsorption only occurred at site occupancies less than 20% ($\phi < 0.2$). At higher surface coverages, nucleation of γ-CrOOH occurred. Thus, it appears that it is more energetically favorable for surface hydroxide nucleation than for complexation of Cr(III) on silica when only 20% surface site occupancy is exceeded. Furthermore, the precipitate does not grow across the silica surface, but instead forms crystalline clustered structures which protrude away from the surface. The correlation between hydrolysis reactions and sorption may be due to precipitation reactions rather than to adsorption. If one views the surface complexation reaction as a type of precipitation, Cr(III) would bind to the surface present and enter a more favorable coordination environment after a hydrolysis reaction. The hydrolysis reaction disrupt the symmetric hexaqua coordination of a metal. This results in a less stable structure in which the H_2O molecule opposite the OH becomes a 'good' leaving group and thus promotes metal ion adsorption and nucleation. As adsorption increases, Cr would continue to bind at isolated sites but would begin to bridge together with O or OH species to further satisfy its coordination shell. On a surface such as α-FeOOH where the structural environment is similar to that for Cr-hydroxides, nucleation progresses over the surface--epitaxial growth. Once the surface has been coated nucleation progresses outward and some distance from the Fe surface undergoes a phase transformation to adopt a more favorable structure (γ-CrOOH). A different scenario, however, arises with Cr(III) sorption on silica. Chromium(III) binds to the surface initially in an isolated site mechanism. Increased retention bridges the Cr species, thus beginning nucleation. The nucleated structure is distorted and therefore of higher energy. In response to the energetics of the strained structure, nucleation begins to progress outward without extending over the surface. In addition, the development of such cluster moieties would lower the surface energy by extensively increasing the surface area.

In conclusion, the predominant factors influencing the sorption mechanism of Cr(III) on oxides are the degree of surface coverage and the type of surface. Solution pH

plays a major role in determining the amount of sorption and therefore influences the sorption mechanism indirectly by influencing the degree of surface coverage. Metal concentration appears to only influence the sorption mechanism by determining the amount of surface coverage.

8.6 References

Bleam, W.F., and M.B. McBride. 1986. The chemistry of adsorbed Cu(II) and Mn(II) in aqueous titanium dioxide suspensions. *J. Colloid Interface Sci.* 110: 335-346.

Burube, Y.G., and P.L. DE Bruyn. 1968. Adsorption at the rutile-solution interface. I: Thermodynamic and experimental study. *J. Colloid Interface Sci.* 27: 305-316.

Charlet, L., and A. Manceau. 1992. X-ray absorption spectroscopic study of the sorption of Cr(III) at the oxide-water interface: II. Adsorption, coprecipitation, and surface precipitation on hydrous ferric oxide. *J. Colloid Interface Sci.* **148**:443-458.

Chisholm-Brause, C.J., P.A. O'Day, G.E. Brown, Jr, and G.A. Parks. 1990a. Evidence for multinuclear metal-ion complexes at solid/solution interfaces from X-ray absorption spectroscopy. *Nature.* **348**:528-530.

Chisholm-Brause, C.J., A.L.Row, K.F. Hayes, G.E. Brown Jr., G.A. Parks, and J.O. Leckie. 1990b. XANES and EXAFS study of aqueous Pb(II) adsorbed on oxide surfaces. *Geochim. Cosmochim. Acta.* **54**: 1897-1909.

Corker, J.M., J. Evans, and J.M. Rummey. 1991. EXAFS study of pillard clay catalysts. *Materials Chem. Phys.* **29**:201-209.

Davis, J.A., R.O. James, and J.O. Leckie. 1978. Surface ionization and complexation at the oxide/water interface. I.Computation of electrical double layer properties in simple electrolytes. *J. Colloid Interface Sci.* 63:480-499.

Eary, L.E., and D. Rai. 1987. Kinetics of chromium(III) oxidation to chromium (VI) by reaction with manganese dioxide. *Environ. Sci. Technol.* 21:547-552.

Farley, K.J., Dzombak, D.A., and F.M.M. Morel. 1985. A surface precipitation model for the sorption of cations on metal oxides. *J. Colloid Interface Sci.* 106:226-242.

Fouad, N.E., H. Knozinger, M.I. Zaki, and A.A. Mansour. Chromia on silica and alumina catalysts: A thermoanalytical and spectroscopic investigation of thermal genesis of the catalysts. *Zeitschfit für* **171**:75-96.

Gurman, S.J., N. Binsted, and I. Ross. 1984. A rapid exact curved-wave theory for EXAFS calculations. *J. Phys.* C **17**: 143-151.

Hayes, K.F., and J.O. Leckie. 1986. Mechanisms of lead ion adsorption at the goethite/water interface. pp.141-158. *In* J.A. Davis and K.F. Hayes (ed.) Geochemical processes at mineral surfaces. ACS Symp. 323. Meet. Am. Chem. Soc., Washington, DC.

Heilman, M.C., D.L. Carter, and C.L. Gonzalez. 1965. The ethylene glycol monoethyl ether (EGME) technique for determing soil-surface area. *Soil Science.* 100:409-413.

Hiemstra, T., W.H. Van Riemsdijk, and G.H. Bolt. 1989a. Multisite proton adsorption modeling at the solid/solution interface of (hydr)oxides: A new approach. I. Model description and evaluation of intrinsic reaction constants. *J. Colloid Interface Sci.* 133:91-104.

Hiemstra, T., J.C.M. De Wit, and W.H. Van Riemsdijk. 1989b. Multisite proton adsorption modeling at the solid/solution interface of (hydr)oxides: A new approach. II. Application to various important (hydr)oxides. *J. Colloid Interface Sci.* 133:105-117.

James, R.O., and T.W. Healy. 1972. Adsorption of hydrolyzable metal ions at the oxide-water interface: II. Charge reversal of SiO_2 and TiO_2 colloids by adsorbed Co(II), La(III), and Th(IV) as model systems. *J. Colloid Interface Sci.* 40:53-65.

Klein, C., and C.S. Hurlbut. 1977. Manual of mineralogy. Wiley and Sons, NY.

Lamble, G.M., and S.M. Heald. 1991. Operation of a dynamically bent sagittally focusing double crystal monochromator for XAFS studies. *Rev. Sci. Instrum.* **63**:880-884.

Manceau, A., and L. Charlet. 1992. X-ray absorption spectroscopic study of the sorpiton of Cr(III) at the oxide-water interface: I. Molecular mechanisms of Cr(III) oxidation on Mn oxides. *J. Colloid Interface Sci.* **148**:425-442.

McBride, M.B. 1982. Cu^{2+}-Adsorption characteristics of aluminum hydroxide and oxyhydroxides. *Clays Clay Miner.* **30**:21-28.

McBride, M.B., A.R. Fraser, and W.J. McHardy. 1984. Cu^{2+} interaction with microcrystalline gibbsite. Evidence for oriented chemisorbed copper ions. *Clays Clay Miner.* **32**:12-18.

Ryskin, Y.I. 1974. The vibrations of protons in minerals: Hydroxl, water and ammonium. pp. 137-181. *In* V.C. Farmer (ed.) The infrared spectra of minerals. Mineralogical Society, London.

Schindler, P.W., and W. Stumm. 1987. The surface chemistry of oxides, hydroxides, and oxide minerals. pp.83-110 *In* W. Stumm (ed.) Aquatic surface chemistry. Wiley and Sons, NY.

Snyder, R.G., and J.A. Ibers. 1962. O-H-O and O-D-O potential envergy curves for chromous acid. *J. Chem. Phys.* **36**:1356-1360.

U.S. EPA. 1984. Code of federal regulations Title 40, national interim primary drinking water regulations, Part 141. U.S. EPA, Washington, D.C.

Yates, D.E., S. Levine, and T.W. Healy. 1974. Site-binding model of the electric double layer at the oxide/water interface. *J.C.S. Faraday* I. 70:1807-1820.

Wason, S.K. 1978. Cosmetic properties and structure of fine-particle synthetic precipitated silicates. *J. Soc. Cosmet. Chem* . **29**:307-314.

CHAPTER 9

SUMMARY AND CONCLUSIONS

Reactions of metals at the solid/solution interface greatly influence their speciation and mobility in the environment. Two types of surface reactions were investigated in this research: redox and retention. The rate and mechanism of Cr(III) oxidation by δ-MnO_2 were ascertained using a composite of kinetic and atomic resolution spectroscopic/microscopic techniques. Atomic level information was also gleaned on the sorption of Al, La, Mn(II), and Cr(VI) on δ-MnO_2 and their effects on Cr(III) oxidation. Finally, the sorption mechanism for Cr(III) on silica was ascertained. Determining the stability of surface bound metal species is necessary for assessing their potential remobilization into the aqueous environment.

A novel kinetic technique for colloidal reactions was developed to study the redox reaction between Cr(III) and δ-MnO_2: an electron paramagnetic resonance spectroscopically monitored stopped-flow (EPR-SF) method. Chromium(III) oxidation proceeds as a four step chemical reaction sequence: (i) Cr(III) adsorption on δ-MnO_2, (ii) two electron transfer, (iii) single electron transfer and ligand exchange, and (iv) desorption of the products. The rate limiting step was adsorption. This finding is supported by the slow ligand exchange reactions of Cr(III) which results from its ligand stable d_3 electron configuration (Taube, 1970). These results are not in agreement with the postulate of Manceau and Charlet (1992) that the electron transfer step is rate-limiting. They proposed that mononuclear Cr(III) must diffuse into the lattice of δ-MnO_2 and bind in site vacancies for electron transfer to occur.

The molecular mechanism hypothesized by Manceau and Charlet (1992) contradicts experimental evidence (Chapter 4; Fendorf and Zasoski, 1992; Amacher and Baker, 1982) that the oxidation rate decreases with time as a function of the MnO_2 surface area. In addition, solid state diffusion on the reaction time scales for Cr(III) oxidation do not appear realistic. The extensive experimental evidence of this study resolves the mechanism for Cr(III) oxidation. A bidentate Cr(III) surface complex forms on δ-MnO_2 (in agreement with Manceau and Charlet, 1992) followed by the electron transfer steps described earlier. The initial oxidation rate increases with increased pH due to the enhancement of Cr(III) sorption, resulting from increased hydrolysis and from the increased surface charge. The oxidation reaction is inhibited at pH greater than 4, though, due to the formation of a Cr-hydroxide surface precipitate.

Based on these results, if Cr(III) were to be dispensed into the surface environment higher concentrations may reduce the potential for oxidation to Cr(VI) by promoting the formation of Cr-hydroxide phases. However, this would depend on the long term stability of these materials. The stability of the surface Cr-hydroxide precipitates on Mn-oxides have not been studied. They have been studied on α-FeOOH and had identical solubilities to homogeneous precipitates. Thus, it appears that solubility data for Cr-hydroxides can be used to assess the potential remobilization of surface precipitated Cr-hydroxide.

The effects of competing metal sorptives on Cr(III) oxidation were investigated. Lanthanum maintained a single sorption mechanism, adsorption, on δ-MnO_2 over the pH range of 3 to 5, and did not influence the oxidation reaction. In contrast, 400 μM Al adsorbed at pH < 4, formed Al-hydroxide surface clusters at pH 4, which expanded over the surface and completely enveloped the Mn-oxide by pH 5. Aluminum did influence Cr(III) oxidation at pH values less than 4, but increasing inhibited oxidation with increased pH above 4. Therefore, of the ions investigated, a surface precipitate was

necessary to inhibit Cr(III) oxidation by δ-MnO_2. Neither of the reaction products, Mn(II) or Cr(VI), influenced the extend of oxidation.

Precipitation of Al-hydroxide on δ-MnO_2 occurred at an ion activity product 10^3 times lower than would be expected in bulk solution. After the Al-hydroxide phase formed, introduction of Cr(III) formed a Cr-hydroxide precipitate on the Al-hydroxide. Although an Al,Cr-hydroxide phase may potentially form, when Al was reacted with δ-MnO_2 prior to Cr(III), separate single metal(Me)-hydroxide precipitates occurred with a distinct phase boundary. The resulting conglomerated colloid was composed of three distinct metal (hydr)oxide phases: δ-MnO_2, Al-, and Cr-hydroxide.

The sorption/desorption rate of Mn(II) on δ-MnO_2 was investigated to determine: the potential rate of Mn(II) readsorption produced from Cr(III) oxidation by Mn-oxides, ascertain the sorption/desorption mechanism, and the ability of the EPR-SF technique for studying rapid reactions. The sorption reaction was complete in less than 1 s, with greater than 80% of the Mn(II) being sorbed within 200 ms. A first-order rate dependence on Mn(II) was observed. Measurement of the initial reaction rate allowed the forward (sorption) rate constant to be determined ($k_f' = 3.74 \times 10^{-3}$ s^{-1}), and the reverse (desorption) rate constant was determined using an integrated reversible first-order rate expression ($k_r' = 3.08 \times 10^{-4}$ s^{-1}). Using these rate constants, the predicted time dependence of Mn(II) sorption was in good agreement with the measured sorption rate. The results indicate that chemical kinetics were measured. Although the Mn(II) sorption reaction on δ-MnO_2 is rapid, sorption was not appreciable in the presence of Cr(III) (Fendorf and Zasoski, 1992). Chromium(III) may competitively displace (desorb) Mn(II), and Cr-hydroxide surface precipitates, which form under pH values conducive for Mn(II) sorption, may not have a high affinity for Mn(II).

The constraints imparted by Cr-hydroxide precipitation on δ-MnO_2 allowed an evaluation of reaction factors controlling precipitation which would otherwise not have

been possible. Surface precipitation results from a decrease in the solvation energy in the interfacial region. This can result from complexation on the surface, from the electrostatics imparted by the charged interface, or from a combination of these factors. When Cr(III) complexes with δ-MnO_2, oxidation results. Therefore, the observed surface precipitate must result from the electrostatic influences of the interfacial region and not from direct complexation with the oxide surface. James and Healy (1972) gave a thermodynamic description of electrostatic influences on the solubility of metal-hydroxides. Based on the surface charge of δ-MnO_2, their model indicates that solubility constants would be lowered at least by 10^2 in the interfacial region (Murray and Dillard, 1979). Our findings indicate that the solubility of Al-hydroxide was lowered by 10^2 at the δ-MnO_2/solution interface (Chapter 6).

The nucleation structure of Cr-hydroxide was of the γ-CrOOH type, similar to that resulting from homogeneous (free) solution precipitation (Chapter 2; Manceau and Charlet, 1992). This supports the conclusion that Cr(III) forming the precipitate was not directly complexed with the Mn-oxide surface because no structural distortions were observed, i.e., the structure formed was not influenced by the structural parameters of the sorbent. The surface precipitate structure of Cr-hydroxide on δ-MnO_2 differs from that on α-FeOOH (Charlet and Manceau, 1992) and silica (Chapter 8). Nucleation on the latter two surfaces resulted in structures that deviated from the γ-CrOOH structure. Chromium(III) nucleation on α-FeOOH yielded an α-CrOOH type structure at the Fe-Cr interface. This suggests that an epitaxial growth occurred on the goethite surface; as nucleation progressed it expanded on the Fe-surface, but with further nucleation away from the Fe interface a phase transition to γ-CrOOH occurred.

The sorption mechanism of Cr(III) on silica differs from that on α-FeOOH or δ-MnO_2. Chromium(III) initially sorbs in a monodentate complex on the silica. However, at 20% surface coverage bridging of the sorbed species occurs. Rather than distributing

over the silica surface, as results on α-FeOOH, the nucleation progresses away from the silica surface--out into the surrounding solution. The initial nucleation at the silica interface resulted in a distorted γ-CrOOH type structure. The silica appears to impart structural constraints on the epitaxial growth of Cr-hydroxide which are not energetically favorable. This results in the higher energy strained structure at the Cr-Si interface, and consequently nucleation progresses away from the silica surface allowing the unstrained γ-CrOOH structure to develop. Comparing the sorption mechanism of Cr(III) on these three oxides, one observes three different processes.

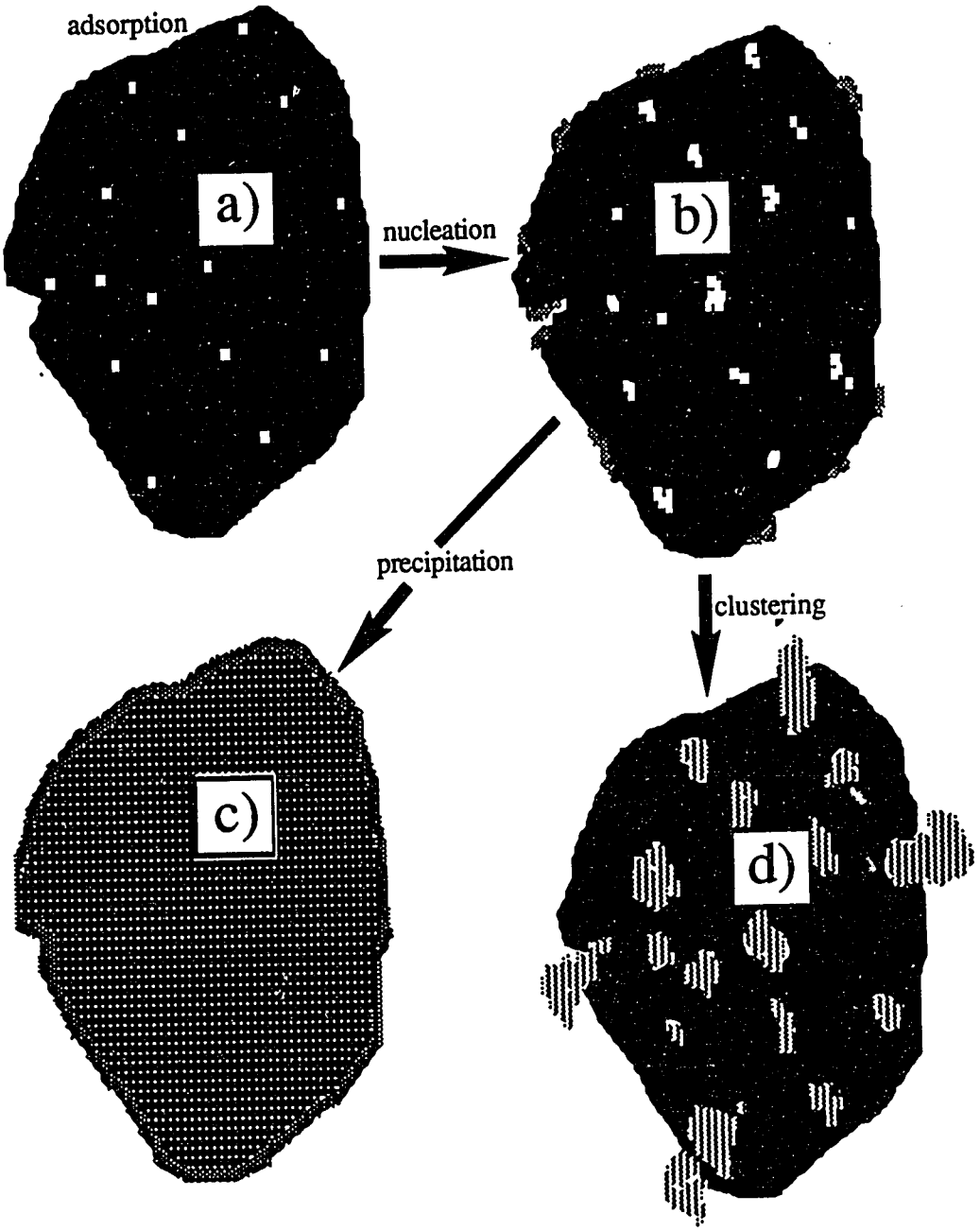

Figure 9-1. An illustration of metal ion sorption reactions on (hydr)oxides. At low surface coverage, isolated site binding (adsorption) is the dominant sorption mechanism(a). With increased metal (Me) levels, Me-hydroxide nucleation begins (b), and further increases in metal levels results in surface precipitation (c) or surface clusters (d). Surface precipitates appear to form under condition in which the structural parameters, e.g., O(H) interatomic distances, of the sorbent and sorbate (Me-hydroxide) are similar. In contrast, discrete surface clusters form when the structure of the surface are not conducive for epitaxial growth of the sorbate.

Figure 9-1 illustrates the sorption mechanisms of metals on oxides. At low surface coverage, adsorption appears to dominate the retention process (Fig. 9-1a). With increased Me levels, nucleation of the Me-hydroxide occurs which may form distinct entities on the surface (this was observed for Al sorption on δ-MnO_2; Chapter 6). Further increases in Me loadings leads either to precipitation (Fig 9-1c) or clustering (Fig 9-1d). Precipitation occurs when the surface site geometry of the sorbent is similar to the interatomic distances of the Me-hydroxide sorbate (i.e., that the O(H)-O(H) distances of the surface are similar to those of the Me-hydroxide sorbate). When the structures are dissimilar, epitaxial growth is energetically unfavorable and the nucleation growth will progress away from the surface to adopt an unstrained structure--the formation of surface clusters. Figure 9-2 shows the structural influences imposed by the surface on nucleation for: (a) structural agreement of the sorbent and sorbate resulting in epitaxial nucleation growth, e.g., Cr(III) sorption on α-FeOOH, (b) structural dissimilarities between the sorbent and sorbate promoting cluster formation, e.g., Cr(III) sorption on silica, and (c) electrostatically induced precipitation inducing a homogeneous type precipitation structure, e.g., Cr(III) sorption on δ-MnO_2.

The sorption of Cr(III) on silica was influenced only by the degree of surface coverage; the pH and metal concentrations only affected the nucleation structure in so much as they influence the amount of sorption (surface coverage). However this may not be the case in all reaction systems. If polymerization occurs in solution, often these species will preferentially adsorb due to their greater charge. Under such conditions, the metal ion concentration will have a dramatic influence on the sorption mechanism. One should carefully evaluate the procedures employed to create an experimental system because often the results may be specific to those reaction conditions (experimental artifacts) rather than representing environmentally realistic situations.

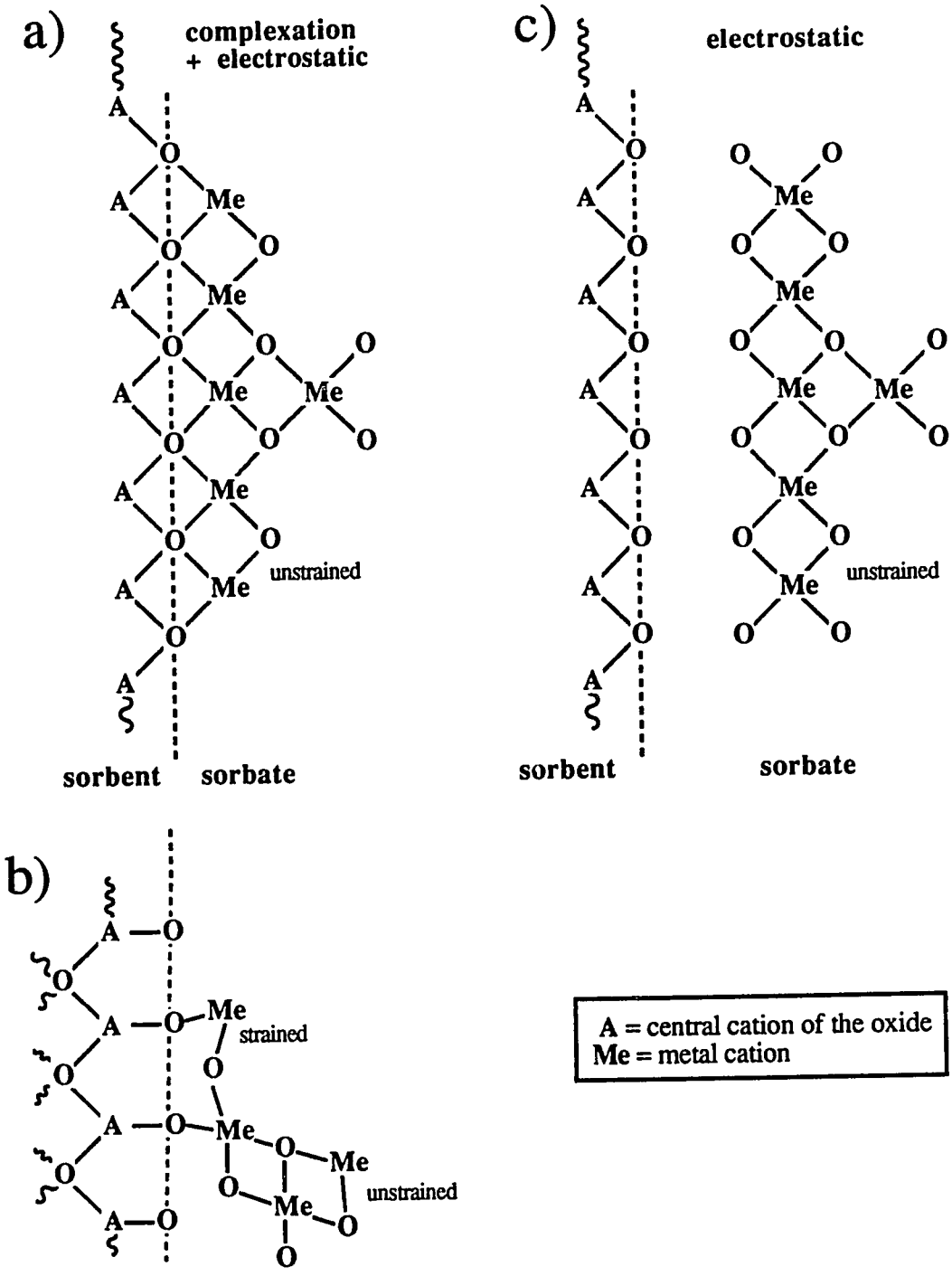

Figure 9-2. Sorbent effects on the nucleation structure of metal-(hydr)oxides at the oxide/water interface. In (a) and (b) the metal (Me) complexes with the oxide and undergoes nucleation. Structural compatibility between the sorbate and sorbent results in an epitaxial nucleation growth mechanism (a) while incompatibility produces a clustered moiety (b). Electrostatically catalyzed nucleation is depicted in (c) in which a structure of the homogeneous precipitate forms.

The electrostatic influences of a charged surface clearly can catalyze precipitation as exemplified by Cr-hydroxide surface precipitation on δ-MnO_2. However, complexation on an oxide can also promote, or at least be the precursor to, nucleation of the metal-hydroxide. Complexation promoted nucleation imparts a structural influence from the sorbent on the nucleation structure. For nucleation on structures with favorable parameters (interatomic site distances) epitaxial type growth occurs until a distance is reached from the sorbent/precipitate interface where the structure of the homogeneous precipitate is adopted. This scenario is observed for Cr-hydroxide nucleation on goethite. When the structural constraints of the sorbent are not favorable for epitaxial growth, nucleation proceeds in discrete clusters which develop away from the surface rather than across it. This was observed for Cr(III) sorption on silica. At present, it is difficult to determine whether, and under what conditions, complexation or electrostatics have a greater effect on metal-hydroxide nucleation. Certainly, electrostatics imparts a large influence on nucleation and are exerted under most conditions (i.e., even variable charged surfaces maintain some charge under most conditions due to protonation reactions of different surface functional groups). Possibly, electrostatic influences dominate the catalysis of nucleation while surface complexation imparts structural influences--as observed for Cr(III) on α-FeOOH (Charlet and Manceau, 1992) and silica (Chapter 8). When complexation does not occur the surface precipitate adopts the structure of the homogeneous precipitate, e.g., Cr(III) precipitation on δ-MnO_2 (Chapter 2).

Determining the sorption mechanism of metal ions at the oxide/solution interface is necessary for evaluating their hazard in the environment. The accuracy of mechanistic models utilized for predicting the fate of metals in colloidal systems will be enhanced by incorporating results from atomic level experimentation. The surface structure of sorbed metals determines their potential for remobilization. The strength of retention will differ depending on whether nucleation of a metal-hydroxide has occurred, and will depend on the structure of the metal-hydroxide (i.e., different polymorphs, solid phase with the same

elemental composition but different structures, often have different solubilities). Furthermore, the sorbent will be modified by the sorption process and the resulting chemical/physical properties determined by the sorption mechanism.

References

Charlet, L. and A.A. Mancaeu. 1992. X-ray absorption spectroscopic study of the sorption of Cr(III) at the oxide-water interface: I. Molecular mechanism of Cr(III) oxidation on Mn oxides. *J. Colloid Interface Sci.* 148: 425-442.

Fendorf, S.E., and R.J. Zasoski. 1992. Chromium(III) oxidation by δ-MnO_2. I: Characterization. *Environ. Sci. Technol.* 26: 79-85.

James, R.O., and T.W. Healy. 1972. Adsorption of hydrolyzable metal ions at the oxide-water interface: II. Charge reversal of SiO_2 and TiO_2 colloids by adsorbed Co(II), La, and Th(IV) as model systems. *J. Colloid Interface Sci.* **40**:53-64.

Manceau, A.A., and L. Charlet. 1992. X-ray absorption spectroscopic study of the sorption of Cr(III) at the oxide-water interface: II. Adsorption, coprecipitation, and surface precipitation on hydrous ferric oxide. *J. Colloid Interface Sci.* **148**: 443-458.

Murray, J.W., and J.G. Dillard. 1979. The oxidation of cobalt(II) adsorbed on manganese dioxide. *Geochim. Cosmochim. Acta.* **43**:781-787.

Taube, H. 1970. Electron transfer reactions of complex ions in solution. Academic Press, New York.

BIBLIOGRAPHY

Allison, J.D., D.S. Brown, and K.J. Novo-Gradac. 1990 MINTEQA2/PRODEFA2, A Geochemical Assessment Model for Environmental Systems: Version 3.0. U.S. Environmental Protection Agency: Athens, GA.

Alvarez, R., and D.L. Sparks. 1985. Polymerization of silicate anions in solution at low concentrations. *Nature* **318**:649-651.

Amacher, M.C., and D.E. Baker. 1982. Redox reactions involving chromium, plutonium, and manganese in soils. DE-AS08-77DPO4515. Inst. for Res. on Land and Water Res., Penn State Univ, PA.

Arrhenius, G., K. Cheung, S. Crane, M. Fisk, J. Frazer, J. Korkisch, T. Mellin, S. Nakao, A. Tsai, and G. Wolf. 1979. Counterions in marine manganates. *Colloques Internationaux du C.N.R.S.* **298**: 333-356.

Atkinson, P.W. 1985. Physical chemistry. Freeman and Company, New York.

Baes, C.F., and B.E. Mesmer. 1976. The hydrolysis of cations. Wiley and Sons, New York.

Balistrieri, L.S., and J.W. Murray. 1982. The surface chemistry of δMnO_2 in major ion seawater. *Geochim. Cosmochim. Acta.* **46**: 1041-1052.

Bartlett, R.J. 1986. Soil redox behavior. pp. 179-207. *In* D.L. Sparks (ed.) Soil physical chemistry. CRC Press, Boca Raton, FL.

Bartlett, R.J., and J.M. Kimble. 1976. Behavior of chromium in soils: I. Trivalent forms. *J. Environ. Qual.* 5:379-383.

Bartlett, R.J., and B.R. James. 1988. Mobility and bioavalability of chromium in soils. pp. 267-303. *In* J.O. Nraigu and E. Nieborer (eds.) Chromium in the Natural and human environments. Wiley and Sons, New York.

Bartlett, R.J., and B. James. 1979. Behavior of chromium in soils: III. Oxidation. *J. Environ. Qual.* 8:31-35.

Benjamin, M.M. 1983. Adsorption and surface precipitation of metals on amorphous iron oxyhydroxide. *Environ. Sci. Technol.* 17:686-692.

Bernasconi, C.F. 1976. Relaxation kinetics. Academic Press, New York.

Bleam, W.F., and M.B. McBride. 1986. The chemistry of adsorbed Cu(II) and Mn(II) in aqueous titanium dioxide suspensions. *J. Colloid Interface Sci.* 110: 335-346.

Blok, C., and J.E. DE Bruyn. 1970. The ionic double layer at the Zn/O solution interface: I. Thermodynamic and experimental study. *J. Colloid Interface Sci.* **32**: 518-525.

Bockris, J.O., and A.K.N. Reddy. 1970. Modern Electrochemistry. Plenum, N.Y.

Bowden, J.W., M.C.A. Bolland, A.M. Posner, and J.P. Quirk. 1973. Generalized model for anion and cation adsorption at oxide surfaces. *Nature* **245**:81-83.

Brown, G.E., G. Calas, G.A. Waychunas, and J. Petiau. 1988. X-ray absorption spectroscopy and its applications in mineralogy and geochemistry. pp. 431-521. *In* F. Hawthorne (ed.) Spectroscopic Methods in Mineralogy and Geology. Rev. Mineral. vol. 18. Mineral. Soc. Am., Book Crafters, MI.

Brown, G.E. Jr., G.A. Parks, and C.J. Chisholm-Brause. 1989. In-situ x-ray absorption spectroscopic studies of ions at oxide-water interfaces. *Chimia.* 43: 248-256.

Bunnett, J.F. 1986. Kinetics in Solution. pp. 171-250. *In* C.F. Bernasconi (ed.) Investigations of rates and mechanisms of reactions, 4th ed. Wiley and Sons, New York.

Burube, Y.G., and P.L. De Bruyn. 1968a. Adsorption at the rutile-solution interface. I: Thermodynamic and experimental study. *J. Colloid Interface Sci.* 27: 305-316.

Burube, Y.G., and P.L. De Bruyn. 1968b. Adsorption at the rutile-solution interface. II: Model of the electrochemical double layer. *J. Colloid Interface Sci.* 28: 92-105.

Buser, W., P. Graf, and W. Feitknecht. 1954. Beitrag zur kenntis der mangen (II)-manganit und des δ-MnO_2. Helv. *Chim. Acta.* **37**: 2322-2333.

Calas, G., and J. Petiau. 1983. Structure of oxide glasses: Spectroscopic studies of local order and crystallochemistry: Geo-chemical implications. *Bull. Mineral.* **106**:33-55.

Charlet, L. and A.A. Mancaeu. 1992. X-ray absorption spectroscopic study of the sorption of Cr(III) at the oxide-water interface: I. Molecular mechanism of Cr(III) oxidation on Mn oxides. *J. Colloid Interface Sci.* 148: 425-442.

Chisholm-Brause, C.J., G.E. Brown, Jr., G.A. Parks, and J.O. Leckie. 1989. XANES and EXAFS study of aqueous Pb(II) absorbed on oxide surfaces. *Physica B* (Amsterdam) 158:674-675.

Citrin, P.H., P. Eisenberger, and R.C. Hewitt. 1976. Transferability of phase shifts in extended X-ray absorption fine structure. *Phy. Rev. Lett.* **36**: 1346-1349.

Clementz, D.M., T.J. Pinnavia, and M.M. Mortland. 1973. Stereochemistry of hydrated copper(II) ions on the interlamellar surfaces of layer silicates. An electron spin resonance study. *J. Phys. Chem.* **77**, 196-200.

Combes, J.M., A. Manceau, G. Calas, and J.Y. Bottero. 1989a. Formation of ferric oxides from aqueous solutions: a polyhedral appraoch by X-ray absorption spectroscopy: I. Hydrolysis and formation of ferric gels. *Geochim. Cosmochim. Acta.* **53**: 583-594.

Combes, J.M., A. Manceau, and G. Calas. 1989b. Formation of ferric oxides from aqueous solutions: A polyhedral appraoch by X-ray absorption spectroscopy: II. Hematite and formation of ferric gels. *Geochim. Cosmochim. Acta.* **54**: 1083-1091.

Corker, J.M., J. Evans, and J.M. Rummey. 1991. EXAFS studies of pillard clay catalysts. *Material Chem. Phys.* **29**: 201-209.

Cowley, J.M. 1981. Diffraction physics. North Holland, Amsterdam.

Crane, S.E. 1981. Structural chemistry of marine manganate minerals. Ph.D. Dissertation. University of California, San Diego.

Crowther, D.L., J.G. Dillard, and J.W. Murray. 1983. The mechanism of Co(II) oxidation on synthetic birnessite. *Geochim. Cosmochim. Acta.* 47:1399-1403.

Davis, J.A., R.O. James, and J.O. Leckie. 1978. Surface ionization and complexation at the oxide/water interface. I.Computation of electrical double layer properties in simple electrolytes. *J. Colloid Interface Sci.* 63:480-499.

Davies, S.H.R., and J.J. Morgan. 1989. Manganese(II) oxidation kinetics on oxide surfaces. *J. Colloid Interface Sci.* **129**: 63-77.

Drago, R.S. 1977. Physical methods in chemistry. Saunders College Publishing, Orlando, FL.

Durham, P.J. 1988. Theory of XANES. pp.52-86. *In* D.C. Knoningsberger and R. Prins (eds.) X-ray absorption. principles, applications, techniques of EXAFS, SEXAFS, and XANES. Wiley and Sons, NY.

Dzombak, D.A., and F.M.M. Morel. 1990. Surface complexation modeling-hydrous ferric oxide. Wiley and Sons, NY.

Eary, L.E., and D. Rai. 1987. Kinetics of chromium(III) oxidation to chromium (VI) by reaction with manganese dioxide. *Environ. Sci. Technol.* 21:547-552.

Farley, K.J., Dzombak, D.A., and F.M.M. Morel. 1985. A surface precipitation model for the sorption of cations on metal oxides. *J. Colloid Interface Sci.* 106:226-242.

Federal Register. 1980a. pp. 33084-33139. Vol. 45, No. 98. Goverment Printing Office, Washington, D.C.

Federal Register. 1980b. pp. 74884-74894. Vol. 45, No. 220. Goverment Printing Office, Washington, D.C.

Fendorf, S.E. 1990. Metal ion influences on chromium oxidation by manganese dioxide. M.S. Thesis, University of California, Davis.

Fendorf, S.E., and R.J. Zasoski. 1992. Chromium(III) oxidation by δ-MnO_2. I: Characterization. *Environ. Sci. Technol.* 26: 79-85.

Fouad, N.E., H. Knozinger, M.I. Zaki, and A.A. Mansour. Chromia on silica and alumina catalysts: A thermoanalytical and spectroscopic investigation of thermal genesis of the catalysts. *Zeitschfit für* **171**:75-96.

Grove, J.H., and B.G. Ellis. 1980. Extractable chromium as releated to soil pH and applied chromium. *Soil Sci. Soc. Am. J.* 44:238-242.

Gurman, S.J., N. Binsted, and I. Ross. 1984. A rapid exact curved-wave theory for EXAFS calculations. *J. Phys. C* **17**: 143-151.

Hachiya, K, M. Ashida, M. Saski, H. Kan, T. Inoue, and T. Yasunaga. 1979. Study of kinetics of adsorption-desorption of Pb^{2+} on γ-Al_2O_3 surface by means of relaxation techniques. *J. Phys. Chem.* 83:1866-1871.

Hayes, K.F., and J.O. Leckie. 1986. Mechanisms of lead ion adsorption at the goethite/water interface. pp.141-158. *In* J.A. Davis and K.F. Hayes (ed.) Geochemical processes at mineral surfaces. ACS Symp. 323. Meet. Am. Chem. Soc., Washington, DC.

Hayes, K.F, A.L. Roe, G.E. Brown, K.O. Hodgson, J.O. Leckie, and G.A. Parks. 1987. *In situ* X-ray adsorption study of surface complexes: selenium oxyanions on α-FeOOH. *Science*. **238**:783-786.

Heald, S.M. 1988. Design of an EXAFS experiment. pp. 87-118. *In* D.C. Knoningsberger and R. Prins (eds.) X-ray Absorption. Principles, applications, techniques of EXAFS, SEXAFS, and XANES. Wiley and Sons, NY.

Healy, T.W., A.P. Herring, and D.W. Furstenau. 1966. The effect of crystal structure on the surface properties of a series of manganese dioxides. *J. Colloid Interface Sci.* **21**:435-444.

Heilman, M.C., D.L. Carter, and C.L. Gonzalez. 1965. The ethylene glycol monoethyl ether (EGME) technique for determing soil-surface area. *Soil Science.* **100**:409-413.

Hiemstra, T., W.H. Van Riemsdijk, and G.H. Bolt. 1989a. Multisite proton adsorption modeling at the solid/solution interface of (hydr)oxides: A new approach. I. Model description and evaluation of intrinsic reaction constants. *J. Colloid Interface Sci.* 133:91-104.

Hiemstra, T., J.C.M. De Wit, and W.H. Van Riemsdijk. 1989b. Multisite proton adsorption modeling at the solid/solution interface of (hydr)oxides: A new approach. II. Application to various important (hydr)oxides. *J. Colloid Interface Sci.* 133:105-117.

Ikeda, T., M. Sasaki, and T. Yasunaga. 1983. Kinetic studies of ion exchange of alkylammonium ion for sodium ion in aqueous suspensions of zeolite 4A using the pressure-jump method. *J. Phys. Chem.* **87**: 745-749.

Ikeda, T., J. Nakahara, M. Sasaki, and T. Yasunaga. 1984. Kinetic behavior of alkali metal ion on zeolite 4A surface using the stopped-flow method. *J. Colloid Interface Sci.* **97**: 278-283.

James, R.O., and T.W. Healy. 1972a. Adsorption of hydrolyzable metal ions at the oxide-water interface: II. Charge reversal of SiO_2 and TiO_2 colloids by adsorbed Co(II), La(III), and Th(IV) as model systems. *J. Colloid Interface Sci.* 40:53-65.

James, R.O., and T.W. Healy. 1972b. Adsorption of hydrolyzable metal ions at the oxide-water interface: III. A thermodynamic model of adsorption. *J. Colloid Interface Sci.* 41:65-80.

Johnson, C.A., and Xyla, A.G. 1991. The oxidation of chromium(III) to chromium(VI) on the surface of manganate (γ-MnOOH). *Geochim Cosmochim Acta.* **55**:2861-2866.

Kinselev, A.V., and V.I. Lygin. 1975. Infrared spectra of surface compounds. Wiley and Sons, NY.

Klimes, N., G. Lassmann, and B. Ebert. 1980. Time-resolved EPR spectroscopy. Stopped-flow EPR apparatus for biological application. J. Mag. Res. 37: 53-59.

Klein, C., and C.S. Hurlbut. 1977. Manual of mineralogy. Wiley and Sons, NY.

Krishnan, K.M. 1989. Electron energy-loss spectroscopy. *In* L.M. Coyne, S.McKeever, and D. F. Blake (eds.) Spectroscopic characterization of minerals and their surfaces. pp.54-74. ACS symposium series 415. American Chemical Society, Washington DC.

Lamble, G.M., and S.M. Heald. 1991. Operation of a dynamically bent sagittally focusing double crystal monochromator for XAFS studies. *Rev. Sci. Instrum.* **63**:880-884.Clementz, D.M., T.J. Pinnavaia, and M.M. Mortland. 1973. Stereochemistry of hydrated copper(II) ions on the interlamellar surfaces of layer silicates. An electron spin resonance study. *J. Phys. Chem.* **77**, 196-200.

Lasaga, A.C. 1981. Rate laws of chemical reactions. pp. 1-68. *In* A.C. Lasaga and R.J. Kirkpatrick (eds.) Kinetics of geochemical processes. Reviews in mineralogy, Vol. 8. Mineral. Soc. Am., Washington D.C.

Lee, P.A., and G. Beni. 1977. New Method for the calculation of atomic phase shifts: Application to extended X-ray absorption fine structure (EXAFS) in molecules and crystals. *Phys. Rev.* B **15**: 2862-2883.

Lee, P.A., and J.B. Pendry. 1975. Theory of the extended X-ray absorption fine structure. *Phys. Rev.* B **11**: 2795-2811.

Loganathan, P., R.G. Burau, and D.W. Furstenau. 1977. Influences of pH on the sorption of Co^{2+}, Zn^{2+} and Ca^{2+} by a hydrous manganese oxide. *Soil Sci. Soc. Am. J.* **41**: 57-62.

Luther, G.W., III. 1990. The frontier-molecular-orbital theory approach in geochemical processes. pp.193-198. *In* W. Stumm (ed.) Aquatic chemical kinetics. Wiley and Sons, NY.

Luther, G.W., III. 1987. Pyrite oxidation and reduction: Molecular orbital theroy considerations. *Geochim. Cosmochim. Acta.* **51**:3193-3199.

Lytle, F.W., R.B. Greegor, D.R. Sandstrom, E.C. Marques, J. Wong, C.L. Spiro, G.P. Huffman, and F.E. Huggins. 1984. Measurements of soft X-ray absorption spectra with a fluorescent ion chamber detector. *Nucl. Instr. and Meth.* **226**:542-548.

Lytle, F.W., D.E. Sayers, and E.A. Stern. 1975. Extended x-ray absorption fine-structure technique. II. Experimental practice and selected results. *Phys. Rev.* B **15**:4825-

4835.Loganathan, P., and R.G. Burau. 1973. Sorption of heavy metal ions by a hydrous manganese oxide. *Geochim. Cosmochim. Acta.* **37**:1277-1294.

Makdisi, R.S. 1992. Tannery wastes definition, risk assessment and cleanup option, Berkeley, California. *J. Haz. Mater.* 29:79-96.

Manceau, A.A., and L. Charlet. 1992. X-ray absorption spectroscopic study of the sorption of Cr(III) at the oxide-water interface: II. Adsorption, coprecipitation, and surface precipitation on hydrous ferric oxide. *J. Colloid Interface Sci.* **148**: 443-458.

Marcelli, A., I. Cavoli, A. Bianconi, J. Garcia, A. Gargano, C.R. Natoli, M Benafatto, P. Chiaradia, M. Fanfoni, E. Fritsch, F. Calas, and J. Petiau. 1985. Local structure in SiO_2 glasses by oxygen K edge XANES. *J. Physique.* **46**, C8:107-112.

McBride, M.B. 1989a. Oxidation of dihydroxybenzene in aerated aqueous suspensions of birnessite. *Clays Clay Miner.* 37:341-347.

McBride, M.B. 1989b. Oxidation of 1,2- and 1,4-dihydroxybenzene by birnessite in acidic aqueous suspensions. *Clays Clay Miner.* 37:479-486.

McBride, M.B. 1987. Adsorption and oxidation of phenolic compounds by iron and manganese oxides. *Soil Sci. Soc. Am. J.* 51:1466-1472.

McBride, M.B. 1982a. Cu^{2+}-Adsorption characteristics of aluminum hydroxide and oxyhydroxides. *Clays Clay Miner.* **30**:21-28.

McBride, M.B. 1982b. Hydrolysis and dehydration reactions of exchangeable Cu^{2+} on hectorite. *Clays Clay Miner.* **30**:200-206.

McBride, M.B., A.R. Fraser, and W.J. McHardy. 1984. Cu^{2+} interaction with microcrystalline gibbsite. Evidence for oriented chemisorbed copper ions. *Clays Clay Miner.* **32**:12-18.

McKenzie, 1977. Manganese oxides and hydroxides. pp. 181-193. *In* J.B. Dixon (ed.) Minerals in the Soil Environment. Soil Sci. Soc. Am, Madison WI.

McMaster, W.H., N. Kerr del Grande, J.H. Mallet, and J.H. Hubell. 1969. Compilation of X-ray cross sections III. *US Atom. Ener. Comm.* UCRL-50174.

Morgan, J.J., and W. Stumm. 1964. Colloid-chemical properties of manganese dioxide. *J. Colloid Sci.* **19**: 347-359.

Murray, J.W. 1975. The interaction of metal ions at the manganese dioxide-solution interface. *Geochim. Cosmochim. Acta* **30**:505-519.

Murray, J.W. 1974. The surface chemistry of hydrous manganese dioxide. J. Colloid Interface Sci. **46**:357-371.

Murray, J.W., and J.G. Dillard, 1979. The oxidation of cobalt(II) adsorbed on manganese dioxide. *Geochim. Cosmochim. Acta.* 43:781-787.

Pauling, L. 1960. The nature of the electrostatic bond, 3rd ed., Cornell Univ. Press, Ithaca, NY.

Pendry, J.B. 1974. Low energy electron diffraction. Academic Press, NY.

Petiau, J. and G. Calas. 1985. EXAFS and edge structure; application to nucleation in oxide glasses. *J. Physique.* **46**, C8:41-50.

Petiau, J., G. Calas, and P. Sainctavit. 1987. Recent developments in the experimental studies of XANES. *J. Physique* **48**, C9:1085-1096.

Potter, R.M., and G.R. Rossman. 1979. The tetravalent manganese oxides: Identification, hydration, and structural relationships by infrared spectroscopy. *Am. Mineral.* **64**: 1199-1218.

Rai, D., B.M. Sass, and D.A. Moore. 1987. Chromium(III) hydrolysis constants and solubility of chromium(III) hydroxide. *Inorg. Chem.* **26**:345-349.

Ryskin, Y.I. 1974. The vibrations of protons in minerals: Hydroxl, water and ammonium. pp. 137-181. *In* V.C. Farmer (ed.) The infrared spectra of minerals. Mineralogical Society, London.

Sass, B.M., and D. Rai. 1987. Solubility of amorphous chromium(III)-iron(III) hydroxide solid solutions. *Inorg. Chem.* **26**:2228-2232.

Sainctavit, P., J. Petiau, G. Calas, M. Benfatto, and C.R. Natoli. 1987. XANES study of sulfur and zinc K-edges in zincblende: Experiments and multiple-scattering calculations. *J. Physique* **48**, C9:1109-1112.

Sayers, D.E., and B. Bunker. 1988. Data Analysis. pp. 211-253. *In* D.C. Knoningsberger and R. Prins (eds.) X-ray Absorption. Principles, applications, techniques of EXAFS, SEXAFS, and XANES. Wiley and Sons, NY.

Sayers, D.E., E.A. Stern, and F.W. Lytle. 1971. New techniques for investigation of noncrystalline structures: Fourier analysis of the extended X-ray-absorption fine structure. *Phys. Rev. Lett.* **64**:1204-1207.

Schindler, P.W. 1981. Surface complexes at oxide-water interfaces. pp. 1-49. *In* M.A. Anderson and A.J. Rubin (eds.) Adsorption of inorganics at solid-liquid interfaces. Ann Arbor Science, MI.

Schindler, P.W., and W. Stumm. 1987. The surface chemistry of oxides, hydroxides, and oxide minerals. pp.83-110. *In* W. Stumm (ed.) Aquatic surface chemistry. Wiley and Sons, NY.

Sparks, D.L. 1989. Kinetics of soil chemical processes. Academic Press, New York.

Stach, J., R. Kirmse, W. Dietzsch, G. Lassmann, V.K. Belyaeva, and I.N. Marov. 1985. Ligand exchange reactions between copper(II)- and nickel(II)-chelates of different sulfur- and selenium-containing ligands. VI [1]. Kinetics of ligand exchange reactions studied by stopped-flow ESR. *Inorgan. Chim. Acta.* 96: 55-59.

Steinfeld, J.E., J.S. Francisco, and W.L. Hase. 1989. Chemical kinetics and dynamics. Prentice Hall, New Jersey.

Stern, E.A. 1974. Theory of extended x-ray absorption fine structure. *Phys. Rev.* B **10**:3027-3037.

Stern, E.A. 1988. Theory of EXAFS. pp.3-51. *In* D.C. Knoningsberger and R. Prins (eds.) X-ray Absorption. Principles, applications, techniques of EXAFS, SEXAFS, and XANES. Wiley and Sons, NY.

Stern, E.A., B.A. Bunker, and S.M. Heald. 1980. Many-body effects on extended X-ray absorption fine structure amplitudes. *Phys. Rev.* B **21**: 5521-5539.

Stone, A.T. 1991. Oxidation and hydrolysis of ionizable organic pollutants at hydrous metal oxide surfaces. pp. 231-254. *In* D.L. Sparks and D.L. Suarez (eds.) Rates of soil chemical processes, Soil Sci. Soc. Am. Special Publication, Soil Sci. Soc. Am., Madison, WI.

Stumm, W., H. Hohl, and F. Dalang. 1976. Interaction of metal ions with hydrous oxide surfaces. *Croat. Chim. Acta.* **48**:491-504.

Taube, H. 1970. Electron Transfer Reactions of Complex Ions in Solution. Academic Press, New York.

Teo, B.K. 1986. EXAFS: Basic Principles and Data Analysis. Springer-Verlag, New York/Berlin.

Teo, B.K., and P.A. Lee. 1979. Ab Initio calculations of amplitude and phase functions for extended X-ray absorption fine structure spectroscopy. *J. Am. Chem. Soc.* **101**:2815-2832.

Tewari, P.H., and W. Lee. 1975. Adsorption of Co(II) at the oxide-water interface. *J. Colloid Interface Sci.* 52:77-88.

Torrent, J., V. Barron, and U. Schwertmann. 1990. Phosphate adsorption and desorption by goethites differing in crystal morphology. *Soil Sci. Soc. Am. J.* **54**:1007-1012.

Traina S.J., and H.W. Doner. 1985. Heavy metal induced release of manganese(II) from a hydrous manganese dioxide. *Soil Sci. Soc. Am. J.* **49**:307-313.

Turner, M.A., and R.H. Rust. 1971. Effects of chromium on growth and mineral nutrition of soybeans. Soil Sci. Soc. Am. Proc. **35**:755-758.

U.S. EPA. 1984. Code of federal regulations Title 40, national interim primary drinking water regulations, Part 141. U.S. EPA, Washington, D.C.

Walker, W.J., C.S. Cronan, H.H. Patterson. 1988. A kinetic study of aluminum adsorption by aluminosilicate clay minerals. *Geochim. Cosmochim. Acta.* **52**:55-62.

Wason, S.K. 1978. Cosmetic properties and structure of fine-particle synthetic precipitated silicates. *J. Soc. Cosmet. Chem .* **29**:307-314.

Waychunas, G.A. 1987. Synchrotron radiation XANES spectroscopy of Ti in minerals: Effects of Ti bonding distances, Ti valence, and site geometry on absorption edge structure. *Am Mineral.* **72**:89-101.

Waychunas, G.A., M.J. Apted, G.E. Brown, Jr. 1983. X-ray K-edge absorpiton spectra of Fe minerals and model compounds: Near-edge structure. *Phys. Chem. Minerals* **10**:1-9.

Wehrli, B., and W. Stumm. 1989. Vanadyl in natural waters: Adsorption and hydrolysis promoted oxygenation. *Geochim. Cosmochim. Acta.* **53**: 69-77.

Westall, J.C. and H. Hohl. 1980. A comparison of electrostatic models for the oxide/soution interface. pp. 265-294. *In* A.C. Zettlemoyer (ed.) Adv. in Colloid and Interface Science. Elsevier Scientific Publishing Company, Amsterdam.

Yates, D.E., S. Levine, and T.W. Healy. 1974. Site-binding model of the electric double layer at the oxide/water interface. *J.C.S. Faraday* I. 70:1807-1820.

Zasoski, R.J., and R.G. Burau. 1988. Sorption and sorptive interactions of cadmium and zinc on hydrous manganese dioxide. *Soil. Sci. Soc. Am. J.* **52**:81-87.

Zhang, P.C., and D.L. Sparks. 1989. Kinetics and mechanism of molybdate adsorption/desorption at the goethite/water interface using pressure-jump relaxation. *Soil Sci. Soc. Am. J.* 53:1028--1034.

Zhang, P.C., and D.L. Sparks. 1990a. Kinetics and mechanisms of sulfate adsorption/desorption at the goethite/water interface using pressure-jump relaxation. *Soil Sci. Soc. Am. J.* 54: 1266-1273.

Zhang, P.C., and D.L. Sparks. 1990b. Kinetics of selenite and selenate adsorption/desorption at the goethite/water interface using pressure-jump relaxation. *Environ. Sci. Technol.* 24: 1848-1856.